The Dissertation Committee for Manuel Joseph Garcia
certifies that this is the approved version of the following dissertation:

Non-Convex Myopic Electricity Markets:
The AC Transmission Network and Interdependent Reserve Types

Committee:

_____

Ross Baldick, Supervisor

_____

Hao Zhu

_____

Constantine Caramanis

_____

Grani Hanasusanto

_____

Surya Santoso

Non-Convex Myopic Electricity Markets:
The AC Transmission Network and Interdependent Reserve Types

by

Manuel Joseph Garcia

DISSERTATION

Presented to the Faculty of the Graduate School of

The University of Texas at Austin

in Partial Fulfillment

of the Requirements

for the Degree of

DOCTOR OF PHILOSOPHY

THE UNIVERSITY OF TEXAS AT AUSTIN

December 2019

Dedicated to my fiancée Rachel Mercer-Smith.

Acknowledgments

I would like to extend my gratitude to everyone who has supported me during my academic pursuits. First and foremost, I would like to thank my supervisor Professor Ross Baldick, without his guidance, encouragement, and thoughtful questions this dissertation would not be complete. Not only has he heavily influenced the work in this dissertation, but he will also have a lasting effect on my career as a researcher. Professor Baldick has taught me how to fish so I can feed myself for a lifetime of research. I leave the program confident in my abilities to sustain a research career. I am fortunate to have had Professor Baldick as my supervisor. I wish him the best in his retirement.

I'm also grateful for my dissertation committee members. Chapter 6 of my dissertation originated as a project for Professor Hao Zhu's course in power system operations and control. I was challenged early in the program by Professor Constantine Caramanis' convex optimization course, which helped motivate me to pursue optimization related research topics. I thank Professor Grani Hanasusanto and Professor Surya Santoso for their constructive advice on my dissertation.

I would also like to thank my colleagues outside of the University of Texas that contributed to this work. During my last two years in the program I met frequently with Dr. Shams Siddiqi from Crescent Power, Inc. He provided valuable insights into the Texas electricity market and contributed significantly to Chapter 4. Dr. Harsha Nagarajan from Los Alamos National Laboratory provided significant contributions to Chapter 6 while I was interning with his research group in New Mexico.

My fellow students at the University of Texas have been very supportive and many of our discussions motivate our work. I'm grateful for the time I've spent in Austin with Bing Huang, Bowen Hua, Mohammad Majidi, Sambuddha Chakrabarti, Qinhao Xing, and Wanki Cho. I'm also thankful for the time I've spent with Jeff Manning and Jian Xu during the preparation of our dissertations and defenses.

I would also like to acknowledge those who supported me before entering the PhD program. Dr. Russell Bent and his research group at Los Alamos National Laboratory encouraged me to return to graduate school to further my career as a national laboratory researcher. Professor Kameshwar Poolla first introduced me to academic research at the University of California at Berkeley and has encouraged my research pursuits over the years. I'm also grateful for Mrs. Anita Maxwell from Shasta College, who taught me that I was capable of succeeding in the academic fields of engineering and mathematics.

The biggest influence in my life is my family. Constant encouragement from my mom (Maggie), dad (Manuel), and sister (Jennifer) has given me the courage to pursue a circuitous path to obtaining a doctorate. They have always been there for me in good times and in bad. Without their support my success in this program would not have been possible.

Finally, the most important thing, my fiancée Rachel Mercer-Smith. Rachel's unconditional love and support has been prevalent throughout my doctoral studies. When I feel lost, she gives me direction. When I lack confidence, she believes in me. Rachel was the first to suggest I apply to this doctoral program and she was there to help me through every test, paper, and presentation. After moving here from New Mexico, we have had a wonderful five year adventure in Texas. It is now time for us to start a new adventure.

Non-Convex Myopic Electricity Markets:
The AC Transmission Network and Interdependent Reserve Types

Publication No. _____

Manuel Joseph Garcia, Ph.D.
The University of Texas at Austin, 2019

Supervisor: Ross Baldick

Electricity markets are particularly complex because they must accommodate the underlying physics that govern the electric power system. These physics present non-convexities in the social welfare maximization problem, also called the economic dispatch problem, solved by the Independent System Operator (ISO), which is the social planner in this context. The non-convexity of this problem presents difficulties in computing the social welfare maximizing dispatch as well as difficulties in deriving a pricing structure that satisfies certain economic requirements such as revenue adequacy of the ISO and non-negative operating profits for market participants. This dissertation analyzes two sources of non-convexity that pertain to two separate market changes that have been recently proposed in Texas. Both proposals pertain to the real-time electricity market, which clears every 5-minutes and is myopic in the sense that only the demand at the end of the upcoming 5-minute interval is considered and no future time intervals are considered in the social welfare maximization problem.

The Electric Reliability Council of Texas (ERCOT) is the ISO in Texas and currently neglects resistive losses along transmission lines when formulating the economic dispatch problem. The first part of this dissertation regards a proposed market change to incorporate transmission losses into the economic dispatch problem. Two general approaches are considered to accommodate associated non-convexity. Similar to current practice, the first approach is based on a marginal pricing structure and uses convex approximations that

facilitate efficient computation. By utilizing various approximations, the aforementioned economic requirements are proven to be satisfied approximately. The second approach is based on an alternative pricing structure in which prices are chosen to explicitly minimize the worst-case violation of these economic requirements. For example the prices may be chosen to minimize the potential revenue shortfall of the ISO. These alternative prices are termed convex hull prices and can be approximated by use of convex relaxations.

The economic dispatch problem currently used by ERCOT does not endogenously represent operating reserves to handle contingencies that may occur. Instead, operating reserves are currently optimized separately from the electric power generation dispatch. The second part of this dissertation regards a proposed market change to co-optimize reserve and generation dispatch in a social welfare maximization problem called a co-optimization problem. Implementation of the real-time co-optimization problem is being pursued simultaneously with a new definition of the primary frequency responsive reserve types considered in the market. One of these reserve types intends to accommodate standard droop control. Another of these reserve types is newly introduced and intends to facilitate participation of fast-acting batteries in primary frequency response. This dissertation derives reserve requirements from first principles that capture the coupling of these two reserve types as well as their ramping abilities. The newly proposed non-convex requirements represent limits on the ramp-constrained primary frequency responsive reserve procurement. Placing these non-convex requirements into a co-optimization problem is proven to result in the satisfaction of the aforementioned economic requirements.

Table of Contents

II Co-Optimization: Interdependent Reserve Types 123

III Conclusions and Future Work 167

List of Tables

List of Figures

Chapter 1

Introduction

Electricity markets enable the trading of electric power as a commodity [36]. The producers of this commodity are *electric generators* that are capable of converting various fuel types into electric power and providing other services while the consumers vary from individual households to large industrial plants that gain utility from electrically powered devices. The exchange of this commodity from producer to consumer occurs through the transmission and distribution systems, which are networks of electric conductors used to transport electric power. Unlike traditional commodities, it is very difficult to store large amounts of electricity, necessitating demand be met identically by supply at all times. Furthermore, electric power demand is traditionally inelastic and uncertain on short time scales, e.g. 24-hours, and is accommodated by adjusting the electricity production of electric generators. As a result, significant coordination is required among electric generators connected to the same transmission network. For this reason, among others, vertically integrated *electricity providers* were established that owned and controlled all electric generators connected to the same transmission system [83]. These electricity providers historically formed geographical monopolies and were subject to various inefficiencies including a lack of competition [48].

In the 1980's and 1990's many electricity markets throughout the world began restructuring in a way that encourages competition [83]. This restructuring requires generator owners and *electric utilities* to respectively sell and purchase electricity in a wholesale electricity market that clears in successive intervals on short time scales in order to satisfy electric power balance. Electric utilities then absorb price variability by reselling the electricity to the consumers, e.g. individual households, at a price that varies on slow time scales, e.g. months, on which these consumers are capable of responding. As of year 2016 approximately two-thirds of the electricity consumers in the United States purchased electric power through these restructured electricity markets [29].

Critical to this restructured market is the Independent System Operator (ISO) that acts as the social planner of the wholesale electricity market. The ISO is a non-profit regulated entity that is given the task of setting prices for electricity and providing coordinated dispatch instructions to generators that maximize social welfare in a way that balances electric power supply and demand, and satisfies various physical constraints imposed by the electric generators and the transmission system. To do this the ISO must solve the social welfare maximization problem, which is an optimization problem also called the economic dispatch problem. Approximate linear models of the underlying power system physics have been traditionally used to formulate the economic dispatch problem, resulting in a convex optimization problem and sound economic principles surrounding the electricity market. This dissertation studies variations of this economic dispatch problem that are non-convex, where the non-convexity arises due to a more accurate representation of the underlying power system physics. As we will see, a non-convex economic dispatch problem will not only make the optimization problem difficult to solve computationally, but will also cause important economic principles surrounding the electricity market to break down. For example, the ISO may not be able to guarantee revenue adequacy as it may realize a deficit after the market is cleared.

There are two types of non-convexities presented in the social welfare maximization problem that are traditionally studied in the literature. First are integer-valued decision variables that represent commitment decisions made by participating generators. These integer-valued decision variables represent hourly start-up and shut-down decisions that are made by each generator throughout the day and allow for start-up costs, no-load costs and minimum up/down times to be considered in an economic dispatch problem that optimizes over a time horizon. This type of economic dispatch problem is called the Unit Commitment (UC) problem and serves as the social welfare maximization problem for the day-ahead market that is cleared every 24 hours [39]. This type of non-convexity is studied extensively in other works but will not be addressed in this dissertation.

This dissertation will study the second non-convexity that is traditionally studied in the literature that pertains to the Alternating Current (AC) model of the transmission network, which operates at a nominal frequency of 60 Hz in the Americas, 50 Hz in Eu-

2

rope, and may vary among other synchronous networks throughout the world. This type of non-convexity arises through continuously differentiable non-linear equations and captures physical phenomena occurring on time scales that are much faster than the hourly commitment decisions being modeled in the UC problem. As a result, this non-convexity is not only relevant to the day-ahead market, but is also relevant to the real-time market, which is cleared on a faster time scales of 5-15 minutes. The economic dispatch problem associated with the real-time market is myopic in the sense that (in its basic formulation) it only optimizes over a single time interval. To isolate the effect of the non-convexity of interest this dissertation will abstract away the day-ahead market and focus solely on the myopic real-time market as well as the associated myopic economic dispatch problem. Issues associated with multiple intervals in a so-called *lookahead* economic dispatch problem will not be addressed in this dissertation.

To operate the system reliably, the ISO is additionally given the task of preparing for contingencies. Ensuring power balance is met at all times requires provision of electric power supply/demand that can be called upon in the event of a contingency. For example, traditional generators may be operated below their maximum power output capability, leaving some headroom that can be quickly called upon in the event of a generator being unexpectedly disconnected from the transmission network. In this case the headroom is interpreted as a *reserve product* that is paid for by the ISO in the context of the electricity market. It is apparent that this reserve product is coupled with the electric power product for each generator since total generator capacity must be apportioned between electric power and reserve products. For this reason, many ISO's in the US have incorporated a reserve product into the social welfare maximization problem, which is termed the *co-optimization problem* as it co-optimizes this reserve product along with the generation. Included in the co-optimization problem is a reserve requirement that is used to guarantee sufficient reserve to accommodate specified contingencies.

Contingencies that cause an excess of electric power demand are typically accommodated by *up reserve*, which represents the ability of a resource to increase its power output. Similarly, contingencies that cause an excess of electric power generation are typically accommodated by *down reserve*, which represents the ability of a resource to decrease its power

output. This dissertation will focus only on up reserve procurement consistent with practice in US markets; however, the analysis can be extended to the case of up and down reserve. Henceforth, all references to *reserve* will imply *up reserve* unless otherwise specified.

Reliably operating the power system has been a major concern in recent years due to a dramatic change in the fuel profile of electric generators. Specifically, traditional generators that burn oil, gas, or coal as fuel are being replaced by cleaner generators that use wind and solar as their primary *fuel*. Unlike traditional electric generators, wind and solar generators exhibit demand-like characteristics in that they are inelastic and uncertain on short time scales. For this reason the term *net demand* has been coined to refer to the combination of traditional demand minus the wind generation and solar generation. As traditional generators are being replaced by wind and solar generators, net demand fluctuations are increasing and fewer traditional generators are available, diminishing the electric power system's ability to achieve power balance.

To improve power system reliability ISOs throughout the world have recently been incorporating new reserve products into the electricity market. In general, these reserve products represent electric power supply that can be called upon in the event of a contingency in order to sustain electric power balance. In contrast to traditional generators adjusting their power output to accommodate contingencies, electricity demand might provide the ability to curtail or electric storage might prepare for discharging during such an event. These different reserve types exhibit varying effectiveness in responding to contingencies and the electricity market should be designed in a way that takes advantage of their diverse properties. This dissertation will study a new reserve type that is capable of exhibiting a nearly instant change in power output and can be interpreted as demand curtailment or battery discharging. A novel reserve requirement will be derived from first principles and is expressed as non-linear constraints that makes the co-optimization problem non-convex.

The Electric Reliability Council of Texas (ERCOT) is the ISO that operates the electricity market in Texas. To date, the economic dispatch problem used by ERCOT in the real-time market does not consider reserve and uses a linear approximation of the AC transmission system that neglects electric power losses along the transmission lines. A high-level

overview of this real-time economic dispatch problem currently used by ERCOT is provided in Chapter 2. ERCOT is governed by the Public Utility Commission of Texas (PUCT), which issues electricity market rule changes in the state of Texas. Over the last few years the PUCT has considered two market rule changes that call for various reserve products to be co-optimized with the generation dispatch and for the inclusion of transmission losses in the model of the transmission network. These two market rule changes have been considered separately by the PUCT and serve as the motivation for the work presented in this dissertation. Accordingly, Part I of this dissertation will address the non-convexity that arises from the inclusion of transmission losses into the economic dispatch problem and Part II will address the inclusion of multiple reserve products into a real-time co-optimization problem. Consistent with the PUCT's analysis, these two market changes will be considered separately [26, 27]. In other words, this dissertation does not consider an economic dispatch problem that both co-optimizes reserve products and incorporates transmission losses although in practice the ERCOT market may eventually include both features. Sections 1.1 and 1.2 further introduce these two topics. Section 1.3 then summarizes the main contributions of this dissertation.

1.1 Economic Dispatch and Transmission Losses

The first non-convexity that will be studied is associated with the Alternating Current (AC) transmission network [11]. Power flow through the AC transmission network is governed by physics that can be represented by continuously differentiable non-linear equations that are traditionally approximated as being linear. The most common approximation makes the key assumption that no real power is lost in the transmission network. This approximation is termed the *Direct Current (DC) approximation* or *DC model* and is used in some electricity markets including the market in Texas [42]. On the other hand, the majority of electricity markets in North America incorporate transmission line losses into the social welfare maximization problem associated with both the real-time and day-ahead markets [21, 22]. ISOs governed by FERC claim to realize significant benefits by incorporating losses into market operation [42]. In fact, PJM has reported 100 million dollars of savings per year in energy and congestion costs [78]. These claims have encouraged other ISOs to consider implementing marginal losses into their economic dispatch [65]. Perhaps more im-

portantly, the implementation of losses into the social welfare maximization problem allows for Locational Marginal Prices (LMPs) to accurately reflect the marginal cost of losses. This allows for LMPs to better guide investment and operational decisions, resulting in long term benefits as well.

Despite the increased prevalence of marginal losses, a standard economic dispatch problem has not emerged in industry, so that energy markets that consider marginal losses have varying implementations [22]. The choice of implementation of marginal losses has both market price and resource dispatch impacts that may significantly benefit some players while significantly disadvantaging other players as compared to *Alternating Current Optimal Power Flow* (AC OPF) outcomes [5, 11, 12], which we will view as the "gold standard" for the dispatch problem. To better understand these various implementations, Part I of this dissertation derives economic dispatch problems from first principles and explains the various assumptions and approximations required to attain different practical formulations. Common and unnecessary assumptions are identified and proper choices of tuning parameters are specified. Certain approximations are shown to increase the error in price and dispatch outcomes. The following four subsections introduce the topic of each chapter in Part I of this dissertation.

1.1.1   Detailed AC OPF Problem

The economic dispatch problem that most accurately accounts for transmission line losses is termed the AC OPF problem. This problem uses the equivalent-Π model for each transmission line in the AC transmission network and uses no significant assumptions or approximations except that the three-phase system is operated at a fixed frequency and is balanced across phases so that per-phase analysis can be used. The AC OPF problem represents distribution system loads as aggregated loads on the transmission system located at distribution substations connecting the transmission system to the distribution system. The aggregated distribution system loads are assumed to be balanced across phases. Distribution system characteristics are not modeled.

To represent the transmission system, complex current, power, and voltages are mod-

eled in detail. As is typical when formulating the AC OPF problem, our formulation will model transmission line capabilities using hard limits on various quantities including real, reactive, and apparent power flow as well as current magnitude flows. Similarly, generator capabilities will be modeled as having hard limits on the amount of real and reactive power they can produce. With this in mind, we recognize that these hard limits can be violated for short time durations and thus may be considered soft limits in practice. Although generators are capable of producing both real and reactive power, their costs will be modeled as being a function of only the real power produced and are assumed convex as is typical in the literature.

Chapter 3 will derive the AC OPF problem from first principles using both a polar and rectangular coordinate representation of the complex voltages in the transmission network. Both formulations include non-convex constraints for each transmission line and bus in the system. This type of non-convexity is difficult to accommodate because it is prevalent among the constraints of the problem. In fact, this non-convexity is so difficult to accommodate that the AC OPF problem has been proven to be generally NP-hard [6, 54]. However, iterative methods, such as interior point algorithms, can be used to effectively approximate the solution to the AC OPF problem. Although these algorithms are only, at best, guaranteed to converge to a local minimum, they often converge to a point that is nearly globally optimal [9, 14].

Throughout Part I of this dissertation various convex approximations of the AC OPF problem will be derived. The solution of the convex problems will then be compared to the identified locally optimal solution of the AC OPF problem, which serves as an intuitive benchmark. Furthermore, convex approximations will be derived from the two AC OPF formulations in Chapter 3. We will see that the polar coordinate formulation of the AC OPF problem yields very accurate approximations that fix voltage magnitudes and assume small voltage angle differences across each transmission line. We will additionally see that the rectangular coordinate formulation of the AC OPF problem yields a very tight relaxation of the AC OPF problem that results in a Semi-Definite Program (SDP).

1.1.2 Non-Linear Approximations of the Economic Dispatch Problem

The AC OPF problem formulated using polar coordinates for the complex voltages facilitates a series of approximations that ultimately result in the DC OPF problem, which uses the DC model of the transmission system. Assumptions used to formulate the DC model of the transmission system require real and reactive power to decouple, voltage magnitudes to be fixed to their nominal values, resistances to be much smaller than reactances, and voltage angle differences across transmission lines to be very small. These assumptions are often well-satisfied in practice, although may be violated under stressed system conditions.

As mentioned earlier, the DC model of the system does not account for transmission losses. For this reason, the lossless DC OPF problem is typically augmented with fixed losses allocated throughout the network as fictitious nodal demand [57, 73, 84]. References [57] and [73] show that introducing a fixed loss representation to the lossless DC OPF problem results in price and dispatch values that more accurately represent those from the AC OPF problem. However, fixed loss representations do not accurately capture the marginal effects of losses as operating conditions vary. In fact, the real power loss of a transmission line is more accurately approximated as the product of the line resistance and the squared real power flowing through the line, and this representation can capture the variation of marginal losses with operating conditions [40, 81].

To account for losses many previous works augment a lossless DC power flow model with the quadratic loss model, eg. [56, 57]. This approach is somewhat self-contradictory because the DC model of the system is only accurate when lines are lossless. Moreover, by assuming lossless transmission lines it is not clear where the additional load due to losses should be allocated. Initial formulations allocated all losses to the slack bus [82], which results in at least some of the losses being modeled as occurring far from the lines that actually incur the losses. This is particularly problematic for remote resources, such as large-scale wind and solar. Reference [58] recognized that the solution to the resulting dispatch problem depended on the choice of slack bus and corrected this problem by introducing *Loss Distribution Factors* (LDFs) that fix the fraction of total system losses allocated to each bus. However, the solution to the dispatch problem in turn depends on the choice of those LDFs

and the authors do not provide a method for determining these factors and do not clarify how to remove this fundamental dependence on the choice of LDFs. More accurate models include the Fictitious Nodal Demand (FND) model from [57] and [40], which allocate half of the losses of each line to each adjacent bus. However, references [57] and [40] do not formally justify this loss allocation model. A main contribution of this dissertation is the rigorous justification of this loss allocation model. Chapter 4 verifies that this is indeed the proper loss allocation by first principles derivation.

Chapter 4 is based on [32] and presents an economic dispatch problem that we term the Transmission Constrained Economic Dispatch (TCED) problem. This economic dispatch problem encompasses the economic dispatch problems from [40, 57] that use the quadratic loss model as well as a more accurate economic dispatch problems that use fewer approximations/assumptions. The most accurate form of the TCED problem is derived from the AC OPF problem in polar coordinates by using the assumptions that real and reactive power decouple and voltages magnitudes are fixed. This TCED problem is derived from first principles and does not utilize many of the aforementioned DC assumptions.

Although the TCED problem is non-convex, it is easily solved under the condition that prices are positive. Under this condition this problem can be solved using the method currently used in practice by Transpower New Zealand Limited (TPNZ), the ISO in New Zealand [77]. Specifically, the load over-satisfaction relaxation, which relaxes power balance by allowing generation to exceed demand (or load) at any location in the transmission network, results in a convex optimization problem. However, this relaxation cannot be used in the case where prices are negative. Negative prices are not typical but may occur in the electricity market for two reasons. First, the offered marginal cost of generation by an electric generator may be negative, reflecting the effective marginal cost of resources that are subsidized volumetrically, as is the case for wind and solar receiving US Federal "Production Tax Credits." Second, even if all marginal cost offers are non-negative, transmission constraints can result in prices that are lower than the lowest marginal cost offer (and therefore possibly negative) and can result in prices that are higher than the highest marginal cost offer. When prices are negative the load over-satisfaction relaxation cannot be used and an alternative method must be used to approximate the solution of the non-convex TCED problem.

1.1.3 Linear Approximations of the Economic Dispatch Problem

The majority of electricity markets in North America intend to approximate the non-convex TCED problem from Chapter 4 by first linearizing the loss function around some base-case state and then introducing loss distribution factors (LDFs) [21]. The resulting linearly constrained economic dispatch (LCED) problem is termed the *common LCED problem* because it closely represents those used in practice as reported in [21] and [58]. Chapter 5 is based on [31], which characterizes the approximation errors associated with each of the three assumptions required to accurately recover the optimal dispatch of the non-convex TCED problem from the solution of the common LCED problem. This characterization is a main contribution of this dissertation.

Reference [21] provides a summary of different linearization techniques implemented by ISOs governed by the Federal Energy Regulatory Commission (FERC), highlighting variations among ISOs in the choice of base-case state. The *common LCED problem* derived in [21] matches that in [58] and is a linearized version of the TCED problem from Chapter 4, which accommodates a general non-linear loss function. Many recent works have attempted to improve upon this linearly constrained formulation in different ways. Reference [94] derives a linear pricing technique that does not rely on a choice of base-case state or LDFs. Reference [56] proposes a dispatch problem resulting in price components that are reference bus independent. Piece-wise linear representations of losses are accommodated by [75] and [76] via the load over-satisfaction relaxation, which is accurate under the assumption that prices are positive. Other work has focused on developing more accurate linear approximations of the AC OPF problem [19, 20, 69, 96]. Similar linearization procedures have also been studied in the context of planning problems [1, 97]. Despite the various linearly constrained formulations suggested in the literature, the common LCED problem from [21] and [58] remains the most commonly used economic dispatch problem in practice.

Using the AC OPF problem as a benchmark, reference [21] illustrates that prices associated with the common LCED problem better capture the marginal effect of losses as compared to economic dispatch problems that represent losses as being fixed. However, using a simple 2-bus example, [21, section V-A] additionally identifies an issue that is missed by current practice. Specifically, using intuitive choices of base-case state and LDFs, the optimal

dispatch of the common LCED problem may be far from feasible for the non-convex TCED problem from which it is derived. Previous work has addressed similar issues by use of post-processing methods [91], which, in our context, intend to identify a dispatch that is feasible for the TCED problem by slightly altering the optimal dispatch of the common LCED problem. Such post-processing methods do not provide optimality guarantees and may identify a costly dispatch, as is illustrated in [21, section V-A]. To mitigate this issue, [21] suggests a successive linearization procedure, which is similar to those from [38] and [13]. This procedure is not guaranteed to converge and requires properly tuned parameters to encourage convergence. Recognizing that the issue exhibited by the 2-bus test case in [21] is difficult to rectify, another contribution of Chapter 5 is to identify the source of this issue. Specifically, this issue occurs if the common LCED problem has multiple minimizers when the ideal choice of base-case state is used (See Remark 5.12).

Despite the prevalence of the common LCED problem, no previous work has established a set of assumptions required to recover the optimal dispatch of the non-convex TCED problem from the common LCED problem. To establish such assumptions Chapter 5 derives the common LCED problem from the TCED problem in Chapter 4. This chapter also shows that the common LCED problem may have multiple minimizers, in which case small perturbations of the base-case state may result in large dispatch approximation error. Furthermore, even if the base-case state matches a minimizer of the non-convex TCED problem, it is proven that there does not always exist a choice of LDFs such that the optimal dispatch of the TCED problem is also optimal for the common LCED problem. On the other hand, such LDFs do exist and are identified for the special case where no line limits are binding.

1.1.4 Convex Hull Pricing

As mentioned earlier, non-convexity associated with the AC OPF problem presents two issues. The first issue, computing a social welfare maximizing dispatch, has been studied extensively and the solution of the AC OPF problem can now be very accurately approximated via iterative algorithms. On the other hand, little attention has been given to the second issue that arises pertaining to market design in the absence of a market equilibrium that guarantees revenue adequacy of the Independent System Operator (ISO). In fact,

reference [8] identifies the problem of pricing non-convexities that arise through the AC transmission network as an emerging challenge in electricity markets. Chapter 6 is based on [33], which addresses this pricing problem by proposing Convex Hull Prices (CHPs) that solve a novel multi-objective minimum uplift problem that balances a trade-off between *generator uplift* and *Financial Transmission Right (FTR) uplift*. For the first time, this chapter presents a method of approximating CHPs in polynomial-time using a transmission network model that is general enough to accommodate the AC OPF problem. The proposed multi-objective minimum uplift problem and the proposed method of approximating CHPs serve as main contributions of this dissertation.

The problem of designing an energy market in the absence of a market equilibrium is well studied in the context of the day-ahead market, which centers around a Mixed Integer Program (MIP) known as the Unit Commitment (UC) problem [72, 74], assuming linearized DC power flow approximations. Similar to the AC OPF problem, the UC problem with DC power flow is non-convex, is NP-hard and is typically solved using heuristic algorithms that perform well in practice but do not identify dispatch values with optimality guarantees. Furthermore, there rarely exist uniform nodal prices that support the optimal dispatch in the day-ahead market. To overcome this problem CHPs have been proposed, also known as extended locational marginal prices, along with side-payments that cover lost opportunity costs of the market participants [35, 43].

CHPs represent a solution of an optimization problem that minimizes various *uplift* quantities including the aforementioned side-payments, which are not directly funded by another revenue stream of the ISO and are typically referred to as *generator uplift*. Reference [95] points out that the ISO may differentiate between generator uplift and all other types of uplift, which they aggregate into a single quantity termed the *settlement residual*, and thus a minimum uplift formulation should be modeled as having multiple competing objectives. Our work studies a recommended extension from [95] by incorporating *FTR uplift* into a multi-objective minimum uplift formulation that generalizes the standard minimum uplift formulation by introducing a weight constant representing the value of FTR uplift relative to generator uplift. We also refer to FTR uplift as *Potential Congestion Revenue Shortfall* (PCRS) because it represents the worst possible shortfall of congestion revenue in

covering FTR payoffs. We will not address other types of uplift in this work, including all reserve related uplift, pointing to this avenue as a sensible extension.

The *Simultaneous Feasibility Condition* (SFC) states that the FTR allocation must represent feasible net real power injections in the transmission network. The SFC is typically defined using a linear model of the transmission network and is a sufficient condition for ensuring FTR payoffs are fully covered by congestion revenue [92]. Under certain assumptions, reference [40] extends this traditional congestion revenue adequacy guarantee to the case where the SFC is defined by a general non-linear model of the transmission network. Traditionally, *congestion revenue shortfalls* occur only in the event of transmission line outages, in which case the SFC would not accurately represent the transmission network at the time of the market clearing. However, reference [55] illustrates that there may be congestion revenue shortfall without the occurrence of a transmission line outage if the SFC is defined by a non-linear model of the transmission network due to a non-convex feasible set of net real power injections. Our work contributes to this literature by relating PCRS to locational prices using a general definition of the SFC and by comparing the standard Locational Marginal Prices (LMPs) to CHPs.

Computing CHPs is generally difficult because the uplift as a function of the locational prices is computationally burdensome to evaluate and is non-smooth. Special-purpose algorithms for computing CHPs have focused on the simple linear transmission constraints that are typically used to formulate the UC problem. For example, references [63, 80, 88–90] either use linear transmission constraints or neglect transmission constraints altogether. Although [43] and [35] provide analysis of CHPs with general non-linear transmission constraints, they later restrict their scope by linearizing these constraints to develop computational methods. We motivate the inclusion of non-linear constraints into this literature by reiterating that computational research pertaining to the AC OPF problem has the ultimate goal of being implemented into ISO market software [11].

Despite utilizing simple transmission models, the aforementioned methods of computing CHPs do not guarantee convergence in polynomial-time. On the other hand, reference [45] frames CHPs as optimal Lagrange multipliers of a polynomially-solvable convex

primal counterpart of the minimum uplift problem that we refer to as the *primal CHP problem.* To date this approach of computing CHPs has only considered linear models of the transmission network. This dissertation extends this work by considering a multi-objective minimum uplift problem along with general non-linear models of the transmission network. Unfortunately, the associated primal CHP problem is expressed in terms of the convex hull of the feasible set of net real power injections, which may not be tractable to evaluate for general transmission network models. In this case we suggest using state-of-the-art relaxations initially developed for the AC OPF problem that result in a *relaxed primal CHP problem* that can be approximately solved in polynomial-time.

1.2   Co-Optimization and Interdependent Reserve Types

The second non-convexity considered in this dissertation is associated with a real-time co-optimization problem that considers both generation dispatch and reserve procurement. Part II is particularly focused on accommodating interdependent reserve types intended to provide primary frequency control, which are collectively referred to as Responsive Reserve (RR) in ERCOT [25]. This dissertation will not consider other reserve types that are deployed on slower time scales, such as reserve types intended to provide secondary frequency control. The reserve types considered in this dissertation contribute to primary frequency control in fundamentally different ways and thus should be considered as different products in the context of an electricity market. Furthermore, the different properties of the interdependent reserve types complicates the reserve requirement that ensures sufficient reserve to accommodate specific contingencies. To better understand these complications we must provide a brief background on frequency control in the electric power system.

Traditional synchronous generators store kinetic energy in the form of a rotating mass called a rotor. Mechanical power is input to the rotor from the prime mover, which may vary from generator to generator. An example of a prime mover is a steam turbine, which may be powered by the burning of oil, gas, or coal. Electro-mechanical power is output from the stator that is realized as electric power injected into the transmission network. When the electric power output of the generator exceeds the mechanical power input to the generator,

the frequency of the rotor decreases and visa versa. Notice this implies that the electrical power output of the stator is equal to the mechanical power input from the prime mover when the frequency is in steady state. When the frequency is not in steady state, the Rate Of Change Of Frequency (ROCOF) depends on the size of the rotor and other mechanically coupled rotating mass, which is referred to as inertia. For example, if the inertia is large then the frequency of the rotor does not change much in response to a power imbalance. Most importantly, synchronous generators can be damaged if their rotor speed is too high or too low. Frequency control in an electric power system aims to prevent this from happening.

The electromechanical physics governing a synchronous generator requires the rotational speed of the rotor to be proportional to the voltage frequency at the generator's terminals. Additionally, the voltage frequency seen by all generators in a transmission system is approximately the same. Frequency control aims to maintain the voltage frequency of a synchronous transmission network at the same nominal voltage frequency, which is 60 Hz in the United States. Frequency control is typically split into two categories. Primary frequency control has the intent of arresting frequency decline/incline in the event of a sudden loss of generation/demand before it reaches some critical voltage frequency threshold at which generator damage may occur. Secondary frequency control aims to return the frequency to its nominal value after such a contingency event occurs. This dissertation will not detail secondary frequency control and will instead focus on primary frequency control.

Primary frequency control is traditionally executed by synchronous generators that provide droop control. *Droop control* aims to respond quickly to a contingency and as a result is performed in a distributed manner with no centralized communication to avoid communication delays. Droop control intends to increase/decrease the mechanical power output of its prime mover proportionally to the locally measured voltage frequency deviation from nominal with an associated dead-band. This proportional signal is called the *droop signal* and the proportionality constant is called the *droop constant*. In fact, the droop signal only serves as a reference signal that is input to a *turbine governor*, which acts as the control system surrounding the prime mover. Indeed the goal of the turbine governor is to attain a mechanical power output of the prime mover that matches the droop signal. Recognizing that the mechanical power output of the turbine governor is the same as the

mechanical power input to the rotor, a frequency decline/incline will cause the mechanical power input to each rotor from each generator in the system to increase/decrease until the frequency decline/incline is arrested. This effectively prevents the rotor speed of each generator from reaching dangerously high or low values.

Traditional droop control operates within Primary Frequency Responsive (PFR) reserve. Part II of this dissertation conservatively assumes that generators providing PFR reserve are the only generators in the system that provide droop control. This assumption deviates slightly from ERCOT requirements, which instead widen the droop control dead-band for all generators not providing PFR reserve [25]. In ERCOT PFR reserve will soon be included in a real-time co-optimization problem. In this context the co-optimization problem must enforce a reserve requirement that ensures sufficient PFR reserve to accommodate a specific large contingency by restoring power balance before the critical frequency threshold is violated. For example, all reserve requirements in ERCOT aim to ensure sufficient reserve to accommodate the simultaneous outage of the two largest generators in the system. Since PFR reserve serves the purpose of arresting frequency decline in response to a generator outage, this requirement necessitates that each generator is capable of deploying its PFR reserve before the critical frequency threshold is met. For this reason, this dissertation will distinguish between *nominal PFR reserve*, which represents an assigned reserve amount that is necessarily less than the generator's headroom, and *available PFR reserve*, which represents the amount of nominal PFR reserve that is capable of being deployed before the critical frequency threshold is met. As we will see, some of the nominal PFR reserve may not be available, particularly if the nominal PFR reserve is very large. Under the assumption that the turbine governor identically follows the droop signal as intended, a simple linear reserve requirement is sufficient to ensure adequate PFR reserve procurement, posing no threat to convexity of the co-optimization problem.

In response to a loss of generation or demand, the Rate Of Change Of Frequency (RO-COF) tends to decrease as the inertia provided by the generators increases and as the number of generators providing droop control increases. Traditionally, wind and solar generation do not provide inertia or primary frequency control because they are inverter-based technologies. As wind and solar generation continue to replace traditional generators, system-wide iner-

tia levels are dropping as are the number of generators providing droop control, effectively increasing the ROCOF in response to a contingency. As the ROCOF increases traditional generators will become more limited by the ramping ability of their turbine governors. In other words, the turbine governors will no longer be able to identically follow the droop signal and the mechanical power input to the rotor will no longer be proportional to the local frequency deviation because the dynamics associated with the turbine governor will restrict the mechanical power's ramping ability. This ramping restriction complicates the reserve requirement because available PFR reserve becomes dependent on the ROCOF.

As wind and solar generation increase and primary frequency control becomes more difficult to perform, ISOs are looking for new technologies to improve primary frequency control. As per Nodal Protocol Revision Request (NPRR) 581 [24], ERCOT has introduced a new Responsive Reserve (RR) type, termed Fast Frequency Responsive (FFR) reserve, intended to improve primary frequency control that aims to take advantage of devices capable of changing their power output nearly instantly. Participants can include fast acting battery storage or demand curtailment that can respond within a few voltage frequency cycles. Rather than reacting proportionally to the locally metered frequency deviation, this new product responds to the frequency in a discrete manner. Specifically, participating devices are expected to fully deploy all reserve nearly instantly if the frequency violates some threshold. For example, if the frequency falls below 59.8 Hz, then all participants providing *FFR reserve* will instantaneously increase their power output to the extent of their procured FFR reserve amount. Introducing this reserve type further complicates the reserve requirement because FFR reserve and PFR reserve serve the same purpose of arresting frequency decline/incline, inherently coupling these two reserve types. The following two subsections explain how these complications are addressed by Chapters 7 and 8.

1.2.1 Reserve Requirement for Sufficient Reserve Procurement

Chapter 7 is based on [30] and provides first principle derivations of reserve requirements that account for the ramping restrictions of PFR reserve as well as the physical coupling between PFR and FFR reserve. The proposed reserve requirements serve as a sufficient condition for maintaining a minimum frequency threshold in response to the two

largest generators being disconnected from the system, as per ERCOT requirements. To account for ramping restrictions of the prime mover a simple piecewise linear model with a ramp rate is adopted from previous work [15].

The proposed reserve requirements are intuitive and provide a straight forward extension to the aforementioned linear reserve requirements. Specifically, in addition to the simple linear requirement an additional constraint on the available PFR reserve is introduced that accounts for the generator's ramping ability. This additional constraint limits the available PFR reserve of a single generator and is referred to as the *rate-based PFR limit*. This limit is represented as a function that increases with the ramp rate exhibited by the prime mover of the generator, the total inertia in the system, and the total FFR reserve procured in the system. We will see that this limit function is non-linear in the total FFR reserve procured.

Chapter 7 further explains the relationship between the proposed rate-based PFR limit and an alternative reserve requirement previously proposed in [59] that uses *equivalency ratios*, which intend to represent the value of FFR reserve relative to PFR reserve. Specifically, under the assumption that the ramp rate of a generator is proportional to its nominal PFR reserve and under the assumption that the rate-based PFR limit does not vary with the total FFR reserve procured, the rate-based PFR limit is identical in form to the equivalency ratio requirement. In other words, this chapter derives the equivalency ratio reserve requirement from first principles under various assumptions. This first principles insight into equivalency ratios is novel because previous work [59] only provided insight into equivalency ratios using empirical results via simulation.

1.2.2   Real-Time Co-Optimization with Rate-Based PFR Limits

Chapter 8 places reserve requirements from Chapter 7 into a real-time co-optimization problem that determines dispatched generation, procured PFR reserve, and procured FFR reserve. Since commitment statuses are assumed constant in myopic real-time co-optimization problems, inertia levels are assumed fixed. With this in mind, the real-time co-optimization problem is still non-convex due to the rate-based PFR limit constraint, which is non-linear in the total procured FFR reserve. We suggest solving this non-convex co-optimization problem

using interior point algorithms that are only guaranteed to converge to a local minimum.

Chapter 8 additionally addresses economic issues associated with the non-convexity of the proposed real-time co-optimization problem. Using a straight-forward pricing structure for reserve the market participants are shown to have zero lost opportunity cost and thus no side-payments are required to ensure their incentives are aligned with the ISO dispatch. The PCRS is additionally shown to be zero and thus congestion revenue adequacy is guaranteed in the presence of FTRs. However, as is the case for all co-optimization problems, revenue adequacy cannot necessarily be guaranteed because reserve payments may be considered out-of-market payments not covered by another revenue stream of the ISO.

Numerical results illustrate the difference between the proposed rate-based PFR limits and the equivalency ratio requirement proposed by previous work [59]. In comparison, the rate-based PFR limit encourages diversity in the procured PFR reserve, effectively dispersing the PFR reserve more evenly among all generators. Furthermore, it is shown that the rate-based PFR limit results in FFR reserve prices that are significantly larger than those resulting from the equivalency ratio requirement. As a result, the rate-based PFR limit results in more out-of-market reserve payments.

1.3   Summary of Contributions

The existing real-time electricity market in ERCOT is myopic and is centered around a convex ED problem. This dissertation studies non-convexities that could arise due to two recently proposed market changes. The first proposed market change introduces losses into the ED problem, resulting in an ED problem with non-linear transmission constraints. The corresponding non-convexity is studied in detail in Part I of this dissertation. The second proposed market change introduces interdependent reserve types for primary frequency response into the ED problem. Part II of this dissertation formulates the resulting co-optimization problem using a non-convex reserve requirement that is derived from first principles. The main contributions of this dissertation are contained within Chapters 4-8 and are summarized as follows:

- First principles derivation of a transmission line model that generalizes the com-

mon quadratic loss model, incorporates an FND representation of losses, and results in a convex TCED problem when using the load over-satisfaction relaxation. This model includes transmission line limits that account for transmission losses. (Chapter 4)

- Rigorous justification that the FND representation of transmission losses should allocate half of the losses of each transmission line to the busses at each end of the line. (Chapter 4)

- Characterization of the approximation errors associated with each of the three assumptions required to accurately recover the optimal dispatch of the non-convex TCED problem from the solution of the common LCED problem. (Chapter 5)

- Observation that the common LCED problem may have multiple minimizers, in which case small perturbations of the base-case state may result in large dispatch approximation error. (Chapter 5)

- Proof that there does not always exist a choice of LDFs such that the optimal dispatch of the TCED problem is also optimal for the common LCED problem even if the ideal base-case state is used. On the other hand, such LDFs do exist and are identified for the special case where no line limits are binding. (Chapter 5)

- Proposal of Convex Hull Prices (CHPs) that solve a novel multi-objective minimum uplift problem that balances a trade-off between *generator uplift* and *Financial Transmission Right (FTR) uplift*. (Chapter 6)

- The first proposed method of approximating CHPs in polynomial-time using a transmission network model that is general enough to accommodate the AC OPF problem. (Chapter 6)

- The distinction between *nominal PFR reserve*, as determined by a generator's head-room, and *available PFR reserve*, as determined by the ramping limitations of a generator's turbine governor. (Chapter 7)

- First principles derivation of a rate-based PFR limit that guarantees sufficient reserve for maintaining a minimum frequency threshold in response to an arbitrarily large generator outage, under certain assumptions. (Chapter 7)

- First principles derivation of the reserve requirement from [59], which provides

insight into the nature of equivalency ratios. When initially proposed, this reserve requirement was derived empirically through simulation. (Chapter 7)

- A novel co-optimization problem formulation using the rate-based PFR limit that is non-convex. This co-optimization problem is proven to result in zero lost opportunity cost for all market participants and zero PCRS when using KKT prices. (Chapter 8)

- The proposed co-optimization problem with rate-based PFR limit is compared to the existing co-optimization problem with equivalency ratio requirement from [59]. In comparison, the proposed co-optimization problem results in higher prices for FFR reserve, more out-of-market reserve payments, and encourages diversity among the procured PFR, meaning that PFR reserve is dispersed among more generators. (Chapter 8)

Chapter 2

Traditional Convex Myopic Electricity Markets

This chapter provides a high-level analysis of myopic electricity markets. A general economic dispatch (ED) problem is presented that may or may not be convex along with associated Locational Marginal Prices (LMPs). In fact, the presented general ED problem and LMPs encompass each of those analyzed in Part I of this dissertation. On the other hand, Part II of this dissertation does not fit into this framework because it considers co-optimization problems that incorporate reserve as decision variables.

The market structure in this chapter intends to encompass the current real-time market structure used in ERCOT with the day-ahead market abstracted away. In this context the economic dispatch problem is convex because transmission constraints are assumed to be convex and reserve procurement is not included. This chapter will highlight important market principles that are satisfied when the economic dispatch problem is convex including the ease of computing a social welfare maximizing dispatch, aligned incentives for generators to follow their dispatch, and the ability to guarantee revenue adequacy of the ISO. Part I and II of this dissertation then intend to explain the complications that arise when introducing ERCOT's newly proposed features into the economic dispatch problem.

We will begin by introducing notation and providing a high-level description of the transmission network in Section 2.1. We then provide description of the market participants in Section 2.2. Section 2.3 will then formulate a general economic dispatch problem that does not consider reserve procurement and may or may not be convex. Locational Marginal Prices are then defined in Section 2.4. Revenue adequacy is then discussed in Section 2.5 and revenue adequacy is proven for the specific case where the economic dispatch problem is convex.

2.1 Notation and Graph Model of Transmission Network

The notation provided in this chapter is consistent with the notation in Parts I and II of this dissertation. Additional notation will be introduced in Parts I and II as needed. Due to an abundance of notation that is required in both Parts I and II, the notation introduced in Part I may not be fully consistent with the notation introduced in Part II and vice versa. In particular, some symbols that are defined in Part I are redefined in Part II.

Throughout this dissertation lower case subscripts are used to index elements of matrices/vectors. For example, $M_{i,j}$ denotes the element in the ith row and j^{th} column of the matrix M. The ith column of a matrix will be denoted M_i. Furthermore, a vector v is designated a column vector and the ith element of v is denoted v_i. The transpose of a matrix or vector is denoted with a superscript dagger $\dagger$. $\mathbb{R}^n$ denotes the set of n-dimensional real vectors. The identity matrix, the matrix of all zeros, and the matrix of all ones are denoted $\mathbf{I}$, $\mathbf{0}$, and $\mathbf{1}$ respectively and are of appropriate dimension. Additional notation will be introduced throughout the dissertation as necessary.

We will also provide a basic graph theoretic model of the transmission network. Although we do not provide a specific model of the transmission network in this chapter, it is important to recognize the existence of this underlying graph in order to understand the various nodal quantities that will be introduced. Specifically, the transmission network is modeled as a directed graph $\mathcal{G} = (\mathbb{V}, \mathbb{E})$ where $\mathbb{V}$ is the set of nodes (buses) and $\mathbb{E}$ is the set of edges (transmission lines). There are n buses and m transmission lines. To simplify notation we will introduce the set of bus indices as $\mathbb{N} = [1, \ldots, n]$, assign an arbitrary unique index to each bus in $\mathbb{V}$, and refer to each bus by its corresponding index. Similarly, we will introduce the set of line indices as $\mathbb{L} = [1, \ldots, m]$, assign an arbitrary unique index to each line in $\mathbb{E}$, and refer to each line by its corresponding index. Furthermore, we will introduce the set $\mathbb{P}$ such that each element of this set represents an ordered pair of bus indices corresponding to each ordered pair of busses in $\mathbb{E}$. With this notation each directed edge $(i, j) \in \mathbb{P}$ connects bus $i \in \mathbb{N}$ to bus $j \in \mathbb{N}$ and corresponds to a unique index $k \in \mathbb{L}$, where i and j are both integers between 1 and n and k is an integer between 1 and m.

Associated with each node $i \in \mathbb{N}$ is a locational price λ_i. This price is said to be

uniform because it is common to each market participant located at bus i. At this point the price λ_i is left general and can take any value.

2.2 Market Participants

The market participants include *generators*, *system demand* and *FTR holders* and they will now be described in detail. Subsequently, a market equilibrium will be defined and the pricing problem will be formulated.

2.2.1 Modeling System Demand

The *system demand* is modeled as constant real power extraction D_i at each node $i \in \mathbb{N}$. The demand at node $i \in \mathbb{N}$ is charged for its consumption in the amount $\lambda_i D_i$. The demand is assumed to be inelastic and is thus not modeled as a profit maximizer.

2.2.2 Modeling Generators and Generator Uplift

Without loss of generality, there is one generator located at each bus in the system indexed by $i \in \mathbb{N}$. The profit of *generator* $i \in \mathbb{N}$ is the difference between its total energy payment and its cost of producing energy. Generator $i \in \mathbb{N}$ generates an amount of real power denoted G_i and is modeled as having a quadratic, convex and increasing cost function $C_i(\cdot)$. The constraints of an individual generator i, termed as *private constraints*, are represented by the set $\mathcal{X}^i$ and enforce simple generation limits $\mathcal{X}^i = \{G_i : \underline{G}_i \leq G_i \leq \overline{G}_i\}$. Each generator is modeled as a profit maximizer whose maximum profit is a function of its corresponding locational price and is expressed as follows:

$$\Upsilon_i(\lambda_i) := \max_{G_i \in \mathcal{X}^i} \ (\lambda_i G_i - C_i(G_i)). \tag{2.1}$$

In the absence of a market equilibrium, some generators may be dispatched at production levels that do not maximize their profit. If the dispatched generation for generator $i \in \mathbb{N}$, denoted G_i^d, does not maximize the generator's profit, that is, $\Upsilon_i(\lambda_i) \neq \left(\lambda_i G_i^d - C_i(G_i^d)\right)$ and therefore $\Upsilon_i(\lambda_i) > \left(\lambda_i G_i^d - C_i(G_i^d)\right)$, then the generator has an incentive to deviate from its dispatched value. If the generator follows its dispatch value, then the generator will experi-

ence lost opportunity cost in the amount that follows:

$$C_i^o(\lambda_i, G_i^d) = \sum_{i \in \mathbb{N}} \Upsilon_i(\lambda_i) - \left(\lambda_i G_i^d - C_i(G_i^d)\right). \qquad (2.2)$$

where $G_i^d \in \mathbb{R}$ represents the dispatched generation for generator i.

As we will see later in this chapter, this issue of misaligned incentives does not occur in todays real-time market in ERCOT, which uses a convex economic dispatch problem. However, this dissertation will analyze non-convex economic dispatch problems that do result in dispatch values that do not maximize generators profits. This issue of misaligned incentives can be overcome by introducing side-payments that cover the generators' lost opportunity cost. In this context a side-payment would be given to a generator under the condition that they follow the dispatched generation. The side-payment aims to neutralize their incentive to deviate.

Side-payments to generators are also referred to as *generator uplift*, are private out-of-market payments, and are unsatisfactory for a number of reasons highlighted by a recent order made by the Federal Energy Regulatory Committee [70]. For example, to remain revenue neutral, the ISO must distribute the cost of these side-payments among market participants introducing potentially unjust tariffs. Additionally, side-payments reduce transparency in the market making it difficult for generator investment decisions to be made. The research in this dissertation is aimed, in part, at designing an electricity market that results in low generator uplift. Chapter 6 will investigate situations where generator uplift is positive.

2.2.3   Modeling Financial Transmission Rights and FTR Uplift

Financial Transmission Rights (FTRs) are financial contracts entitling FTR holders to a specific revenue stream that results from price differences at system buses. FTRs are allocated among FTR holders before prices are cleared. There are typically two types of FTRs, Point-to-Point (PTP) obligations and PTP options [40]. For sake of brevity, we will only consider PTP obligations in this dissertation.

Let Ξ denote the set of all FTR holders. In its most general form, a PTP obligation for FTR holder $\xi \in \Xi$ can be represented by an *FTR allocation vector* $f^{(\xi)} \in \mathbb{R}^n$ where each element $f_k^{(\xi)}$ represents a megawatt value injected into the transmission system at node

k. Each FTR holder receives an FTR payoff in the amount of $-\lambda^\dagger f^{(\xi)}$. The *total FTR payoff* to all FTR holders is in the amount of $-\lambda^\dagger f$, where $f := \sum_{\xi \in \Xi} f^{(\xi)}$ is the sum of all FTR allocation vectors. Different energy markets may choose the allocation vectors $f^{(\xi)}$ in different ways. These allocation vectors are often chosen using an FTR allocation process that is beyond the scope of this dissertation. For example, see [40] for a description of FTR allocation processes.

To elaborate on this model of FTRs, we will provide an intuitive example. In particular, let's see how FTRs can be used by market participants to hedge locational price uncertainty. Consider a simple example where the generator at bus i has a bilateral contract with the demand at bus j that has been arranged outside of the wholesale electricity market where the generator plans to produce in the amount G_i^* and the demand plans to consume D_j. In this case the net wholesale market payment by both market participants is in the amount $\lambda_i G_i^* - \lambda_j D_j$. Suppose these market participants also hold a sparse FTR allocation vector together such that $f_i^{(\xi)} = G_i^*$ and $f_j^{(\xi)} = -D_j$. Then they will receive an FTR payoff in the amount $-\lambda_i G_i^* + \lambda_j D_j$, which is the negative of their net market payment. These two payments cancel out for any possible price vector λ and so the market participants are effectively able to avoid any uncertainty in the locational prices at bus i and bus j for dispatch and demand quantities that match their FTR allocation vector.

Energy markets typically choose FTR allocation vectors to satisfy the *Simultaneous Feasibility Condition* (SFC) for reasons pertaining to revenue adequacy that will soon become clear. For the remainder of this chapter, we assume the FTR allocation satisfies the SFC, which states that the sum of all FTR allocation vectors represent a feasible net real power injection in the transmission system. The set of feasible net real power injections, denoted $\mathcal{T} \subset \mathbb{R}^n$, represents constraints on the net real power injections imposed by the transmission network that are referred to as *coupling constraints* as they ultimately relate the demand and generation at each node to one another. At this point we leave this set general, encompassing both linear and non-linear power flow models of the transmission system.

Definition 2.1. The FTR allocation satisfies the *simultaneous feasibility condition* (SFC) if the sum of all FTR allocation vectors lies in the feasible set of net real power injec-

tions, e.g., $f \in \mathcal{T}$.

Remark 2.1. The feasible set of net real power injections $\mathcal{T}$ is left general in the main body of this chapter and will be further elaborated in Part I of this dissertation. The definition of this set will include implicit variables such as voltages, net reactive power injections at buses and power flows on transmission lines. Physical constraints in the transmission network are enforced, which may include reactive power injection and voltage magnitude limits at each bus $i \in \mathbb{N}$ as well as real, reactive or apparent power flow limits on each transmission line $\ell \in \mathbb{L}$. This set does not place generator limits on net real power injections at buses, effectively allowing FTRs to be allocated to any bus in the system even if no device is connected to that bus. □

Remark 2.2. Electricity markets today require each FTR allocation vector $f^{(\xi)}$ to be *balanced* in the sense that the elements sum to zero, e.g. $\mathbf{1}^\dagger f^{(\xi)} = 0$. Accordingly, the aforementioned example would have $G_i^\star = -D_j$. Of course, requiring each FTR allocation vector to be balanced is only sensible if the SFCs are defined using a lossless model of the transmission network. With the goal of introducing loss modeling into the electricity market, this dissertation uses a more general definition of FTRs that allow FTR allocation vectors to be *unbalanced* in the sense that their elements may not sum to zero, e.g. $\mathbf{1}^\dagger f^{(\xi)} \neq 0$. Accordingly, the aforementioned example may have $G_i^\star \neq -D_j$. Unbalanced FTRs have been studied well in the literature [37, 40] and allow FTRs to hedge locational price differences caused by losses as well as congestion.

Once the generators (demand) are paid (charged) for producing (consuming) energy, the ISO is left with additional revenue, called *congestion revenue*. Let's denote the realized net real power injections as $T^d := G^d - D \in \mathcal{T}$. The congestion revenue is

$$\lambda^\dagger \left(D - G^d \right). \tag{2.3}$$

Congestion revenue is used to fund the FTR payoffs. The congestion revenue is said to be *adequate* if it is larger than the total FTR payoffs. It is important for the electricity market to be structured in a way that encourages congestion revenue adequacy. For this reason the prices should be chosen such that the congestion revenue covers the worst case FTR

allocation. The maximum FTR payoff can be written as a function of the prices as follows:

$$\Psi(\lambda) := \max_{f \in \mathcal{T}} \quad -\lambda^\dagger f. \tag{2.4}$$

The Potential Congestion Revenue Shortfall or *PCRS*, also referred to as *FTR uplift*, is written as follows and represents the maximum possible shortfall of congestion revenue:

$$C^s(\lambda, G^d) = \Psi(\lambda) - \lambda^\dagger \left(D - G^d \right). \tag{2.5}$$

This value can be interpreted as the maximum FTR payoff $\Psi(\lambda)$ less the congestion revenue and is non-negative. It is important to recognize that the PCRS $C^s(\lambda, G^d)$ represents a worst case shortfall over all possible FTR allocations. In fact the realized FTR allocation may allow congestion revenue to cover FTR payoffs even if the PCRS is positive. If the PCRS satisfies $C^s(\lambda, G^d) = 0$, then congestion revenue adequacy is guaranteed, meaning that there does not exist an FTR allocation that causes a congestion revenue shortfall. In the event that congestion revenue is unable to cover FTR payoffs then the ISO must allocate the shortfall among market participants introducing an allocation problem. Proper allocation of congestion revenue shortfall has been a point of controversy [41]. The research in this dissertation is aimed, in part, at designing an electricity market that results in low FTR uplift. Chapter 6 will illustrate a trade-off between achieving low FTR uplift and achieving low generator uplift in the context of selecting optimal locational prices λ.

2.3 General Economic Dispatch Problem

The economic dispatch problem is central to the proposed market structure. This problem is written as follows where $\mathcal{X} = \{G \in \mathbb{R}^n : G_i \in \mathcal{X}^i \quad \forall i \in \mathbb{N}\}$ enforces generator limits at each node and the feasible set of net real power injections $\mathcal{T}$ is left general, as in Section 2.2.3.

$$\min_{G \in \mathcal{X}, \ T \in \mathcal{T}} \quad \sum_{i \in \mathbb{N}} C_i(G_i) \tag{2.6}$$

$$st : D_i - G_i + T_i = 0 \quad \forall i \in \mathbb{N} \tag{2.6a}$$

Notice that this problem is written generally to accommodate any non-convexity associated with the feasible set of net real power injections. In fact, this problem is a generalization of each optimization problem to be derived in Part I of this dissertation. In contrast to the specific formulations to appear in Part I, the general ED problem (2.6) is written in a way that is conceptually convenient for analysis purposes but is not necessarily written in a way that is convenient computationally. For example it is often possible to eliminate the decision variable T after specifying the feasible set of net real power injections $\mathcal{T}$.

A solution to this problem consists of a *social welfare maximizing dispatch*. This solution may be difficult to compute if the feasible set of net real power injections is non-convex. As a result, we do not assume that dispatch values represent a social welfare maximizing dispatch. Instead we will assume that the dispatched generation, denoted G^d, solves the KKT conditions of the general economic dispatch problem (2.6) (See Remarks 2.3 and 2.4). Of course, if the problem is convex, then any solution satisfying the KKT conditions is also a global minimizer, in which case G^d would represent the social welfare maximizing dispatch.

At this point we should note that the economic dispatch problem (2.6) directly minimizes generator fuel costs. However, there may be other costs that affect social welfare that are not considered in the objective function of this problem. For example, lost opportunity costs for generators and PCRS may be interpreted as decreasing social welfare but are not considered in the objective function of problem (2.6).

2.4 Locational Marginal Prices (KKT Prices)

Many concepts associated with price setting are closely related to the Lagrange multipliers of the power balance constraints (2.6a). Electricity markets commonly use uniform prices that we term *KKT prices* and denote by $\lambda^\star \in \mathbb{R}^n$. These prices are set by first identifying a solution of problem (2.6) that satisfies the KKT conditions and then setting the prices to be the Lagrange multipliers of the power balance constraints (2.6a). Under certain conditions further elaborated in the next section of this chapter, the KKT prices represent the marginal cost of serving load at each location in the system. For this reason, KKT prices are often referred to as Locational Marginal Prices (LMPs). Furthermore, LMPs are specific

to the identified solution of the general ED problem and as a result are algorithm dependent. In other words, different algorithms may produce different LMPs. Below is a general definition of a KKT price/dispatch pair that only introduces Lagrange multipliers for the power balance constraints and leaves the sets $\mathcal{T}$ and $\mathcal{X}$ implicit. This definition follows from the normal cone definition of the First Order Necessary Conditions (FONCs) as described in Appendix A (See [71] as well as Remarks 2.4 and 2.3).

Definition 2.2. A *KKT price/dispatch pair* $(\lambda^\star, G^\star) \in \mathbb{R}^n \times \mathcal{X}$ are such that constraint (2.6a) holds for some $T^\star \in \mathcal{T}$ along with the following generalized stationarity conditions.

$$
\begin{aligned}
-\lambda^\star &\in \mathcal{N}_{\mathcal{T}}(T^\star) \quad \text{and} \\
0 &\in \partial \left(C_i(G_i) - \lambda_i^\star G_i \right) |_{G_i^\star} + \mathcal{N}_{\mathcal{X}^i}(G_i^\star) \quad \forall i \in \mathbb{N}
\end{aligned} \tag{2.7}
$$

where $\mathcal{N}_{\mathcal{T}}(T^\star)$ is the normal cone of the set $\mathcal{T}$ at the point $T^\star$ and $\mathcal{N}_{\mathcal{X}^i}(G_i^\star)$ is the normal cone of the set $\mathcal{X}^i$ at the point $G_i^\star$. The subdifferential of a general function $g(x)$ evaluated at a point $x^\star$ is denoted $\partial(g(x))|_{x^\star}$. A formal definition of the normal cone is provided in [71] and is explained intuitively in Appendix A.

Remark 2.3. We emphasize that a KKT price/dispatch pair may not exist in our general framework because constraint qualifications may not be satisfied within the set $\mathcal{T}$. It is also possible that an identified solution satisfying the KKT conditions could represent a saddle point, local maximum, or local minimum. However, in practice a local minimum to the AC OPF problem satisfying the KKT conditions is almost always attainable using standard off-the-shelf software, as is the case for each test case in this dissertation. Furthermore, our results regarding KKT prices hold if the solution represents a saddle point, local maximum, or local minimum.

Remark 2.4. Appendix A provides an elaborate description of how the conditions from Definition 2.2 are related to the common KKT conditions that will be further analyzed in future chapters. For the special case where the cost function and constraint functions are smooth, Appendix A proves any dispatch $G^\star$ that satisfies the traditional KKT conditions for the general economic dispatch problem (2.6) will also satisfy the conditions from Definition 2.2 for some Lagrange multipliers $\lambda^\star$. In fact, there may be multiple such Lagrange multipliers $\lambda^\star$ that satisfy the KKT conditions for generation dispatch $G^\star$. Our results do not require such Lagrange multipliers to be unique.

2.5 A Revenue Adequate Market Equilibrium

In accordance with [43], a *decentralized market equilibrium* refers to a set of prices, side-payments and dispatch values for which generators have no incentive to deviate from their dispatch values. As explained in Section 2.2.2, the proposed side-payments always ensure a decentralized market equilibrium is realized, whereas payments on the basis of energy prices alone do not necessarily have this property. To recover the cost introduced by these side-payments the ISO must introduce tariffs to market participants. In our context these tariffs must also accommodate any realized congestion revenue shortfall due to FTRs. The formal definition of a decentralized market equilibrium from [43] addresses this issue by proposing tariffs be applied to the consumers. By modeling consumers as fixed demand as in Section 2.2.1, their individual rationality is not compromised by imposing these tariffs. However, this simple model of fixed demand does not consider more elastic consumers that respond to energy prices or the long term effects these tariffs may have on consumer behavior. Furthermore, the allocation of revenue shortfalls by the ISO has been a point of controversy as pointed out in Sections 2.2.2 and 2.2.3.

This dissertation will expand upon the notion of a decentralized market equilibrium by additionally requiring revenue adequacy of the ISO to be guaranteed. We will refer to such a decentralized market equilibrium as a *revenue adequate market equilibrium*. Note that our definition of a revenue adequate market equilibrium is consistent with the *Competitive Equilibrium Model (CEM) 1* from [52]. Specifically, we will define a revenue adequate market equilibrium to be a price dispatch pair (λ, G) that results in zero PCRS and zero side-payments (or equivalently zero lost opportunity cost for generators). Intuitively, a revenue adequate market equilibrium guarantees revenue adequacy in the form of side-payments and FTR payoffs.

Definition 2.3. A *revenue adequate market equilibrium* is defined to be a price/dispatch pair (λ, G) that result in zero side-payments and zero PCRS, e.g.

$$C^s(\lambda, G) = 0 \text{ and } C_i^o(\lambda_i, G_i) = 0 \ \forall i \in \mathbb{N}$$

Reference [52] shows that a revenue adequate market equilibrium does not always exist when defining the feasible set of net real power injections using the full AC-model of the transmission system. Even if a revenue adequate market equilibrium does exist we still may not achieve it. Specifically, by theorem 1 of [52] a revenue adequate market equilibrium, as in Definition 2.3, can only occur if the dispatched generation is a social welfare maximizing dispatch. As explained in Section 2.3, we do not assume that the dispatched generation maximizes social welfare and so it is apparent that the market may not be operating in a revenue adequate equilibrium in general.

Recognizing that the side-payments and PCRS are always non-negative, the lack of a revenue adequate market equilibrium implies that at least one of these values are positive, and thus additional costs accrue in the form of generator opportunity costs and/or FTR underfunding that may be difficult to account for when setting prices. In fact, these costs are not accounted for in the objective function of the general ED problem. As a result, if the market is not operating in a revenue adequate market equilibrium, then KKT prices do not actually represent the marginal cost of serving load at each location in the system. In fact, this marginal price interpretation of the KKT prices only holds if a revenue adequate market equilibrium exists, the dispatched generation represents a global minimizer of the general ED problem, the global minimizer of the general ED problem solves the KKT conditions with unique Lagrange multipliers, and the AC OPF problem satisfies certain constraint qualifications [5] that allow KKT prices to exist in the first place. Despite the fact that KKT prices do not necessarily represent the marginal cost of serving load, we will still use this term interchangeably with the term LMPs, as is standard practice.

Traditional electricity market formulations are convenient in that the feasible set of net real power injections is represented by a polytope and thus the general ED problem is convex. In this case, it is easy to solve the general ED problem for a global minimizer and KKT prices result in a revenue adequate market equilibrium allowing for the convenient marginal pricing interpretation to hold. This is formally stated by the following theorem.

Theorem 2.1. *Under the assumption that the general ED problem (2.6) is convex, a KKT price/dispatch pair $(\lambda^\star, G^\star)$ as in Definition 2.2 will result in a revenue adequate market equilibrium as in Definition 2.3.*

Proof: The generalized stationarity conditions for (2.7) include necessary conditions for optimality of each profit-maximizing generation problem (2.1). (Note that the normal cone definition of the FONCs are generally represented by (A.6) in Appendix A). The generalized stationarity conditions for (2.7) include necessary conditions for optimality of the maximum FTR payoff problem (2.4). Since each of these problems are convex, these conditions are also sufficient for global optimality. □

In contrast to Theorem 2.1, numerical results from Section 3.5 will show that a revenue adequate market equilibrium is not always attainable if the feasible set of net real power injections $\mathcal{T}$ is non-convex. It is important to recognize that approximate convex models create problems of their own, including the need to make the dispatch satisfy the underlying non-convex constraints. Numerical results in Section 6.5 illustrate the costs associated with adjusting the dispatch on fast time scales to achieve feasible net real power injections.

2.6   Summary

This chapter provided a high-level overview of a myopic electricity market structure that centers around a general ED problem. Market participants are defined to be demand that consumes electric power, generators that produce electric power, and FTR holders. Generators that experience lost opportunity cost are provided side-payments, also referred to as generator uplift. PCRS is defined to be the worst possible shortfall of congestion revenue in covering FTR payoffs and is referred to as FTR uplift. These uplift quantities are unsatisfactory because they represent a potential revenue shortfall of the ISO and thus revenue adequacy cannot be guaranteed when uplift is positive. The remainder of this dissertation is aimed, in part, at designing an electricity market that results in little uplift.

The market structure presented in this chapter is general enough to encompass the real-time market structure currently used by ERCOT, which additionally restricts the feasible set of net real power injections to be a polytope. In this special case, the ED problem becomes convex and LMPs are proven to result in zero generator uplift and zero FTR uplift. The remainder of this dissertation will focus on two sources of non-convexity that may be introduced by recently proposed market changes in ERCOT. Part I introduces transmission

losses into the feasible set of net real power injections, making this set non-convex. It is shown that revenue adequacy cannot be guaranteed in this setting. Part II introduces interdependent reserve types for primary frequency response, resulting in a co-optimization problem with a non-convex reserve requirement. It is shown that this co-optimization problem results in zero generator uplift and zero FTR uplift when using marginal prices; however, out-of-market reserve payments may cause the ISO to experience revenue inadequacy. Part III provides a brief conclusion and future work.

Part I
Economic Dispatch: Non-Linear Transmission Models

Part I of this dissertation incorporates accurate non-linear transmission models into the myopic economic dispatch problem. This part is motivated by Texas' recent consideration of implementing transmission loss models into the economic dispatch problem [27]. As explained in Chapter 1, the Public Utility Commission of Texas (PUCT) has considered the introduction of transmission losses separately from the introduction of real-time co-optimization. Consistent with the PUCT's analysis, this part of the dissertation will not consider reserve products in the economic dispatch problem.

Chapter 3 formulates the economic dispatch problem that most accurately accounts for the equivalent-Π model of a transmission line, which is termed the Alternating Current Optimal Power Flow (AC OPF) problem. Due to the inherent non-convexity of the AC OPF problem it is generally difficult to solve and results in an electricity market that cannot guarantee congestion revenue adequacy. This is one reason why ISOs today solve economic dispatch problems that serve as convex approximations of the AC OPF problem. These convex approximations are derived in Chapters 4 and 5. Specifically, Chapter 4 formulates the non-convex Transmission Constrained Economic Dispatch (TCED) problem that can be solved using a convex relaxation under the condition that prices are positive. Chapter 5 formulates the convex Linearly Constrained Economic Dispatch (LCED) problem from the TCED problem. Finally, Chapter 6 attempts to accommodate the AC OPF problem by using algorithms that may only identify a locally optimal solution and suggests mitigating the congestion revenue adequacy problem using convex hull prices.

Chapter 3

The AC OPF problem

The most accurately formulated myopic economic dispatch problem is termed the Alternating Current Optimal Power Flow (AC OPF) problem. The AC OPF problem is non-convex and NP-hard in general [6, 54]. With this in mind, the AC OPF problem has a long history pertaining to the way it is formulated and solved [11]. This chapter will derive two different formulations that are prevalent in the literature [67]. These two formulations are derived using polar coordinates and rectangular coordinates to represent the complex voltages at each bus in the transmission network and facilitate very accurate approximations that will be further investigated in Chapters 4 and 6 respectively. This chapter will show that the two formulations provided are specific cases of the general ED problem (2.6) from Chapter 2. Numerical results will provide examples that illustrate how certain economic principles breakdown due to the non-convexity of the AC OPF problem. Specific test cases are studied for which there does not exist a revenue adequate market equilibrium.

This chapter will be organized as follows. Section 3.1 will introduce the equivalent-Π model of a transmission line and derive complex power flow quantities associated with this model from first principles. Section 3.2 will introduce a simple model for an electrical bus in a transmission system that may experience shunt losses. Using the derived expressions from Sections 3.1 and 3.2 two different forms of the AC OPF problem will be derived in Sections 3.3 and 3.4. Section 3.3 formulates an AC OPF problem using polar coordinates to express the complex voltages at each bus. This form of the AC OPF problem is convenient for utilizing standard approximations such as fixed voltage magnitudes and small voltage angle approximations as will be illustrated in Chapter 4. Section 3.4 formulates the AC OPF problem in rectangular coordinates, which will ultimately be used to derive a relaxed version of the AC OPF problem in Chapter 6.

3.1 Generalized Equivalent Π-Model of a Transmission Line

This section derives complex power flow quantities along an arbitrary transmission line $(i,j) \in \mathbb{P}$ using the equivalent-Π model of a transmission line. Figure 3.1 provides a circuit diagram of the general equivalent-Π model of a transmission line operated at a nominal frequency. The transmission line $(i,j) \in \mathbb{P}$ connects bus $i \in \mathbb{N}$ to bus $j \in \mathbb{N}$ and is indexed by $\ell \in \mathbb{L}$. The series impedance of the line is denoted $z_\ell = \frac{1}{y_\ell}$ where y_ℓ is the series admittance. The complex voltage at bus i is denoted v_i. An ideal transformer is located near bus i with complex off-nominal turns ratio of a_ℓ. Shunt admittances are denoted $y_\ell^{(c)}$ where the c superscript indicates that this shunt admittance is largely capacitive. In fact, this shunt admittance is typically assumed to be purely imaginary; however, in this chapter we will allow $y_\ell^{(c)}$ to have non-zero real part.
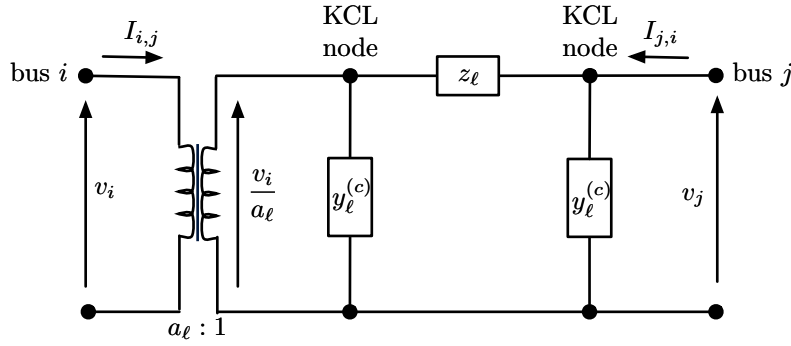
Figure 3.1: Circuit diagram of transmission line $(i,j) \in \mathbb{P}$ indexed by $\ell \in \mathbb{L}$.

The current flowing into the line can be derived using Kirchhoff's Current Law (KCL) by summing the currents into the nodes on both sides of the series impedance. The current flowing into the line from bus i is denoted $I_{i,j}$ and the current flowing into the line from bus j is denoted $I_{j,i}$. These values satisfy the following expressions:

$$a_\ell^* I_{i,j} = \frac{\frac{v_i}{a_\ell} - v_j}{z_\ell} + \frac{v_i}{a_\ell} y_\ell^{(c)} = \frac{1}{a_\ell}\left(y_\ell + y_\ell^{(c)}\right) v_i - y_\ell v_j \tag{3.1}$$

$$I_{j,i} = \frac{\frac{-v_i}{a_\ell} + v_j}{z_\ell} + v_j y_\ell^{(c)} = \left(y_\ell + y_\ell^{(c)}\right) v_j - \frac{1}{a_\ell} y_\ell v_i \tag{3.2}$$

where superscript $*$ denotes complex conjugate (and should be distinguished from superscript $\star$, which will denote optimal quantities).

Notice that the two terms in the middle expression represent the current flowing through the series impedance and the current flowing through the shunt element. The expression on the far right-hand side (RHS) simply groups like terms in v_i and v_j. Furthermore, the current flowing into the line from bus i traverses a transformer yielding a factor of a_ℓ^* in (3.1).

The complex power flowing into the line can then expressed using Ohms law. Using the expressions from (3.1) and (3.2) the complex power flowing into the line from bus i and from bus j are respectively written as follows:

$$P_{i,j} + \mathbf{i}Q_{i,j} = v_i I_{i,j}^* = \left(\frac{y_\ell + y_\ell^{(c)}}{a_\ell^* a_\ell} \right)^* v_i v_i^* - \frac{y_\ell^*}{a_\ell^*} v_i v_j^*, \tag{3.3}$$

$$P_{j,i} + \mathbf{i}Q_{j,i} = v_j I_{j,i}^* = \left(y_\ell + y_\ell^{(c)} \right)^* v_j v_j^* - \frac{y_\ell^*}{a_\ell^*} v_j v_i^*. \tag{3.4}$$

To simplify this expression it is common to introduce admittance matrices. With this in mind we will now introduce a branch admittance matrix $Y^{(i,j)} \in \mathbb{C}^{n \times n}$.

$$Y^{(i,j)} := \frac{1}{a_\ell a_\ell^*} (y_\ell + y_\ell^{(c)}) \mathbf{I}_i \mathbf{I}_i^\dagger - \frac{1}{a_\ell} y_\ell \mathbf{I}_i \mathbf{I}_j^\dagger \tag{3.5}$$

$$Y^{(j,i)} := (y_\ell + y_\ell^{(c)}) \mathbf{I}_i \mathbf{I}_i^\dagger - \frac{1}{a_\ell} y_\ell \mathbf{I}_i \mathbf{I}_j^\dagger \tag{3.6}$$

where $\mathbf{I}_i$ is the ith column of the identity matrix, which also represents the ith standard unit vector. The complex power flow expressions (3.3) and (3.4) can now be consolidated into a single expression that is valid for both directions. Notice that the second of the following two expressions simply reverses i and j compared to the first and so they will be collectively referred to as expression (3.7):

$$P_{i,j} + \mathbf{i}Q_{i,j} = Y_{i,i}^{(i,j)*} v_i v_i^* + Y_{i,j}^{(i,j)*} v_i v_j^* \tag{3.7a}$$

$$P_{j,i} + \mathbf{i}Q_{j,i} = Y_{j,j}^{(j,i)*} v_j v_j^* + Y_{j,i}^{(j,i)*} v_j v_i^* \tag{3.7b}$$

The expression (3.7) can be easily shown to be equivalent to (3.3) and (3.4) algebraically. The expression (3.7) can then be placed in matrix form by treating $v \in \mathbb{C}^n$ as a vector of complex voltages. Notice that the second of the following two expressions again simply reverses i and j compared to the first and so they will be collectively referred to as expression (3.8):

$$P_{i,j} + \mathbf{i}Q_{i,j} = v^\dagger Y^{(i,j)*} v^* \tag{3.8a}$$

$$P_{j,i} + \mathbf{i}Q_{j,i} = v^\dagger Y^{(j,i)*} v^* \tag{3.8b}$$

where we interpret superscript $*$ for a vector to mean the complex conjugate of the vector. The complex power expressions (3.7) and (3.8) will be used to formulate the AC OPF problem in polar coordinates and rectangular coordinates respectively.

3.2 Bus Model with Shunt Losses

A bus $i \in \mathbb{N}$ is a connection point at which generators or demand can inject or extract complex power from the transmission network. The sum of complex power injected into bus i is termed the net complex power injection. This subsection derives net complex power injection quantities for an arbitrary bus $i \in \mathbb{N}$ that may experience complex power loss due to shunt admittance. With this in mind the net complex power injection at each bus represents the sum of the complex powers flowing out of the bus through transmission lines less the shunt losses. The complex shunt element at bus i has admittance denoted $y_i^{(s)} = g_i^{(s)} + \mathbf{i}b_i^{(s)}$. The net complex power injection at each bus is written as follows:

$$T_i + \mathbf{i}U_i = \sum_{(i,j)\in\mathbb{P}} (P_{i,j} + \mathbf{i}Q_{i,j}) + \sum_{(j,i)\in\mathbb{P}} (P_{j,i} + \mathbf{i}Q_{j,i}) - v_i(v_i y_i^{(s)})^* \tag{3.9}$$

where the third term on the RHS represents the real power loss through the shunt element located at bus i. With this in mind the value $v_i y_i^{(s)}$ represents the complex current flowing through the shunt element.

Once again, admittance matrices will be introduced to simplify notation. The network admittance matrix $Y \in \mathbb{C}^{n\times n}$ will now be defined in terms of the branch admittance matrices $Y^{(i,i)}$ as follows:

$$Y := \sum_{(i,j)\in\mathbb{P}} Y^{(i,j)} + \sum_{(j,i)\in\mathbb{P}} Y^{(i,j)} - \mathrm{diag}(y^{(s)}) \tag{3.10}$$

where $\mathrm{diag}(y^{(s)}) \in \mathbb{C}^{n\times n}$ a diagonal matrix with diagonal elements represented by the vector of bus shunt admittances $y^{(s)} \in \mathbb{C}^n$. The net complex power injection expression (3.9) can

now be simply written as follows:

$$T_i + \mathbf{i}U_i = v_i \sum_{j=1}^{n} Y_{i,j}^* v_j^* \tag{3.11}$$

The expression (3.11) can be easily shown to be equivalent to (3.9) algebraically. The expression (3.11) can then be placed in matrix form by treating $v \in \mathbb{C}^n$ as a vector of complex voltages and by introducing the bus admittance matrix as $Y^{(i)} := \mathbf{I}_i \mathbf{I}_i^\dagger Y$. The net complex power injections can now be expressed as follows:

$$T_i + \mathbf{i}U_i = v^\dagger Y^{(i)*} v^* \tag{3.12}$$

The complex power expressions (3.11) and (3.12) will be used to formulate the AC OPF problem in polar coordinates and rectangular coordinates respectively.

3.3   AC OPF Problem in Polar Coordinates

First use polar coordinates to formulate the AC OPF problem. In this case the complex voltage at bus i is denoted $v_i = V_i \angle (\theta_i)$, where V_i is the voltage magnitude and θ_i is the voltage angle. Using polar coordinates the feasible set of net real power injections is defined by constraints that are sinusoidal in the voltage angle variables and quadratic in the voltage magnitude variables.

The complex power flow in a transmission line expressed in terms of voltage angle and voltage magnitude follows from the expression (3.7). With this in mind, denote the admittance quantities in this expression using polar coordinates as follows: $Y_{i,i}^{(i,j)} = |Y_{i,i}^{(i,j)}| \angle \varsigma_{i,j}$ and $Y_{i,j}^{(i,j)} = |Y_{i,j}^{(i,j)}| \angle \varpi_{i,j}$. Multiplying the complex quantities in polar coordinates and using Eulers formula the complex power flowing into the line from bus i and bus j can be rewritten as follows:

$$P_{i,j} = |Y_{i,i}^{(i,j)}| V_i^2 \cos(-\varsigma_{i,j}) + |Y_{i,j}^{(i,j)}| V_i V_j \cos(\theta_i - \theta_j - \varpi_{i,j}) \quad \forall (i,j) \in \mathbb{P} \text{ and } \forall (j,i) \in \mathbb{P} \tag{3.13}$$

$$Q_{i,j} = |Y_{i,i}^{(i,j)}| V_i^2 \sin(-\varsigma_{i,j}) + |Y_{i,j}^{(i,j)}| V_i V_j \sin(\theta_i - \theta_j - \varpi_{i,j}) \quad \forall (i,j) \in \mathbb{P} \text{ and } \forall (j,i) \in \mathbb{P} \tag{3.14}$$

Similarly, an expression for the net complex power injection into a bus in terms of the voltage angle and voltage magnitude follows from expression (3.11). With this in

mind, denote the admittance quantities in this expression using polar coordinates as follows: $Y_{i,j} = |Y_{i,j}| \angle \varphi_{i,j}$. Multiplying the complex quantities in polar coordinates leads to the following expressions for the net real and reactive power injections into bus i:

$$T_i = V_i \sum_{j=1}^{n} |Y_{i,j}| V_j \cos(\theta_i - \theta_j - \varphi_{i,j}) \quad \forall i \in \mathbb{N} \tag{3.15}$$

$$U_i = V_i \sum_{j=1}^{n} |Y_{i,j}| V_j \sin(\theta_i - \theta_j - \varphi_{i,j}) \quad \forall i \in \mathbb{N} \tag{3.16}$$

These expressions are written in terms of real valued variables and so they can then be placed in an economic dispatch problem that is suitable for standard optimization software. This economic dispatch problem is termed the AC OPF problem and optimizes over the vector of nodal generation $G \in \mathbb{R}^n$ as well as the voltage magnitude and voltage angle vectors. The AC OPF problem minimizes the cost of generation and is written as follows:

$$\min_{G \in \mathbb{R}^n, V \in \mathbb{R}^n, \theta \in \mathbb{R}^n} \quad \sum_{i \in \mathbb{N}} C_i(G_i) \tag{3.17}$$

$$st: D_i - G_i = V_i \sum_{j=1}^{n} |Y_{i,j}| V_j \cos(\theta_i - \theta_j - \varphi_{i,j}) \quad \forall i \in \mathbb{N} \tag{3.17a}$$

$$\underline{U}_i \leq V_i \sum_{j=1}^{n} |Y_{i,j}| V_j \sin(\theta_i - \theta_j - \varphi_{i,j}) \leq \bar{U}_i \quad \forall i \in \mathbb{N} \tag{3.17b}$$

$$-\bar{P}_{i,j} \leq |Y_{i,i}^{(i,j)}| V_i^2 \cos(-\varsigma_{i,j}) + |Y_{i,j}^{(i,j)}| V_i V_j \cos(\theta_i - \theta_j - \varpi_{i,j}) \leq \bar{P}_{i,j} \quad \forall (i,j) \in \mathbb{P} \text{ and } \forall (j,i) \in \mathbb{P} \tag{3.17c}$$

$$-\bar{Q}_{i,j} \leq |Y_{i,i}^{(i,j)}| V_i^2 \sin(-\varsigma_{i,j}) + |Y_{i,j}^{(i,j)}| V_i V_j \sin(\theta_i - \theta_j - \varpi_{i,j}) \leq \bar{Q}_{i,j} \quad \forall (i,j) \in \mathbb{P} \text{ and } \forall (j,i) \in \mathbb{P} \tag{3.17d}$$

$$|Y_{i,i}^{(i,j)}|^2 V_i^4 + |Y_{i,j}^{(i,j)}|^2 V_i^2 V_j^2 + 2|Y_{i,i}^{(i,j)}||Y_{i,j}^{(i,j)}| V_j V_i^3 \cos(\theta_i - \theta_j) \leq \bar{S}_{i,j}^2 \quad \forall (i,j) \in \mathbb{P} \text{ and } \forall (j,i) \in \mathbb{P} \tag{3.17e}$$

$$0 \leq V_i \leq \bar{V}_i \quad \forall i \in \mathbb{N} \tag{3.17f}$$

$$\underline{G}_i \leq G_i \leq \bar{G}_i \quad \forall i \in \mathbb{N} \tag{3.17g}$$

This AC OPF problem bears resemblance to the economic dispatch problem (2.6). Generation costs are being minimized in the objective function. The constraint (3.17a) enforces real power balance at each node, where the RHS of the constraint is the net real power injection as expressed in (3.15). Constraint (3.17b) enforces limits on the net reactive power injection at each bus, where the net reactive power quantity is written as in (3.16).

Constraints (3.17f) and (3.17g) enforce nodal generation and nodal voltage magnitude constraints.

Constraints (3.17c)-(3.17e) enforce line limits where each line limit is assumed symmetric in that each flow quantity has the same limit regardless of flow direction. Constraints (3.17c) and (3.17d) limit the real and reactive power flows on each transmission line and use the expressions from (3.13) and (3.14). Constraint (3.17e) enforces apparent power constraints on each transmission line. With this in mind the squared apparent power flow is represented by the expression $P_{i,j}^2 + Q_{i,j}^2$. The left-hand side (LHS) of constraint (3.17e) is derived by first substituting the expressions for $P_{i,j}$ and $Q_{i,j}$ from (3.13) and (3.14) and then applying the angle difference trigonometric identity, which allows for the following equivalence:

$$\cos(\theta_i - \theta_j) = \cos(-\varpi_{i,j})\cos(\theta_i - \theta_j - \varpi_{i,j}) + \sin(-\varpi_{i,j})\sin(\theta_i - \theta_j - \varpi_{i,j})$$

The AC OPF problem can be written in the form presented as the general ED problem (2.6) from Chapter 2. In this context the AC OPF problem uses a feasible set of net real power injections written as follows:

$$\mathcal{T} = \{T \in \mathbb{R}^n : \exists (V, \theta) \text{ where } (3.15), (3.17b), (3.17c), (3.17d), (3.17e), (3.17f), (3.17g)\} \quad (3.18)$$

It should be apparent that this feasible set of net real power injections is non-convex due to the sinusoidal and high-order polynomial terms. However, this AC OPF problem has constraints defined by smooth functions in the decision variables and is able to be solved to a local minimizer by use of standard iterative algorithms. Also notice that the AC OPF problem does not enforce contingency constraints as stated in Remark 3.1.

Remark 3.1. Economic dispatch problems used in practice define the feasible set of net real power injections in a way that ensures the system is capable of operating within short-term or emergency limits in the event of any single line outage. We do not consider these contingency constraints in any of the considered problems in this dissertation. In fact, such contingency constraints are typically not studied in the context of the AC OPF problem because they would require the introduction of voltage decision variables V and θ for each

of the m possible line outages, making the AC OPF problem intractable to solve. Such contingency-constrained problems could be approximated within the framework we develop by representing the detailed AC equations for the expected non-contingency case, and using linearized constraints to represent the conditions in the contingency cases. It is typical to use such linearized constraints in practice.

3.4 AC OPF Problem in Rectangular Coordinates

Let us now use rectangular coordinates to formulate the AC OPF problem. In this case the complex voltage at bus i is denoted $v_i = v_{\mathrm{Re},i} + \mathbf{i} v_{\mathrm{Im},i}$. Using rectangular coordinates the feasible set of net real power injections is defined by constraints that are quadratic in the real and imaginary parts of the voltage variables.

The complex power flow in a transmission line expressed in terms of the real and imaginary parts of the complex voltage follows from the expression (3.8). With this in mind, denote the admittance quantities in this expression using rectangular coordinates as follows: $Y^{(i,j)} = G^{(i,j)} + \mathbf{i} B^{(i,j)}$. Multiplying the complex quantities in rectangular coordinates leads to the following expressions, which hold for each transmission line in both directions, eg. $(i,j) \in \mathbb{P}$ and $(j,i) \in \mathbb{P}$:

$$Q_{i,j} = -B_{i,i}^{(i,j)}\left(v_{\mathrm{Re},i}^2 + v_{\mathrm{Im},i}^2\right) + G_{i,j}^{(i,j)}(v_{\mathrm{Im},i}v_{\mathrm{Re},j} - v_{\mathrm{Re},i}v_{\mathrm{Im},j}) - B_{i,j}^{(i,j)}(v_{\mathrm{Re},i}v_{\mathrm{Re},j} + v_{\mathrm{Im},i}v_{\mathrm{Im},j}) \quad (3.19)$$

$$P_{i,j} = G_{i,i}^{(i,j)}\left(v_{\mathrm{Re},i}^2 + v_{\mathrm{Im},i}^2\right) + G_{i,j}^{(i,j)}(v_{\mathrm{Re},i}v_{\mathrm{Re},j} + v_{\mathrm{Im},i}v_{\mathrm{Im},j}) + B_{i,j}^{(i,j)}(v_{\mathrm{Im},i}v_{\mathrm{Re},j} - v_{\mathrm{Re},i}v_{\mathrm{Im},j}) \quad (3.20)$$

Similarly, an expression for the net complex power injection into a bus in terms of the real and imaginary parts of the complex voltage follows from expression (3.12). With this in mind, denote the admittance quantities in this expression using polar coordinates as follows: $Y^{(i)} = G^{(i)} + \mathbf{i} B^{(i)}$. Multiplying the complex quantities in rectangular coordinates leads to the following expressions for the net real and reactive power injections into bus i:

$$T_i = G_{i,j}^{(i)}(v_{\mathrm{Re},i}v_{\mathrm{Re},j} + v_{\mathrm{Im},i}v_{\mathrm{Im},j}) + B_{i,j}^{(i)}(v_{\mathrm{Im},i}v_{\mathrm{Re},j} - v_{\mathrm{Re},i}v_{\mathrm{Im},j}) \quad (3.21)$$

$$U_i = G_{i,j}^{(i)}(v_{\mathrm{Im},i}v_{\mathrm{Re},j} - v_{\mathrm{Re},i}v_{\mathrm{Im},j}) - B_{i,j}^{(i)}(v_{\mathrm{Re},i}v_{\mathrm{Re},j} + v_{\mathrm{Im},i}v_{\mathrm{Im},j}) \quad (3.22)$$

Table 3.1: Admittance related matrices used to express the constraints of the AC OPF problem in a standard quadratic form.

Power Flow Matrices for line $(i,j) \in \mathbb{P}$	Power Injection Matrices for bus $i \in \mathbb{N}$	Voltage Matrix for bus $i \in \mathbb{N}$
$H^{(i,j)} = \frac{1}{2} \begin{bmatrix} G^{(i,j)}+G^{(i,j)\dagger} & B^{(i,j)\dagger}-B^{(i,j)} \\ B^{(i,j)}-B^{(i,j)\dagger} & G^{(i,j)}+G^{(i,j)\dagger} \end{bmatrix}$ $Z^{(i,j)} = \frac{-1}{2} \begin{bmatrix} G^{(i,j)}+G^{(i,j)\dagger} & B^{(i,j)\dagger}-B^{(i,j)} \\ B^{(i,j)}-B^{(i,j)\dagger} & G^{(i,j)}+G^{(i,j)\dagger} \end{bmatrix}$	$H^{(i)} = \frac{1}{2} \begin{bmatrix} G^{(i)}+G^{(i)\dagger} & B^{(i)\dagger}-B^{(i)} \\ B^{(i)}-B^{(i)\dagger} & G^{(i)}+G^{(i)\dagger} \end{bmatrix}$ $Z^{(i)} = \frac{-1}{2} \begin{bmatrix} G^{(i)}+G^{(i)\dagger} & B^{(i)\dagger}-B^{(i)} \\ B^{(i)}-B^{(i)\dagger} & G^{(i)}+G^{(i)\dagger} \end{bmatrix}$	$M^{(i)} = \begin{bmatrix} \mathbf{I}_i\mathbf{I}_i^\dagger & 0 \\ 0 & \mathbf{I}_i\mathbf{I}_i^\dagger \end{bmatrix}$

To simplify these expressions introduce vector $w := [v_{\text{Re}}^\dagger, v_{\text{Im}}^\dagger]^\dagger$. Admittance related matrices can now be defined as shown in Table 3.1. The expressions (3.19)-(3.22) can now be expressed as standard quadratic expressions as follows:

$$Q_{i,j} = w^\dagger H^{(i,j)} w \tag{3.23}$$

$$P_{i,j} = w^\dagger Z^{(i,j)} w \tag{3.24}$$

$$T_i = w^\dagger H^{(i)} w \tag{3.25}$$

$$U_i = w^\dagger Z^{(i)} w \tag{3.26}$$

The RHS of the expressions (3.23)-(3.26) are written in standard quadratic form and can be easily placed into an AC OPF problem that optimizes over $w \in \mathbb{R}^{2n}$. This AC OPF problem minimizes the cost of generation and is written as follows:

$$\min_{G \in \mathbb{R}^n, w \in \mathbb{R}^{2n}} \sum_{i \in \mathbb{N}} C_i(G_i) \tag{3.27}$$

$$st : D_i - G_i = w^\dagger H^{(i)} w \quad \forall i \in \mathbb{N} \tag{3.27a}$$

$$\underline{U}_i \le w^\dagger Z^{(i)} w \le \bar{U}_i \quad \forall i \in \mathbb{N} \tag{3.27b}$$

$$-\bar{P}_{i,j} \le w^\dagger Z^{(i,j)} w \le \bar{P}_{i,j} \quad \forall (i,j) \in \mathbb{P} \text{ and } \forall (j,i) \in \mathbb{P} \tag{3.27c}$$

$$-\bar{Q}_{i,j} \le w^\dagger H^{(i,j)} w \le \bar{Q}_{i,j} \quad \forall (i,j) \in \mathbb{P} \text{ and } \forall (j,i) \in \mathbb{P} \tag{3.27d}$$

$$\left(w^\dagger Z^{(i,j)} w\right)^2 + \left(w^\dagger H^{(i,j)} w\right)^2 \le \bar{S}_{i,j}^2 \quad \forall (i,j) \in \mathbb{P} \text{ and } \forall (j,i) \in \mathbb{P} \tag{3.27e}$$

$$0 \le w^\dagger M_i w \le \bar{V}_i \quad \forall i \in \mathbb{N} \tag{3.27f}$$

$$\underline{G}_i \le G_i \le \bar{G}_i \quad \forall i \in \mathbb{N} \tag{3.27g}$$

Similarly to the polar formulation in (3.17), this rectangular formulation of the AC OPF problem bears resemblance to the economic dispatch problem (2.6). Generation costs are being minimized in the objective function. The constraint (3.27a) enforces real power balance at each node, where the RHS of the constraint is the net real power injection as expressed in (3.25). Constraint (3.27b) enforces limits on the net reactive power injection at each bus, where the net reactive power quantity is written as in (3.26). Constraint (3.27f) enforces nodal voltage magnitude constraints, where the limited quantity is equivalent to $v_{\text{Re},i}^2 + v_{\text{Im},i}^2$ and $M^{(i)}$ is defined in Table 3.1. Constraint (3.27g) enforces nodal generation constraints.

Constraints (3.27c)-(3.27e) enforce line limits where each line limit is assumed symmetric in that each flow quantity has the same limit regardless of flow direction. Constraints (3.27c) and (3.27d) limit the real and reactive power flows on each transmission line and use the expressions from (3.24) and (3.23). Constraint (3.27e) enforces apparent power constraints on each transmission line. With this in mind the squared apparent power flow is represented by the expression $P_{i,j}^2 + Q_{i,j}^2$. The LHS of constraint (3.17e) is derived by first substituting the expressions for $P_{i,j}$ and $Q_{i,j}$ from (3.24) and (3.23).

Under the assumption that the cost is quadratic, this is very nearly a Quadratically Constrained Quadratic Program (QCQP), which is a common class of optimization problem that is well studied and may be easier to solve than general smooth non-convex optimization problems. Unfortunately, the apparent power flow constraint (3.27e) is fourth order. However, this constraint can be made quadratic by introducing intermediate variables and constraints $Q_{i,j} = w^\dagger Z^{(i,j)} w$ and $P_{i,j} = w^\dagger H^{(i,j)} w$. In this case the apparent power flow constraint (3.27e) can be introduced to the formulation in order to make the apparent power flow constraint quadratic, in which case this constraint appears as $P_{i,j}^2 + Q_{i,j}^2 \leq \bar{S}_{i,j}^2$. As a result, this problem can indeed be written as a QCQP with the drawback of introducing additional optimization variables.

This problem is written similarly to the economic dispatch problem (2.6) from Chapter 1. In this context the feasible set of net real power injections is written as follows:

$$\mathcal{T} = \{T \in \mathbb{R}^n : \exists w \in \mathbb{R}^n \text{ where } (3.25), (3.27b), (3.27c), (3.27d), (3.27e), (3.27f), (3.27g)\} \quad (3.28)$$

It should be noted that this definition of the feasible set of net real power injections is equivalent to the definition from (3.18) in that a vector T exists in one of these sets if and only if it exists in the other. The difference between the two definitions lies in the way the AC OPF problem is formulated. Either form may see benefits as compared to the other. For example, the rectangular coordinate version of the AC OPF problem yields a very tight semi-definite programming relaxation that will be discussed in Chapter 6. On the other hand, the polar coordinate version of the AC OPF problem yields very accurate simplifying approximations that make the problem easier to solve. These simplifying approximations will be discussed in Chapters 4 and 5.

3.5   Numerical Results

This section will study situations where a revenue adequate market equilibrium is not achieved. In Chapter 6 these test cases will be reinvestigated in the context of convex hull prices, which aim to minimize the worst case revenue shortfall of the ISO.

3.5.1   Simple 3-bus System

This section studies a simple 3-bus power system similar to that in [66] that can be visualized by the one-line diagram shown in Figure 3.2. This three bus test case will be revisited in Chapter 6. The net real power injection at buses 1, 2, and 3 are denoted T_1, T_2, and T_3. The net reactive power injections at buses 1 and 2 are unconstrained. The voltage magnitudes at buses 1 and 2 are fixed to $V_1 = 1$p.u. and $V_1 = 1.21$p.u. respectively. Bus 3 is a null bus whose net real and reactive power injection, denoted T_2 and U_2, are fixed to zero and has no voltage magnitude constraint. A real power flow limit of 3.5p.u. is placed on the line connecting bus 1 and bus 2. The maximum feasible voltage angle difference between bus 1 and bus 2 is approximately 40 degrees and occurs when the system is operating at the limit of line 1-2.

Notice that the feasible set of net real power injections $\mathcal{T}$ is three dimensional; however, the system will physically operate on a slice of this set along the plane $T_3 = 0$ because there is neither generation nor load at bus 3. As explained in Remark 2.1, the feasible set of net
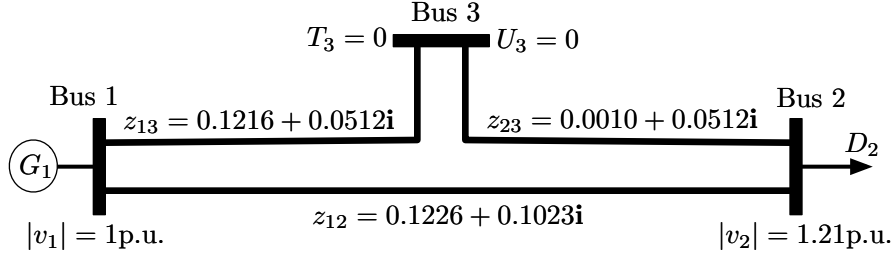
Figure 3.2: One-line diagram of the 3-bus test case with positive PCRS. Impedance values are given in p.u.

real power injections does not enforce constraints on the net real power injections at buses. (Note: these constraints are accommodated by the feasible set of each generator $\mathcal{X}^i$ in the economic dispatch problem (2.6)). This means that FTRs can be allocated to bus 3 even though its net real power injection is physically restricted to zero.

The consumption at bus 2 is fixed to 1p.u., so the net real power injection at bus two is $T_2 = -1$p.u. In this case there is only one feasible point that represents the solution to the AC OPF problem $(T_1^\star, T_2^\star, T_3^\star) \approx (5.4077, -1, 0)$ and therefore $G_1^d = 5.4077$p.u. Notice this operating point accrues large line losses of approximately 4.5p.u. Bus 1 consists of one generator whose cost in dollars is represented by the following piece-wise linear cost function:

$$C_1(G_1) = \begin{cases} 0.5G_1 & \text{if } G_1 \leq 2 \\ G_1 & \text{if } G_1 > 2 \end{cases}$$

Remark 3.2. We assume that the load is valuable enough to maintain operation of the grid at such high line losses (as opposed to opening a circuit breaker on the transmission line to terminate grid operation). □

Let's now identify the LMPs as described in Section 2.4. These prices were found by solving the AC OPF problem in MATLAB using an interior point method available in the function 'fmincon.' The feasible voltages at buses 1, 2, and 3 are $v_1 = 1$, $v_2 = 1.0026 - 0.6774\mathbf{i}$, and $v_3 = 0.8381 - 0.5356\mathbf{i}$ respectively in units of per unit (p.u.). The solver provided the Lagrange multipliers for the real power balance constraint (6.5a) that solve the KKT conditions for this point. The LMPs for bus 1, 2 and 3 are $\lambda_1^\star = \$1/\text{p.u.}$, $\lambda_2^\star = \$9.455/\text{p.u.}$, and $\lambda_3^\star = \$9.461/\text{p.u.}$ respectively. The congestion revenue can be easily computed as $CR = \$4.05$.

The side-payment to the only generator in the 3-bus system (or equivalently the lost opportunity cost) as defined in Section 2.2.2 is numerically found to be zero. This is illustrated in Table 3.2. Specifically, the marginal cost of the generator and the LMP seen by the generator are both equal to $1/p.u.. As a result the generator's profit will always be zero and it will not experience any lost opportunity cost. In fact, it can be proven that side-payments to generators are always zero when using a KKT price-dispatch pair. This is proven explicitly in Chapter 6 by Theorem 6.1.

Table 3.2: Evaluating lost opportunity cost for the only generator rounding to nearest cent.

Payment ($)	Profit ($)	Max Profit ($)	Lost Opp. Cost ($)
$\lambda_1^\star G_1^d$	$\lambda_1^\star G_1^d - C_1(G_1^d)$	$\Upsilon_1(\lambda_1^\star)$	$C_i^o(\lambda_1^\star, G_1^d)$
5.41	0	0	0

The PCRS using the identified LMPs as defined in Section 2.2.3 is numerically found to be $0.26 with an optimal FTR allocation $f^\star = [5.5929, 6.3464, -7.3892]$ in units of $p.u.$. The optimal FTR allocation is computed by solving the FTR payoff maximization problem (2.4). Typically, in high-dimension, it is not easy to identify the optimal FTR allocation vector that falls in the non-convex feasible set of net real power injections. However, in our simple example this can be done by randomly sampling feasible points to initialize a Newton-Raphson algorithm. The PCRS computation is illustrated in Table 3.3. Specifically, the congestion revenue is easily found to be $4.05 and the maximum FTR payoff can be computed as $-\lambda^{\star\dagger} f^\star = 4.31$. The PCRS is the difference between the two, amounting to $0.26.

Table 3.3: Evaluating PCRS for the 3-bus test case rounding to the nearest cent.

Demand Charge ($)	Congestion Revenue($)	Max. FTR Payoff ($)	PCRS ($)
$\lambda_2^\star D_2$	$\lambda_2^\star D_2 - \lambda_1^\star G_1^d$	$\Psi(\lambda^\star) = -\lambda^{\star\dagger} f^\star$	$C^s(\lambda^\star, G^d)$
9.46	4.05	4.31	0.26

Since we are using LMPs the lost opportunity cost of generators is zero as expected from Chapter 2. However, the PCRS is non-zero, illustrating that a revenue adequate market

equilibrium does not exist for this simple test case. Furthermore, the PCRS is approximately five percent of the total operating cost and is therefore non-negligible.

3.5.2 Examples on Standard Test Cases

The example in the previous section is contrived to show extreme characteristics. To see whether similar results might occur in more practical systems, consider the much larger test cases available from the NESTA archive [17]. The AC OPF problem in polar coordinates is solved using the PowerModels package in Julia [16] along with the interior point solver IPOPT [87]. It is important to recognize that the interior point algorithm is only capable of converging to a local minimum, so the identified dispatch may not be a global minimum of the AC OPF problem. As stated in Section 2.5, the PCRS must be positive if the dispatch is not globally optimal for the AC OPF problem.

Table 3.4 provides a comparison of side-payments and PCRS when using LMPs. We provide results for six systems with 162 buses, 189 buses, 300 buses, 2224 buses, 2383 buses, and 3012 buses. Computing the PCRS for a given set of prices requires solving the non-convex max FTR payoff problem (2.4). The provided PCRS values are computed using an interior point solver in Julia that identifies a local maximum of problem (2.4). Since we are only guaranteeing a local maximimum of the FTR maximization problem, the PCRS values provided in the table underestimate the true PCRS value.

As expected, LMPs result in zero side-payments to generators and positive PCRS. The PCRS may be very large with respect to the total operating cost as in test case 162_ieee_dtc (approximately 32%) or very small as in test case 3012wp_mp (approximately 0.07%). Aside from the test cases studied in this dissertation, many of the test cases in the NESTA archive result in PCRS values that are greater than 0.1% of total operating cost. On the other hand, very few test cases in the NESTA archive result in PCRS values that are greater than 1% of total operating cost.

3.6 Conclusions

This chapter derived the AC OPF problem using both rectangular and polar coordinates from first principles. Both versions are non-convex but are significantly different in

Table 3.4: Results for NESTA Test Cases. All amounts are in dollars per hour. Computational time is determined using a computer with a 2.7 GHz processor.

Test Case	LMPs (for AC OPF)		Total Operating Cost	Computational Time (sec)
	Side Payments	PCRS		
162_ieee_dtc	~ 0	1,352.92	4,230.23	0.66
189_edin	~ 0	1.22	849.29	0.59
300_ieee	~ 0	36.87	16,891.27	1.14
2224_edin	~ 0	520.76	38,127.69	17.23
2383wp_mp	~ 0	13,681.00	1,868,511.77	15.42
3012wp_mp	~ 0	1,815.44	2,600,842.72	33.47

form. Chapters 4 and 5 will show that the polar coordinate formulation is convenient for deriving simplifying approximations. Chapter 6 will show that the rectangular coordinate formulation is convenient for deriving a convex relaxation that results in a semi-definite program.

Numerical results illustrate two problems associated with the AC OPF problem. First is the difficulty in solving the AC OPF problem. Interior point algorithms seem to work well; however, they are only guaranteed to converge to local minima. The second problem is the general lack of a revenue adequate market equilibrium. Specifically, the test cases studied in this section result in positive PCRS.

Since the PCRS is positive for each test case in this chapter the ISO is not guaranteed revenue adequacy because congestion revenue may not cover FTR payoffs. Now that we have identified a problem associated with revenue adequacy for the ISO, we should naturally consider how to fix this problem. Chapter 6 directly addresses this problem by proposing a different pricing structure called convex hull pricing that aims to minimize the weighted sum of PCRS and generator side-payments. Chapter 6 will explain how to approximate convex hull prices using relaxations and will revisit these examples to illustrate the improvement in PCRS when using convex hull prices.

Chapter 4

Non-Linear Approximations of the AC OPF Problem

Standard economic dispatch problems that consider line losses are linear approximations of a non-convex economic dispatch problem formulated by fixing voltage magnitudes and assuming the decoupling of real and reactive power, which we term the *Transmission Constrained Economic Dispatch (TCED) problem.* This chapter formulates and analyzes a general form of the TCED problem, incorporating and generalizing the Fictitious Nodal Demand (FND) model [57], resulting in a slack bus independent formulation that provides insight into standard formulations by pointing out commonly used but unnecessary assumptions and by deriving proper choices of "tuning parameters." The proper choice of loss allocation is derived to assign half of the losses of each transmission line to adjacent buses, justifying approaches in the literature. Line constraints are proposed in the form of voltage angle difference limits and are proven equivalent to various other line limits including current magnitude limits and mid-line power flow limits. The formulated TCED problem with marginal losses consistently models flows and loss approximations, results in approximately correct outcomes and is proven to be reference bus independent. Various approximations of this problem are compared using realistically large transmission network test cases.

This chapter is an extension of the work in [32] and is organized as follows. Section 4.1 provides a model of a transmission line using the assumption that voltage magnitudes are fixed. We explain how this model is a generalization of other models used in the literature and outline various common approximations. Section 4.2 uses a general transmission line model to formulate the non-convex TCED problem that utilizes line constraints in the form of voltage angle difference limits across each transmission line. The *relaxed TCED problem* is then formulated using the load over-satisfaction relaxation. The relaxed TCED problem is shown to have the same global minimizer as the TCED problem under the condition that the LMPs are positive and is shown to be convex when using specific approximations.

Section 4.2 continues to explain how the voltage angle limit parameters can be chosen to indirectly enforce limits on various physical parameters associated with a transmission line. Section 4.3 provides empirical results analyzing the error of the various approximations as well as their relation to the AC OPF problem.

4.1 Transmission Line Model

Figure 4.1 provides a circuit diagram of the general equivalent-Π model of a transmission line $(i, j) \in \mathbb{P}$ that is operated at a nominal frequency. The transmission line is indexed by $\ell \in \mathbb{L}$ and connects bus $i \in \mathbb{N}$ to bus $j \in \mathbb{N}$. This circuit is similar to that in Figure 3.1 but differs from it in the treatment of the series element. In particular, to facilitate discussion of loss models, the series impedance of the line is divided into two parts and separated by an intermediate node c located at a fractional distance d from from bus j. The total series impedance is denoted $z_\ell = r_\ell + \mathbf{i}x_\ell$ where r_ℓ is the series resistance and x_ℓ is the series reactance. The series impedance separating node c from bus j is in the amount dz_ℓ. We assume that the shunt conductances are zero, ie. the real part of $y_\ell^{(c)}$ is zero, and thus no real power flows through the shunt elements. As in Chapter 3, the complex voltage at bus i is denoted $v_i = V_i \angle(\theta_i)$ in polar coordinates, where V_i is the voltage magnitude and θ_i is the voltage angle. An ideal transformer is located near bus i with complex off-nominal turns ratio of $a_\ell = \tau_\ell \angle(\psi_\ell)$.
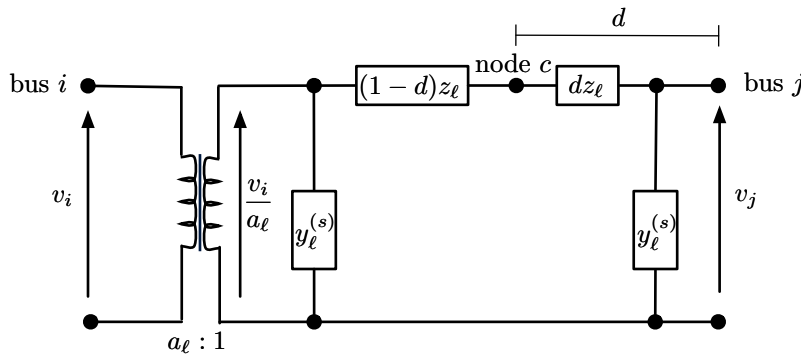
Figure 4.1: Circuit diagram of an arbitrary line ℓ connecting bus i to bus j.

4.1.1 Real Power Flow on a Transmission Line

We consider the flow of real power in the series element of the equivalent-Π model of a transmission line. Assuming fixed voltage magnitudes, the real power flowing through node c in the series element in the direction of bus j at an arbitrary fractional distance d is represented by the following function:

$$\hat{F}_\ell(\Theta_\ell, d) := g_\ell(\tfrac{d}{\tau_\ell^2}V_i^2 - (1-d)V_j^2) - \tfrac{b_\ell}{\tau_\ell}V_iV_j\sin(\Theta_\ell - \psi_\ell) - \tfrac{g_\ell}{\tau_\ell}V_iV_j(2d-1)\cos(\Theta_\ell - \psi_\ell), \quad (4.1)$$

where $y_\ell = 1/z_\ell = g_\ell + \mathbf{i}b_\ell$ and $\Theta_\ell = \theta_i - \theta_j$. This model is a generalization of that in [84] and is derived explicitly in Appendix C.1. Notice that this function requires knowledge of the fixed voltage magnitudes. Reference [84] suggests different ways of choosing the fixed voltage magnitudes including using the state estimated values or a local minimizer of the AC OPF problem.

4.1.2 Loss Function and Approximations

From (4.1), the real power flowing into the line from bus i and from bus j are respectively expressed as $\hat{F}_\ell(\Theta_\ell, 1)$ and $-\hat{F}_\ell(\Theta_\ell, 0)$. The loss function for the line represents the real power loss across the line and is derived by summing these two values:

$$\hat{L}_\ell(\Theta_\ell) := g_\ell(V_j^2 + \tfrac{1}{\tau_\ell^2}V_i^2) - 2\tfrac{g_\ell}{\tau_\ell}V_iV_j\cos(\Theta_\ell - \psi_\ell). \quad (4.2)$$

ISOs may desire a simpler quadratic approximation in order to utilize quadratic programming software. A very accurate approximation uses a third order Taylor expansion of the cosine function in (4.2) around $\Theta_\ell = \psi_\ell$. This approximation results in a quadratic model of losses since the coefficient of the third order term is zero, with quartic error on the order of $\frac{g_\ell V_iV_j}{24\tau_\ell}\Theta_\ell^4$:

$$\hat{L}_\ell(\Theta_\ell) \approx g_\ell(V_j^2 + \tfrac{1}{\tau_\ell^2}V_i^2) - \tfrac{g_\ell}{\tau_\ell}V_iV_j(2 - (\Theta_\ell - \psi_\ell)^2). \quad (4.3)$$

Note that this approximation does not rely on any assumption that the line resistance is small compared to the reactance. Though very accurate, using this approximation in practice still requires some knowledge of how to fix the voltage magnitudes and tap ratios. An ISO may desire a simpler model that fixes voltage magnitudes to 1 p.u. and tap ratios to $a_\ell = 1$. Fixing these values results in the following approximation:

$$\hat{L}_\ell(\Theta_\ell) \approx g_\ell\Theta_\ell^2. \quad (4.4)$$

Perhaps the most commonly used approximation equates the line losses to the product of resistance of the line and squared DC power flow across the line. We can arrive at this approximation from (4.4) by additionally assuming $r_\ell \ll x_\ell$:

$$\hat{L}_\ell(\Theta_\ell) \approx r_\ell (\tfrac{1}{x_\ell}\Theta_\ell)^2. \tag{4.5}$$

This final approximation of the loss function is by far the simplest and carries the interpretation that losses are equal to the resistance times the squared DC power flow where the DC power flow is given by $\frac{1}{x_\ell}\Theta_\ell$. This interpretation is often used naively without an understanding of the several approximations used to get to this point.

4.1.3 Fictitious Nodal Demand Representation

An FND representation of our transmission line model can be derived from (4.1) and (4.2). Notice that we can express the real power flowing into the line from adjacent buses as follows, for an arbitrary fractional distance d:

$$\hat{F}_\ell(\Theta_\ell, 1) = \hat{F}_\ell(\Theta_\ell, d) + (1 - d)\hat{L}_\ell(\Theta_\ell), \tag{4.6}$$

$$-\hat{F}_\ell(\Theta_\ell, 0) = -\hat{F}_\ell(\Theta_\ell, d) + d\hat{L}_\ell(\Theta_\ell). \tag{4.7}$$

These expressions lead to an FND model depicted in Figure 4.2 that is similar to that shown in [84]. Specifically, a lossless transfer of real power from bus i to bus j occurs in the amount $\hat{F}_\ell(\Theta_\ell, d)$. Losses are then represented as fictitious demand at bus i in the amount $(1 - d)\hat{L}_\ell(\Theta_\ell)$ and at bus j in the amount $d\hat{L}_\ell(\Theta_\ell)$. This FND model is equivalent to (4.1) in the sense that the buses see the same net real power injection.
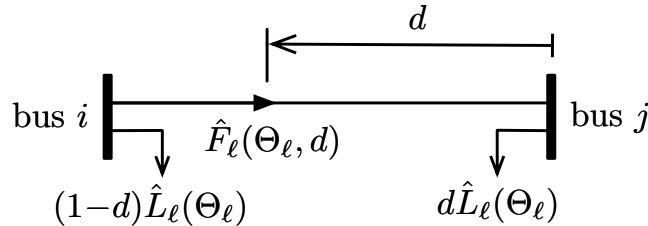
Figure 4.2: One-line diagram of the FND representation of the proposed transmission line model.

4.1.4 Mid-line Power Flows and Approximations

A crucial observation is that d can be chosen to simplify the form of the resulting model. When $d = \frac{1}{2}$ the cosine term in (4.1) drops out, simplifying the expression for the lossless real power flow $\hat{F}_\ell(\Theta_\ell, \frac{1}{2})$ in the FND model (4.6) and (4.7). This value is termed the *mid-line power flow* and is written as follows:

$$\hat{F}_\ell\left(\Theta_\ell, \tfrac{1}{2}\right) = \tfrac{1}{2}g_\ell(\tfrac{1}{\tau_\ell^2}V_i^2 - V_j^2) - \tfrac{b_\ell}{\tau_\ell}V_iV_j\sin(\Theta_\ell - \psi_\ell). \tag{4.8}$$

We will see that with this choice of d, a linear approximation to $\hat{F}_\ell$ is accurate to second order in Θ_ℓ. This choice of d is also convenient because of the symmetry of losses that occur around the mid-point of the line. Specifically, the second term on the RHS of (4.6) and (4.7) are identically $\frac{1}{2}\hat{L}_\ell(\Theta_\ell)$. This expression for the mid-line power flow is also in [84].

Unfortunately, the exact expression for the mid-line power flow (4.8) is not convex in the vicinity of $\Theta_\ell \approx 0$. However, a very accurate linear approximation can be attained through a second order Taylor expansion at $\Theta_\ell = \psi_\ell$. This approximation results in a linear model since the coefficient of the second order term is zero, with cubic error on the order of $\frac{b_\ell V_i V_j}{6\tau_\ell}\Theta_\ell^3$:

$$\hat{F}_\ell\left(\Theta_\ell, \tfrac{1}{2}\right) \approx \tfrac{1}{2}g_\ell(\tfrac{1}{\tau_\ell^2}V_i^2 - V_j^2) - \tfrac{b_\ell}{\tau_\ell}V_iV_j(\Theta_\ell - \psi_\ell). \tag{4.9}$$

Fixing the voltage magnitudes to 1p.u. and off-nominal tap ratios to $a_\ell = 1$ further simplifies the previous approximation to:

$$\hat{F}_\ell\left(\Theta_\ell, \tfrac{1}{2}\right) \approx -b_\ell\Theta_\ell. \tag{4.10}$$

Similar to the derivation of loss approximations in Section 4.1.2, a final approximation often utilized in practice assumes $r_\ell \ll x_\ell$, leading to the following expression:

$$\hat{F}_\ell\left(\Theta_\ell, \tfrac{1}{2}\right) \approx \tfrac{1}{x_\ell}\Theta_\ell. \tag{4.11}$$

With respect to the FND representation of our model, this approximation can be interpreted as the combination of lossless DC power flow and line losses distributed equally to adjacent buses. In fact, this interpretation is also consistent with with the FND formulation from [57] and [40], which suggest half losses of each line be allocated to both adjacent buses. Our

derivation shows that the allocation resulting from the choice $d = \frac{1}{2}$ is particularly advantageous in that it results in a simple expression for the flow that is well approximated by a linear function. This observation does not appear to have been recognized previously in the literature; however, the authors of [40, 57] may have had this advantage in mind in proposing FND.

4.1.5 Squared Current Magnitude and Approximations

The squared magnitude of the current flowing into the transmission line from bus i and bus j can be represented as functions of the voltage angle difference Θ_ℓ and will be denoted $\hat{\mathcal{J}}_{ij}(\Theta_\ell)$ and $\hat{\mathcal{J}}_{ji}(\Theta_\ell)$ respectively. These functions are explicitly derived in Appendix C.2 and are respectively written as follows:

$$\hat{\mathcal{J}}_{ij}(\Theta_\ell) := \frac{|y_\ell|^2}{\tau_\ell^2} \left(\frac{\chi_\ell^2}{\tau_\ell^2} V_i^2 + V_j^2 - \frac{2\chi_\ell}{\tau_\ell} V_i V_j \cos(\phi_\ell - \psi_\ell + \Theta_\ell) \right), \tag{4.12}$$

$$\hat{\mathcal{J}}_{ji}(\Theta_\ell) := |y_\ell|^2 \left(\frac{1}{\tau_\ell^2} V_i^2 + \chi_\ell^2 V_j^2 - \frac{2\chi_\ell}{\tau_\ell} V_i V_j \cos(\phi_\ell + \psi_\ell - \Theta_\ell) \right), \tag{4.13}$$

where χ_ℓ and ϕ_ℓ are defined to be the magnitude and angle of the complex number $z_\ell(y_\ell^{(c)} + y_\ell)$ respectively, so that $z_\ell(y_\ell^{(c)} + y_\ell) = \chi_\ell \angle(\phi_\ell)$. Notice that this complex number is approximately 1 because the shunt admittance is typically much smaller than the series admittance. As a result $\chi_\ell \approx 1$ and $\phi_\ell \approx 0$. In the following, we consider $\hat{\mathcal{J}}_{ij}(\Theta_\ell)$. The function $\hat{\mathcal{J}}_{ji}(\Theta_\ell)$ can be handled similarly.

Similar approximations to those in Sections 4.1.2 and 4.1.4 can be used for the squared current magnitude function. The first approximation uses a third order Taylor expansion of the cosine function in (4.12) around $\Theta_\ell = -\phi_\ell + \psi_\ell$. This approximation results in a quadratic function, with quartic error on the order of $\frac{2\chi_\ell |y_\ell|^2 V_i V_j}{24\tau^3}(\Theta_\ell + \phi_\ell - \psi_\ell)^4$:

$$\hat{\mathcal{J}}_{ij}(\Theta_\ell) \approx \left(\frac{\chi_\ell^2}{\tau_\ell^2} V_i^2 + V_j^2 - \frac{\chi_\ell}{\tau_\ell} V_i V_j \left(2 - (\Theta_\ell + \phi_\ell - \psi_\ell)^2 \right) \right) \frac{|y_\ell|^2}{\tau_\ell^2}. \tag{4.14}$$

In the case where shunt admittance $y_\ell^{(c)}$ is negligible we have $\chi_\ell = 1$ and $\phi_\ell = 0$. Additionally fixing the voltage magnitudes to 1p.u. and the off-nominal tap ratio to $a = 1$ simplifies the previous approximation as follows:

$$\hat{\mathcal{J}}_{ij}(\Theta_\ell) \approx |y_\ell|^2 \Theta_\ell^2. \tag{4.15}$$

In the case where $r_\ell \ll x_\ell$ we have $y_\ell \approx \mathbf{i}b_\ell$. The approximation (4.15) then simplifies to the following:

$$\hat{\mathcal{J}}_{ij}(\Theta_\ell) \approx (\tfrac{1}{x_\ell}\Theta_\ell)^2. \tag{4.16}$$

This final approximation of the squared current magnitude is the simplest and carries the interpretation that the per unit current magnitude is equal to the per unit magnitude of the DC power flow.

4.1.6 General Transmission Line Model

We have now introduced multiple approximations of the loss function $\hat{L}_\ell(\cdot)$, the mid-line power flow function $\hat{F}_\ell(\cdot, \tfrac{1}{2})$, and the squared current magnitude function $\hat{\mathcal{J}}_{ij}(\cdot)$. We now introduce definitions of more general functions that encompass all outlined approximations. We begin with the general loss function $\check{L}_\ell(\cdot)$ that encompasses exact expressions for losses and any realistic loss function approximation, including any one of the forms on the RHSs of (4.2)-(4.5). Consistent with properties of losses, the general loss function is required to be convex in the vicinity of the origin as well as symmetric about the point ψ_ℓ. Resistances are realistically assumed to be positive, resulting in strict convexity. Note that a function with a check mark $\check{\ }$ represents an approximation to its *exact* counterpart denoted with a hat symbol $\hat{\ }$.

Definition 4.1. A *general loss function* of angles, denoted $\check{L}_\ell : \mathbb{R} \to \mathbb{R}$, is a function with the following properties: strictly convex on the subdomain $\mathcal{D}_\ell := [-\tfrac{\pi}{2} + \psi_\ell, \tfrac{\pi}{2} + \psi_\ell]$, continuously differentiable, non-negative, symmetric about the point ψ_ℓ and strictly monotonically increasing on the subdomain $\mathcal{D}_{\ell+} := [\psi_\ell, \tfrac{\pi}{2} + \psi_\ell]$.

Similarly, the general mid-line power flow function $\check{F}_\ell(\cdot)$ encompasses all functional forms on the RHSs of (4.8)-(4.11). This general function highlights the monotonic property of the mid-line power flow function for angle differences near the origin. Although the mid-line power flow function is typically monotonically increasing this definition is left general to accommodate potentially positive susceptance values (or equivalently negative reactance values), in which case the function would be monotonically decreasing.

Definition 4.2. A *general mid-line power flow function* of angles, denoted $\check{F}_\ell : \mathbb{R} \to \mathbb{R}$, is strictly monotonic on the subdomain $\mathcal{D}_\ell$ and is continuously differentiable.

The general squared current magnitude function $\check{\mathcal{I}}_{ij}(\cdot)$ encompasses all functional forms outlined by (4.12)-(4.16). This general function highlights the convexity of the squared current magnitude function near the origin as well as its symmetry about the point $-\phi_\ell + \psi_\ell$.

Definition 4.3. A *general squared current magnitude function* of angles, denoted $\check{\mathcal{I}}_{ij} : \mathbb{R} \to \mathbb{R}$, is a function with the following properties: convex on the subdomain
$\tilde{\mathcal{D}}_\ell := [-\frac{\pi}{2} - \phi_\ell + \psi_\ell, \frac{\pi}{2} - \phi_\ell + \psi_\ell]$, strictly monotonically increasing on the subdomain
$\tilde{\mathcal{D}}_{\ell+} := [-\phi_\ell + \psi_\ell, \frac{\pi}{2} - \phi_\ell + \psi_\ell]$, symmetric about the point $-\phi_\ell + \psi_\ell$, and continuously differentiable.

The remainder of this chapter provides results using these more general functions and is therefore pertinent to typical dispatch formulations that utilize the simplest functional forms outlined by (4.5), (4.11), and (4.16) and also pertinent to the exact functional forms outlined by (4.2), (4.8), and (4.12).

4.2 Transmission Constrained Economic Dispatch

This section formulates a non-convex economic dispatch problem using the general transmission line model from the previous section that we refer to as the Transmission Constrained Economic Dispatch (TCED) problem. This problem formulation enforces line limits using simple bounds on the voltage angle difference across each transmission line. We then explain that this TCED problem can be represented as a convex relaxed TCED problem under the condition that prices are positive and an affine approximation of the mid-line power flow function is used. Finally, we explain how the voltage angle difference bounds can be chosen to enforce limits on a variety of line related quantities.

4.2.1 Real Power Injections and Loss Distribution Factor Approximation

The net real power injections at each bus can be expressed by summing the associated injections into each transmission line incident to it. To express the net real power injections as a function of voltage angles we will utilize the FND model (4.6) and (4.7) evaluated at the

midpoint of each line $d = \frac{1}{2}$ along with arbitrary approximations for the loss function and mid-line power flows outlined in Section 4.1. For convenience, we introduce a vector valued function $L : \mathbb{R}^m \to \mathbb{R}^m$ that maps voltage angle differences to line losses. The ℓth element of this vector valued loss function is defined as $L_\ell(\Theta) := \check{L}_\ell(\Theta_\ell)$ where $\Theta \in \mathbb{R}^m$ is a vector of voltage angle differences, consistent with the established notation. Similarly, the vector valued function $F : \mathbb{R}^m \to \mathbb{R}^m$ maps voltage angle differences to mid-line power flows. The ℓth element of this vector valued function is defined as $F_\ell(\Theta) := \check{F}_\ell(\Theta_\ell)$.

The net real power injections at each bus in the system can be represented as a vector valued function of voltage angle differences, denoted $T : \mathbb{R}^m \to \mathbb{R}^n$:

$$T(\Theta) := \tfrac{1}{2}\, |A|^\dagger L(\Theta) + A^\dagger F(\Theta), \tag{4.17}$$

where the branch-bus incidence matrix of the graph $\mathcal{G}$ is denoted $A \in \mathbb{R}^{m \times n}$. Specifically, A is sparse and the row representing line ℓ connecting bus i to bus j has element i equal to 1 and j equal to -1. The element-wise absolute value of the branch-bus incidence matrix is denoted $|A|$, also known as the unoriented incidence matrix of graph $\mathcal{G}$. Intuitively, the function $T(\cdot)$ can be interpreted at each bus as being the sum of net real injections into incident lines due to lossless real power transfers together with half of the losses of each incident line.

Since the voltage angles $\theta \in \mathbb{R}^n$ only enter each equation through the differences Θ_ℓ, one degree of freedom can be removed by assigning an arbitrary *angle reference bus* $\rho \in \mathbb{N}$ and setting $\theta_\rho = 0$. The vector of voltage angle differences can now be written as $\Theta = \dot{A}\dot{\theta}$ where $\dot{\theta} \in \mathbb{R}^{n-1}$ is the vector of voltage angles with element ρ removed and the matrix $\dot{A} \in \mathbb{R}^{m \times (n-1)}$ is the incidence matrix A with column ρ removed.

Reference [58] introduced loss distribution factors to distribute losses throughout the transmission system. Loss distribution factors can be thought of as an approximation to the function of net real power injections $T(\Theta)$. A vector of distribution factors denoted $\eta \in \mathbb{R}^n_+$ sum to one and represent the fraction of total system losses allocated to each bus. The associated approximation to the function representing net real power injections is written as follows:

$$T(\Theta) \approx \eta \mathbf{1}^\dagger L(\Theta) + A^\dagger F(\Theta). \tag{4.18}$$

At a particular operating point, it is possible to choose η so that the left and RHS of (4.18) match exactly. However, it is not generally possible to choose η to make this true generally and not possible to make partial derivatives of the LHS and RHS of (4.18) match exactly (See Section 5.2.5). In particular, notice that the rank of $\eta \mathbf{1}^\dagger$ is one and the rank of the unoriented incidence matrix $|A|$ is at least $n-1$ under the assumption that the system graph is fully connected [86]. That is, we cannot choose η to satisfy $\eta \mathbf{1}^\dagger = \frac{1}{2} |A|^\dagger$. Thus the approximation on the RHS of (4.18) is never an exact representation of the function $T(\Theta)$. Instead, the proper choice of loss distribution factors will change with state $\dot{\theta}$. The proper choice of loss distribution factors is further addressed in Section 5.2.5.

4.2.2 Transmission Constrained Economic Dispatch Problem

The TCED problem optimizes over the nodal generation represented by vector $G \in \mathbb{R}^n$ and the voltage angle vector $\dot{\theta} \in \mathbb{R}^{n-1}$. The cost of generation is represented by the function $C(G) := \sum_{i \in \mathbb{N}} C_i(G_i)$ where $C : \mathbb{R}^n \to \mathbb{R}$ is assumed convex. The nodal demand is considered fixed and is represented by $D \in \mathbb{R}^n$. The *Transmission Constrained Economic Dispatch (TCED) problem* is:

$$\min_{G \in \mathbb{R}^n, \dot{\theta} \in \mathbb{R}^{n-1}} C(G) \tag{4.19}$$

$$st : T(\dot{A}\dot{\theta}) = G - D \tag{4.19a}$$

$$\underline{G} \le G \le \bar{G} \tag{4.19b}$$

$$\underline{\Theta} \le \dot{A}\dot{\theta} \le \overline{\Theta} \tag{4.19c}$$

Constraint (4.19a) is a vector equality constraint that represents real power balance at each node. Constraints (4.19b) enforce generator output limits and constraints (4.19c) represent limits on voltage angle differences across each transmission line. Section 4.2.4 will explain how to choose the voltage angle difference limits to indirectly enforce limits on various line related quantities including current magnitude and mid-line power flow.

Remark 4.1. Throughout this chapter we will assume that any vector of voltage angle differences Θ satisfying (4.19c) also satisfies the constraint $\Theta_\ell \in \mathcal{D}_\ell \cap \tilde{\mathcal{D}}_\ell$ for each line ℓ, where $\mathcal{D}_\ell$ and $\tilde{\mathcal{D}}_\ell$ are from Definitions 4.1 and 4.3. This assumption effectively enforces limits on the voltage angle differences Θ that should hold for any practical power system.

Note that there is no explicit slack bus in this formulation, since real power balance is represented at each bus, so the formulation is independent of choice of slack bus. There is an explicit reference bus and Theorem 4.1 below shows that the formulation is independent of choice of reference bus.

Theorem 4.1. Consider two instances of the TCED problem (4.19) defined using different reference buses. The reduced voltage angle vectors associated with the first and second instances of the problem are defined to be $\dot{\theta} \in \mathbb{R}^{n-1}$ and $\ddot{\theta} \in \mathbb{R}^{n-1}$ respectively. Let $(G^\star, \dot{\theta}^\star)$ be a solution to the first instance of the problem. There exists some $\ddot{\theta}^\star \in \mathbb{R}^{n-1}$ such that $(G^\star, \ddot{\theta}^\star)$ is a solution to the second instance of the problem.

Proof: Let $\dot{A}$ and $\ddot{A}$ be the reduced brach-bus incidence matrices for the first and second instances of the problem respectively. The matrices $\dot{A}$ and A have the same range space because any given row of A can be written as a linear combination of the other rows in A (ie. $A1 = 0$). Similarly $\ddot{A}$ and A have the same range space. Thus $\dot{A}$ and $\ddot{A}$ have the same range space. As a result, there must exist some $\ddot{\theta}^\star$ such that $\ddot{A}\ddot{\theta}^\star = \dot{A}\dot{\theta}^\star$. It follows that there exists a $\ddot{\theta}^\star$ such that $(G^\star, \ddot{\theta}^\star)$ is feasible for the second instance of the problem. Notice that this implies the second instance of the problem has an optimal value no greater than the optimal value of the first instance. Furthermore, there does not exist a feasible point of the second instance of the problem that achieves a lower optimal value than the first instance, else a similar argument shows that a feasible point can be constructed for the first instance that has a lower cost than $(G^\star, \dot{\theta}^\star)$. Thus both instances have the same optimal value and there exists a $\ddot{\theta}^\star$ such that $(G^\star, \ddot{\theta}^\star)$ is optimal for the second instance of the problem. $\square$

The Locational Marginal Prices (LMPs), denoted $\lambda^\star \in \mathbb{R}^n$, represent the sensitivity of the optimal value of the TCED problem (4.19) with respect to the demand vector D, assuming such sensitivities exist. In fact, the LMPs are independent of the choice of reference bus because the optimal value of the TCED problem (4.19) is independent of the choice of reference bus for any $D \in \mathbb{R}^n$ as stated in Theorem 4.1. Of course this simple analysis assumes that LMPs are well defined. Section 5.1.4 explicitly defines LMPs and decomposes the LMP into energy, loss and congestion components.

Remark 4.2. A clear relationship must be established between the TCED problem and the gold standard AC OPF problem, as specified in Chapter 3. Under the assumption that shunt conductances are negligible, the *exact* TCED problem defined by (4.2), (4.8), and (4.12) can be derived from the AC OPF problem by fixing the voltage magnitudes and removing all constraints that involve reactive power quantities, including reactive power balance constraints at buses. Thus, if the voltage magnitudes are fixed to values that match the solution of the AC OPF problem, then the TCED problem formulated here will act as a relaxation of the AC OPF problem, obtaining a lower optimal objective value. Of course, in practice the solution to the AC OPF problem will not be available when fixing the voltage magnitudes, so these quantities must be approximated.

4.2.3 Load Over-Satisfaction Relaxation

A relaxed version of the TCED problem that uses the *load over-satisfaction relaxation* can be obtained from problem (4.19) by replacing the real power balance equality constraints (4.19a) with inequality constraints that permit the delivery of excess generation [75]. With this in mind, the *relaxed TCED problem* is written as follows:

$$\min_{G \in \mathbb{R}^n, \dot{\theta} \in \mathbb{R}^{n-1}} C(G) \tag{4.20}$$

$$st : T(\dot{A}\dot{\theta}) \leq G - D \tag{4.20a}$$

$$\underline{G} \leq G \leq \bar{G} \tag{4.20b}$$

$$\underline{\Theta} \leq \dot{A}\dot{\theta} \leq \overline{\Theta} \tag{4.20c}$$

If this *relaxed TCED problem* results in positive LMPs, then its solution also solves the TCED problem (4.19). To understand this intuitively, first assume that the optimal solution of this problem solves the Karush-Kuhn-Tucker (KKT) conditions and then recognize that the LMPs of the relaxed TCED problem are represented by the optimal Lagrange multipliers of constraint (4.20a). If these Lagrange multipliers are positive, then constraint (4.20a) must be binding at optimality by the complementary slackness condition [5]. As a result, the optimal solution of the relaxed TCED problem (4.20) is feasible and thus optimal for the TCED problem (4.19).

The relaxed TCED problem (4.20) is convex under the condition that an affine ap-

proximation of the mid-line power flow function $F(\cdot)$ is used as is the case for approximations (4.9), (4.10), and (4.11). To see this, first notice that the objective function is convex by assumption and constraints (4.20b) and (4.20c) are convex because they are linear. Finally, the function $T(\cdot)$ is convex as defined in (4.17) because the mid-line power flow function is affine and the vector valued loss function $L(\cdot)$ is convex on the domain of the TCED problem (4.20) as follows from Definition 4.1 and Remark 4.1. Constraint (4.20a) is additionally convex because the function $T(\cdot)$ is convex and appears on the LHS of the inequality.

The relaxed TCED problem (4.20) is written similarly to the general economic dispatch problem (2.6) from Chapter 1. In this context the feasible set of net real power injections is written as follows:

$$\mathcal{T} = \{T(\dot{A}\dot{\theta}) : \exists \dot{\theta} \in \mathbb{R}^{n-1} \text{ where } (4.20a), (4.20b), (4.20c)\} \tag{4.21}$$

It should be emphasized that this definition of the feasible set of net real power injections is convex when using approximations (4.9), (4.10), and (4.11) of the mid-line power flow function $F(\cdot)$ and thus LMPs achieve a revenue adequate market equilibrium as follows from Theorem 2.1. Similar results regarding revenue adequacy using the load over-satisfaction relaxation appear in previous work [77].

4.2.4 Characterizing Line Limits

The TCED problem (4.19) should enforce line limits that represent the physical abilities of the transmission line. For this reason it is appropriate to limit a real power quantity or current quantity using approximations outlined in the previous section. Unfortunately, such constraints are non-linear and may even be non-convex. This subsection explains how to enforce such limits by reformulating them to be in the standard form of constraints (4.19c), which place bounds on the voltage angle difference across each transmission line.

We will consider three types of line limits. Namely, limits on the real power flow enforced at the mid-point of the transmission line, limits on the squared current magnitude flowing into either side of the transmission line, and limits on the real-power loss across the transmission line. Remark 4.3 additionally explains that the apparent power flowing

into either side of a transmission line can be enforced using limits on the squared current magnitude flowing into either side of the transmission line. By reformulating these line limits to the same form as constraints (4.19c) this section implies that the TCED problem (4.19) encompasses all such limits without loss of generality.

4.2.4.1   Mid-Line Power Flow Limits

First consider real power flow limits enforced at the mid-point of the transmission line. Interpreted as lossless real power flow limits in the FND model from Section 4.1.3, these constraints are written as follows.

$$-\bar{F}_\ell \leq \check{F}_\ell(\Theta_\ell) \leq \bar{F}_\ell \tag{4.22}$$

We assume $\bar{F}_\ell$ is in the image of $\check{F}_\ell(\cdot)$ on the subdomain $\mathcal{D}_\ell$, denoted $\check{F}_\ell[\mathcal{D}_\ell]$. As a result, limits on the mid-line power flow are easy to enforce because the function $\check{F}_\ell(\cdot)$ is strictly monotonic on the specified subdomain. Define the function $\check{F}_\ell^{-1} : \check{F}_\ell[\mathcal{D}_\ell] \to \mathcal{D}_\ell$ as the inverse of $\check{F}_\ell(\cdot)$ on the specified subdomain. This inverse function is strictly monotonic on $\check{F}_\ell[\mathcal{D}_\ell]$, allowing constraints (4.22) to be written as follows. Notice that these constraints are in the same form as (4.19c).

$$\check{F}_\ell^{-1}(-\bar{F}_\ell) \leq \Theta_\ell \leq \check{F}_\ell^{-1}(\bar{F}_\ell) \tag{4.23}$$

4.2.4.2   Real Power Loss Limits

Line limits are typically chosen to prevent transmission lines from overheating. The production of heat is a direct result of the real-power loss across the line. For this reason it may be appropriate to limit the real-power loss across the transmission line. Such a constraint would be of the following form for a given line indexed by ℓ.

$$\check{L}_\ell(\Theta_\ell) \leq \bar{L}_\ell \tag{4.24}$$

where $\bar{L}_\ell$ is the constant real-power loss limit and is assumed to lie in the image of $\check{L}_\ell(\cdot)$ on the subdomain $\mathcal{D}_\ell$, denoted $\check{L}_\ell[\mathcal{D}_\ell]$. In fact, this constraint is convex because the function $\check{L}_\ell(\Delta\theta_\ell)$ is convex on the subdomain $\mathcal{D}_\ell$ and can be directly implemented into an economic

dispatch problem. However, this limit can also be enforced using simple bounds on the voltage angle difference across the line, as in constraints (4.19c).

Recall that $\check{L}_\ell(\cdot)$ is symmetric about the point ψ_ℓ and so constraint (4.24) can be written as $\check{L}_\ell(|\Theta_\ell - \psi_\ell| + \psi_\ell) \leq \bar{L}_\ell$. From definition 4.1, $\check{L}_\ell(\cdot)$ is strictly monotonically increasing on the subdomain $\mathcal{D}_{\ell+}$ and so it is invertible on this subdomain. Define $\check{L}_\ell^{-1} : \check{L}_\ell[\mathcal{D}_{\ell+}] \to \mathcal{D}_{\ell+}$ to be the inverse of the function $\check{L}_\ell(\cdot)$ restricted to the subdomain $\mathcal{D}_{\ell+}$. This inverse function is also strictly monotonically increasing on $\check{L}_\ell[\mathcal{D}_{\ell+}]$, allowing constraints (4.24) to be written as follows. Notice that this constraint can be easily placed in the same form as (4.19c).

$$|\Theta_\ell - \psi_\ell| + \psi_\ell \leq \check{L}_\ell^{-1}(\bar{L}_\ell) \tag{4.25}$$

4.2.4.3 Current Magnitude Limits

It may be more appropriate to limit the magnitude of the current flowing into the transmission line. A limit on the squared magnitude of the current flowing into the line is represented by the following constraint.

$$\check{\mathfrak{I}}_{ij}(\Theta_\ell) \leq \bar{\mathfrak{I}}_\ell^2 \tag{4.26}$$

where $\bar{\mathfrak{I}}_\ell$ is the constant current magnitude limit and $\bar{\mathfrak{I}}_\ell^2$ is assumed to lie in the image of $\check{\mathfrak{I}}_{ij}(\cdot)$ on the subset $\tilde{\mathcal{D}}_\ell$, denoted $\check{\mathfrak{I}}_{ij}[\tilde{\mathcal{D}}_\ell]$. Notice that $\check{\mathfrak{I}}_{ij}(\cdot)$ is symmetric about the point $-\phi_\ell + \psi_\ell$ and is strictly monotonically increasing on the domain $\tilde{\mathcal{D}}_{\ell+}$ and so it is invertible on this subdomain. Define $\check{\mathfrak{I}}_{ij}^{-1} : \check{\mathfrak{I}}_{ij}[\tilde{\mathcal{D}}_{\ell+}] \to \tilde{\mathcal{D}}_{\ell+}$ to be the inverse of the function $\check{\mathfrak{I}}_{ij}(\cdot)$ restricted to the subdomain $\tilde{\mathcal{D}}_{\ell+}$. This inverse function is also strictly monotonically increasing on $\check{\mathfrak{I}}_{ij}[\tilde{\mathcal{D}}_{\ell+}]$, allowing constraint (4.26) to be rewritten as constraint (4.27).

$$|\Theta_\ell + \phi_\ell - \psi_\ell| - \phi_\ell + \psi_\ell \leq \check{\mathfrak{I}}_{ij}^{-1}(\bar{\mathfrak{I}}_\ell^2) \tag{4.27}$$

This constraint can be easily placed in the same form as (4.19c).

$$-\check{\mathfrak{I}}_{ij}^{-1}(\bar{\mathfrak{I}}_\ell^2) + 2\psi_\ell - 2\phi_\ell \leq \Theta_\ell \leq \check{\mathfrak{I}}_{ij}^{-1}(\bar{\mathfrak{I}}_\ell^2) \tag{4.28}$$

Remark 4.3. Since voltage magnitudes are assumed fixed, the magnitude of current flowing into either side of a transmission line is proportional to the magnitude of the apparent power flowing into that side of the transmission line. Thus limits on the magnitude of apparent power flow (MVA limits) can be enforced using squared current magnitude limits (4.26) and (4.27).

4.3   Numerical Results

This section provides an empirical analysis of three realistically large test cases provided by version 6.0 of the MATPOWER toolbox in MATLAB [98]. The *3375wp* test case is a 3,375 bus representation of the Polish power system during the winter 2007-2008 winter evening peak with a total fixed demand of $48,362$ MW. The *2869pegase* test case is a 2,869 bus representation of the European high voltage transmission network with a total fixed demand of $132,437$ MW. The *6515rte* test case is a 6,515 bus representation of the French transmission network with a total fixed demand of $107,264$ MW. The two larger test cases are fully described in [47]. For each test case the MVA rating of each transmission line is interpreted as a current magnitude limit and line limits are enforced as in Section 4.2.4.3.

We consider six different optimization problems for each test case: the AC OPF problem, the exact TCED problem and four approximations to the exact TCED problem. Each optimization problem is solved by the interior-point algorithm provided by the MATLAB function FMINCON with user supplied analytical gradients/Hessians using a standard laptop with a 2.7 GHz processor. Due to the non-convexity of each problem, global optimality cannot be guaranteed in general and the interior point algorithm may converge to a local minimizer. That being said, we are able to verify that a global minimizer was identified for each of the four approximations for test cases *6515rte* and *2869pegase* by use of the load over-satisfaction relaxation.

The AC OPF problem fully captures the coupling of real and reactive power and optimizes over voltage magnitudes. At the optimal dispatch of the AC OPF problem, the operating cost of test cases *6515rte*, *2869pegase*, and *3375wp* are $\$109,767$, $\$133,993$, and $\$7,404,635$ respectively. The *exact* TCED problem (4.19) is defined by the exact expressions of each function provided earlier in this chapter (4.2), (4.8), (4.12) and (4.17) and is formu-

lated by fixing voltage magnitudes to the identified local minimizer of the AC OPF problem. As described in Remark 4.2, this problem should act as an approximation to the AC OPF problem but should obtain a lower optimal objective value. The identified local minimizer of the AC OPF problem is used to initialize the interior point algorithm for the exact TCED problem. The dispatch approximation error $\Delta G \in \mathbb{R}^n$ represents the difference between the identified optimal dispatch of the TCED problem of interest and that of the exact TCED problem. Similarly the objective approximation error ΔC represents the difference between $C(G)$ evaluated at the identified optimal dispatch of the TCED problem of interest and that of the exact TCED. Finally, $\Delta\lambda$ represents the difference between the identified price vector associated with the problem of interest and that of the TCED problem.

As explained in Section 4.2.3, the TCED problem and the relaxed TCED problem have the same global minimizer if the LMPs are positive. Furthermore, the relaxed TCED problem is convex when using any of the approximations to the mid-line power flow function in Section 4.1.4. This allows us to verify that the interior point methods identified global

Table 4.1: This table compares the solution of multiple different TCED problems to that of the exact TCED problem using three realistically large test cases. The error quantities are denoted with Δ and represent the difference between identified optimal quantities of the problem of interest and those of the exact TCED problem. The reported time is an average over 10 runs. The total dispatched generation for each problem is denoted $\mathbf{1}^\dagger G$.

Test Case	Aprx. Num.	Aprx. Eqns. $\check{F}_\ell$ / $\check{L}_\ell$ / $\check{J}_{ij}$ / T	ΔC ($)	$\mathbf{1}^\dagger G$ (MW)	$\|\Delta G\|_1$ (MW)	$\|\Delta G\|_\infty$ (MW)	mean($\lambda^\star$) ($/MW)	min($\lambda^\star$)/max($\lambda^\star$) ($/MW)	$\max_{i\in\mathbb{N}} \frac{\|\Delta\lambda_i\|}{\lambda_i^\star}$	$\|\Theta\|_\infty$ (rad)	time (sec)
6515 rte	Exact	(4.2)/(4.8)/(4.12)/(4.17)	0	109764	0	0	1.08	0.87 / 2.52	0	0.3822	10
	1	(4.3)/(4.9)/(4.14)/(4.17)	2.36	109762	159.29	31.06	1.08	0.87 / 2.53	0.0891	0.3730	8
	2	(4.4)/(4.10)/(4.15)/(4.17)	-184.57	109949	8622.52	658.90	1.07	0.97 / 1.43	0.4306	0.4255	8
	3	(4.5)/(4.11)/(4.16)/(4.17)	-72.21	109837	8793.72	664.70	1.07	0.97 / 1.41	0.4394	0.4254	24
	4	(4.5)/(4.11)/(4.16)/(4.18)	47.92	109717	8012.29	679.46	1.07	0.96 / 1.55	0.3829	0.4255	27
	AC OPF		-3.38	109768	908.16	103.87	1.08	0.56 / 2.48	0.5257	0.3822	152
2869 pegase	Exact	(4.2)/(4.8)/(4.12)/(4.17)	0	133982	0	0	1.02	0.99 / 1.12	0	0.2429	4
	1	(4.3)/(4.9)/(4.14)/(4.17)	2.14	133980	58.06	5.21	1.02	0.99 / 1.12	0.0011	0.2422	3
	2	(4.4)/(4.10)/(4.15)/(4.17)	-167.57	134150	2124.47	190.99	1.02	0.98 / 1.14	0.0330	0.2780	3
	3	(4.5)/(4.11)/(4.16)/(4.17)	-134.32	134117	1971.91	188.48	1.02	0.98 / 1.13	0.0177	0.2743	7
	4	(4.5)/(4.11)/(4.16)/(4.18)	-94.62	134077	3739.75	972.89	1.02	0.98 / 1.12	0.0132	0.2710	10
	AC OPF		-11.29	133993	581.57	22.25	1.02	0.99 / 1.11	0.0222	0.2438	6
3375 wp	Exact	(4.2)/(4.8)/(4.12)/(4.17)	0	49190	0	0	146.70	0.00 / 454.89	0	0.2639	8
	1	(4.3)/(4.9)/(4.14)/(4.17)	344.10	49188	32.79	16.58	146.66	0.00 / 454.58	0.9604	0.2624	5
	2	(4.4)/(4.10)/(4.15)/(4.17)	-33629.36	49266	2267.75	309.97	151.26	0.00 / 971.06	5.7514	0.2625	6
	3	(4.5)/(4.11)/(4.16)/(4.17)	-13737.40	49228	1011.08	245.73	149.27	0.00 / 460.28	1.6180	0.2726	6
	4	(4.5)/(4.11)/(4.16)/(4.18)	-7382.55	49184	911.03	244.28	148.55	0.00 / 459.67	539.2388	0.2612	7
	AC OPF		-8.43	49188	118.84	54.03	147.42	0.00 / 469.40	0.9943	0.2629	180

optima for test cases *6515rte* and *2865pegase* when using each of the four approximations to the exact TCED problem. However, we emphasize that this approach cannot always be taken in the case where there exists an LMP that is non-positive as in test case *3375wp*. See [77] for a description of the problems that may arise when LMPs are non-positive. In fact, the identified optimal dispatch for test case *3375wp* using the relaxed TCED problem results in a generation dispatch that does not satisfy real power balance with equality as in (4.19a). We found no large test cases with any strictly negative LMPs.

The remainder of this section analyzes Table 4.1, which provides detailed information about the six aforementioned optimization problems solved for each test case. The identified local minimizers of the AC OPF problem and the approximations 1-4 are directly compared to that of the exact TCED problem. Approximation 1 uses Taylor expansions to obtain a very accurate quadratically constrained program. Approximation 2 additionally assumes voltage magnitudes are nominal, tap ratios are nominal and shunt susceptances are much smaller than series susceptances. Approximation 3 additionally assumes that series resistances are much smaller than series reactances. Approximation 4 additionally uses the load distribution factor approximation with the LDFs chosen to allocate all losses to the slack bus, which is designated by each individual test case description. The third column of the table explicitly states the equations used in each approximation.

Remark 4.4. From Table 4.1, the voltage angle difference across each line falls well within the limits from Remark 4.1, which approximately constrains $|\Theta_\ell|$ to be lower than $\frac{\pi}{2} \approx 1.5707$.

4.3.1 TCED Problem vs. AC OPF

We begin by comparing the TCED problem (4.19) to the AC OPF problem provided by MATPOWER. Each test case follows the trend outlined in Remark 4.2. Specifically, the *exact* TCED problem acts as a relaxation to the AC OPF problem as it attains a lower optimal value. However, the optimal values of both problems are close to each other relative to the total system cost.

It is perhaps more important to analyze the difference in the generation dispatch between the exact TCED problem and the AC OPF problem. The 1-norm of the nodal dispatch approximation error, denoted $\|\Delta G\|_1$, is relatively small, realizing values of no more

than 1% of total system demand. In contrast, the infinity norm of the nodal dispatch error is potentially significant because it represents a MW value that is seen entirely by a single bus. In fact, marginal generators see the largest change in dispatch. The sum of all dispatched generation is denoted $\mathbf{1}^{\dagger}G$ and is similar across all approximations.

A similar conclusion can be drawn for the LMPs identified by both problems. In general LMPs are very similar for both problems, illustrated by nearly identical mean LMPs. However, the LMP at an individual bus may be significantly different between the problems as illustrated by the maximum normalized difference of nodal price denoted $\frac{|\Delta\lambda_i|}{\lambda_i^\star}$. Although this value is very small for test case *2869pegase*, at least one bus in test case *3375wp* has an LMP change of over 99% in magnitude.

4.3.2   Approximations of the Exact TCED Problem

Table 4.1 quantifies how well the solution of each TCED formulation approximates the solution of the exact formulation. Approximation 1 is the most accurate in terms of nodal dispatch and LMP approximation error. This is expected because only accurate Taylor expansion approximations are used.

Approximation 2 experiences a drastic increase in approximation error because it introduces multiple assumptions including nominal tap ratios, negligible shunt susceptances and nominal voltage magnitudes.

Approximation 3 additionally assumes $r_\ell \ll x_\ell$ and the resulting approximate loss function tends to underestimate real power losses as compared to approximation 2. This can be seen by noticing that the total dispatched generation is lower for approximation 3.

Approximation 4 is equivalent to approximation 3 but with all losses allocated to the slack bus. Notice that the nodal dispatch error has a large infinity norm, $\|\Delta G\|_\infty$, because the load profile changes significantly. For this reason approximation 4 can be very inaccurate. For example the 1-norm of the nodal dispatch error is nearly doubled in test case *2869pegase*. This underlines the concern about loss formulations having potentially adverse affect on particular generators due to the location of the slack bus.

4.4 Summary

This chapter derives a generalized non-convex TCED problem with marginal losses that consistently models flow and loss approximation, results in approximately correct outcomes and is proven to be reference bus independent. A hierarchy of approximations for this problem are outlined and common unnecessary assumptions are identified along with proper choices of "tuning parameters." For example, nodal loss allocation is derived from first principles to assign half losses of each line to its adjacent buses. Additionally, line limit constraints are derived in the form of current magnitude limits and mid-line power flow limits and are enforced as simple bounds on the voltage angle difference on each transmission line. Empirical results are provided that illustrate the general trend of increasing approximation error as more approximations are used. Furthermore, the identified local minimizer of the exact TCED problem is shown to very closely match the certified global minimizer of an approximate TCED problem solved via the load over-satisfaction relaxation. Certain approximations increase the error in price and dispatch outcomes; however, the approximation that allocates losses to the slack bus is very inaccurate and results in significant dispatch and LMP errors.

Each of the formulations in this chapter have been nonlinear and have been solved using a general interior-point method intended for nonlinear problems. The numerical results illustrated that these problems can be solved quickly (less than 30 seconds) even at large scale. In the next chapter, we consider linearized approximations that can be solved by large-scale linear programming software, which converges an order of magnitude faster than the solvers used for the nonlinear problems. Although easier to solve, these linear programs require more approximations to formulate. The next chapter additionally analyzes this approximation error.

Chapter 5

Linearly Constrained Economic Dispatch Problems

The underlying TCED problem derived in Chapter 4 is non-convex. Although the TCED problem can be represented as a convex problem when LMPs are positive using the load over-satisfaction relaxation, this technique cannot be used if LMPs are generally non-positive. For this and other reasons the non-convex TCED problem is typically approximated by the convex problem obtained by linearizing the constraints around some base-case state. Electricity prices and dispatch decisions are then chosen based on the resulting linearly-constrained economic dispatch (LCED) problem. Different LCED problems have been suggested in the literature and they are all derived using one of two linearization techniques, which we call *direct* and *indirect* linearization, respectively. Various formulations in the literature use Loss Distribution Factors (LDFs), as introduced in Section 1.1.2 and discussed in Section 4.2.1. An LCED problem often used in practice that uses LDFs as reported in [22] and [58] is derived using indirect linearization and is termed the *common LCED problem*. This chapter studies the assumptions required to recover the optimal dispatch of the non-convex TCED problem from the solution of the common LCED problem. We show that the common LCED problem may have multiple minimizers, in which case small perturbations of the base-case state may result in large dispatch approximation error. Furthermore, even if the base-case state matches a minimizer of the non-convex TCED problem, it is proven that there does not always exist a choice of LDFs such that the optimal dispatch of the TCED problem is also optimal for the common LCED problem. On the other hand, such LDFs do exist and are identified for the special case where no line limits are binding.

71

Despite the prevalence of the common LCED problem, no previous work has established a set of assumptions required to recover the optimal dispatch of the non-convex TCED problem from the common LCED problem. To establish such assumptions this chapter derives the common LCED problem from the non-convex TCED problem in Chapter 4 restricted to linear approximations of the mid-line power flow function, which we label as the *TCED problem with angles* or Optimization A (Opt. A). To illustrate the assumptions used to attain the common LCED problem, four intermediate problems, namely, Opt. B, C, D, and E, are also derived that are not individually novel but constitute a convenient route for the derivation. Figure 5.1 outlines the sequence of problems derived to attain the common LCED problem or Opt. F. This derivation ultimately proves that a specific dispatch that is optimal for the TCED problem with angles (Opt. A) is also optimal for the common LCED problem (Opt. F) under two key assumptions. This specific dispatch can be efficiently recovered from the common LCED problem (Opt. F) under the additional assumption that the common LCED problem has a unique optimal dispatch.
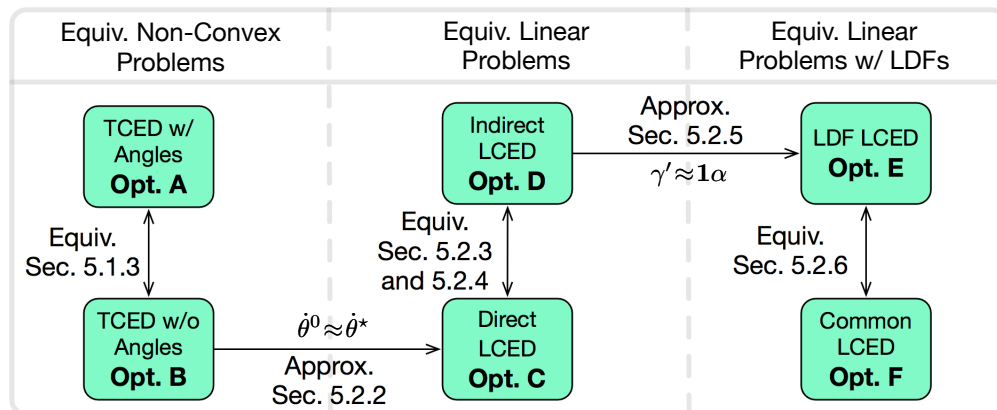
Figure 5.1: Diagram outlining the derivation structure of Chapter 5. Vertical connections with arrows pointing in both directions indicate equivalence of the two connected problems, meaning any dispatch that is optimal for one is also optimal for the other. Horizontal connections pointing in only one direction indicate that both problems share an optimal dispatch, namely the base-case dispatch, under the appropriate assumptions.

The derivation begins in Section 5.1 by eliminating voltage angles from the TCED problem with angles (Opt. A) yielding an ED problem that optimizes over generation dispatch and nodal loss allocation variables. This problem is termed the *TCED problem without*

angles (Opt. B) and is shown to be equivalent to the TCED problem with angles (Opt. A), where two problems are said to be *equivalent* if any dispatch that is optimal for one is also optimal for the other.

The fundamental linearization theory in [40] uses a first order Taylor expansion of the constraints with respect to all optimization variables about the base-case state and its associated base-case dispatch. We call this *direct linearization*. Section 5.2.2 derives the *direct LCED* problem (Opt. C) by applying direct linearization to the TCED problem without angles (Opt. B). The first key assumption, termed *Assumption 5.1*, requires the base-case dispatch to satisfy the Karush-Kuhn-Tucker (KKT) conditions and represent an optimal dispatch of the TCED problem without angles (Opt. B). A result from [40] can then be applied to show that the same base-case dispatch is optimal for the *direct LCED* problem (Opt. C). A related practical question is how close does the base-case state need to be to a minimizer of the underlying non-convex problem for the approximate LCED problem to result in a good dispatch approximation (See Remark 5.5).

Another approach is to linearize with respect to only the net real power injections using total derivatives of implicit functions. We call this *indirect linearization*. In fact, the common LCED problem (Opt. F) is derived using indirect linearization as in [21] and [58]. Section 5.2.3 derives the intermediate *indirect LCED* problem (Opt. D) by applying indirect linearization to the TCED problem without angles (Opt. B). Section 5.2.3 establishes equivalence of the indirect LCED problem (Opt. D) and the direct LCED problem (Opt. C), showing any dispatch that is optimal for one of these problems is also optimal for the other. Section 5.2.4 then explains how to compute the LMPs from Lagrange multipliers of the indirect LCED problem (Opt. D), which differ from those of the direct LCED problem (Opt. C). We additionally emphasize that the indirect linearization technique requires loss sensitivities to be computed as the solution of equations with a large Jacobian matrix during each market interval, e.g. every 5-15 minutes for the real-time market, which may be computationally burdensome.

Section 5.2.5 introduces LDFs to the indirect LCED problem (Opt. D) to obtain the *LDF LCED problem* (Opt. E). Section 5.2.5 additionally explains that under Assumption 5.1

there do not generally exist LDFs that allow the base-case dispatch to solve the LDF LCED problem. However, under the assumption that no line limits are binding such LDFs do exist and are identified in Section 5.2.5. The second key assumption, termed *Assumption 5.2*, effectively asserts that no line limits are binding.

Finally, Section 5.2.6 formulates the *common LCED problem* (Opt. F) by eliminating the loss allocation variables and introducing a single loss variable in their place. The *LDF LCED problem* (Opt. E) is shown to be equivalent to the common LCED problem (Opt. F). Furthermore, the derivation outlined in Figure 5.1 shows that the base-case dispatch is optimal for the common LCED problem under Assumptions 5.1 and 5.2. However, Section 5.2.7 emphasizes that the common LCED problem (Opt. F) may have multiple optimal dispatches, some of which may not be feasible for the TCED problem with angles (Opt. A). As a result, it may be difficult to recover an optimal dispatch of the TCED problem with angles (Opt. A) by solving the common LCED problem (Opt. F) using standard off-the-shelf optimization software. The third and final key assumption, termed *Assumption 5.3*, requires the common LCED problem (Opt. F) to have a unique optimal dispatch. Under Assumptions 5.1, 5.2, and 5.3 the base-case dispatch, which is optimal for the TCED problem with angles (Opt. A), is the unique optimal dispatch of the common LCED problem (Opt. F), and can be easily recovered.

Section 5.3 provides numerical results intended to illustrate two key findings that point out significant dispatch approximation errors may occur when certain assumptions are violated. The first key finding states that very small perturbations to the ideal base-case state can result in significantly large dispatch approximation error if the common LCED problem (Opt. F) has multiple minimizers. This is illustrated in Section 5.3.1 using an intuitive 2-bus example as well as a larger more realistic test case. The second key finding states that significant dispatch approximation error may occur when Assumption 5.2 is violated, even if Assumptions 5.1 and 5.3 hold. This is illustrated in Section 5.3.2 using an intuitive 3-bus example that is highly resistive and heavily congested. However, a larger more realistic test case is used to illustrate that violating Assumption 5.2 typically results in insignificant dispatch approximation error.

5.1 Transmission Constrained Economic Dispatch

We begin by reiterating previously established notation from Chapter 2. Lower case subscripts are used to indicate elements of matrices. For example the element in the ith row and j^{th} column of matrix M is denoted $M_{i,j}$. The ith column of matrix M is denoted M_i. The transpose of a matrix is denoted with a superscript $\dagger$, for example $M^\dagger$, and a superscript $-\dagger$ represents the inverse transpose of a matrix. The set of n dimensional real numbers is denoted $\mathbb{R}^n$. A vector $v \in \mathbb{R}^n$ is designated a column vector and its ith element is denoted v_i. The element-wise absolute value of a matrix or vector is denoted $|M|$ or $|v|$ respectively. The identity matrix, the matrix of all zeros, and the matrix of all ones are denoted $\mathbf{I}$, $\mathbf{0}$, and $\mathbf{1}$ respectively and are of appropriate dimension. The branch-bus incidence matrix of the graph $\mathcal{G}$ is denoted $A \in \mathbb{R}^{m \times n}$. Specifically, A is sparse and the row representing line k connecting bus i to bus j has element i equal to 1 and element j equal to -1. In this context bus i is arbitrarily assigned to be the *sending bus* and power flow is designated positive when flowing from bus i to bus j.

5.1.1 Transmission-Constrained Economic Dispatch with Angles

The Transmission-Constrained Economic Dispatch (TCED) problem (4.19) from Section 4.2.2 with a linear form of the mid-line power flow function $F(\cdot)$ is adopted. This problem optimizes over the nodal generation dispatch vector $G \in \mathbb{R}^n$ and the vector of voltage angles excluding the known angle at the bus $\rho \in \mathbb{N}$, which will be termed the *angle reference bus*. A dot over a vector represents that vector with element ρ removed. For example the vector of voltage angles is denoted $\theta \in \mathbb{R}^n$ and the vector of voltage angles excluding the angle at the angle reference bus is denoted $\dot{\theta} \in \mathbb{R}^{n-1}$. Similarly, a dot over a matrix represents that matrix with column ρ removed. For example, the matrix $\dot{A} \in \mathbb{R}^{m \times (n-1)}$ is equivalent to A with column ρ removed.

The *TCED problem with angles* (Opt. A) is written as follows. Voltage magnitudes are assumed constant and all equal to one per unit. The nodal demand is considered fixed and is represented by $D \in \mathbb{R}^n$. The cost of generation is represented by the function $C(G) := \sum_{i \in \mathbb{N}} C_i(G_i)$ where $C : \mathbb{R}^n \to \mathbb{R}$ is assumed convex.

$$\min_{P \in \mathbb{R}^n, \dot{\theta} \in \mathbb{R}^{n-1}} \quad C(G) \tag{Opt. A}$$

$$st : \tfrac{1}{2} |A|^\dagger L(\dot{A}\dot{\theta}) + H^\dagger \dot{\theta} = G - D \tag{A1}$$

$$\underline{G} \leq G \leq \bar{G} \tag{A2}$$

$$\underline{F} \leq B\dot{A}\dot{\theta} \leq \bar{F} \tag{A3}$$

Constraint (A1) represents the real power balance at each bus in the system as in constraint (4.19a). The vector valued loss function is denoted $L : \mathbb{R}^m \to \mathbb{R}^m$ and maps voltage angle differences to line losses. This function is assumed to be convex on the domain of the problem and is assumed to be continuously differentiable. Half of each line's losses are assigned to its incident buses as Fictitious Nodal Demand (FND) as in Chapter 4. In the interest of deriving a linearly-constrained economic dispatch problem, we assume a linear approximation of the mid-line power flow function described in Section 4.1.4 and represented by $H^\dagger \dot{\theta}$, where $H := \dot{A}^\dagger BA$ is termed the *reduced weighted Laplacian matrix* and represents the weighted Laplacian matrix of the underlying system graph with row ρ removed. In the expression for H, the matrix $B \in \mathbb{R}^{m \times m}$ is full rank and diagonal where the diagonal elements represent the edge weights of the underlying system graph and can be interpreted as transmission line susceptances. Constraint (A2) enforces generator output limits and constraint (A3) enforces line limits in the form of mid-line power flow limits as described in Section 4.2.4.1.

Remark 5.1. The *lossless DC OPF problem* is identical to the TCED problem with angles (Opt. A) if the loss function $L(\cdot)$ is replaced by the zero vector $\mathbf{0}$. This lossless DC OPF problem is linearly constrained, convex, and easy to solve.

5.1.2 General TCED Problem without Angles

Many references, e.g. [21] and [58], analyze the energy market with respect to an economic dispatch problem that optimizes over dispatch and loss variables. We will derive four such problems that optimize over the nodal dispatch vector and a nodal loss allocation vector $N \in \mathbb{R}^n$. These four problems, Opt. B, C, D, and E respectively, can each be expressed as the following *general TCED problem without angles*. The *price reference bus* (or slack

bus) is designated as bus $\sigma \in \mathbb{N}$. Throughout this chapter a ring over a vector represents that vector with element σ removed. Similarly, a ring over a matrix represents that matrix with column σ removed, e.g. $\mathring{A}$.

$$\min_{G \in \mathbb{R}^n, N \in \mathbb{R}^n} \quad C(G) \qquad \qquad (\text{Opt. } j)$$

$$st : \mathbf{1}^\dagger (G - D - N) = 0 \qquad \qquad (j1)$$

$$\Lambda_j(\mathring{P}, N; \mathring{D}) = \mathbf{0} \qquad \qquad (j2)$$

$$\underline{G} \leq G \leq \bar{G} \qquad \qquad (j3)$$

$$\underline{F} \leq S(\mathring{G} - \mathring{D} - \mathring{N}) \leq \bar{F} \qquad \qquad (j4)$$

Constraint $(j1)$ represents real power balance. Constraint $(j3)$ represents generator output limits. Constraint $(j4)$ represents limits on the mid-line power flow on each transmission line expressed in terms of shift factors $S := B \mathring{A} \mathring{H}^{-\dagger}$. Note that the matrix $\mathring{H}$ is invertible under the standard assumption that the system graph is fully connected. The nodal loss allocation constraint $(j2)$ incorporates a general function $\Lambda_j(\cdot, \cdot; \mathring{D}) : \mathbb{R}^{n-1} \times \mathbb{R}^n \to \mathbb{R}^n$, which takes the constant parameter $\mathring{D} \in \mathbb{R}^{n-1}$ as an additional argument. This general function will be defined differently for each of the next four optimization problems formulated in this chapter. These four problems will be differentiated by j taking values B, C, D, and E.

Remark 5.2. Opt. j has one more decision variable and equality constraint than Opt. A. Opt. j is also conveniently formulated because there is one linear *overall* real power balance constraint and all non-convexity is concentrated to constraint $(j2)$.

The Lagrangian function is central to the First Order Necessary Conditions (FONCs) for optimality. The Lagrangian function of Opt. j is written as follows. The arguments of this function are partitioned into three categories, namely: primal variables, dual variables, and constant parameters. An equation number is assigned to each term for future reference.

$$\Phi_j(N, G; \kappa, \gamma, \bar{\mu}, \underline{\mu}, \bar{\beta}, \underline{\beta}; D) := \tag{5.1}$$

$$C(G) \tag{5.1a}$$

$$+ \kappa \mathbf{1}^\dagger (-G + D + N) \tag{5.1b}$$

$$+ \gamma^\dagger \Lambda_j(\mathring{G}, N; \mathring{D}) \tag{5.1c}$$

$$+ \underline{\beta}^\dagger (\underline{G} - G) \tag{5.1d}$$

$$+ \bar{\beta}^\dagger (G - \bar{G}) \tag{5.1e}$$

$$+ \bar{\mu}^\dagger \left(S(\mathring{G} - \mathring{D} - \mathring{N}) - \bar{F} \right) \tag{5.1f}$$

$$+ \underline{\mu}^\dagger \left(\underline{F} - S(\mathring{G} - \mathring{D} - \mathring{N}) \right). \tag{5.1g}$$

Here the Lagrangian function is defined with: $\kappa \in \mathbb{R}$ representing the Lagrange multiplier of the overall real power balance constraint $(j1)$; $\gamma \in \mathbb{R}^n$ representing the Lagrange multipliers of the nodal loss allocation constraint $(j2)$; $(\bar{\beta}, \underline{\beta}) \in \mathbb{R}^n \times \mathbb{R}^n$ representing the Lagrange multipliers of the generator output constraint $(j3)$; and $(\bar{\mu}, \underline{\mu}) \in \mathbb{R}^m \times \mathbb{R}^m$ representing the Lagrange multipliers of the line limit constraint $(j4)$.

The KKT conditions for some pair of primal variables (G, N) require the existence of corresponding Lagrange multipliers that jointly satisfy the primal feasibility, dual feasibility, complementary slackness, and stationarity conditions [5]. Primal feasibility requires the primal variables to satisfy constraint $(j1)$-$(j4)$. Dual feasibility requires the dual variables associated with inequality constraints $\bar{\beta}, \underline{\beta}, \bar{\mu}$ and $\underline{\mu}$ to be non-negative. Complementary slackness requires each of the terms (5.1d)-(5.1g) to equate to zero. The stationarity condition requires the partial derivative of the Lagrangian function to be zero with respect to the primal variables G and N. The stationarity condition is as follows, where the partial derivatives of Φ_j with respect to N_σ, G_σ, $\mathring{N}$, and $\mathring{G}$ are represented by (5.2), (5.3), (5.4), and (5.5) respectively:

$$0 = \kappa + \nabla_{N_\sigma} \Lambda_j(\mathring{G}, N; \mathring{D})\gamma, \tag{5.2}$$

$$0 = \nabla_{G_\sigma} C(G) - \kappa + \bar{\beta}_\sigma - \underline{\beta}_\sigma, \tag{5.3}$$

$$\mathbf{0} = \kappa\mathbf{1} + \nabla_{\mathring{N}} \Lambda_j(\mathring{G}, N; \mathring{D})\gamma + S^\dagger(\underline{\mu} - \bar{\mu}), \tag{5.4}$$

$$\mathbf{0} = \nabla_{\mathring{G}} C(G) - \kappa\mathbf{1} + \nabla_{\mathring{G}} \Lambda_j(\mathring{G}, N; \mathring{D})\gamma - S^\dagger(\underline{\mu} - \bar{\mu}) + \bar{\mathring{\beta}} - \underline{\mathring{\beta}}. \tag{5.5}$$

5.1.3 Transmission-Constrained Economic Dispatch without Angles

By choosing the function Λ_j appropriately Opt. j can be made equivalent to the *TCED problem with angles* (Opt. A) in that any optimal dispatch for one of these problems is also optimal for the other. In particular, Sections 5.1.3.1-5.1.3.3 show that Opt. A is equivalent to the following *TCED problem without angles.*

Optimization B. The *TCED problem without angles* is defined to be Opt. j with Λ_j specified by:

$$\Lambda_{\mathrm{B}}(\mathring{G}, N; \mathring{D}) := N - \tfrac{1}{2} |A|^\dagger L \left(\dot{A} \mathring{H}^{-\dagger}(\mathring{G} - \mathring{D} - \mathring{N}) \right). \tag{5.6}$$

Sections 5.1.3.1 through 5.1.3.3 derive the TCED problem without angles (Opt. B) from the TCED problem with angles (Opt. A). Each step taken in the reformulation preserves the set of feasible dispatch variables G, implying any dispatch that is optimal for one of these problems is also optimal for the other. Both problems additionally have the same optimal objective value and as a result the sensitivity of the optimal objective value with respect to D is the same for both problems under the assumption that the sensitivity is well defined.

5.1.3.1 Loss Allocation Vector

We first introduce the nodal loss allocation vector $N \in \mathbb{R}^n$ as a decision variable in Opt. A along with the constraint:

$$N = \tfrac{1}{2} |A|^\dagger L(\dot{A}\dot{\theta}). \tag{5.7}$$

5.1.3.2 Real Power Balance Constraint

By (5.7), we can replace the first term in the real power balance constraint (A1) in Section 5.1.1 by N to obtain:

$$N + H^\dagger \dot\theta = G - D. \tag{5.8}$$

Note that $H\mathbf{1} = 0$, left multiply the LHS and RHS of (5.8) by the full rank matrix $[\mathbf{1}, \mathring{\mathbf{I}}]^\dagger$ and re-arrange to obtain:

$$
\begin{aligned}
0 &= \mathbf{1}^\dagger (G - D - N), \tag{5.9} \\
\mathring{H}^\dagger \dot\theta &= \mathring{G} - \mathring{D} - \mathring{N}. \tag{5.10}
\end{aligned}
$$

Since $[\mathbf{1}, \mathring{\mathbf{I}}]^\dagger$ is full rank, constraints (5.9) and (5.10) hold if and only if constraint (5.8) holds. Since $\mathring{H}$ is invertible, constraint (5.10) can be re-arranged to:

$$\dot\theta = \mathring{H}^{-\dagger} (\mathring{G} - \mathring{D} - \mathring{N}). \tag{5.11}$$

5.1.3.3 Eliminate Voltage Angles

In summary, we first introduced constraint (5.7) along with variable N. We then replaced the real power balance constraint (A1) from Section 5.1.1 with equivalent constraints (5.11) and (5.9). We now substitute the expression for $\dot\theta$ from constraint (5.11) into constraints (5.7) and (A3). The resulting optimization problem is equivalent to Opt. B but with additional constraint (5.11). Since $\dot\theta$ is otherwise unconstrained, constraint (5.11) can be removed resulting in Opt. B.

Definition 5.1. Let the generation dispatch $G^\star$ and the nodal loss allocation $N^\star$ represent a local minimizer of the TCED problem without angles (Opt. B) with associated Lagrange multipliers $\kappa^\star$, $\gamma^\star$, $\bar\mu^\star$, $\underline\mu^\star$, $\bar\beta^\star$, and $\underline\beta^\star$ that solve the KKT conditions for the TCED problem without angles (Opt. B) under the assumption that such a local minimizer exists.

5.1.4   Locational Marginal Prices

The Locational Marginal Prices (LMPs), denoted $\lambda^\star$, are defined to be the partial derivative of the Lagrangian function with respect to the demand vector D:

$$\lambda^\star := \nabla_D \Phi_{\mathrm{B}}(N^\star, G^\star; \kappa^\star, \gamma^\star, \bar{\mu}^\star, \underline{\mu}^\star, \bar{\beta}^\star, \underline{\beta}^\star; D). \tag{5.12}$$

where Φ_{B} represents the Lagrangian function (5.1) for the TCED problem without angles (Opt. B). The LMP can be decomposed as $\lambda^\star := e + l + c$, where e is the energy component associated with Lagrange multiplier κ, l is the loss component associated with Lagrange multipliers γ, and c is the congestion component associated with Lagrange multipliers $(\bar{\mu}, \underline{\mu})$. The congestion and loss components of the LMP at the price reference bus are zero, that is $c_\sigma := 0$ and $l_\sigma := 0$. The remaining LMP components are explicitly written as follows:

$$e := \kappa^\star \mathbf{1}, \tag{5.13}$$

$$\mathring{l} := \tfrac{1}{2} \mathring{H}^{-1} \mathring{A}^\dagger \nabla L(\mathring{A} \mathring{\theta}^\star) \, |A| \, \gamma^\star, \tag{5.14}$$

$$\mathring{c} := S^\dagger (\underline{\mu}^\star - \bar{\mu}^\star). \tag{5.15}$$

where $\mathring{\theta}^\star = \mathring{H}^{-\dagger}(\mathring{G}^\star - \mathring{D} - \mathring{N}^\star)$.

Remark 5.3. As explained in Section 5.1.3 the sensitivity of the optimal objective value with respect to D is the same for Opt. A and Opt. B under the assumption that the sensitivity is well defined. This implies that the LMPs for both problems are the same. Furthermore, Opt. A is a special case of the TCED problem (4.19), with the mid-line power flow function restricted to a linear form. As a result, Opt. B and the TCED problem (4.19) have the same LMPs when the mid-line power flow function is restricted to a linear form.

Remark 5.4. The loss and congestion components of the LMP are zero at the price reference bus highlighting the dependency of these components of the LMP on the choice of price reference bus. On the other hand, the LMP is not dependent on the choice of price reference bus as explained in Section 4.2.2 with respect to the TCED problem (4.19).

5.1.5   FTRs and Congestion Revenue Adequacy

The TCED problem without angles (Opt. B) is non-convex. ISOs governed by FERC intend to solve this problem by linearizing the non-linear constraints of the TCED problem

without angles (Opt. B) around some base-case state resulting in a convex LCED problem as will be discussed elaborately in the next section. It is important to note that the congestion revenue adequacy guarantee from Section 2.5 does not apply to the TCED problem without angles (Opt. B) or to the LCED problems in the next section. Specifically, the revenue adequacy guarantee from Section 2.5 does not hold for Opt. B because it is non-convex. Furthermore, the revenue adequacy guarantee from Section 2.5 does not apply to the LCED problems in the next section because the base-case state changes on a day-to-day basis and the SFCs must be fixed at the time of the FTR auction, which may occur months or even years in advance of market clearing. For this reason and others, ISOs governed by FERC do not consider losses when defining the SFCs. Specifically, the SFCs are defined by the following polytope, which matches the line limit constraints ($j4$) and power balance constraints ($j1$). Notice that this definition of the SFCs is convex and does not depend on the base-case state, allowing it to be fixed far in advance of the market clearing.

$$\mathcal{T} := \left\{ f \in \mathbb{R}^n : \underline{F} \le S\mathring{f} \le \bar{F} \ \text{ and } \ \mathbf{1}^\dagger f = 0 \right\}. \tag{5.16}$$

As explained in Remark 2.2, electricity markets today require each FTR allocation vector $f^{(\xi)}$ to be *balanced* in the sense that the elements sum to zero, e.g. $\mathbf{1}^\dagger f^{(\xi)} = 0$. This requirement is possible to enforce because the SFCs are lossless as in (5.16), which requires $\mathbf{1}^\dagger f = 0$.

ISOs in the US typically price FTRs based on the congestion component c of the LMP defined by (5.15) as opposed to the LMP $\lambda^\star$ defined by (5.12). In this case, the payoff received by the FTR holder will be very close to the value $-\lambda^{\star\dagger} f^{(\xi)}$ under the assumption that the loss component of the LMP l is very small. To see this, notice that $-\lambda^{\star\dagger} f^{(\xi)} = -(c+l)^\dagger f^{(\xi)}$ because $e^\dagger f^{(\xi)} = 0$ when the FTR allocation vector is balanced $\mathbf{1}^\dagger f^{(\xi)} = 0$. For this reason, FTRs can still be used to approximately hedge the LMP uncertainty as described intuitively in Section 2.2.3. More specifically, FTRs in practice can only be used to hedge the congestion component of the LMP c and not the loss component of the LMP l.

In this section, the congestion revenue remains $\lambda^{\star\dagger}(D-G)$ as previously stated in (2.3); however, the total FTR payoff now differs from Section 2.2.3 and is now written as $-c^\dagger f$. As a result, we must give a congestion revenue adequacy guarantee that differs from the guarantee provided in Section 2.5. This subsection will provide a different revenue adequacy

guarantee that accommodates this alternative payoff. Specifically, the following theorem states that the total FTR payoff is upper bounded by the congestion revenue under the condition that the LMPs are non-negative. This theorem can be applied when using the SFCs defined in (5.16) along with FTR payoffs defined by $-c^\dagger f$. Reference [40] provides a similar revenue adequacy guarantee and also explains intuitively why the potential congestion revenue shortfall (PCRS) is typically small when prices are negative.

Theorem 5.1. Suppose the FTR allocation satisfies the SFCs so that $f \in \mathcal{T}$ where $\mathcal{T}$ is defined in (5.16). Let the point $(G^\star, N^\star)$ satisfy the KKT conditions of the TCED problem without angles (Opt. B). If the LMPs $\lambda^\star$ as defined in (5.12) are all non-negative, then the congestion revenue $\lambda^{\star\dagger}(D - G^\star)$ is greater than or equal to the FTR payoff $c^\dagger f$, where c is the congestion component of the LMP as defined in (5.15).

$$f \in \mathcal{T} \quad and \quad \lambda^\star \geq \mathbf{0} \Rightarrow \lambda^{\star\dagger}(D - G^\star) \geq c^\dagger f$$

Proof: See Appendix B.

It also is important to recognize that FTR payoffs $-c^\dagger f^{(\xi)}$ do not depend on the choice of angle reference bus ρ or slack reference bus σ if the FTR allocations vectors $f^{(\xi)}$ are balanced. Proof of this is not provided in this dissertation, see [58] for a discussion of this issue. Reference [58] explains that the congestion component of the LMP c at any given bus will depend on the choice of slack reference bus σ; however, the differences across busses, e.g. Ac, will not.

5.2 Linearly Constrained Economic Dispatch

The economic dispatch problems formulated in the previous section are non-convex and may be difficult to solve. For this reason it is typical for ISOs to use approximations that result in a convex problem. Today ISOs use linearization techniques to simplify non-convex economic dispatch problems into convex linearly-constrained problems. In this section we present a sequence of four linearly-constrained economic dispatch problems, respectively, Opt. C, D, E, and F, ultimately resulting in the common LCED problem (Opt. F) used in [21]

and [58]. Presenting the sequence of problems highlights the nature of the approximations used in practice.

Section 5.2.1 describes linearization about a base-case state, which is fundamental to all of the linearization approaches. Section 5.2.2 derives the *direct LCED* problem (Opt. C), which serves as an approximation to the TCED problem without angles (Opt. B) as explained by a result from [40]. Section 5.2.3 introduces the *indirect LCED problem* (Opt. D) and proves that it is equivalent to Opt. C. Section 5.2.4 then explains how to compute the loss component of the LMP from Lagrange multipliers of the indirect LCED problem (Opt. D). LDFs are then introduced to the indirect LCED problem in Section 5.2.5 to obtain the *LDF LCED problem* (Opt. E). This problem is shown to be a good approximation of the indirect LCED problem under the additional assumption that no line limits are binding. The *common LCED problem* (Opt. F) is derived in Section 5.2.6 and is shown to be equivalent to the LDF LCED problem (Opt. E). Section 5.2.7 then introduces a uniqueness assumption required to efficiently recover an optimal dispatch of the TCED problem with angles (Opt. A).

5.2.1 Linearization about Base-Case State

The linearization procedure will use a first order approximation around a base-case state $\dot{\theta}^0$. Associated with the base-case state are the base-case nodal loss allocation vector $N^0 := \frac{1}{2}|A|^{\dagger}L(\dot{A}\dot{\theta}^0)$ and the base-case generation dispatch vector $G^0 := H^{\dagger}\dot{\theta}^0 + N^0 + D$. Note that by construction the base-case values $\dot{\theta}^0$ and G^0 satisfy all equality constraints in Opt. A and the base-case values N^0 and G^0 satisfy all equality constraints in Opt. B.

In the real-time market the base-case state is often chosen to match the output of the state estimator. Similarly, in the day ahead market the base-case state is often chosen by predicting the future system state based on historical data. However, other choices of base-case state are used in practice. For example, another common method constructs a base-case state from the optimal dispatch of an alternative form of the economic dispatch problem [21]. A simple example of an alternative form of the economic dispatch problem is the lossless DC OPF problem. Note that previous work has concluded that a minimizer of the lossless DC OPF problem can be used as the base-case to effectively approximate

losses [79].

5.2.2 Direct Linearization

Reference [40] suggests directly linearizing the nodal loss allocation constraint $\Lambda_{\mathrm{B}}(\mathring{G}, N; \mathring{D}) = \mathbf{0}$ with respect to decision variables $\mathring{G}$ and N using a first order Taylor expansion. The gradient of the LHS with respect to $\mathring{G}$ is $-\frac{1}{2}\mathring{H}^{-1}\dot{A}^{\dagger}\nabla L(\dot{A}\dot{\theta}^0)|A|$ and the gradient of the LHS with respect to $\mathring{N}$ is $\mathbf{\mathring{I}}^{\dagger} + \frac{1}{2}\mathring{H}^{-1}\dot{A}^{\dagger}\nabla L(\dot{A}\dot{\theta}^0)|A|$. With this in mind, the direct LCED problem is defined as follows.

Optimization C. The *direct LCED problem* is defined to be Opt. j with Λ_j specified by:

$$\Lambda_{\mathrm{C}}(\mathring{G}, N; \mathring{D}) := N - \tfrac{1}{2}|A|^{\dagger}L\left(\dot{A}\mathring{H}^{-\dagger}(\mathring{G}^0 - \mathring{D} - \mathring{N}^0)\right)$$
$$- \tfrac{1}{2}|A|^{\dagger}\nabla L^{\dagger}(\dot{A}\dot{\theta}^0)\dot{A}\mathring{H}^{-\dagger}((\mathring{G} - \mathring{G}^0) - (\mathring{N} - \mathring{N}^0)). \tag{5.17}$$

Note that with the specification of Λ_{C} as in (5.17), Opt. C has linear constraints. With cost function $C(\cdot)$ assumed convex, Opt. C is a convex problem. If the cost function $C(\cdot)$ is linear, then Opt. C is a linear program.

The following assumption provides conditions under which an optimal dispatch of the TCED problem without angles (Opt. B) is also optimal for the direct LCED problem (Opt. C).

Assumption 5.1. *The base-case dispatch and nodal loss allocation vectors (G^0, N^0) represent a local minimizer of the TCED problem without angles (Opt. B) and solve the KKT conditions for the TCED problem without angles (Opt. B) along with some Lagrange multipliers κ^0, γ^0, $\bar{\mu}^0$, $\underline{\mu}^0$, $\bar{\beta}^0$, and $\underline{\beta}^0$.*

We will employ this assumption for the remainder of this section. Notice that the LMPs are well defined under Assumption 5.1 and are expressed as in Section 5.1.4. Under Assumption 5.1, [40] proves that (G^0, N^0) along with Lagrange multipliers κ^0, γ^0, $\bar{\mu}^0$, $\underline{\mu}^0$, $\bar{\beta}^0$, $\underline{\beta}^0$ satisfy the KKT conditions for the direct LCED problem (Opt. C), implying that the base-case dispatch P^0 is optimal for the direct LCED problem, which is a convex program with linear constraints as mentioned above. This result is easy to verify by noting that

these values satisfy the stationarity condition and the primal feasibility condition for both problems. Additionally note that the dual feasibility condition and complementary slackness conditions are identical for both problems.

Remark 5.5. A base-case state $\dot{\theta}^0$ satisfying Assumption 5.1 is termed an *ideal base-case state*. However, in practice Assumption 5.1 will only be approximately true and the base-case values (G^0, N^0) will fall in the vicinity of a minimizer of the TCED problem without angles (Opt. B). Section 5.3 explains the conditions under which this is a reasonable approximation. Specifically, Section 5.3.1 studies test cases where this approximation does not work well and Section 5.3.2 studies test cases where this approximation does work well.

5.2.3   Indirect Linearization

In this section we take another approach, similar to that of [21] and [58], by deriving loss sensitivities with respect to nodal net real power injections about the base-case state. To do this we must first define the nodal loss allocation as an implicit vector valued function of the net real power injections at the non-price reference buses $\tilde{N} : \mathbb{R}^{n-1} \to \mathbb{R}^n$. The vector of net real power injections is denoted $T \in \mathbb{R}^n$ and is interpreted as the generation dispatch vector less the demand vector $G - D$. The function $\tilde{N}$ is defined implicitly by the relationship between N and $\mathring{G} - \mathring{D}$ in the constraint $\Lambda_\mathrm{B}(\mathring{G}, N; \mathring{D}) = \mathbf{0}$ from the TCED problem without angles (Opt. B), and therefore satisfies:

$$\tilde{N}(\mathring{T}) := \tfrac{1}{2}|A|^\dagger L \left(\dot{A} \mathring{H}^{-\dagger}(\mathring{T} - \mathring{\tilde{N}}(\mathring{T})) \right). \tag{5.18}$$

The *loss sensitivity matrix* is denoted $\nabla \tilde{N} : \mathbb{R}^{n-1} \to \mathbb{R}^{(n-1) \times n}$ and is defined to be the Jacobian of $\tilde{N}$ with respect to its argument. The nodal loss allocation vector can then be approximated using a simple first order Taylor expansion of the function $\tilde{N}(\mathring{T})$ evaluated at the base-case net real power injections $\mathring{T}^0 := \mathring{G}^0 - \mathring{D}$. The indirect LCED problem is as follows.

Optimization D. The *indirect LCED problem* is defined to be Opt. j with Λ_j specified by:

$$\Lambda_\mathrm{D}(\mathring{G}, N; \mathring{D}) := N - \tilde{N}(\mathring{G}^0 - \mathring{D}) - \nabla \tilde{N}(\mathring{G}^0 - \mathring{D})^\dagger (\mathring{G} - \mathring{G}^0). \tag{5.19}$$

86

We derive the loss sensitivity matrix $\nabla\tilde{N}$ in Theorem 5.2 below. Theorem 5.2 allows us to prove equivalence of linear constraints $\Lambda_{\mathrm{C}}(\mathring{G}, N; \mathring{D}) = \mathbf{0}$ and $\Lambda_{\mathrm{D}}(\mathring{G}, N; \mathring{D}) = \mathbf{0}$. Specifically, these constraints are equivalent in that one constraint holds if and only if the other holds. This can be proven algebraically by substituting the expression for the loss sensitivity matrix, $\nabla\tilde{N}$, from Theorem 5.2 into the expression for $\Lambda_{\mathrm{D}}(\mathring{G}, N; \mathring{D})$ from (5.19). As a result, the direct LCED problem (Opt. C) and the indirect LCED problem (Opt. D) are equivalent in that any optimal dispatch of one of these problems is also optimal for the other. Also notice that computing the loss sensitivity matrix, $\nabla\tilde{N}$, requires the inversion of a large Jacobian matrix.

Theorem 5.2. *Assuming the matrix* $\mathbf{I} + \frac{1}{2}\mathring{H}^{-1}\mathring{A}^{\dagger}\nabla L(\mathring{A}\mathring{\theta}^0)|\mathring{A}|$ *is invertible, the columns of the loss sensitivity matrix evaluated at* $\mathring{T}^0$ *corresponding to the non-price reference buses are expressed as:*

$$\nabla\mathring{\tilde{N}}(\mathring{T}^0) = \tfrac{1}{2}\mathring{H}^{-1}\mathring{A}^{\dagger}\nabla L(\mathring{A}\mathring{\theta}^0)|\mathring{A}|(\mathbf{I} + \tfrac{1}{2}\mathring{H}^{-1}\mathring{A}^{\dagger}\nabla L(\mathring{A}\mathring{\theta}^0)|\mathring{A}|)^{-1}.$$

The column of the loss sensitivity matrix evaluated at $\mathring{T}^0$ *corresponding to the price reference bus is expressed as:*

$$\nabla\tilde{N}_{\sigma}(\mathring{T}^0) = \tfrac{1}{2}(\mathbf{I} - \nabla\mathring{\tilde{N}}(\mathring{T}^0))\mathring{H}^{-1}\mathring{A}^{\dagger}\nabla L(\mathring{A}\mathring{\theta}^0)|A_{\sigma}|.$$

Proof: Differentiating all rows of (5.18) excluding the price reference bus around the point $\mathring{T}^0$ yields the following:

$$\nabla\mathring{\tilde{N}}(\mathring{T}^0) = \tfrac{1}{2}\mathring{H}^{-1}\mathring{A}^{\dagger}\nabla L(\mathring{A}\mathring{\theta}^0)|\mathring{A}| - \tfrac{1}{2}\nabla\mathring{\tilde{N}}(\mathring{T}^0)\mathring{H}^{-1}\mathring{A}^{\dagger}\nabla L(\mathring{A}\mathring{\theta}^0)|\mathring{A}|.$$

Algebraic manipulation yields the following and the result then follows by the assumption on invertibility:

$$\nabla\mathring{\tilde{N}}(\mathring{T}^0)(\mathbf{I} + \tfrac{1}{2}\mathring{H}^{-1}\mathring{A}^{\dagger}\nabla L(\mathring{A}\mathring{\theta}^0)|\mathring{A}|) = \tfrac{1}{2}\mathring{H}^{-1}\mathring{A}^{\dagger}\nabla L(\mathring{A}\mathring{\theta}^0)|\mathring{A}|.$$

Differentiating the row of (5.18) corresponding to the price reference bus yields the expression for $\nabla\tilde{N}_{\sigma}(\mathring{T}^0)$. $\qquad\square$

5.2.4 Equivalent Loss Component of LMP

The expression for the loss component of the LMP in terms of the Lagrange multipliers of the indirect LCED problem (Opt. D) evaluated at the base-case point (G^0, N^0) is as follows:

$$\mathring{l} = \nabla_{\mathring{D}} \Lambda_D(\mathring{G}^0, N^0; \mathring{D})\gamma' = \nabla \tilde{N}(\mathring{G}^0 - \mathring{D})\gamma', \tag{5.20}$$

where $l_\sigma = 0$ and (G^0, N^0) along with Lagrange multipliers κ^0, γ', $\bar{\mu}^0$, $\underline{\mu}^0$, $\bar{\beta}^0$, $\underline{\beta}^0$ satisfy the KKT conditions for the indirect LCED problem (Opt. D). Of course this expression is slightly different than the expression given for the loss component of the LMP from (5.14). This is because the Lagrange multipliers γ' corresponding to the indirect LCED problem (Opt. D) do not match the Lagrange multipliers γ^0 corresponding to the direct LCED problem (Opt. C). For the remainder of this chapter γ' will denote the optimal Lagrange multiplier for the constraint $\Lambda_D(\mathring{G}, N; \mathring{D}) = \mathbf{0}$ of the indirect LCED problem (Opt. D).

The following theorem derives a relationship between the Lagrange multipliers of the direct LCED problem (Opt. C) and the indirect LCED problem (Opt. D). By Theorem 5.3 below, the KKT point from Assumption 5.1, with γ^0 replaced by γ', solves the KKT conditions for the indirect LCED problem (Opt. D). As a result, the base-case dispatch G^0 is optimal for the indirect LCED problem (Opt. D). In addition, the expressions of the loss component of the LMP from (5.14) can be obtained from the expression (5.20) by substituting γ' and $\nabla \tilde{N}(\mathring{G}^0 - \mathring{D})$ using the expressions from Theorems 5.2 and 5.3.

Theorem 5.3. Let (G^0, N^0) along with Lagrange multipliers κ^0, γ^0, $\bar{\mu}^0$, $\underline{\mu}^0$, $\bar{\beta}^0$, $\underline{\beta}^0$ satisfy the KKT conditions for the direct LCED problem (Opt. C). Then (G^0, N^0) along with Lagrange multipliers κ^0, γ', $\bar{\mu}^0$, $\underline{\mu}^0$, $\bar{\beta}^0$, $\underline{\beta}^0$ satisfy the KKT conditions for the indirect LCED problem (Opt. D) where $\gamma'_\sigma = \gamma^0_\sigma$ and

$$\mathring{\gamma}' = (\mathbf{I} + \tfrac{1}{2} \mathring{H}^{-1} \dot{A}^\dagger \nabla L(\dot{A}\dot{\theta}^0)|\mathring{A}|)\mathring{\gamma}^0 + \tfrac{1}{2} \mathring{H}^{-1} \dot{A}^\dagger \nabla L(\dot{A}\dot{\theta}^0)|A_\sigma|\gamma^0_\sigma.$$

Proof: Notice that the primal feasibility, dual feasibility, and complementary slackness conditions do not include γ and are identical for Opt. C and Opt. D. Therefore, by hypothesis these conditions also hold for Opt. D. It remains to show that the stationarity conditions (5.2)-(5.5) hold for Opt. D. Notice that the stationarity conditions for Opt. C and Opt. D

differ only by their loss terms and so we need only show equivalence of the partial derivatives of the loss terms for both problems.

1) Stationarity Condition w.r.t. N_σ

For Opt. D we have $\nabla_{N_\sigma} \Lambda_D(\mathring{G}^0, N^0; \mathring{D})\gamma' = \gamma'_\sigma$. Replacing γ'_σ with its given expression yields $\gamma^0_\sigma = \nabla_{N_\sigma} \Lambda_C(\mathring{G}^0, N^0; \mathring{D})\gamma^0$, matching Opt. C.

3) Stationarity Condition w.r.t. $\mathring{N}$

For Opt. D we have $\nabla_{\mathring{N}} \Lambda_D(\mathring{G}^0, N^0; \mathring{D})\gamma' = \mathring{\gamma}'$. Substituting the given expression for $\mathring{\gamma}'$ results in $\nabla_{\mathring{N}} \Lambda_C(\mathring{G}^0, N^0; \mathring{D})\gamma^0$, matching Opt. C.

2) Stationarity Condition w.r.t. $\mathring{G}$

For Opt. D we have

$$\nabla_{\mathring{G}} \Lambda_D(\mathring{G}^0, N^0; \mathring{D})\gamma' = -\nabla\mathring{\tilde{N}}(\mathring{G}^0 - \mathring{D})\mathring{\gamma}' - \nabla\tilde{N}_\sigma(\mathring{G}^0 - \mathring{D})\gamma'_\sigma.$$

Substituting the expression for $\nabla\mathring{\tilde{N}}(\mathring{G}^0 - \mathring{D})$ from Theorem 5.2, substituting the given expressions for $\mathring{\gamma}'$ and γ'_σ, and rearranging the expression algebraically results in the following:

$$\begin{aligned}
\nabla_{\mathring{G}} \Lambda_C(\mathring{G}^0, N^0; \mathring{D})\gamma^0 = &-\tfrac{1}{2}\mathring{H}^{-1}\dot{A}^\dagger \nabla L(\dot{A}\dot{\theta}^0)|\mathring{A}|\mathring{\gamma}^0 \\
&-\tfrac{1}{2}\mathring{H}^{-1}\dot{A}^\dagger \nabla L(\dot{A}\dot{\theta}^0)|A_\sigma|\gamma^0_\sigma,
\end{aligned}$$

again matching Opt. C. $\qquad\square$

5.2.5 Loss Distribution Factor LCED Problem

To reduce the number of optimization variables many references, including [21] and [58], introduce *Loss Distribution Factors* (LDFs) in the form of a vector $\eta \in \mathbb{R}^n$ where $\mathbf{1}^\dagger \eta = 1$ and typically $\eta \in \mathbb{R}^n_+$. Each LDF represents the fraction of total system losses allocated to node i. Recognizing that the total system losses are represented by the function $\mathbf{1}^\dagger \tilde{N}(\mathring{G} - \mathring{D})$, the LDF LCED problem is defined as follows.

Optimization E. The *LDF LCED problem* is defined to be Opt. j with Λ_j specified by:

$$\Lambda_E(\mathring{G}, N; \mathring{D}) = N - \eta\Big(\mathbf{1}^\dagger \tilde{N}(\mathring{G}^0 - \mathring{D}) + \mathbf{1}^\dagger \nabla\tilde{N}(\mathring{G}^0 - \mathring{D})^\dagger(\mathring{G} - \mathring{G}^0)\Big). \tag{5.21}$$

References [21] and [58] only provide *intuitive* choices of LDFs that are not proven optimal. In fact, there may not exist LDFs that allow the base-case dispatch to be optimal for the LDF LCED problem (Opt. E). To see this notice that the constraint $\Lambda_{\mathrm{E}}(\mathring{G}, N; \mathring{D}) = \mathbf{0}$ reduces to $N^0 = \eta \mathbf{1}^\dagger N^0$ when evaluated at the base-case values (G^0, N^0). For this constraint to be satisfied we must have the following choice of LDFs:

$$\eta := \tfrac{1}{\mathbf{1}^\dagger N^0} N^0. \tag{5.22}$$

Remark 5.6. References [21] and [58] suggest the use of LDFs according to (5.22). However, these references do not prove if or when such LDFs are optimal. Section 5.3.2 illustrates that the LDFs from (5.22) are not always optimal but typically result in very small approximation error.

Unfortunately, the LDFs in (5.22) do not generally allow the stationarity condition for the LDF LCED problem (Opt. E) to be satisfied at the KKT point from Assumption 5.1. To see this notice that the stationarity conditions for the LDF LCED problem (Opt. E) and the indirect LCED problem (Opt. D) differ only by their loss terms. In order for these problems to be equivalent, the partial derivative of the loss term in the Lagrangian function from Opt. E with respect to $\mathring{G}$ must be equivalent to that of Opt. D. This partial derivative is written as follows:

$$\nabla_{\mathring{G}} \Lambda_{\mathrm{E}}(\mathring{G}, N; \mathring{D})\gamma' = -\nabla \tilde{N}(\mathring{G}^0 - \mathring{D})\mathbf{1}\eta^\dagger \gamma',$$
$$= -\nabla \tilde{N}(\mathring{G}^0 - \mathring{D})\mathbf{1}(\tfrac{1}{\mathbf{1}^\dagger N^0} N^0)^\dagger \gamma'. \tag{5.23}$$

In general this partial derivative does not match that of the indirect LCED problem (Opt. D), which is expressed as $\nabla_{\mathring{G}} \Lambda_{\mathrm{D}}(\mathring{G}, N; \mathring{D})\gamma' = -\nabla \tilde{N}(\mathring{G}^0 - \mathring{D})\gamma'$. A sufficient condition for the base-case dispatch to be optimal for the LDF LCED problem (Opt. E) requires that γ' be proportional to the vector of ones as embodied in Assumption 5.2 below. We will employ Assumption 5.2 for the remainder of this section and we will consider some test cases for which it is also satisfied; however, it is important to note that this assumption is not generally true.

Assumption 5.2. *The optimal Lagrange multipliers γ' associated with the indirect LCED problem (Opt. D) are uniform. E.g. there exists some $\alpha \in \mathbb{R}$ such that $\gamma' = \mathbf{1}\alpha$.*

To understand Assumption 5.2 it is useful to analyze the stationarity condition for the indirect LCED problem (Opt. D) with respect to N as defined by (5.2) and (5.4), which is as follows:

$$\kappa^0 + \gamma'_\sigma = 0 \quad \text{and} \quad \mathbf{1}\kappa^0 + \mathring{\gamma}' + S^\dagger(\underline{\mu}^0 - \bar{\mu}^0) = \mathbf{0}$$

This shows that the Lagrange multipliers $\gamma' = -\mathbf{1}\kappa^0 - c$ are indeed uniform if and only if the congestion component of the LMP c is zero as defined in Section 5.1.4, in which case $\gamma' = -\mathbf{1}\kappa^0$. In turn, the congestion component of the LMP is zero if no line limits from constraint ($j4$) are binding at the base-case values (G^0, N^0), leading to the statement in Remark 5.7. This is because non-binding line limits require that $\underline{\mu}^0 = \bar{\mu}^0 = \mathbf{0}$ by the complementary slackness condition.

Remark 5.7. Assumption 5.2 holds if no line limits from constraint ($j4$) are binding at the base-case values (G^0, N^0).

The following theorem states that the base-case dispatch G^0 is optimal for the LDF LCED problem (Opt. E) under Assumptions 5.1 and 5.2.

Theorem 5.4. *Let (G^0, N^0) along with Lagrange multipliers κ^0, γ', $\bar{\mu}^0$, $\underline{\mu}^0$, $\bar{\beta}^0$, $\underline{\beta}^0$ satisfy the KKT conditions for the indirect LCED problem (Opt. D) where $\gamma' = \mathbf{1}\alpha$. Then (G^0, N^0) along with the same Lagrange multipliers also satisfy the KKT conditions for the LDF LCED problem (Opt. E).*

Proof: Notice that the primal feasibility, dual feasibility, and complementary slackness conditions are identical for Opt. D and Opt. E and by hypothesis these conditions therefore hold for Opt. E. It remains to show that the stationarity conditions (5.2)-(5.5) hold for Opt. E. Notice that the stationarity conditions for Opt. D and Opt. E differ only by their loss terms and so we need only show equivalence of the partial derivatives of the loss terms for both problems. First, the partial derivatives with respect to N and G_σ are equivalent for both problems:

$$\nabla_N \Lambda_j(\mathring{G}^0, N^0; \mathring{D})\mathbf{1}\alpha = \mathbf{1}\alpha \quad \text{and} \quad \nabla_{G_\sigma} \Lambda_j(\mathring{G}^0, N^0; \mathring{D})\mathbf{1}\alpha = 0.$$

Furthermore, the partial derivative with respect to $\mathring{G}$ is equivalent for both problems. This is shown as follows:

$$\nabla_{\mathring{G}}\Lambda_{\mathrm{E}}(\mathring{G}^0, N^0; \mathring{D})\mathbf{1}\alpha = -\nabla\tilde{N}(\mathring{G}^0 - \mathring{D})\mathbf{1}(\tfrac{1}{\mathbf{1}^\dagger N^0}N^0)^\dagger\mathbf{1}\alpha,$$
$$= -\nabla\tilde{N}(\mathring{G}^0 - \mathring{D})\mathbf{1}\alpha.$$

$\square$

5.2.6 Common LCED Problem

The commonly formulated economic dispatch problem represents the total system losses as a single decision variable $\nu \in \mathbb{R}$ as opposed to representing the loss allocation to each node as individual decision variables. This effectively eliminates $n-1$ decision variables and $n-1$ constraints, making the problem much easier to solve. Using notation similar to [21], the *common LCED problem* (Opt. F) is written as follows:

$$\min_{G\in\mathbb{R}^n, \nu\in\mathbb{R}} \quad C(G) \tag{Opt. F}$$
$$st : \mathbf{1}^\dagger(G - D - \eta\nu) = \mathbf{0} \tag{F1}$$
$$\nu = LF^\dagger(G - D) + q \tag{F2}$$
$$\underline{G} \leq G \leq \bar{G} \tag{F3}$$
$$\underline{F} \leq S(\mathring{G} - \mathring{D} - \mathring{\eta}\nu) \leq \bar{F} \tag{F4}$$

This formulation is similar to the general TCED problem without angles (Opt. j). In fact, the objective function and the generation output limit constraint are identical to those of Opt. j. The power balance constraint (F1) and line limit constraint (F4) represent constraints ($j1$) and ($j4$) after replacing the nodal loss allocation vector N with the expression $\eta\nu$. Constraint (F2) represents the total system losses where $q \in \mathbb{R}$ is an offset constant and $LF \in \mathbb{R}^n$ represents the sensitivity of the total system losses with respect to the net real power injections. Notice this formulation enforces transmission line limits despite the use of Assumption 5.2, which effectively assumes no line limits are binding.

References [21] and [58] observe that different approximations of LF can be used and they derive three different versions of LF using total derivatives and implicit functions. With respect to our formulation the loss sensitivity vector is defined based on the loss sensitivity

matrix as $L\mathring{F} = \nabla\tilde{N}(\mathring{G}^0 - \mathring{D})\mathbf{1}$ and $LF_\sigma = \mathbf{0}$. Our formulation also uses a constant offset term of $q = \mathbf{1}^\dagger\tilde{N}(\mathring{G}^0 - \mathring{D}) + \mathbf{1}^\dagger\nabla\tilde{N}(\mathring{G}^0 - \mathring{D})^\dagger(\mathring{D} - \mathring{G}^0)$. Using these definitions of LF and q the loss constraint (F2) is as follows:

$$\nu = \mathbf{1}^\dagger\tilde{N}(\mathring{G}^0 - \mathring{D}) + \mathbf{1}^\dagger\nabla\tilde{N}(\mathring{G}^0 - \mathring{D})^\dagger(\mathring{G} - \mathring{G}^0). \tag{5.24}$$

Using this proposed definition of the loss sensitivity vector LF and offset constant q, it should now be apparent that the common LCED problem (Opt. F) is equivalent to the LDF LCED problem (Opt. E) in that any optimal dispatch of one problem is also optimal for the other. This is because both problems have the same feasible set of dispatch variables G. In fact, a feasible solution of the common LCED problem (G, ν) can be constructed from any feasible solution of the LDF LCED problem (G, N) where $\nu = \mathbf{1}^\dagger N$. Similarly, a feasible solution of the LDF LCED problem (G, N) can be constructed from any feasible solution of the common LCED problem (G, ν) where $N = \eta\nu$.

Remark 5.8. Although we do not prove this explicitly, the base-case values G^0 and $\nu^0 = \mathbf{1}^\dagger N^0$ indeed satisfy the KKT conditions of the common LCED problem (Opt. F) along with Lagrange multipliers κ^0, α, $\bar{\mu}^0$, $\underline{\mu}^0$, $\bar{\beta}^0$, $\underline{\beta}^0$ under Assumptions 5.1 and 5.2. Furthermore, in agreement with (5.20) the loss price can now be expressed as $l = LF\alpha$. It is interesting to note that this expression of the loss price can also be derived from the common LCED problem (Opt. F) when considering the loss sensitivity matrix LF and the offset constant q to be constant parameters independent of the demand vector D. This may be counter-intuitive because LF and q are indeed (implicitly) defined in terms of the demand vector D.

5.2.7 Recovering a Locally Optimal Dispatch

Recall that, by Assumption 5.1, the base-case values (G^0, N^0) represent a local minimizer of the TCED problem without angles (Opt. B). Thus far we have shown that the base-case generation dispatch G^0 is locally optimal for the TCED problem with angles (Opt. A) and is globally optimal for the common LCED problem (Opt. F) under Assumptions 5.1 and 5.2. However, as mentioned in the introduction, the common LCED problem (Opt. F) may have multiple optimal dispatch vectors, some of which may not be optimal or even feasible for the TCED problem with angles (Opt. A). This is an issue because standard

93

off-the-shelf optimization software used to solve the common LCED problem (Opt. F) only identifies one of potentially multiple optimal dispatch vectors. An additional assumption is required to guarantee the identified dispatch matches the base-case dispatch G^0.

Assumption 5.3. *The common LCED problem (Opt. F) has a unique minimizer* (G, ν).

Remark 5.9. The common LCED problem (Opt. F) is said to have a *unique optimal dispatch* if Assumption 5.3 holds true. Similarly, the common LCED problem (Opt. F) is said to have *multiple minimizers* or *multiple optimal dispatch vectors* if Assumption 5.3 does not hold true.

Assumption 5.3 ensures that the common LCED problem has a unique optimal dispatch. Under Assumptions 5.1, 5.2, and 5.3 the unique optimal dispatch for the common LCED problem (Opt. F) is indeed locally optimal for the TCED problem with angles (Opt. A) and represents the base-case dispatch G^0. Under these three assumptions a locally optimal dispatch for the TCED problem with angles (Opt. A) can be identified by solving the common LCED problem (Opt. F) using standard off-the-shelf optimization software. The numerical results section investigates errors associated with relaxing each of these three assumptions.

5.3 Numerical Results

This section provides numerical results intended to illustrate two key findings that point out significant dispatch approximation errors may occur when certain assumptions are violated. Section 5.3.1 illustrates the first key finding that small perturbations to the ideal base-case state can result in significantly large dispatch approximation error if Assumption 5.3 fails to hold. Associated errors are illustrated using an intuitive 2-bus test case as well as a realistically large test case with 2383 buses, neither of which enforce line limits so that Assumption 5.2 holds. Section 5.3.2 then illustrates the second key finding that significant dispatch approximation error may occur when Assumption 5.2 fails to hold even if Assumptions 5.1 and 5.3 hold. Associated errors are illustrated using an intuitive 3-bus test case as well as the same 2383 bus test case as in Section 5.3.1 but with line limits enforced. In this specific example, introducing transmission line limits to the 2383 bus test

94

case causes the common LCED problem (Opt. F) to have a unique optimal dispatch and we show that there is no dispatch approximation error despite the presence of transmission congestion. This suggests that realistic systems may not experience significant approximation error when Assumption 5.2 fails to hold. Section 5.3.2 continues to select different base-case states that introduce dispatch approximation error into the 2383 bus test case when enforcing line limits. Since the uniqueness Assumption 5.3 holds for this specific test case, small perturbations to the ideal base-case state result in little dispatch approximation error.

In this section the kth diagonal element of B is $B_{kk} = \frac{1}{x_k}$ and the kth element of the vector valued loss function is $L_k(\Theta) = \frac{r_k}{x_k^2}\Theta_k^2$ where the impedance of line $k \in \mathbb{L}$ is $r_k + \mathbf{i}x_k$ and $\Theta \in \mathbb{R}^m$ represents the voltage angle difference across each transmission line $\dot{A}\dot{\theta}$. The LDFs η are chosen as in (5.22). A computer with a 2.0 GHz processor is used.

5.3.1 Multiple Minimizers of the Common LCED Problem

This subsection studies two test cases that satisfy Assumptions 5.1 and 5.2; however, the common LCED problem (Opt. F) has multiple minimizers for these two test cases, violating Assumption 5.3. In this context small perturbations to the ideal base-case state are shown to result in a common LCED problem (Opt. F) with a unique optimal generation dispatch; however, this unique optimal generation dispatch differs significantly from the desired generation dispatch $G^\star$ that solves the TCED problem with angles (Opt. A), resulting in large generation dispatch approximation error. This is shown using an intuitive 2-bus test case as well as a large test case with 2383 buses. In this subsection neither test case enforces line limits so that Assumption 5.2 holds (See Remark 5.7).

5.3.1.1 2-Bus Test Case

A one-line diagram of the 2-bus test case is provided in Figure 5.2 along with various parameters of the test case. Notice that the transmission line is highly resistive and has no transmission limit. All system demand is located at bus 2 and is fixed to $D_2 = 100$p.u. The demand is co-located with *expensive* generation with cost function $C_2(G_2) = G_2$. The generation at bus 2 is unlimited so that $0 \leq G_2 \leq \infty$. *Inexpensive* generation is located remotely at bus 1 as the cost of this generator is $C_1(G_1) = 0.6G_1$. The inexpensive generation is limited

as $0 \leq G_1 \leq 60$p.u. The total system cost $C(G)$ is the sum of the individual generator costs. Bus 1 is designated the angle reference bus and the price reference bus so that $\sigma = \rho = 1$. The resulting system state is $\dot{\theta} = \theta_2$.
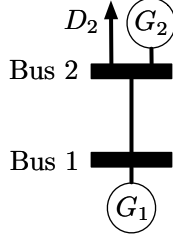
Figure 5.2: 2-bus system one-line diagram. The demand is fixed at $D_2 = 100$p.u. The generators have cost functions $C_1(G_1) = 0.6G_1$ and $C_2(G_2) = G_2$. The line has per-unit impedance of $0.01 + \mathbf{i}0.01$ and has no limit so that $\bar{F}_1 = -\underline{F}_1 = \infty$.

Figure 5.3 plots the set of all feasible generation dispatch vectors for the TCED problem with angles (Opt. A) as a black curve. The gray arrows in this figure represent the objective descent direction. The unique optimal generation dispatch vector is $G^\star = [28.125, 78.125]^\dagger$p.u., is represented by the star in the figure, and is intuitively the feasible generation dispatch vector that is furthest downstream in the descent direction. The associated optimal vector of voltage angles is $\dot{\theta}^\star = \theta_2^\star = -0.25$ radians.

The black dashed line represents the set of all feasible generation dispatch vectors for the common LCED problem (Opt. F) when using the ideal base-case state $\dot{\theta}^0 = \dot{\theta}^\star$. Notice that the descent direction is perpendicular to the black dashed line and as a result all feasible generation dispatch vectors are optimal. Since the common LCED problem (Opt. F) has multiple minimizers, Assumption 5.3 does not hold. Additionally, only one of the infinitely many minimizers of Opt. F is feasible for the TCED problem with angles (Opt. A).

In practice the ideal base-case state is typically estimated. To emulate this, linearize around the base-case state $\dot{\theta}^\star + \delta$ where $\delta = 0.07$ radians represents a small perturbation. The resulting linear feasible set of generation dispatch vectors is represented by the dashed gray line. Furthermore, the common LCED problem (Opt. F) now has a unique optimal generation dispatch vector $G \approx [60, 55.559]^\dagger$p.u. that is represented by the black circle and also significantly differs from the desired generation dispatch vector $G^\star$. The dispatch ap-
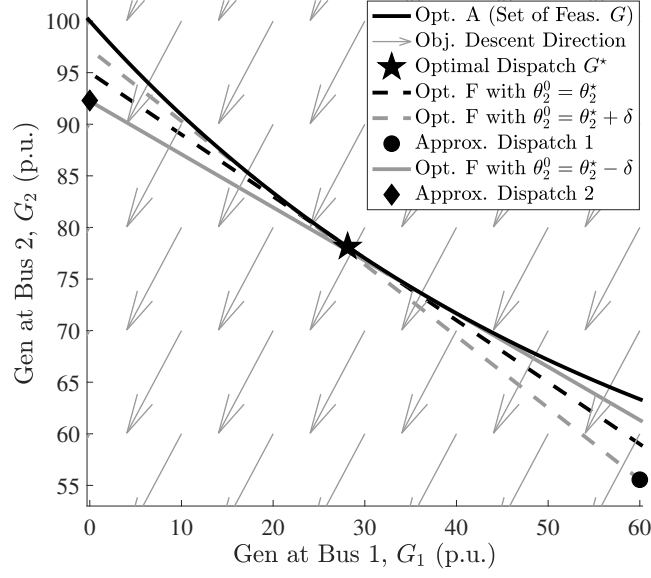
Figure 5.3: Illustration of the feasible set of dispatch vectors G for various ED problems associated with the 2-bus test case.

proximation error vector is $\Delta G = G - G^\star \approx [31.875, -22.566]^\dagger$p.u., which is large compared to $G^\star$.

Perturbing the ideal base-case state in the other direction also results in large dispatch approximation error. Specifically, linearizing around the base-case state $\dot\theta^\star - \delta$ results in the linear feasible set of generation dispatch vectors represented by the solid gray line. In this case the common LCED problem (Opt. F) has a unique optimal generation dispatch vector $G \approx [0, 92.242]^\dagger$p.u. that is represented by the black diamond and also significantly differs from the desired generation dispatch vector $G^\star$. The dispatch approximation error vector is $\Delta G = G - G^\star \approx [-28.125, 14.117]^\dagger$p.u., which is again large compared to $G^\star$.

Remark 5.10. Similarly large approximation error remains for an arbitrarily small perturbation $\delta > 0$. Alternatively, similarly large approximation error remains after adding slight curvature to the objective descent direction that might arise from a small positive quadratic coefficient in the cost function.

Remark 5.11. The lossless DC OPF problem yields a unique optimal generation dispatch vector of $G = [60, 40]^\dagger$p.u. for the 2-bus test case. In fact, the lossless DC OPF problem and the TCED problem with angles (Opt. A) both have unique optimal generation dispatch

vectors; however, the common LCED problem (Opt. F) has multiple optimal generation dispatch vectors when the base-case state matches its ideal value $\dot{\theta}^\star$.

Remark 5.12. Reference [21, section V-A] makes a similar observation regarding a different 2-bus test case. In their example the common LCED problem (Opt. F) also has multiple minimizers when the ideal base-case state is chosen. Rather than perturbing the base-case state, as is done in this chapter, they perturb the bids of the generators. Keeping the base-case state fixed, they show that a small perturbation in generator bids can result in significant dispatch approximation error. This observation is consistent with the observations made here.

5.3.1.2 Test Case 2383wp without Line Limits Enforced

Now consider the test case *2383wp* from the NESTA archive, which represents the Polish power system during the 1999-2000 winter evening peak [17]. Line limits are not enforced to ensure that Assumption 5.2 holds. The identified minimizer of the TCED problem with angles (Opt. A) is found using the interior point algorithm provided by the MATLAB function FMINCON and takes 17.10sec. to converge. The optimal objective value of this problem is $C(G^\star) = \$1865459.40$.

Let's first analyze the common LCED problem (Opt. F) with the base-case state chosen to match the identified minimizer of the TCED problem with angles (Opt. A) $\dot{\theta}^0 = \dot{\theta}^\star$ in order to satisfy Assumption 5.1. In this case the loss sensitivity matrix $\nabla \tilde{N}(\mathring{G}^0 - \mathring{D})$ takes 26.13sec. to compute due to the inverse computation. There exist multiple optimal dispatch vectors G for the common LCED problem (Opt. F), some of which are not feasible for the TCED problem with angles (Opt. A). To illustrate this we use an interior point algorithm provided by Artelys KNITRO software to solve the common LCED problem (Opt. F) with different supplied initial guesses [10]. Table 5.1 compares the identified minimizers of both problems where $\Delta G \in \mathbb{R}^n$ represents the difference between $G^\star$ and the identified optimal dispatch of the common LCED problem (Opt. F) and ΔC represents the difference between $C(G^\star)$ and the optimal objective value of the common LCED problem (Opt. F).

Turning to the first row of Table 5.1, the main body of this chapter proves that

$G = G^\star$ and $\nu = \mathbf{1}^\dagger N^\star$ is a minimizer of the common LCED problem (Opt. F). When supplying this as the initial guess, the algorithm immediately converges to a dispatch that nearly matches $G^\star$. Notice that the associated errors, ΔG, are very small relative to the total dispatch generation $\|G^\star\|_1 = 49231.67$MW and the optimal objective values of both problems are nearly identical. However, ΔG is not identically zero due to insignificant computational error.

Table 5.1: Results for test case 2383wp without line limits enforced and with the ideal base-case state $\dot{\theta}^0 = \dot{\theta}^\star$. The error quantities are denoted with Δ and represent the difference between identified optimal quantities of Opt. A and Opt. F.

Initial Guess for the Interior Point Algorithm	$\|\Delta G\|_1$ (MW)	$\|\Delta G\|_\infty$ (MW)	$|\Delta C|$ ($)	Solver Time (s)
$G = G^\star$ and $\nu = \mathbf{1}^\dagger N^\star$	1.73	0.88	0.00	5.52
Typical Operating Point	21.65	10.70	0.00	5.33
Minimizer of lossless DC OPF	308.77	152.77	0.00	7.61

To demonstrate that Opt. F has multiple minimizers, two alternative initial guesses were supplied as shown in the second and third rows of Table 5.1. The first alternative was constructed from the typical operating point provided by the test case description. The second alternative was constructed from the minimizer of the lossless DC OPF problem, which was solved using the DC OPF function available in MATPOWER [98]. When using these alternative initial guesses the algorithm converges to dispatch values that do not match $G^\star$ but do attain the same optimal objective value $C(G^\star)$. Furthermore, these identified dispatch values are not feasible for the TCED problem with angles (Opt. A).

Similar to the simple 2-bus example, a small perturbation of the base-case state results in significantly large dispatch approximation error. To illustrate this we perturb the ideal base-case state $\dot{\theta}^\star$ by a perturbation vector $\delta \in \mathbb{R}^{n-1}$ that was sampled from a normal distribution with zero mean and a diagonal covariance matrix of $10^{-10} \times \mathbf{I}$. The specific sample drawn from this distribution has the properties $\|\delta\|_\infty = 3.6 \times 10^{-5}$ radians and $\|\delta\|_1 = 0.018$ radians. The resulting common LCED problem appears to have a unique optimal dispatch because the same dispatch is identified when using any initial guess for

the interior point algorithm. The dispatch approximation error is $\|\Delta G\|_1 = 314.70$ MW and $\|\Delta G\|_\infty = 156.19$ MW. This dispatch approximation error is significant compared to the small perturbation δ.

5.3.2 LDF Approximation Error with Congestion

This subsection studies test cases that satisfy Assumptions 5.1 and 5.3; however, transmission line congestion causes Assumption 5.2 to be violated. A highly resistive 3-bus test case with significant transmission congestion is used to illustrate the potential dispatch approximation errors associated with Assumption 5.2. Although associated errors are large for this extreme 3-bus test case, they are typically very small in practice as is illustrated by the 2383 bus test case with line limits enforced. In fact, this test case exhibits no error despite having transmission congestion. To illustrate error associated with Assumption 5.1 alternative choices of base-case state are investigated that introduce dispatch approximation error into the 2383 bus test case.

5.3.2.1 3-Bus Test Case

Figure 5.4 provides the details of the 3-bus test case in a one-line diagram. The generation dispatch values G have no upper limit but are restricted to be non-negative, e.g. $\underline{G} = 0$. The system is highly resistive as the impedance of each line is $r_k + \mathbf{i} x_k = 0.01 + \mathbf{i} 0.01$ in units of p.u. The cost function is given by $C(G) = C_1(G_1) + C_2(G_2) + C_3(G_3)$. Bus 1 is assigned to be the slack bus and the reference bus.
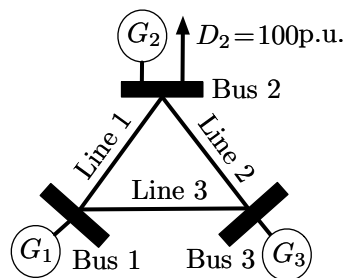

Figure 5.4: 3-bus system one-line diagram. The line limits $\bar{F} = -\underline{F}$ are such that $\bar{F}_2 = \bar{F}_3 = \infty$ and $\bar{F}_1 = 11$p.u. The generators have cost functions $C_1(G_1) = G_1^2$, $C_2(G_2) = 100G_2^2$ and $C_3(G_3) = 0.01G_3^2$.

The minimizer of the TCED problem with angles (Opt. A) is $G^\star \approx [82.38, 6.81, 123.61]^\dagger$ and $\dot\theta^\star \approx [-0.690, 0.110]^\dagger$ in units of p.u. and radians respectively. The ideal base-case state is chosen $\dot\theta^0 = \dot\theta^\star$ and thus the base-case dispatch is $G^0 = G^\star$. The line limit for line 1 is binding and the congestion component of the LMP is non-zero, taking the value $c = [0, 137.26, -137.26]^\dagger$ in units of dollars per p.u. Notice that Section 5.2.5 draws no conclusion regarding whether or not G^0 is optimal for the LDF LCED problem (Opt. E).

As expected the base-case point G^0 and $\nu^0 := \mathbf{1}^\dagger N^0$ is feasible for the common LCED problem (Opt. F); however, this point is not optimal. An alternative unique optimal dispatch G of Opt. F is identified that is not feasible for the TCED problem with angles (Opt. A). The optimal objective value for the common LCED problem (Opt. F) is \$11512.63, which is \$62.36 lower than the optimal objective value for the TCED problem with angles (Opt. A). The optimal dispatch for the common LCED problem (Opt. F) is $G = [86.96, 6.17, 122.41]^\dagger$ p.u. and the dispatch approximation error is $G^\star - G = [-4.58, 0.64, 1.20]^\dagger$. This highly resistive network exhibits small error, suggesting this approximation is typically accurate.

5.3.2.2 Test Case 2383wp with Line Limits Enforced

Consider the same test case as Section 5.3.1 but with line limits enforced. The identified minimizer of the TCED problem with angles (Opt. A) is found using the interior point algorithm provided by FMINCON and takes 18.81sec. to converge. The optimal objective value of this problem is $C(G^\star) = \$1890940.57$. There are 4 congested lines with binding limits, which is a small amount relative to the 2896 total transmission lines.

When using the ideal base-case state $\dot\theta^0 = \dot\theta^\star$ the common LCED problem (Opt. F) appears to have a unique minimizer because the interior point algorithm converges to the same point with any choice of initial guess. Notice that test case 2383wp has the unusual property that its common LCED problem (Opt. F) has a unique minimizer when enforcing line limits but has multiple minimizers when line limits are not enforced. This property is not typical as many other test cases in the NESTA archive do not have this property.

We consider four different base-case states when formulating the common LCED problem (Opt. F). Each of the four versions of this problem appear to have a unique

minimizer because the interior point algorithm converges to the same point for any choice of initial guess. Since there is a unique minimizer, we are able to take advantage of the much faster dual simplex algorithm provided by MOSEK, which does not allow for a user supplied initial guess [4]. Table 5.2 provides numerical results for each of the four choices of base-case state. Notice that the solver times are much faster and the optimal generation dispatch vector $G^\star$ is exactly recovered when setting the base-case state to its ideal value $\dot\theta^0 = \dot\theta^\star$. Note that the loss sensitivity matrix $\nabla\tilde{N}(\mathring{G}^0 - \mathring{D})$ requires approximately 28 seconds of computation time for each base-case state.

Since the common LCED problem (Opt. F) now has a unique optimal dispatch when using the ideal base-case state, small perturbations of the base-case state should result in small approximation errors. This is illustrated by using the same perturbed base-case state $\dot\theta^\star + \delta$ as in Section 5.3.1.2. Notice that the dispatch approximation error is very small as compared to the error witnessed in Section 5.3.1.2. In fact, we should expect the dispatch approximation error to disappear as the perturbation becomes smaller, e.g. $\|\delta\| \to 0$.

Table 5.2: Results for test case 2383wp with line limits enforced. The error quantities are denoted with Δ and represent the difference between identified optimal quantities of Opt. A and Opt. F.

Choice of Base-Case State, $\dot\theta^0$	$\|\dot\theta^\star - \dot\theta^0\|_1$ (radians)	$\|\Delta G\|_1$ (MW)	$\|\Delta G\|_\infty$ (MW)	$|\Delta C|$ ($)	Solver Time (s)
Local Min. of Opt. A, $\dot\theta^\star$	0.00	0.00	0.00	0.00	1.26
Small Perturbation, $\dot\theta^\star + \delta$	0.02	0.08	0.04	0.95	1.33
Min. of Lossless DC OPF	34.15	73.95	29.67	1061.11	1.10
Typical Operating Point	257.68	501.37	306.58	24007.79	1.37

As discussed in Section 5.2.1, the ideal base-case state $\dot\theta^\star$ is not known in practice. We now consider two alternative choices of base-case state $\dot\theta^0$. First, is the minimizer of the lossless DC OPF problem. The second alternative is determined by solving power flow equations at the typical operating point provided by the test case description. The power flow equations and the lossless DC OPF problem are solved using MATPOWER. Table 5.2 shows that the generation dispatch error is small relative to the total generation, which satisfies

$\|G^\star\|_1 = 25108.74\text{MW}$. Furthermore, the minimizer of the lossless DC OPF problem serves as a better base-case state in terms of the generation dispatch error.

5.4 Summary

Using first-order Taylor expansions, this chapter derived several convex linearly constrained approximations to the non-convex economic dispatch problem from Chapter 4. A sequence of four linearly constrained approximations are derived, ultimately resulting in the common Linearly Constrained Economic Dispatch (LCED) problem, which is characterized with respect to the underlying non-convex economic dispatch problem. Throughout the chapter various approximation errors are identified including errors pertaining to the choice of base-case state and errors pertaining to the common LCED problem having multiple solutions. This chapter also highlights that there may not exist LDFs that recover the solution to the underlying non-convex economic dispatch problem under congested conditions even if the base-case state matches the solution to the underlying non-convex economic dispatch problem. However, if no transmission line limits are binding, then such LDFs do exist and are identified.

Chapter 6

Convex Hull Pricing

The previous two chapters provided convex approximations of the non-convex AC OPF problem for which there exist algorithms that provably converge to a globally optimal solution. On the other hand, the there exist algorithms to solve the non-convex AC OPF problem that perform well in practice but do not identify a generation dispatch with general optimality guarantees. Over the past decade a significant amount of research has focused on developing such algorithms. With this in mind, many recent works have developed relaxations to tightly approximate the AC OPF problem, e.g. [18, 49, 51, 60–62, 67, 85]. Although these methods identify a dispatch that is not guaranteed to be feasible, a nearly optimal feasible dispatch along with corresponding LMPs can be recovered via primal-dual interior point methods.

This chapter investigates the use of a potentially sub-optimal dispatch that is feasible for the AC OPF problem and may be identified using any of the aforementioned algorithms. However, as explained in Section 2.5, reference [52] shows that a revenue adequate market equilibrium does not always exist for the AC OPF problem. Furthermore, by theorem 1 of [52] a revenue adequate market equilibrium, as in Definition 2.3, can only occur if the globally optimal dispatch is identified for the AC OPF problem. For this reason our proposed pricing structure should account for costs associated with generator uplift and FTR uplift.

Convex Hull Prices (CHPs) are proposed and are defined to solve a novel multi-objective minimum uplift problem that captures the trade-off between generator side-payments

and potential congestion revenue shortfall. A convex primal counterpart of this multi-objective minimum uplift problem, termed the *primal CHP problem*, is formulated in terms of the convex hull of the set of feasible net real power injections. Indeed the term *Convex Hull Price* derives from the result that the CHPs are equivalent to the optimal Lagrange multipliers of the *primal CHP problem*. However, depending on the chosen model of the transmission network, the convex hull of the feasible set of net real power injections may be intractable to evaluate. In this case CHPs are approximated using state-of-the-art convex relaxations that are efficiently solvable. This is the first proposed method of approximating CHPs in polynomial-time that is general enough to accommodate the non-linear transmission constraints in the AC OPF problem. In our abstract myopic market setting we show that tight relaxations of the AC OPF problem can be used to effectively approximate CHPs that decrease potential congestion revenue shortfall significantly with little effect to side-payments.

This chapter serves as an initial effort to incorporate non-linear models of the transmission network into a general convex hull pricing framework. As mentioned in Section 1.1.4, all special-purpose algorithms for computing CHPs have focused the Unit Commitment (UC) problem with linear transmission constraints. In an initial effort to incorporate non-linear transmission models, this chapter focuses on an abstract myopic market that considers only a single time period, consistent with the entirety of this dissertation. In other words, we focus on the non-convexity of interest by analyzing CHPs associated with the AC OPF problem, which does not incorporate integer decision variables representing generator commitment statuses. However, similar relaxation techniques can be used to approximate a solution of a multi-objective minimum uplift problem in a more general setting that includes generator commitment (See Remark 6.1).

In the context of the AC OPF problem, we show that standard LMPs always result in zero generator uplift and non-negative FTR uplift because the generator models are convex and the transmission network model is non-convex. Using LMPs, the total FTR uplift reaches over 32% of the total operating cost for an IEEE test case with 162 buses and over 13% of the total operating cost for a NESTA test case with 2224 buses [17]. This implies that the consideration of non-linear transmission constraints may be significant in the context of FTR

105

uplift. Since generator uplift is zero when using LMPs, CHPs will actually increase generator uplift as compared to LMPs, which is starkly different from the typical observations made in the context of the UC problem. We also find that CHPs can be effectively approximated using the Semi-Definite Programming (SDP) relaxation. In fact, if the weight parameter representing the relative value of FTR uplift to generator uplift is set lower than 0.72, then approximate CHPs for the 162 bus test case reduce the total uplift by over 30% of the total operating cost without introducing any generator uplift. This promising result is dampened by noting that the SDP relaxation is unable to be solved efficiently for large test cases with over 1000 buses. We emphasize the difficulty of solving large SDPs and point out that SDPs are only approximately solvable in polynomial-time, with arbitrarily small fixed approximation error [2]. Two other state-of-the-art convex relaxations are also analyzed that are more computationally efficient, but tend to result in higher uplift payments for the test cases analyzed.

This chapter is organized as follows. Section 6.1 explains that LMPs may result in positive FTR uplift and proves that LMPs always result in zero side-payments to generators. Section 6.2 formulates the CHP optimization problem as a multi-objective minimum uplift problem and shows that CHPs support a revenue adequate market equilibrium if such prices exist. Section 6.3 then derives the primal CHP problem from a general form of the AC OPF problem and CHPs are proven to be the optimal Lagrange multipliers of the primal CHP problem. A general relaxation technique is then proposed to approximate the primal CHP problem. Throughout the main body of this chapter, the model of the transmission network is left general. In fact, many of the results may be general enough to apply to other systems that are subject to non-linear transportation constraints, provided the respective relaxations well approximate the feasible regions. Section 6.5 then focuses on the fully detailed AC model of the transmission network, provides examples where a revenue adequate market equilibrium does not exist and illustrates many of the concepts discussed. Section 6.6 concludes and provides directions to pursue in future work.

6.1 LMPs and Revenue Inadequacy

The following theorem states that a KKT price/dispatch pair as in Definition 2.2 always results in zero side-payments to generators, which is a byproduct of the private constraint sets $\mathcal{X}^i$ being convex. This highlights a fundamental difference between LMPs and CHPs in the context of the AC OPF problem. While CHPs minimize the sum of side-payments and PCRS, LMPs result in zero side-payments. As a result CHPs tend to increase side-payments and decrease PCRS as compared to LMPs. This tendency of CHPs in the context of the AC OPF problem is starkly different from from the tendency that has been observed in previous work. Specifically, CHPs tend to lower side-payments to generators in the context of the Unit Commitment (UC) problem with a linear model of the transmission network, as in [80] and [45]. The difference is due to the fact that the private constraints $\mathcal{X}^i$ are the source of non-convexity in the UC problem, whereas the network constraints are the source of the non-convexity in the AC OPF problem.

Theorem 6.1. *A KKT price/dispatch pair as in Definition 2.2 results in zero side-payments to generators, eg.* $C_i^o(\lambda_i^\star, G_i^\star) = 0 \ \forall i \in \mathbb{N}$.

Proof: The generalized stationarity conditions (2.7) include necessary conditions for optimality of each profit-maximizing generation problem (2.1). Since each problem (2.1) is convex, these conditions are also sufficient for global optimality. $\qquad\square$

6.2 Multi-objective Minimum Uplift Problem

To reduce deficit it is in the interest of the ISO to have low side-payments and PCRS. CHPs are defined as an optimal solution to a pricing problem that minimizes the weighted sum of these values and is referred to as the *CHP problem* or the *multi-objective minimum uplift problem.*

Definition 6.1. The *Convex Hull Prices* (CHPs) minimize the weighted sum of potential congestion revenue shortfall and total side-payments, are denoted $\hat{\lambda}$, and are defined using a positive weight parameter $\alpha > 0$ that represents the value of PCRS relative to generator side-payments.

$$\hat{\lambda} \in \underset{\lambda \in \mathbb{R}^n}{\operatorname{argmin}} \ \left(\alpha C^s(\lambda, G^d) + \underset{i \in \mathbb{N}}{\Sigma} \ C_i^o(\lambda_i, G_i^d) \right) \tag{6.1}$$

Recalling that side-payments and PCRS are always non-negative and recognizing that the weight parameter α is defined to be positive, it is apparent that CHPs must form a revenue adequate market equilibrium, as in Definition 2.3, with any given dispatch values G^d if such prices exist. Furthermore, the ISO may prefer PCRS over side-payments because the PCRS only represents a potential shortfall whereas the side-payments represent an actual shortfall. For this reason, the weight parameter will likely be chosen to be less than one.

The CHP problem (6.1) is similar to the multi-objective minimum uplift problem from [95], but explicitly incorporates FTR uplift into the formulation as suggested in their future work section. Our formulation also includes non-linear transmission constraints, which has not been investigated in a multi-objective setting. When the weight parameter is set to $\alpha = 1$ the CHP problem (6.1) is consistent with the formulation in [43] and [35], which provide a high-level analysis that is capable of accommodating non-linear transmission models. However, the special-purpose algorithm designed to solve the minimum uplift problem in [43] and [35] is restricted to linear transmission models.

The objective function of the CHP problem (6.1) is intuitively convex in the price variables λ because it is the sum of individual functions that represent the maximum of affine functions in λ. However, despite convexity, this problem is still difficult to solve in general because its objective function is difficult to evaluate and is non-smooth. In fact, references [6] and [54] show that it is generally NP-hard to identify a feasible point of the maximum FTR payoff problem from (2.4), which must be solved to evaluate the PCRS function from (2.5) denoted $C^s(\lambda, G^d)$.

6.3   Approximating Extended Locational Marginal Prices

This section explains how CHPs can be approximated as the optimal Lagrange multipliers of a convex optimization problem. We begin by formulating the convex primal CHP problem. The CHPs are then proven equivalent to optimal Lagrange multipliers of the convex primal CHP problem. We then explain how to approximate the convex primal version of the CHP problem using convex relaxations. This section leaves the feasible set of net real power injections $\mathcal{T}$ general.

6.3.1 Primal Formulation of the CHP Problem

The primal CHP problem is very similar in form to the general ED problem. This formulation incorporates the dispatched net real power injections $T^d := G^d - D$ and the weight parameter α into the real power balance constraints. Notice that the this generalized version of the real power balance constraints reduces to the standard real power balance constraints when $\alpha = 1$. The *primal CHP problem* is written as follows:

$$\min_{G \in \mathcal{X}, \; T \in \text{conv}(\mathcal{T})} \quad \sum_{i \in \mathbb{N}} C_i(G_i) \tag{6.2}$$

$$st : D_i - G_i + \alpha T_i + (1 - \alpha)T_i^d = 0 \quad \forall i \in \mathbb{N} \tag{6.2a}$$

where $\text{conv}(\mathcal{T})$ is the convex hull of $\mathcal{T}$.

A key insight that helps in computing CHPs is that any optimization problem with a linear objective function and a compact feasible set has the same optimal value after relaxing the feasible set to its convex hull [28]. Under the assumption that $\mathcal{T}$ is compact we have the following equivalence:

$$\min_{T \in \mathcal{T}} \lambda^\dagger T \;\; = \;\; \min_{T \in \text{conv}(\mathcal{T})} \lambda^\dagger T \tag{6.3}$$

This fact allows for the partial Lagrangian dual function of the primal CHP problem, denoted $\mathcal{L}(\lambda)$ to be written in the following convenient form:

$$\mathcal{L}(\lambda) := \sum_{i \in \mathbb{N}} \min_{G_i \in \mathcal{X}^i} \left(C_i(G_i) - \lambda_i G_i\right) + \alpha \min_{T \in \mathcal{T}} \lambda^\dagger T + \lambda^\dagger \left((1 - \alpha)T^d + D\right). \tag{6.4}$$

The following Theorem 6.2 establishes CHPs as a maximizer of this partial Lagrangian dual function. Though similar to results in other work regarding CHPs, e.g. [80], this result accounts for weight constant α and general non-linear transmission models assumed by the set $\mathcal{T}$. If the weight parameter is set to $\alpha = 1$ then the partial Lagrangian dual function is independent of the dispatched generation G^d, and thus CHPs do not depend on the dispatched generation. As opposed to LMPs, this is a potential benefit using CHPs with $\alpha = 1$. It should be noted that there are analogous observations in the context of the UC problem, where CHPs are also independent of, for example, sub-optimality of the UC solution.

Theorem 6.2. *A maximizer of the partial Lagrangian dual function* $\mathcal{L}(\lambda)$ *from (6.4) is also a minimizer of the CHP problem (6.1) and thus represents CHPs.*

Proof: A maximizer of the partial Lagrangian dual function (6.4) is unchanged by adding and subtracting the term $\sum_{i\in\mathbb{N}} \lambda_i T_i^d$ and subtracting the constant $\sum_{i\in\mathbb{N}} C_i(G_i^d)$. Noting that $T_i^d = G_i^d - D_i$, we obtain the following expression:

$$\mathcal{L}(\lambda) - \sum_{i\in\mathbb{N}} C_i(G_i^d) = \sum_{i\in\mathbb{N}} \left(\lambda_i G_i^d - C_i(G_i^d) - \Upsilon_i(\lambda_i) \right) - \alpha(\lambda^\dagger T^d + \Psi(\lambda)).$$

By (2.5) and (2.2), this expression is equivalent to the negative of the objective function of the CHP problem (6.1). The result directly follows. □

As summarized in the following theorem, a maximizer of the partial Lagrangian dual function $\mathcal{L}(\lambda)$ from (6.4) can be recovered as the optimal Lagrange multipliers of constraints (6.2a). Indeed the term *Convex Hull Price* is derived from this key result, which is similar to results in other work, e.g. [45].

Theorem 6.3. *Optimal Lagrange multipliers of constraints (6.2a) minimize the CHP problem (6.1) and thus represent CHPs.*

Proof: Equation (6.3) implies that the function $\mathcal{L}(\lambda)$ from (6.4) represents the partial Lagrangian dual function for problem (6.2). Furthermore, strong duality holds for problem (6.2) when dualizing only linear constraints because it is a convex problem with a non-empty feasible set. The result follows from Theorem 6.2. □

6.3.2   Approximating CHPs

Unfortunately, the convex hull of the set of feasible net real power injections $\text{conv}(\mathcal{T})$ may be intractable to evaluate, as is the case when using the fully detailed AC model of the transmission network [53]. In this case the primal CHP problem must be relaxed using a conservative convex set $\text{relax}(\mathcal{T}) \supseteq \text{conv}(\mathcal{T})$ that can be expressed in closed form. The *relaxed primal CHP problem* is written as follows and the *approximate CHPs*, denoted $\bar{\lambda}$, are found as the optimal Lagrange multipliers of the nodal real power balance constraint (6.5a).

$$\min_{G\in\mathcal{X},\ T\in\text{relax}(\mathcal{T})} \quad \sum_{i\in\mathbb{N}} C_i(G_i) \tag{6.5}$$

$$st : D_i - G_i + \alpha T_i + (1-\alpha)T_i^d = 0 \quad \forall i \in \mathbb{N} \tag{6.5a}$$

The Lagrange multipliers of constraint (6.5a) can be recovered from a slightly reformulated

problem that represents a general convex relaxation of the AC OPF problem. To see this, reformulate the relaxed primal CHP problem by dividing the real power balance constraint by α to yield an equivalent problem that can be interpreted as a general convex relaxation of the AC OPF problem where the demand vector is represented as $\tilde{D}_i = \frac{1}{\alpha} D_i + \frac{1-\alpha}{\alpha} T_i^d$. In this context the generators must be redefined to have a generation amount of $\tilde{G}_i = \frac{1}{\alpha} G_i$, a cost function of $\tilde{C}_i(\tilde{G}_i) = C_i(\alpha \tilde{G}_i)$, and private constraints of $\tilde{\mathcal{X}}^i := \{\tilde{G}_i : \frac{1}{\alpha} G_i^{\min} \le \tilde{G}_i \le \frac{1}{\alpha} G_i^{\max}\}$. The resulting reformulation will produce Lagrange multipliers that differ from those of constraint (6.5a) by a factor of α. This allows CHPs to be approximated using algorithms initially developed to approximately solve convex relaxations of the AC OPF problem that are proven to converge in polynomial-time.

Intuitively, approximate CHPs minimize a function that represents an upper bound on the weighted sum of side-payments and PCRS. The conservative nature of this upper bound is dependent on the how well the convex relaxation represents the convex hull and on the magnitude of the weight parameter α. The following theorem makes this result explicit.

Theorem 6.4. Approximate CHPs, denoted $\bar{\lambda}$ and defined as the optimal Lagrange multipliers of constraint (6.5a), satisfy:

$$\bar{\lambda} \in \underset{\lambda \in \mathbb{R}^n}{argmin}\left(\alpha C^s(\lambda, G^d) + \underset{i \in \mathbb{N}}{\Sigma} C_i^o(\lambda_i, G_i^d) + \alpha\left(\Psi^r(\lambda) - \Psi^c(\lambda)\right)\right) \tag{6.6}$$

$$where \quad \Psi^r(\lambda) := \underset{f \in relax(\mathcal{T})}{max} \quad -\lambda^\dagger f \tag{6.7}$$

$$and \quad \Psi^c(\lambda) := \underset{f \in conv(\mathcal{T})}{max} \quad -\lambda^\dagger f \tag{6.8}$$

Proof: From the same process as the proof in Theorem 6.2, the prices $\bar{\lambda}$ maximize the following equation:

$$\underset{i \in \mathbb{N}}{\Sigma}(\lambda_i G_i^d - C_i(G_i^d) - \Upsilon_i(\lambda_i)) - \alpha(\lambda^\dagger T^d + \Psi^r(\lambda)) \tag{6.9}$$

By substituting the expression for generator uplift $C_i^o(\lambda_i, G_i^d)$, adding and subtracting the term $\alpha \Psi(\lambda)$, and noting that (6.3) implies $\Psi(\lambda) = \Psi^c(\lambda)$ we attain the following:

$$\underset{i \in \mathbb{N}}{\Sigma} C_i^o(\lambda_i, G_i^d) - \alpha(\lambda^\dagger T^d + \Psi(\lambda)) + \alpha(\Psi^c(\lambda) - \Psi^r(\lambda))$$

This is the negative of the objective function of (6.6). □

From Theorem 6.4, the objective function minimized by approximate CHPs is similar to that of CHPs from Definition 6.1. When the relaxed set relax($\mathcal{T}$) accurately represents the convex hull conv($\mathcal{T}$), CHPs match approximate CHPs because $\Psi^r(\lambda) = \Psi^c(\lambda)$. Also notice that the upper bound being minimized will be tighter if the weight parameter $\alpha > 0$ is smaller. Fortunately, as we discussed in Section 6.2, this weight parameter should be less than one. Of course approximate CHPs may match CHPs even if the relaxed set of feasible net real power injections does not match the convex hull. Future work will identify sufficient conditions for exactness.

Remark 6.1. Further studies should generalize Theorems 6.2, 6.3, and 6.4 to accommodate the UC problem over a 24 hour period. Such a generalization requires problems (6.2) and (6.5) to be restated such that the private constraint set of each generator $\mathcal{X}^i$ is replaced by its convex hull conv($\mathcal{X}^i$) and the cost function of each generator is replaced by its convex envelope, both of which are explicitly characterized in [45].

6.4 Shor's Rank Relaxation

This section provides a specific relaxation that will be used to approximate CHPs in Section 6.5. This relaxation is derived from the AC OPF problem in rectangular coordinates as described in Section 3.4 and is similar to other formulations in the literature [51,68]. First recognize that the decision variable $w \in \mathbb{R}^{2n}$ in problem (3.27) only appears in quadratic terms of the form $w^\dagger M w$, where M is an appropriately chosen quadratic coefficient matrix. Using properties of the trace operator, each of these quadratic terms can be generally rewritten as $w^\dagger M w = \text{Tr}(M w w^\dagger)$. Subsequently, the decision variable w will only appear in the form of $w w^\dagger$ and can thus be replaced by a matrix W restricted to be positive definite and rank 1. These restrictions are written as $W \in \mathbb{S}_+^{2n \times 2n}$ and rank(W) = 1 where $\mathbb{S}_+^{2n \times 2n}$ represents the set of symmetric positive semi-definite $2n \times 2n$ matrices. With this in mind problem (3.27) can be equivalently rewritten as follows:

$$\min_{G\in\mathbb{R}^n, W\in\mathbb{S}_+^{2n\times 2n}} \quad \underset{i\in\mathbb{N}}{\Sigma}\, C_i(G_i) \tag{6.10}$$

$$st: D_i - G_i = \mathrm{Tr}(H^{(i)}W) \quad \forall i \in \mathbb{N} \tag{6.10a}$$

$$\underline{U}_i \leq \mathrm{Tr}(Z^{(i)}W) \leq \bar{U}_i \quad \forall i \in \mathbb{N} \tag{6.10b}$$

$$-\bar{P}_{i,j} \leq \mathrm{Tr}(Z^{(i,j)}W) \leq \bar{P}_{i,j} \quad \forall(i,j)\in\mathbb{P} \text{ and } \forall(j,i)\in\mathbb{P} \tag{6.10c}$$

$$-\bar{Q}_{i,j} \leq \mathrm{Tr}(H^{(i,j)}W) \leq \bar{Q}_{i,j} \quad \forall(i,j)\in\mathbb{P} \text{ and } \forall(j,i)\in\mathbb{P} \tag{6.10d}$$

$$\mathrm{Tr}(Z^{(i,j)}W)^2 + \mathrm{Tr}(H^{(i,j)}W)^2 \leq \bar{S}_{i,j}^2 \quad \forall(i,j)\in\mathbb{P} \text{ and } \forall(j,i)\in\mathbb{P} \tag{6.10e}$$

$$0 \leq \mathrm{Tr}(M_iW) \leq \bar{V}_i \quad \forall i \in \mathbb{N} \tag{6.10f}$$

$$\underline{G}_i \leq G_i \leq \bar{G}_i \quad \forall i \in \mathbb{N} \tag{6.10g}$$

$$\mathrm{rank}(W) = 1 \tag{6.10h}$$

Shor's rank relaxation is attained by removing the rank constraint. This relaxation results in a convex optimization problem; however, the problem still must be placed in standard SDP form, which requires a linear objective function and constraints that are only linear and semi-definite. With this in mind we will assume that the cost function for each generator takes the quadratic form $C_i(G_i) = c_{i,2}G_i^2 + c_{i,1}G_i + c_{i,0}$. To make the objective function linear we will enforce the constraint $C_i(G_i) \leq t_i$ for each generator $i \in \mathbb{N}$ and minimize the value $\underset{i\in\mathbb{N}}{\Sigma}\, t_i$. The final step required to attain an SDP in standard form uses Schur's complement to reformulate the convex quadratic constraints. The SDP relaxed AC OPF problem is as follows:

$$\min_{t\in\mathbb{R}^n,G\in\mathbb{R}^n,W\in\mathbb{S}_+^{2n\times 2n}} \quad \sum_{i\in\mathbb{N}} t_i \tag{6.11}$$

$$st: D_i - G_i = \mathrm{Tr}(H^{(i)}W) \quad \forall i \in \mathbb{N} \tag{6.11a}$$

$$\underline{U}_i \leq \mathrm{Tr}(Z^{(i)}W) \leq \bar{U}_i \quad \forall i \in \mathbb{N} \tag{6.11b}$$

$$-\bar{P}_{i,j} \leq \mathrm{Tr}(Z^{(i,j)}W) \leq \bar{P}_{i,j} \quad \forall (i,j) \in \mathbb{P} \text{ and } \forall (j,i) \in \mathbb{P} \tag{6.11c}$$

$$-\bar{Q}_{i,j} \leq \mathrm{Tr}(H^{(i,j)}W) \leq \bar{Q}_{i,j} \quad \forall (i,j) \in \mathbb{P} \text{ and } \forall (j,i) \in \mathbb{P} \tag{6.11d}$$

$$\begin{bmatrix} \bar{S}_{i,j}^2 & -\mathrm{Tr}(Z^{(i,j)}W) & -\mathrm{Tr}(H^{(i,j)}W) \\ -\mathrm{Tr}(Z^{(i,j)}W) & 1 & 0 \\ -\mathrm{Tr}(H^{(i,j)}W) & 0 & 1 \end{bmatrix} \succeq \mathbf{0} \tag{6.11e}$$

$$0 \leq \mathrm{Tr}(M_iW) \leq \bar{V}_i \quad \forall i \in \mathbb{N} \tag{6.11f}$$

$$\underline{G}_i \leq G_i \leq \bar{G}_i \quad \forall i \in \mathbb{N} \tag{6.11g}$$

$$\begin{bmatrix} -c_{i,1}G_i - c_{i,0} + t_i & -\sqrt{c_{i,2}}G_i \\ -\sqrt{c_{i,2}}G_i & 1 \end{bmatrix} \succeq \mathbf{0} \quad \forall i \in \mathbb{N} \tag{6.11h}$$

This problem is written in standard SDP form. In fact, it can also be expressed in the form provided in (6.5) recognizing that the net real power injections are expressed as follows:

$$T_i = \mathrm{Tr}(H^{(i)}W) \quad \forall i \in \mathbb{N}. \tag{6.12}$$

In this case the relaxed feasible set of net real power injections is written as follows:

$$\mathrm{relax}(\mathcal{T}) = \{T \in \mathbb{R}^n : \exists W \text{ where } (6.12), (6.11b), (6.11c), (6.11d), (6.11e), (6.11f), (6.11g)\} \tag{6.13}$$

It should be apparent that this relaxed feasible set of net real power injections is convex because it is described by linear and semi-definite constraints. However, this set also requires a large number of variables to be introduced to the problem, increasing the dimension of the search space, and making the problem difficult to solve.

6.5   Numerical Results

This section extends the examples from Section 3.5. Specifically, Section 3.5 identifies positive PCRS for various test cases when using the fully detailed non-convex feasible set of net real power injections $\mathcal{T}$ defined in Chapter 3, which models real and reactive power as well as voltage magnitude. We will begin with the simple 3-bus example from Section 3.5.1 and

114

we will compute approximate CHPs by applying the standard Semi-Definite Programming (SDP) relaxation to obtain the convex relaxed set relax($\mathcal{T}$) as described in Section 6.4. We then move onto larger, more realistic networks, to which we apply three different relaxations including the SDP relaxation, the Quadratic Convex (QC) relaxation, and the Second-Order Cone (SOC) relaxation. The standard LMPs from Section 3.5 are compared to approximate CHPs for each relaxation. The weight parameter α from Definition 6.1 is set to one for all examples except the final example that illustrates the effect of varying α for a test case with 162 buses.

The loss-less DC approximation of the feasible set of net real power injections will be denoted $\mathcal{T}_{DC}$. This section will additionally analyze prices, termed DCLMPs, that are found as the Lagrange multipliers of the real power balance constraint of the DC OPF problem, which is equivalent to problem (2.6) with $\mathcal{T} = \mathcal{T}_{DC}$ where $\mathcal{T}_{DC}$ is defined by the loss-less DC approximation from Chapter 4.

The optimal dispatch as determined by the DC OPF problem should be dispatched along with DCLMPs; however, this dispatch may not be feasible for the true transmission network, whose feasible set of net real power injections is represented by the set $\mathcal{T}$. For this reason control action must be taken on fast time scales to attain a feasible dispatch. This section will assume that fast control action adjusts generator outputs to attain the optimal dispatch from the AC OPF problem $T^\star$. This assumption idealizes fast time scale control, which typically does not minimize cost.

In this section the SFC is defined using the true set of feasible net real power injections $\mathcal{T}$; however, when using the DC OPF problem the SFC is typically defined using the DC approximation $\mathcal{T}_{DC}$. This alternative definition of the SFC would not allow all financial transactions to achieve a full hedge because it does not consider losses. This is out of the scope of this dissertation. See [41] for a more detailed description of FTRs. To avoid confusion the remainder of this section will not specify PCRS when using DCLMPs.

6.5.1 Simple 3-bus System

This section studies the simple 3-bus power system described in detail in Section 3.5.1. The one-line diagram of this system is provided in Figure 6.1. The feasible set of net real

power injections at buses 1 and 2 form an elliptical shape illustrated in Figure 6.2. Notice that the feasible set of net real power injections $\mathcal{T}$ is now three dimensional; however, the elliptical shape in Figure 6.2 represents a slice of this set at the plane $T_3 = 0$. As explained in Remark 2.1, the feasible set of net real power injections does not enforce constraints on the net real power injections at buses. (Note: these constraints are accommodated by the feasible set of each generator $\mathcal{X}^i$ in the general ED problem (2.6)). This means that FTRs can be allocated to bus 3 even though its net real power injection is physically restricted to zero.
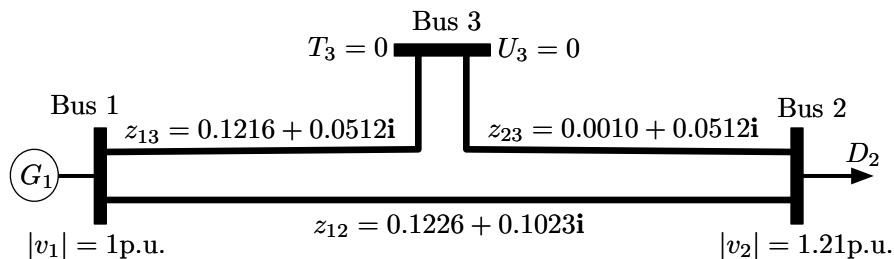
Figure 6.1: One-line diagram of the 3-bus test case. Repeated from Figure 3.2.

The consumption at bus 2 is fixed to 1p.u., so the net real power injection at bus two is $T_2 = -1$p.u. In this case the only feasible point is the green dot in Figure 6.2. This green dot will represent the solution to the AC OPF problem $(T_1^\star, T_2^\star, T_3^\star) \approx (5.4077, -1, 0)$. Notice this operating point accrues large line losses of approximately 4.5p.u. Bus 1 consists of one generator whose cost in dollars is represented by the following piece-wise linear cost function:

$$C_1(G_1) = \begin{cases} 0.5G_1 & \text{if } G_1 \leq 2 \\ G_1 & \text{if } G_1 > 2 \end{cases}$$

6.5.1.1 DCLMPs

The loss-less DC approximation of the feasible set of net real power injections $\mathcal{T}_{\text{DC}}$ is represented by the red line in Figure 6.2a. The black dot represents the optimal dispatch produced by the DC OPF problem; however, this point is not feasible for the true system. We assume that control on a fast time scale is able to adjust the generator dispatch values
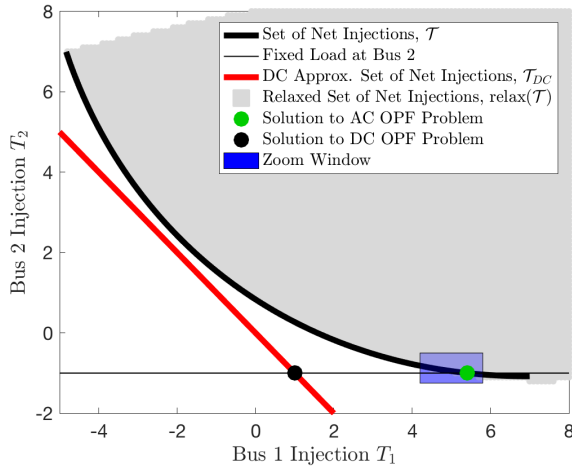
(a) Feasible Set of Net Real Power Injections
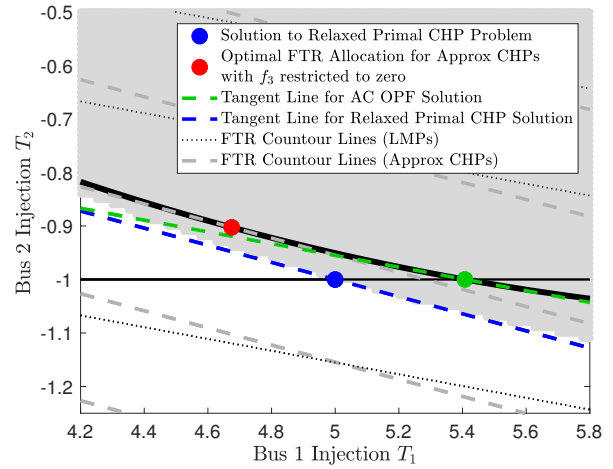
(b) Zoomed version of Fig.6.2a

Figure 6.2: This figure illustrates the feasible set of net real power injections along with its rank relaxed counterpart and its approximate DC counterpart. Figure 6.2a illustrates the feasible set of net real power injections in black along with its SDP relaxed version in grey and its DC approximated version in red. This feasible set is represented in two dimensions because bus three is a null-bus. Figure 6.2b is a zoomed in version of Figure 6.2a. Contours of the objective function in problem (2.4) are shown for the case of approximate CHPs and LMPs.

to attain the solution to the AC OPF problem, which is represented by the green dot in Figure 6.2.

The DCLMPs can be recovered as the Lagrange multipliers of the real power balance constraints of the DC OPF problem. Since no line limits are binding these prices are the same at each bus $\lambda_1^{\text{DC}} = \lambda_2^{\text{DC}} = \lambda_3^{\text{DC}} = \$0.5/\text{p.u.}$. These prices along with the optimal dispatch of the AC OPF problem $P^\star$ result in a generator side-payment of $C_1^o(\lambda_1^{\text{DC}}, T_1^\star) = (1 - \lambda_1^{\text{DC}})T_1^\star = \$2.7$.

6.5.1.2 LMPs

The LMPs were identified in Section 3.5.1, as described in Section 2.4. The LMPs for bus 1, 2 and 3 are $\lambda_1^\star = \$1/\text{p.u.}$, $\lambda_2^\star = \$9.455/\text{p.u.}$, and $\lambda_3^\star = \$9.461/\text{p.u.}$ respectively. The congestion revenue can be easily computed as $CR = \$4.05$. The side-payments to the generator is zero as proven by Theorem 6.1 and the payment to the generator is in the amount \$5.41. We found the PCRS to be \$0.26 with an optimal FTR allocation $f = [5.5929, 6.3464, -7.3892]$ in units of $p.u.$

117

The contour lines represented by the objective function of the FTR payoff maximization problem (2.4) are shown in Figure 6.2. The contour lines associated with the LMPs are represented by black dotted lines and are parallel to the tangent line at the green dot. The optimal FTR allocation occurs at the point where the contour lines are tangent to the feasible set of net real power injections $\mathcal{T}$. This point coincides with the dispatched set point represented by the green dot. Furthermore, at this point the Congestion Revenue Shortfall (CRS) is zero. This means that there does not exist an FTR allocation in the plane plotted in Figure 6.2 that results in congestion revenue shortfall. However, this plane restricts the FTR allocation for bus 3, f_3, to be zero. Since the set of net real power injections $\mathcal{T}$ is three dimensional, we need to expand our analysis to three dimensional FTR allocation vectors. In fact, Section 3.5.1 identified the PCRS to be \$0.26 with an optimal FTR allocation $f = [5.5929, 6.3464, -7.3892]$ in units of $p.u.$.

6.5.1.3 Approximate CHPs

Let's now identify the approximate CHPs using the SDP relaxation from [66]. These prices were found by solving the relaxed primal CHP problem (6.5) with $\alpha = 1$ using the CVX package in MATLAB [34]. The solver provides the optimal Lagrange multipliers for the real power balance constraint (6.5a), which are equivalent to the approximate CHPs. The approximate CHPs for bus 1, 2 and 3 are $\bar{\lambda}_1 = \$1/p.u.$, $\bar{\lambda}_2 = \$5.890/p.u.$, and $\bar{\lambda}_3 = \$5.920/p.u.$. Since $\bar{\lambda}_1 = \hat{\lambda}_1$ the generator side-payment remains zero and the generator payment remains \$5.41.

The contour lines associated with the FTR payoff maximization problem (2.4) when using approximate CHPs are represented by gray dashed lines in Figure 6.2 and are parallel to the tangent line at the blue dot. The optimal FTR allocation when using the approximate CHPs occur at the point where the contour lines are tangent to the feasible set of net real power injections $\mathcal{T}$. This point is represented by the red dot. Since the red dot does not coincide with the green dot, the FTR payoff at this point will be larger than the congestion revenue. We can conclude that the approximate CHPs introduce the possibility of positive CRS in the plane of FTR allocation vectors where $f_3 = 0$. As mentioned previously, this analysis should be extended to the three dimensional SFCs.

The PCRS using the identified CHPs is numerically found to be \$0.21 with an optimal FTR allocation $f^\star = [4.7284, -9.2816, 8.3189]$ in units of $p.u.$. The optimal FTR allocation is computed by solving the FTR payoff maximization problem (2.4). The PCRS computation is illustrated in Table 6.1. Specifically, the congestion revenue is easily found to be \$0.48 and the maximum FTR payoff can be computed as $-\lambda^{\star\dagger}f^\star = \$0.69$. The PCRS is the difference between the two, amounting to \$0.21.

Table 6.1: Evaluating PCRS for using approximate CHPs rounding to the nearest cent.

Demand Charge (\$)	Congestion Revenue(\$)	Max. FTR Payoff (\$)	PCRS (\$)
$\lambda_2^\star D_2$	$\lambda_2^\star D_2 - \lambda_1^\star G_1^d$	$\Psi(\lambda^\star) = -\lambda^{\star\dagger}f^\star$	$C^s(\lambda^\star, G^d)$
5.89	0.48	0.69	0.21

6.5.2 Examples on Standard Test Cases

Let's now consider the much larger NESTA test cases that were studied in Section 3.5.2 [17]. We consider three different relaxations of the feasible set of net real power injections when formulating the relaxed primal CHP problem (6.5). First is the SDP relaxation, which is implemented using the MATPOWER toolbox in MATLAB [68]. Some of the NESTA test cases can be solved exactly using the SDP relaxation. Such test cases yield zero side-payments and zero PCRS when using LMPs. Instead, we focus on test cases that cannot be solved exactly using the SDP relaxation and yield positive PCRS when using LMPs. We also consider the QC relaxation described in [18] and the SOC relaxation described in [46]. Both the QC and SOC relaxations are implemented using the PowerModels package in Julia [16].

Table 6.2 provides a comparison of side-payments and PCRS when using LMPs, approximate CHPs and DCLMPs. We provide results for six systems with 162 buses, 189 buses, 300 buses, 2224 buses, 2383 buses, and 3012 buses. When computing approximate CHPs we set the weight parameter to $\alpha=1$. By varying the weight parameter $0 < \alpha < 1$ we would expect to achieve PCRS and side-payments that fall between the two extremes produced by approximate CHPs and LMPs. Computing the PCRS for a given set of prices requires solving the non-convex max FTR payoff problem (2.4). The provided PCRS values

Table 6.2: Results for NESTA test cases. All amounts are in dollars per hour. For large test cases, a penalty is added to the objective function in the SDP-relaxed problem, associated values are denoted with an asterisk. The side-payments when using DCLMPs are ideal, assuming that fast control action optimizes cost, associated values are denoted with a triangle. PCRS values are omitted for DCLMPs to avoid confusion regarding the definition of the SFC. The weight parameter is $\alpha = 1$. The results pertaining to LMPs and total operating costs match those in Table 3.4

Test Case	LMPs (for AC OPF) Side Payments	PCRS	DCLMPs (for DC OPF) Side Payments	PCRS	Approximate CHPs with SDP Relaxation Side Payments	PCRS	Approximate CHPs with QC Relaxation Side Payments	PCRS	Approximate CHPs with SOC Relaxation Side Payments	PCRS	Total Operating Cost
162_ieee_dtc	~ 0	1,352.92	6.66$^\triangle$	-	0.11	42.55	127.48	26.87	127.33	28.94	4,230.23
189_edin	~ 0	1.22	4.66$^\triangle$	-	0.05	0.74	0.25	0.77	0.25	0.77	849.29
300_ieee	~ 0	36.87	257.40$^\triangle$	-	0.03	14.77	3.12	128.18	3.15	130.88	16,891.27
2224_edin	~ 0	520.76	75.92$^\triangle$	-	79.26*	343.47*	1,392.20	738.48	1,838.29	430.59	38,127.69
2383wp_mp	~ 0	13,681.00	289.12$^\triangle$	-	1,572.55*	4,023.87*	5,552.60	7,145.92	5,601.56	7,513.18	1,868,511.77
3012wp_mp	~ 0	1,815.44	6,303.82$^\triangle$	-	2,411.54*	1,348.35*	12,907.15	6,179.91	12,882.12	6,924.57	2,600,842.72

are computed using an interior point solver in Julia that identifies a local maximum of problem (2.4).

As explained in Section 3.5.2, LMPs result in zero side-payments to generators and positive PCRS. The PCRS may be very large with respect to the total operating cost as in test case 162_ieee_dtc (approximately 32%) or very small as in test case 3012wp_mp (approximately 0.07%). Furthermore, DCLMPs introduce a small amount of side-payments to generators, although these values will likely be much larger in practice where control on fast time scales is imperfect.

Approximate CHPs from the SDP relaxation perform well for the three smallest test cases. That is, as compared to LMPs, they tend to increase side-payments by a small amount and decrease PCRS significantly. Furthermore, approximate CHPs result in much lower side-payments as compared to DCLMPs.

Unfortunately, the MATPOWER algorithm used to solve the SDPs was unable to converge for the three largest test cases. For these cases we use a software package that employs an additional approximation by placing a penalty in the objective of the SDP-relaxed problem to encourage convergence [64] (associated quantities are denoted with an asterisk). The penalty parameters were adjusted for each individual test case. Despite using an additional approximation, the resulting approximate CHPs are still able to reduce PCRS as compared to LMPs.

Approximate CHPs from the QC and SOC relaxations result in similar PCRS and generator side-payments. These approximate CHPs result in higher generator side-payments and PCRS as compared to approximate CHPs from the SDP relaxation. In fact, these approximate CHPs increase the PCRS as compared to LMPs for test cases 300_ieee and 3012wp_mp.
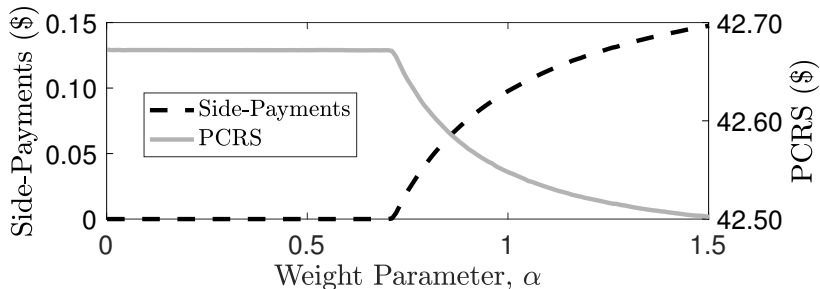
Figure 6.3: Competing objectives for test case 162_ieee_dtc.

To provide insight into the trade-off between PCRS and side-payments, let's analyze approximate CHPs for the test case 162_ieee_dtc using the SDP relaxation. Figure 6.3 shows the generator side-payments and PCRS as the weight parameter α varies from 0 to 1.5. As expected, side-payments increase in α, PCRS decreases in α, and the trajectories pass through their associated values in Table 6.2 when $\alpha = 1$. Interestingly, as the parameter α decreases, the side-payments reach zero at the point $\alpha = 0.72$ and cannot decrease further. At this point the PCRS remains constant at \$42.67. In fact, choosing parameter α below 0.72 results in approximate CHPs that achieve savings in PCRS of over 30% of the total operating cost as compared to LMPs while still maintaining zero side-payments.

6.6   Conclusions and Future Directions

This chapter incorporates non-linear models of the transmission system into the existing Convex Hull Pricing framework. In the context of the AC OPF problem we theoretically prove and empirically observe the tendency of CHPs to increase generator side-payments as compared to LMPs, which is significantly different from the behavior of CHPs in the context of the UC problem with linear network models. We define CHPs as the optimal solution to a novel multi-objective minimum uplift problem that captures the trade-off between generator

side-payments and PCRS. For the first time, we present a method of approximating CHPs using non-linear transmission constraints that are general enough to accommodate the AC OPF problem. Specifically, CHPs are approximated by the optimal Lagrange multipliers of the relaxed primal CHP problem, which can be approximately solved using well-known polynomial-time algorithms that approximately solve relaxed versions of the AC OPF problem. We provide a theoretical result illustrating that approximation accuracy can be improved by tightening the relaxation used or by placing more value in generator side-payments as compared to PCRS using the parameter α.

Examples show that FTR uplift may be large when using LMPs, motivating the inclusion of non-linear models of the transmission network into the CHP framework. We then approximate CHPs using SDP, QC, and SOC relaxations of the AC transmission network. The SDP relaxation is shown to effectively approximate CHPs; however, existing algorithms used to solve this relaxed SDP problem do not scale well with the size of the transmission network. In fact, using the SDP relaxation we are able to identify CHPs that significantly reduce PCRS while hardly effecting generator side-payments.

Future work will extend the concepts from this chapter to the unit commitment problem. Of course the unit commitment problem does not incorporate the full AC model of the transmission system as it is implemented today. However, the unit commitment problem implemented today does account for a non-linear transmission model using the linearization techniques derived in Chapters 4 and 5. For this reason future work will define the feasible set of net real power injections $\mathcal{T}$ using the approximate non-linear transmission models derived in Chapter 4. In fact, when using these approximate non-linear transmission models we believe the exact CHPs can be recovered by use of the load over-satisfaction relaxation under the condition that all CHPs are positive.

Part II
Co-Optimization: Interdependent Reserve Types

Part II of this dissertation incorporates reserve procurement into the economic dispatch problem. The resulting problem is called a co-optimization problem because it optimizes the reserve products along with the electric generation product. The Electric Reliability Council of Texas (ERCOT) is currently planning to implement a co-optimization problem into the real-time electricity market in Texas [26]. As explained in Chapter 1, the Public Utility Commission of Texas (PUCT) has considered the introduction of real-time co-optimization separately from the introduction of transmission losses. Consistent with the PUCT's analysis, this part of the dissertation will use a linear model of the transmission network that does not account for transmission losses.

Co-optimization problems enforce a reserve requirement that necessitates the procurement of sufficient reserve to accommodate specific contingencies. For example, ERCOT requires reserve capable of withstanding the simultaneous outage of the two largest generators [59]. Chapter 7 derives various reserve requirements from first principles including a novel requirement termed the *rate-based PFR limit* and an existing requirement termed the *equivalency ratio requirement*, which has only been studied empirically in previous work [59]. Chapter 8 places the derived reserve requirements into a co-optimization problem. This chapter compares and contrasts the *equivalency ratio requirement*, which results in a convex co-optimization problem, and the *rate-based PFR limit*, which results in a non-convex co-optimization problem.

Chapter 7

Reserve Requirements

ERCOT recently redefined the reserve types considered in the electricity market in Texas. As per Nodal Protocol Revision Request (NPRR) 863, all reserve types that contribute to primary frequency response are referred to as Responsive Reserve (RR) and include Primary Frequency Responsive (PFR) reserve and Fast Frequency Responsive (FFR) reserve [25]. All other reserve types considered in ERCOT are deployed on slower time scales and will not be considered throughout Part II of this dissertation. This chapter derives requirements for RR that are unaffected by all the neglected slower acting reserve types.

PFR reserve is defined to accommodate standard droop control provided by traditional generators. The amount of PFR reserve provided by generator i will be denoted r_i. This chapter conservatively assumes that generators contracting to provide PFR reserve are the only generators in the system that actually do provide droop control. This assumption deviates slightly from ERCOT requirements, which instead widen the droop control dead-band for all generators that are not contracting to provide PFR reserve [25]. The definition and implementation of FFR reserve was recently introduced by NPRR 581 and accommodates fast acting resources that are capable of changing their power output almost instantaneously [24]. Any resource can provide FFR reserve if it experiences little to no ramping limitations; however, this type of reserve is primarily intended for new battery technologies such as lithium ion batteries and so, for brevity, the word battery will generally be used in reference to FFR reserve. The amount of FFR reserve provided by battery j will be denoted b_j.

This introduction section will first outline a general reserve requirement that ensures the system is capable of accommodating a large loss of generation of size L. Intuitively, this requirement will additionally ensure sufficient reserve to accommodate any less severe

contingencies (See Remark 7.1). To ensure reserve procurement is capable of accommodating a generator outage (possibly including multiple simultaneous unit outages) of size L, we must satisfy the following general requirement:

$$\mathbf{1}^\dagger r + \mathbf{1}^\dagger b \geq L \tag{7.1}$$

In the context of primary frequency control, accommodating a generator outage of size L requires that the voltage frequency trajectory remain above some critical frequency threshold denoted $\omega_{\min}$, which is 59.4Hz in ERCOT. This critical frequency threshold typically represents the point at which firm load begins to disconnect from the system as an emergency precaution to avoid a system wide blackout (See Remark 7.2). As explained in Section 1.2, this requires power balance between mechanical prime mover power and net electrical consumption to be met before the frequency falls below the critical frequency threshold. Unlike FFR reserve, PFR reserve may not be capable of providing all procured reserve within this time constraint due to turbine governor ramping limitations. With this in mind, the PFR reserve amount appearing in the requirement (7.1), denoted r_i, must be available to be deployed before the critical frequency threshold is met and thus we will hence-forth refer to this quantity as the *available PFR reserve.* In contrast, the *nominal PFR reserve*, denoted R_i, will refer to the product quantity that generator i is contracting to provide in the electricity market. Intuitively, the nominal PFR reserve will represent the minimum of the head-room of the generator and the generator's offered PFR capacity. In our context the *head-room* of the generator is the generator's capacity $\bar{G}_i$ less its generation dispatch value G_i and the generator's *offered PFR capacity*, denoted $\bar{R}_i$, is an offered quantity in the electricity market representing the maximum amount of nominal PFR reserve the generator is willing to provide. The distinction between nominal PFR reserve, as determined by the head-room, and the available PFR reserve, as determined by governor ramping limitations, is essential to understanding and analyzing the role and value of FFR reserve.

Remark 7.1. All reserve requirements in ERCOT aim to ensure sufficient reserve to accommodate the simultaneous outage of the two largest generators in the system and thus L is chosen to be the combined capacity of the two largest generators, which approximately amounts to 2750MW [59]. Additionally, the requirement (7.1) intuitively ensures sufficient

reserve to accommodate any less severe contingencies. For example, this requirement will ensure sufficient Responsive Reserve to accommodate fluctuations in net demand caused by variable wind generation. This is because net demand fluctuations are small compared to L on the short time scales pertaining to primary frequency response.

Remark 7.2. Although the critical frequency threshold intuitively represents the point at which firm load begins to disconnect from the system, firm load in ERCOT begins to disconnect from the system at a frequency of 59.3Hz, which is conservatively set 0.1Hz below the critical frequency threshold of $\omega_{\min} = 59.4$Hz. In other words, reserve requirements are designed to maintain the frequency above $\omega_{\min} = 59.4$Hz, which is 0.1Hz higher than the frequency at which firm load begins to disconnect from the system [59]. This 0.1Hz margin accommodates, for example, errors in frequency measurement that may occur during the transient conditions accompanying a large generator outage.

It is apparent that the available PFR reserve should be constrained to be less than the nominal PFR reserve, e.g. $r_i \leq R_i$. However, the available PFR reserve for a generator may also be limited by other factors including the ramping ability of the generator and the time taken to reach the critical frequency threshold. With this in mind, this chapter will provide different limits that can be placed on the available PFR reserve to ensure it can be delivered before the critical frequency threshold is met. Each of these PFR reserve limits utilize different turbine governor models that account for the ramping ability of PFR reserve. The first such limit, presented in Section 7.3, is termed the *rate-based PFR limit*, and is derived from a turbine governor model that assumes a constant ramp rate. The second such limit, presented in Section 7.4.1, is termed the *proportional PFR limit*, and is derived from a turbine governor model that assumes the ramp rate is proportional to the generator's nominal PFR reserve. The third such limit, presented in Section 7.4.2, is termed the *equivalency ratio PFR limit* and is consistent with the reserve requirement provided by [59] that is based on empirical analysis of ERCOT system responses under various conditions of inertia.

The rest of this chapter discusses the following. Section 7.1 provides a model of the three contributors to arresting frequency decline in the event of a large generator outage: inertia, PFR reserve, and FFR reserve. This section distinguishes between *nominal PFR*

reserve and *available PFR reserve.* This section additionally explains the traditional offered PFR capacity limit, which is derived from a droop signal that is proportional to frequency deviations. The remainder of the chapter builds towards the derivation of other PFR reserve limits that consider turbine governor ramping limitations and guarantee that the critical frequency threshold is not violated. Section 7.2 models the ramping limitations of a turbine governor using a simple time delay followed by a constant ramp rate. This section continues by providing a system wide model of the frequency response that also utilizes a simple time delay followed by a constant ramp rate. Section 7.3 then uses the constant ramp rate models from Section 7.2 to derive the rate-based PFR limit that guarantees the frequency does not fall below the critical frequency threshold and is proportional to the ramp rate of the corresponding generator. Section 7.4 derives the proportional PFR limit by assuming that a generator's ramp rate is proportional to its nominal PFR reserve. Section 7.4 continues by presenting the equivalency ratio PFR limit which is derived from the reserve requirement from [59]. A connection is then drawn between the proportional PFR limit and the equivalency ratio PFR limit that gives first principles insight into equivalency ratios. Finally, the reserve requirements are summarized in Section 7.5, which explains that any combination of the derived limits on available PFR reserve can be enforced in a co-optimization problem.

7.1 Three Contributors to Arresting Frequency

The three main contributors to arresting frequency decline in response to a large generator outage are inertia, PFR reserve, and FFR reserve. Each of these three contributors to arresting frequency decline will now be modeled in detail.

7.1.1 Inertia and Frequency Dynamics

Voltages in the system are modeled as quasi-steady state sinusoids whose frequency may be slowly varying. Moreover, this voltage frequency at time t is modeled as being the same at each generator in the system and is denoted $\omega(t)$. The total post-outage inertia is M (in units of Watt-seconds or Ws) and represents the sum of inertia values for all generators that are still in service after the outage. The simplified system dynamics are represented by

127

the *swing equation* [3], which is expressed as follows:

$$\frac{d\omega(t)}{dt} = \frac{\omega_0}{2M}(\mathbf{1}^{\dagger}\mathbf{m}(t) - \mathbf{e}(t)), \tag{7.2}$$

where $\mathbf{m}(t) \in \mathbb{R}^n$ represents the vector of mechanical power input from the turbine governor of each generator in the system and $\mathbf{e}(t) \in \mathbb{R}$ represents the total net electrical demand in the system. Notice that $\mathbf{m}(t)$ is in bold font to distinguish it from the number of transmission lines in the system, which is denoted m. The number of generators in the system is denoted n, the vector of ones is denoted $\mathbf{1}$, and a superscript dagger $\dagger$ represents the transpose operator. This model makes the common assumption that there is no system damping, which is a conservative assumption since damping will tend to reduce the frequency excursions. The *nominal frequency* is denoted ω_0 and will be assumed to be the frequency just prior to the time of the generator outage.

7.1.2 Fast Frequency Responsive Reserve

We assume that Fast Frequency Responsive (FFR) reserve can be fully deployed instantaneously and can be provided by any device that does not exhibit ramping constraints. FFR capable devices include fast-acting battery storage and load-shedding. For brevity, we will henceforth refer to devices providing FFR reserve as *batteries* and we will refer to each battery by its corresponding index in the set $\mathbb{B} = [1, \dots, \beta]$ where β is the total number of FFR resources. Despite referring to these resources as batteries, the analysis covers both batteries and load-shedding as FFR resources. The amount of FFR reserve provided by each battery is denoted b_j and each battery provides an *offered FFR capacity* in the amount of $\bar{b}_j$. The private battery constraints exhibited by each battery are then written as follows:

$$\mathcal{B}^j := \{b_j \in \mathbb{R} : 0 \le b_j \le \bar{b}_j\}. \tag{7.3}$$

The FFR reserve is triggered when the frequency drops below a frequency threshold of $\omega_2 < \omega_1$, where ω_1 is the frequency corresponding to the dead-band of droop control. Note that ω_2 is typically significantly lower than the frequency ω_1 corresponding to the dead-band of droop control. In fact, FFR reserve is considered a reserve type that is deployed only during emergencies involving the largest generator outages as opposed to PFR reserve which

is used for essentially all contingencies. When deployed, the FFR reserve instantaneously decreases the net electrical demand in the system $\mathbf{e}(t)$ by an amount $\mathbf{1}^\dagger b$. We additionally introduce the non-negative constant $\Delta_2 := \omega_1 - \omega_2$.

7.1.3 Primary Frequency Responsive Reserve and Droop Control

Primary Frequency Responsive (PFR) reserve is intended to be compatible with conventional generator droop control, which increases the mechanical power output of the turbine governor $\mathbf{m}_i(t)$ in response to a large generator outage. PFR reserve is provided by generators that may also be selling power into the electricity market. The nominal PFR reserve R_i must satisfy $G_i + R_i \leq \bar{G}_i$, where G_i is the dispatched electric power generation of generator i and $\bar{G}_i$ is its capacity. Furthermore, each generator has an *offered PFR capacity* denoted $\bar{R}_i$. With this in mind, the private constraints of generator i can be generalized from the previous definition in Section 2.2.2. Specifically, the private constraints for generator i are now written as follows:

$$\mathcal{X}^i := \{(G_i, R_i) \in \mathbb{R} \times \mathbb{R} : \underline{G}_i \leq G_i \leq \bar{G}_i - R_i \text{ and } 0 \leq R_i \leq \bar{R}_i\}, \tag{7.4}$$

The ISO typically has qualification requirements that implicitly or explicitly determine a limit on the offered PFR capacity $\bar{R}_i$ that a generator can offer into the market. To derive this limit on the offered PFR capacity $\bar{R}_i$ we first must describe standard droop control in detail. Subsequently, the concept of available PFR reserve will be introduced, which further limits the amount of PFR that can be deployed in particular system conditions, to account for turbine governor ramping limitations.

7.1.3.1 Standard Droop Control

Generators providing PFR reserve respond to local frequency via droop control by adjusting the reference mechanical power output of their turbine governor $\mathbf{m}_i^{\text{ref}}(t)$ on the time scale of $\frac{1}{\omega^0} \approx 0.016$ seconds. In the context of droop control, the generation value G_i represents the nominal value of $\mathbf{m}_i^{\text{ref}}(t)$ around which the adjustments are made and is updated when the real-time market clears on the time scale of minutes. Furthermore, during droop control the reference mechanical power output of each generator's turbine governor is

129

limited implicitly by the need to preserve capacity for reserves, is adjusted depending on the generator's local frequency deviation, and has a dead-band of $\Delta_1 := \omega_0 - \omega_1$ where $\omega_1 < \omega_0$ represents the low end of the dead-band. This reference signal is written as follows and is illustrated in Figure 7.1.

$$\mathbf{m}_i^{\text{ref}}(t) = \begin{cases} G_i & \text{if } -\Delta_1 \leq \omega(t) - \omega_0 \leq \Delta_1 \\ G_i + R_i & \text{if } -\gamma_i(\omega(t) - \omega_0) - \gamma_i\Delta_1 \geq R_i \\ G_i - R_i^{\text{down}} & \text{if } -\gamma_i(\omega(t) - \omega_0) + \gamma_i\Delta_1 \leq R_i^{\text{down}} \\ G_i - \gamma_i(\omega(t) - \omega_0) - \gamma_i\Delta_1 & \text{if } 0 < -\gamma_i(\omega(t) - \omega_0) - \gamma_i\Delta_1 < R_i \\ G_i - \gamma_i(\omega(t) - \omega_0) + \gamma_i\Delta_1 & \text{else} \end{cases} \quad (7.5)$$

where ω^0 is the nominal frequency, $\omega(t)$ is the system frequency at time t, γ_i is the droop constant for generator i, and R_i^{down} is the nominal down PFR reserve. Notice that the droop reference signal is limited by the nominal PFR reserve R_i. This is because the nominal PFR reserve R_i intuitively represents either the PFR reserve capacity $\bar{R}_i$ or the headroom of the generator $\bar{G}_i - G_i$. If this limit is not imposed by the droop reference signal, then droop control could cause the generator to violate its capacity, denoted $\bar{G}_i$.
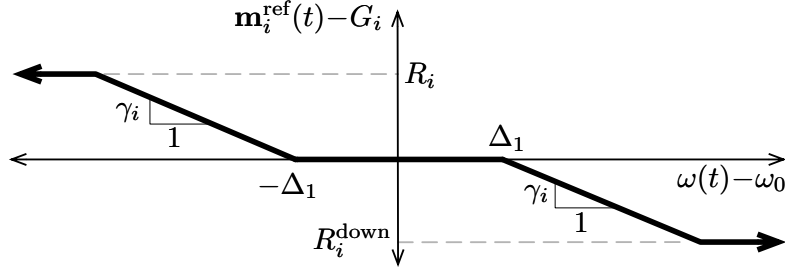
Figure 7.1: Droop signal with dead-band.

The reference mechanical power output then traverses the turbine governor dynamics of the generator to produce the realized mechanical power output, denoted $\mathbf{m}_i(t)$. These turbine governor dynamics can be very complicated and are not detailed in our work. See [50] for a description of turbine governor dynamics.

7.1.3.2 Offered PFR Capacity Limits

Notice that the reference mechanical power output $\mathbf{m}_i^{\text{ref}}(t)$ cannot attain a value larger than $G_i + \gamma_i(\omega_0 - \omega_{\text{min}}) - \gamma_i\Delta_1$ without the critical frequency threshold ω_{min} being violated. For this reason, ISOs should impose the following offered PFR capacity limit for

each generator i:

$$\bar{R}_i \leq \gamma_i(\omega_0 - \omega_{\min}) - \gamma_i\Delta_1 \tag{7.6}$$

The droop constant γ_i is chosen based on a required droop percentage imposed by the ISO. The droop percentage represents the percent change in frequency required to achieve a governor change of 100 percent capacity. Let ν_i represent the droop percentage for each generator expressed as a fraction. For example, in ERCOT the droop percentage is typically set to 5% and so $\nu_i = 0.05$. The proportionality droop constant γ_i used during droop control satisfies $\gamma_i\nu_i\omega_0 - \gamma_i\Delta_1 = \bar{G}_i$ and can be determined as follows:

$$\gamma_i = \frac{\bar{G}_i}{\nu_i\omega_0 - \Delta_1} \tag{7.7}$$

This definition of the droop constant is consistent with BAL-001-TRE-1, the reliability standard that details primary frequency response requirements in ERCOT [23]. Following from (7.6) and (7.7) the offered PFR capacity limit is written as follows:

$$\bar{R}_i \leq \frac{\bar{G}_i(\omega_0 - \omega_{\min} - \Delta_1)}{\nu_i\omega_0 - \Delta_1} \approx \frac{\bar{G}_i(\omega_0 - \omega_{\min})}{\nu_i\omega_0}. \tag{7.8}$$

The approximation assumes that the dead-band for droop control Δ_1 is very small. Although the approximation over estimates the offered PFR capacity limit, the approximation error is typically very small and is easily accommodated by the conservatively chosen critical frequency threshold $\omega_{\min}$ (See Remark 7.2). In fact, the typical dead-band in ERCOT is $\Delta_1 = 0.017$Hz, which is significantly smaller than the value $\omega_0 - \omega_{\min} = 0.6$Hz and the typical value of $\nu_i\omega_0 = 3$Hz for the typical droop percentage of 5%. Furthermore, the critical frequency threshold is $\omega_{\min} = 59.4$Hz in ERCOT and ERCOT uses the approximation outlined in (7.8). In this case the offered PFR capacity limit is $0.2\bar{G}_i$ for a generator i with 5% droop. This is consistent with ERCOT protocols.

7.1.3.3 Available PFR Reserve and Ramping Limitations

The reference mechanical power output must traverse the turbine governor dynamics of the generator to produce realized mechanical power output, denoted $\mathbf{m}_i(t)$. As mentioned above, these turbine governor dynamics can be very complicated and are not detailed in our

work. However, a salient feature of these turbine governor dynamics is that the mechanical power output $\mathbf{m}_i(t)$ tends to lag the reference mechanical power input $\mathbf{m}_i^{\mathrm{ref}}(t)$, particularly if the reference signal changes quickly. For this reason, it is possible that a generator's PFR reserve is not fully available before the critical frequency threshold is met, effectively exhibiting ramp limitations that restrict its power output. Current practices do not account for these ramping limitations. This chapter addresses this shortfall of current practices by differentiating between the nominal PFR reserve, denoted R_i, and the *available* PFR reserve, denoted r_i, which represents the amount of PFR reserve that is actually available as increased generation before the critical frequency threshold is reached.

In general, the available PFR reserve r_i may depend on the generator's nominal PFR reserve R_i, turbine governor ramping capabilities, and the time taken for the system frequency to reach the critical frequency threshold, which in turn will depend on various system-wide parameters. This chapter will provide various limits that restrict the amount of available PFR reserve based on the generators' ramping restrictions. The first limit on the available PFR reserve is very simple and follows from the fact that a generator's mechanical power output will never rise above its reference input. With this in mind the available PFR reserve should be less than the generator's nominal PFR reserve and thus the following holds:

$$r_i \leq R_i \tag{7.9}$$

Note that the available reserve quantity r_i will be eliminated as a decision variable in the co-optimization problems in Chapter 8. On the other hand, this chapter will explicitly represent the available reserve quantity as r_i to clearly distinguish it from the nominal PFR reserve quantity R_i.

7.2 Approximating Ramp Limitations of PFR Reserve

This section will approximate turbine governor dynamics using a simple ramp rate approximation. We will first describe the model of the turbine governors and then describe a model of the system as a whole. The subsequent section will then use these models to derive a limit on the available PFR reserve.

7.2.1 Simple Turbine Governor Model

We need only characterize each generator's turbine governor response to the very specific situation where a large loss of generation occurs since all smaller contingencies will result in smaller frequency excursions. Such a response is similar to that of a step response in the reference mechanical power output because of the fast frequency drop. This type of response is illustrated in Figure 7.2, where the amount of available PFR reserve for generator i is denoted by r_i and the mechanical power output of the turbine governor for generator i at time t is denoted $\mathbf{m}_i(t)$. The approximate piecewise linear model shown in this figure is adopted from [15].
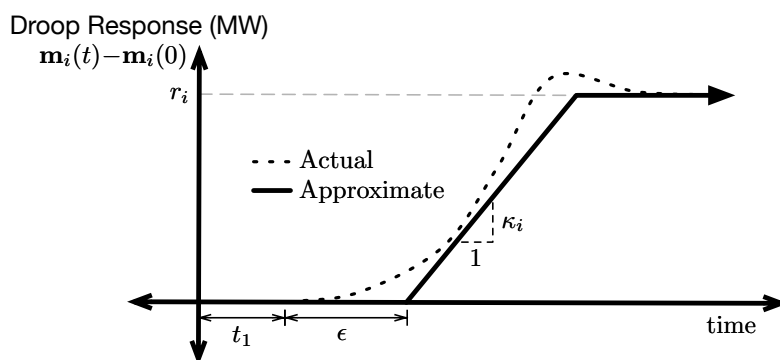
Figure 7.2: Turbine governor response to generator outage.

The mechanical power output of generator i is assumed to match its dispatched generation G_i^d at the time of the generator outage $t = 0$, e.g. $\mathbf{m}_i(0) = G_i^d$. Following the outage at $t = 0$ the frequency begins to drop. At the time $t = t_1$ the frequency reaches the lower end of the frequency dead-band $\omega(t_1) = \omega_0 - \Delta_1$. Subsequently, the turbine governor is modeled as experiencing a small time delay ϵ. Although this time delay will be assumed the same for all generators, this is only a simplifying assumption that can be easily extended. After exhibiting this time delay, the mechanical power output will be modeled as having a constant governor ramp rate κ_i that will continue until all available PFR reserve r_i is deployed. This constant ramp rate should be chosen conservatively in a way that underestimates the mechanical power output of the turbine governor. Since this model underestimates the mechanical power output of the turbine governor, the modeled frequency trajectory will have a larger excursion than the realized frequency trajectory and so the analysis will be conservative.

7.2.2 System-Wide Frequency Response Model

This subsection provides a simple model of the frequency response exhibited by the system in response to a large generator outage. The response in system frequency $\omega(t)$ and power imbalance $\mathbf{1}^\dagger\mathbf{m}(t)-\mathbf{e}(t)$ is shown by the solid black trajectories in Figure 7.3. These trajectories satisfy the swing equation (7.2) and so the frequency $\omega(t)$ is proportional to the integral of the energy imbalance curve.
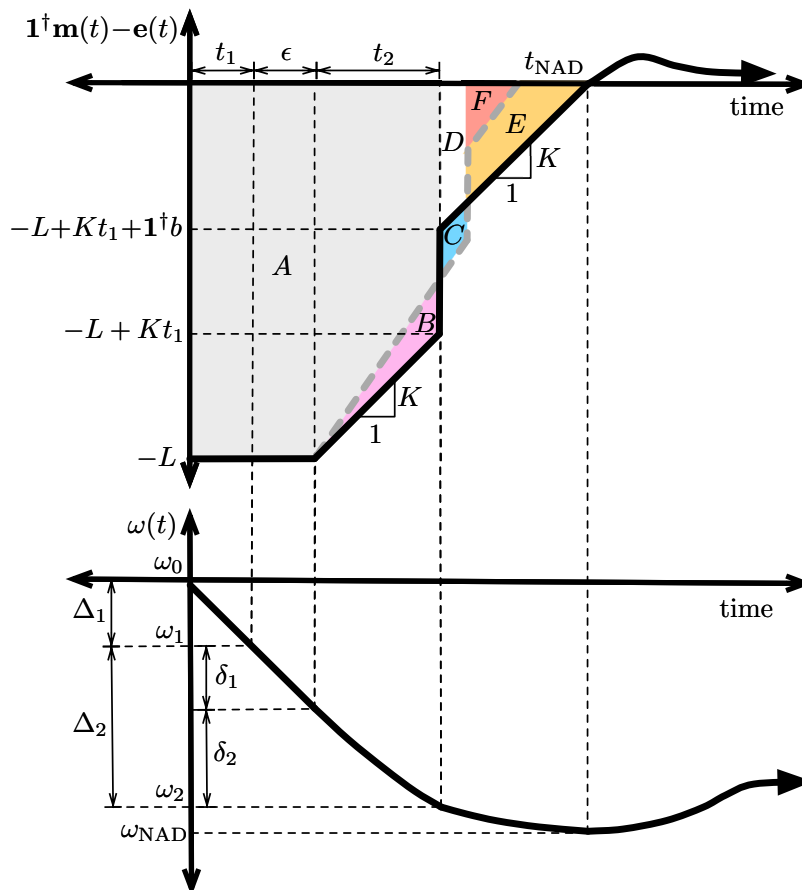
Figure 7.3: This plot is not drawn to scale. The top plot shows the energy imbalance over time. The main power trajectory is shown as a solid black line with aggregate ramp rate K. The dashed gray line represents a trajectory with a slightly increased aggregate ramp rate K'. Six non-overlapping regions are colored and labeled A through F. The bottom plot shows the frequency trajectory corresponding to the main power trajectory.

As shown in Figure 7.3, the PFR reserve is deployed at time t_1 when the frequency falls below the dead-band threshold of $\omega_1 = \omega_0 - \Delta_1$; however, the ramp of mechanical power

$\mathbf{1}^{\dagger}\mathbf{m}(t)$ begins after a further time delay of ϵ. The frequency is $\omega_0 - \Delta_1 - \delta_1$ at the time $t_1 + \epsilon$ of the beginning of the ramp. The PFR reserve is modeled as ramping with constant *aggregate ramp rate* K. While the PFR reserve is ramping up the FFR reserve is deployed. The FFR is instantaneously deployed at time $t_1 + \epsilon + t_2$ when the frequency falls below the dead-band threshold of $\omega_2 = \omega_0 - \Delta_1 - \Delta_2$. Subsequently, the ramp continues until the mechanical power input of the turbine governors meet the electric power demand of the system at time t_{NAD}, at which point the frequency nadir is realized, denoted ω_{NAD}. We assume that the PFR reserve ramps at the rate K throughout the time from $t_1 + \epsilon$ to t_{NAD}.

Remark 7.3. Based on the model from the previous subsection the summed mechanical power output of PFR generators $\mathbf{1}^{\dagger}\mathbf{m}(t)$ will not exhibit a constant aggregate ramp rate, K. In fact, some generators may deploy all PFR reserve before the frequency nadir is reached, in which case the aggregate ramp rate will effectively decrease over time. Section 7.3.2 will explain why using a constant aggregate ramp rate K is a conservative model of the aggregate behavior of the PFR reserve.

Notice that ϵ, Δ_1, Δ_2, ω_0, ω_1, and ω_2 are all non-negative constant parameters. The swing equation (7.2) allows us to derive expressions for the other parameters by computing the integral of the power imbalance curve in Figure 7.3. In this way it can be shown that:

$$\delta_1 = \frac{\omega_0}{2M}\epsilon L \quad \text{and} \quad \delta_2 = \Delta_2 - \frac{\omega_0}{2M}\epsilon L, \tag{7.10}$$

$$t_1 = \frac{2M\Delta_1}{L\omega_0} \quad \text{and} \quad t_2 = \frac{1}{K}\left(L - \sqrt{L^2 - \frac{4M}{\omega_0}K\delta_2}\right). \tag{7.11}$$

We will additionally impose a few assumptions regarding the response of the system. Specifically, we assume the deployment of FFR reserve occurs in the middle of the PFR reserve ramp. We claim that this is a reasonable assumption because PFR reserve is typically deployed at a dead-band threshold Δ_1 that is much tighter than the FFR reserve dead-band threshold $\Delta_1 + \Delta_2$ consistent with the intention that PFR reserve is deployed for all contingencies, but FFR reserve is deployed only for the largest of contingencies. Furthermore, we assume there is enough reserve to restore power balance and we assume that the power imbalance $\mathbf{1}^{\dagger}\mathbf{m}(t) - \mathbf{e}(t)$ remains non-positive after the FFR reserve is deployed. These assumptions are stated as follows:

Assumption 7.1. We assume the constant parameters are such that the FFR reserve is deployed during the PFR reserve ramp:

$$\delta_1 = \tfrac{\epsilon L \omega_0}{2M} \leq \Delta_2 \quad \text{and} \quad \Delta_1 + \Delta_2 \leq \omega_0 - \omega_{\text{NAD}} \tag{7.12}$$

We assume there is sufficient reserve to restore power balance and the power imbalance remains non-positive immediately after the FFR reserve is deployed:

$$\mathbf{1}^\dagger b + \mathbf{1}^\dagger r \geq L \quad \text{and} \quad K t_2 + \mathbf{1}^\dagger b \leq L \tag{7.13}$$

The frequency thresholds are set according to the ERCOT NPRR 863 [25], resulting in $\omega_0 = 60\text{Hz}$, $\omega_1 = 59.9833\text{Hz}$, and $\omega_2 = 59.8\text{Hz}$. These parameters will be used in all numerical results in Part II of this dissertation along with a PFR time delay of $\epsilon = 0.5$ seconds. Furthermore, L is set to 2750MW to represent the loss of the two largest generators in ERCOT. With these parameters, the assumption from (7.12) holds.

Remark 7.4. Future work should focus on situations where Assumption 7.1 does not hold. For example, we could accommodate FFR reserve being triggered before or after the PFR reserve ramp. We could also accommodate the situation where FFR reserve deployment immediately results in a positive energy imbalance.

7.3   Rate-Based PFR Reserve Limit

This section derives an additional condition that the available PFR reserve should satisfy in order to ensure adequate reserve procurement. This condition is called the rate-based PFR limit and is sufficient in guaranteeing adequate reserve procurement under the assumption that the approximate ramping models from Section 7.2.1 underestimate the mechanical power output of each individual generator.

7.3.1   Minimum Aggregate Ramp Rate

The frequency nadir increases (that is, improves) with increasing aggregate ramp rate K. Equivalently, the frequency deviation $\Delta\omega := \omega_0 - \omega_{\text{NAD}}$ decreases with the aggregate ramp

rate. To see this first notice that the frequency deviation corresponding to the main power trajectory illustrated in Figure 7.3 can be expressed as $\Delta\omega := \frac{\omega_0}{2M}(A+B+D+E+F)$, where capital letters represent their corresponding shaded area indicated in the figure. Now consider a slight increase in aggregate ramp rate from K to K', resulting in the energy imbalance curve illustrated by the dashed gray line. Notice that the FFR reserve is now triggered later in time because the frequency does not decline as fast. The frequency deviation can now be expressed as $\Delta\omega' := \frac{\omega_0}{2M}(A+C+D+F)$. Since the FFR reserve is always deployed instantaneously and fully at the same frequency ω_2, the area under the curve prior to the FFR deployment will remain constant for all aggregate ramp rates. As a result we must have $B = C + D$ and thus the following holds:

$$\Delta\omega = \tfrac{\omega_0}{2M}(A + C + 2D + E + F) > \tfrac{\omega_0}{2M}(A + C + D + F) = \Delta\omega' \qquad (7.14)$$

This analysis implies that the frequency deviation $\Delta\omega$ is strictly monotonically decreasing in the aggregate ramp rate K. Equivalently, the frequency nadir ω_{NAD} is strictly monotonically increasing with the aggregate ramp rate K. As a result there exists a unique ramp rate $K_{\min}$ such that the frequency nadir is $\omega_{\mathrm{NAD}} = \omega_{\min}$. Furthermore, all aggregate ramp rates greater than this *minimum aggregate ramp rate* $K_{\min}$ will satisfy the minimum frequency threshold, e.g. $\omega_{\mathrm{NAD}} \geq \omega_{\min}$. The following result provides an expression for $K_{\min}$ where the *total FFR reserve* is denoted $\tilde{b} := \mathbf{1}^\dagger b$ and a constant is introduced as $\Delta_3 := \omega_0 - \Delta_1 - \Delta_2 - \omega_{\min}$.

Theorem 7.1. Under Assumption 7.1, the frequency nadir satisfies the minimum frequency threshold $\omega_{NAD} \geq \omega_{min}$ if the aggregate ramp rate satisfies $K \geq K_{min}$ where:

$$K_{min} = \frac{\left(\tilde{b}\sqrt{\Delta_3} - \sqrt{(\Delta_2 + \Delta_3 - \frac{\omega_0}{2M}\epsilon L)L^2 - (\Delta_2 - \frac{\omega_0}{2M}\epsilon L)\tilde{b}^2} \right)^2}{\frac{4M}{\omega_0}(\Delta_2 + \Delta_3 - \frac{\omega_0}{2M}\epsilon L)^2} \qquad (7.15)$$

Proof: The nadir frequency can be related to the aggregate ramp rate using the swing equation (7.2). From the integral of the energy imbalance curve in Figure 7.3, this relationship is as follows. Notice that Assumption 7.1 preserves the geometry of Figure 7.3, allowing for the integral of the energy imbalance curve to be explicitly represented using the

area covered by a combination of triangles and rectangles.

$$\tfrac{2M}{\omega_0}(\omega_0 - \omega_{\text{NAD}}) = A + B + D + F + E \tag{7.16}$$

$$= L(t_1 + \epsilon) + (L - Kt_2)t_2 + \tfrac{1}{2}t_2^2 K + \tfrac{1}{2K}(L - Kt_2 - \tilde{b})^2 \tag{7.17}$$

$$= \tfrac{2M}{\omega_0}\Delta_1 + L\epsilon + \tfrac{1}{2K}(L - \tilde{b})^2 + \tilde{b}t_2 \tag{7.18}$$

$$= \tfrac{2M}{\omega_0}\Delta_1 + L\epsilon + \tfrac{1}{2K}(L - \tilde{b})^2 + \tilde{b}\tfrac{1}{K}\left(L - \sqrt{L^2 - \tfrac{2M}{\omega_0}2K\delta_2}\right) \tag{7.19}$$

The initial expression (7.16) represents the integral of the power imbalance curve, where capital letters represent their corresponding shaded area indicated in the figure. Step (7.16)-(7.17) expresses this integral as the area covered by a combination of triangles and rectangles. Step (7.17)-(7.18) uses $t_1 = \frac{2M\Delta_1}{L\omega_0}$ and performs additional algebra. Step (7.18)-(7.19) expresses t_2 as

$$t_2 = \frac{1}{K}L - \frac{1}{K}\sqrt{L^2 - \tfrac{4M}{\omega_0}K\delta_2}.$$

We will now set $\omega_{\text{NAD}} = \omega_{\min}$ and solve (7.19) for $K_{\min}$. Note that there is only one such $K_{\min}$ and any $K > K_{\min}$ will result in a nadir frequency $\omega_{\text{NAD}} > \omega_{\min}$ because ω_{NAD} is strictly monotonically increasing in K.

First, let's introduce the constant $\omega = \omega_0 - \omega_{\min} - \Delta_1 - \frac{\omega_0}{2M}\epsilon L$ to simplify notation. From (7.19) we have the following:

$$\tilde{b}\sqrt{L^2 - \tfrac{4M}{\omega_0}K\delta_2} = \tfrac{1}{2}L^2 + \tfrac{1}{2}\tilde{b}^2 - \tfrac{2M}{\omega_0}K\omega \tag{7.20}$$

Note that both sides of this equation are real and non-negative, else t_2 from (7.11) would be complex. Squaring both sides and rearranging gives the following quadratic equation in K:

$$\tfrac{4M^2}{\omega_0^2}\omega^2 K^2 + \left(\tfrac{4M}{\omega_0}\tilde{b}^2\delta_2 - (L^2 + \tilde{b}^2)\tfrac{2M}{\omega_0}\omega\right)K + \tfrac{1}{4}(L^2 + \tilde{b}^2)^2 - \tilde{b}^2 L^2 = 0 \tag{7.21}$$

This quadratic equation has two solutions, denoted $K_+^\star$ and $K_-^\star$, written as follows:

$$\frac{\tfrac{2M}{\omega_0}\omega(L^2 + \tilde{b}^2) - \tfrac{4M}{\omega_0}\tilde{b}^2\delta_2 \pm \sqrt{(\tfrac{4M}{\omega_0}\tilde{b}^2\delta_2 - \tfrac{2M}{\omega_0}\omega(L^2 + \tilde{b}^2))^2 - \tfrac{4M^2}{\omega_0^2}\omega^2((L^2 + \tilde{b}^2)^2 - 4\tilde{b}^2 L^2)}}{\tfrac{8M^2}{\omega_0^2}\omega^2}$$

Algebraically rearranging the descriminant results in the following equivalent expression for $K_+^\star$ and $K_-^\star$:

$$K_\pm^\star = \frac{\omega(L^2 + \tilde{b}^2) - 2\tilde{b}^2\delta_2 \pm 2\tilde{b}\sqrt{\omega - \delta_2}\sqrt{\omega L^2 - \delta_2\tilde{b}^2}}{\tfrac{4M}{\omega_0}\omega^2} \tag{7.22}$$

Under the assumption that $K_{\min} = K_-^\star$ where $\pm$ takes the sign $-$, the result follows by factoring the numerator of the previous expression and replacing $\omega = \Delta_2 + \Delta_3 - \frac{\omega_0}{2M}\epsilon L$ and $\delta_2 = \Delta_2 - \frac{\omega_0}{2M}\epsilon L$.

We now show that $\pm$ cannot take the sign $+$. Suppose it can take the sign $+$. Then $K_+^\star$ solves (7.20) and thus results in a real non-negative LHS and RHS of (7.20). Furthermore, $K_-^\star \leq K_+^\star$ and so the LHS and RHS of (7.20) remain real and non-negative when evaluated at $K_-^\star$. Since $K_-^\star$ solves (7.21) and results in a real non-negative LHS and RHS of (7.20), $K_-^\star$ must also solve (7.20). Thus $K_-^\star$ and $K_+^\star$ result in the same nadir frequency. This contradicts the fact that the nadir frequency is strictly monotonically increasing in the aggregate ramp rate K. □

7.3.2   Sufficient Condition for Satisfying Frequency Threshold

As stated in Remark 7.3, the system model of a constant aggregate ramp rate does not fully capture the response of each individual generator. In fact, each individual generator will exhibit a ramp rate of κ_i until their reserve has been fully deployed as explained in Section 7.1.3. Some generators may deploy all PFR reserve before the frequency nadir is reached, in which case the aggregate ramp rate will effectively decrease over time. That being said, the frequency threshold is guaranteed to be satisfied if we assume the generators are capable of fully deploying all of their PFR reserve before the time $t_{\min}$, which represents the time of the frequency nadir at the minimum aggregate ramp rate $K_{\min}$. This is implied by the intuitive fact that the frequency nadir rises when a generator ramps faster than expected. This intuitive fact was illustrated in Section 7.3.1 but is not formally proven. This logic leads to the following result:

Theorem 7.2. Under Assumption 7.1, the frequency nadir satisfies the minimum frequency threshold $\omega_{NAD} \geq \omega_{min}$ if the following holds for each generator $i \in [1, \ldots, n]$:

$$r_i \leq \kappa_i h(M, \mathbf{1}^\dagger b) \tag{7.23}$$

where the limit function $h(M, \tilde{b})$ is as follows:

$$h(M, \tilde{b}) := \frac{\frac{4M}{\omega_0}(\Delta_2 + \Delta_3 - \frac{\omega_0}{2M}\epsilon L)^2(L - \tilde{b})}{\left(\tilde{b}\sqrt{\Delta_3} - \sqrt{(\Delta_2 + \Delta_3 - \frac{\omega_0}{2M}\epsilon L)L^2 - (\Delta_2 - \frac{\omega_0}{2M}\epsilon L)\tilde{b}^2}\right)^2} \tag{7.24}$$

Proof: Following from the discussion, the frequency threshold will be met if each generator is capable of deploying all of its PFR reserve before the time t_{min}. This requirement is mathematically written as follows:

$$r_i \leq \kappa_i(t_{min} - t_1 - \epsilon) = \kappa_i \frac{L - \mathbf{1}^\dagger b}{K_{min}} \tag{7.25}$$

Substituting K_{min} with its expression from (7.15) gives the result. $\qquad\square$

The rate-based PFR limit from (7.23) can be interpreted as a condition that the available PFR reserve must satisfy. With this in mind, any additional nominal PFR reserve in excess of this limit cannot be utilized before the critical frequency threshold is met. Intuitively, any nominal PFR reserve R_i that exceeds the amount $\kappa_i h(M, \mathbf{1}^\dagger b)$ is not classified as being *available*, meaning that it cannot be provided before the critical frequency threshold is met.

The function $h(M, \tilde{b})$ is convex in its second argument. Figure 7.4 provides example plots of $h(M, \tilde{b})$ versus its second argument $\tilde{b}$ for several different values of inertia M. Notice that this function is increasing in M and $\tilde{b}$. As a result constraint (7.23) allows the nominal PFR reserve for a generator to increase if the system inertia increases, if the total FFR reserve increases, or if its ramp rate κ_i increases.

As we will see in Chapter 8, the rate based-PFR limit (7.23) can be enforced as a constraint in a co-optimization problem. Unfortunately, enforcing this constraint would make the co-optimization problem non-convex because the limit function $h(M, \tilde{b})$ is strictly convex in its second argument and appears on the Right Hand Side (RHS) of the inequality. For this
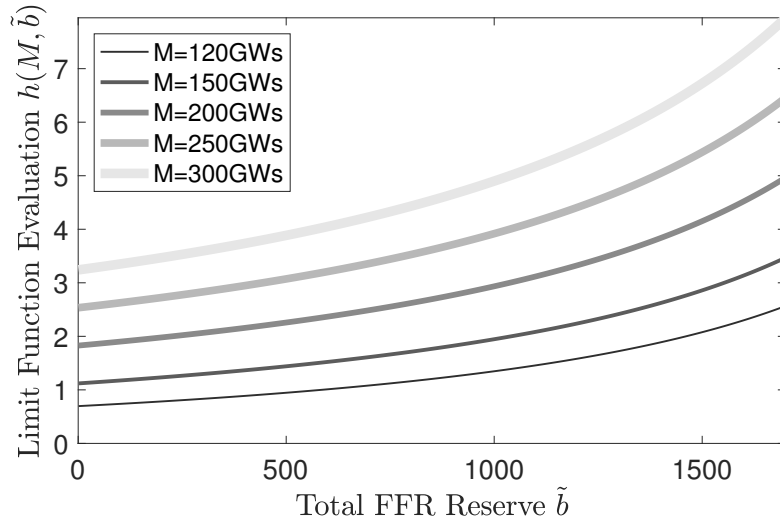
Figure 7.4: Function $h(M, \tilde{b})$ with parameters consistent with Sections 7.2.2 and 8.4.

reason, it may be beneficial to approximate this function as being linear, which would result in a convex co-optimization problem. In fact, as shown in Figure 7.4, the limit function $h(M, \tilde{b})$ is approximately linear for low values of total FFR reserve, e.g. $\mathbf{1}^\dagger b = 100$MW. Furthermore, a conservatively low linear approximation can be easily constructed as a tangent line of the convex limit function $h(M, \tilde{b})$. Future work will further investigate linear approximations of the limit function $h(M, \tilde{b})$.

7.4 Proportional PFR Reserve Limits

This subsection provides a connection between the rate-based PFR limit (7.23) and equivalency ratios from [59]. To make this connection Section 7.4.1 first introduces a turbine governor model that assumes the ramp rate κ_i is proportional to the nominal PFR reserve R_i. This model results in a *proportional PFR reserve limit* that depends on the nominal PFR reserve. Section 7.4.2 then provides the equivalency ratio requirement from [59] and explains how this requirement can also be represented as a limit on the PFR reserve that is proportional to the nominal PFR reserve R_i. Section 7.4.3 then explains how the equivalency ratio can be approximated using the simple ramp rate model of a turbine governor and provides first principles insight into the behavior of equivalency ratios.

7.4.1 Proportional Ramp Rate Model

Empirically, in the case of large contingencies, the governor ramp rate of a generator, κ_i, tends to increase with its nominal PFR reserve, R_i. This is because the frequency drop in response to a large generator outage is so fast that the droop signal as described in Section 7.1.3.1 will nearly represent a step change, where the size of the step is equal to the nominal PFR reserve R_i. Assuming a low-pass filter type response from the droop signal to the generator mechanical output power, the ramp rate of the turbine governor's mechanical power output will increase with the size of the step reference input to the turbine governor.

To emulate this, a model is proposed that is new to the literature and assumes the generator's ramp rate is proportional to the nominal PFR reserve R_i. Let's denote the proportionality constant by τ_i, which may vary among generators. Then the governor ramp rate of the generator is $\kappa_i = \tau_i R_i$. Notice that the nominal PFR reserve amount R_i is changed on 5-15 minute time scales corresponding to the real-time market clearing. On the other hand, primary frequency control occurs on time scales of $\frac{1}{\omega^0} \approx 0.016$ seconds. As a result, the nominal PFR reserve amount and the ramp rate κ_i can be considered constant on the time scales that primary control is being performed. With this in mind, the same rate-based PFR limit (7.23) can be enforced as follows:

$$r_i \leq \tau_i R_i h(M, \mathbf{1}^\dagger b) \tag{7.26}$$

Intuitively, any nominal PFR reserve R_i that exceeds the amount $\tau_i R_i h(M, \mathbf{1}^\dagger b)$ is not classified as being *available*, meaning that it cannot be provided before the critical frequency threshold is met. This model attempts to capture the way in which a turbine governor response ramps faster when it has larger head-room.

7.4.2 Equivalency Ratio Requirement

Reference [59] uses an *equivalency ratio reserve requirement* of the following form:

$$\mathbf{1}^\dagger R + \alpha(M)\mathbf{1}^\dagger b \geq \upsilon(M) \tag{7.27}$$

where $\alpha(M)$ is termed the *equivalency ratio* and $\upsilon(M)$ is the *frequency responsive reserve requirement (Rfrr)*, both of which are functions of the total system inertia. Reference [59]

determines these two functions empirically based on simulation studies so that satisfaction of constraint (7.27) will ensure sufficient reserve to prevent the frequency from violating the minimum frequency threshold of $\omega_{\min} = 59.4$Hz in response to an outage of size L, where $L = 2750$MW in their work.

The simulation studies in [59] fix the inertia to some particular values of M and identify pairs of total FFR reserve $\mathbf{1}^\dagger b$ and total nominal PFR reserve $\mathbf{1}^\dagger R$ that result in a frequency nadir that exactly meets the frequency threshold $\omega_{\min}$. The corresponding total FFR reserve and PFR reserve pairs are found to have a linear relationship for each fixed value of inertia. When plotting these values against each other, the slope of the line is $\alpha(M)$ and the intercept along the PFR reserve axis is $\upsilon(M)$. The first three columns of Table 7.1 replicate the data from [59, table I] and shows the values of $\alpha(M)$ and $\upsilon(M)$ for different values of inertia M.

Table 7.1: Parameters required to enforce the equivalency ratio requirement from [59]. The equivalency ratio $\alpha(M)$ and reserve requirement $\upsilon(M)$ are provided for various values of total system inertia M.

Total Inertia M (GWs)	Rfrr $\upsilon(M)$ (MW)	Equivalency Ratio $\alpha(M)$	Ratio $\frac{\upsilon(M)}{\alpha(M)}$ (MW)
120	5200	2.2	2363.6
136	4700	2.0	2350.0
152	3750	1.5	2500.0
177	3370	1.4	2407.1
202	3100	1.3	2384.6
230	3040	1.25	2432.0
256	2640	1.13	2336.3
278	2640	1.08	2444.4
297	2240	1	2240.0
316	2280	1	2280.0
332	2140	1	2140.0
350	2140	1	2140.0

In its fourth column, Table 7.1 additionally presents the ratio $\frac{\alpha(M)}{\upsilon(M)}$, which is approximately constant across all inertia values for $\alpha(M) > 1$. In fact, this ratio is approximately equal to but slightly less than the magnitude of the outage being accommodated $L = 2750$. We will suggest that this observation merits the approximation of $\upsilon(M) \approx \alpha(M)L$. For this

reason, the constraint (7.27) can be approximated as follows:

$$\frac{1}{\alpha(M)}\mathbf{1}^\dagger R + \mathbf{1}^\dagger b \geq L \tag{7.28}$$

Notice that this equivalency ratio requirement is similar to the general reserve requirement (7.1) but with r_i replaced with $\frac{1}{\alpha(M)}R_i$. This suggests that an equivalency ratio PFR limit should be placed on the available PFR reserve in the following form:

$$r_i \leq \frac{1}{\alpha(M)}R_i \tag{7.29}$$

In fact, the equivalency ratio reserve requirement (7.28) holds if and only if there exists a vector $r \in \mathbb{R}^n$ such that constraints (7.29) and (7.1) hold.

7.4.3 Relationship Between Proportional Ramp Rate and Equivalency Ratios

Although [59] initially justified the use of equivalency ratios empirically, our analysis provides insight into equivalency ratios established from first principles. Specifically, the PFR limits from (7.29) and (7.26) are both proportional to the nominal PFR reserve R_i, suggesting that the proportionality constants should be similar. With this in mind, under the assumption that all proportionality constants τ_i are approximately the same across generators, the equivalency ratios can be approximated as follows:

$$\alpha(M) \approx \frac{1}{\tau_i h(M, \mathbf{1}^\dagger b)} \tag{7.30}$$

To better understand this approximation, Figure 7.5 plots the function $\frac{1}{h(M,\mathbf{1}^\dagger b)}$ versus the total FFR reserve $\mathbf{1}^\dagger b$ for different values of inertia M. Notice that this function varies only somewhat in the total FFR reserve argument at high inertia levels. In other words, the function $\frac{1}{h(M,\mathbf{1}^\dagger b)}$ can be reasonably approximated as being constant in the total FFR reserve $\mathbf{1}^\dagger b$ when the inertia level is high, further justifying the approximation (7.30).

Notice that the approximation (7.30) provides important insight into equivalency ratios from first principles. Specifically, equivalency ratios may be appropriately approximated as being constant in the total FFR reserve, $\mathbf{1}^\dagger b$, at the high inertia levels that are similar in magnitude to the inertia levels seen today in ERCOT. However, as the inertia levels drop, the
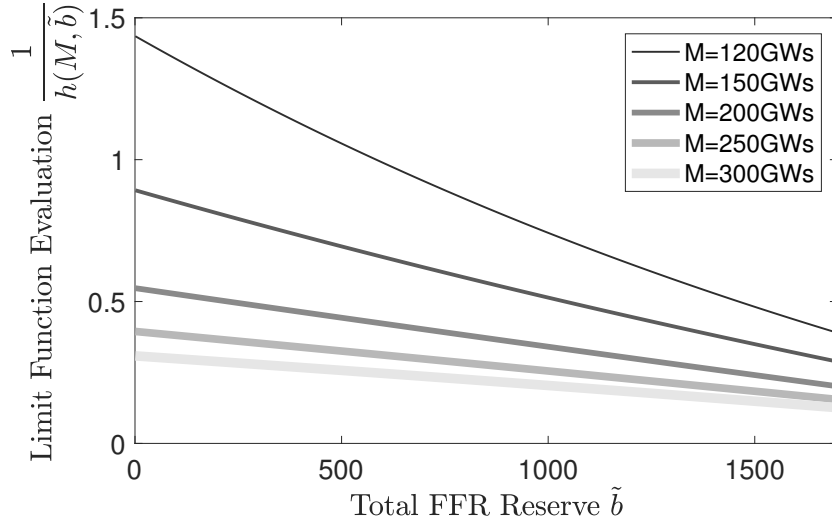
Figure 7.5: Function $h(M, \tilde{b})$ with parameters consistent with Sections 7.2.2 and 8.4.

equivalency ratio may vary significantly with the total FFR reserve. As is seen in Figure 7.5, the slope of the equivalency ratio with respect to the total FFR reserve is approximately an order of magnitude larger when the inertia is $M = 120$GWs as opposed to $M = 300$GWs. Future work will extend the empirical results from reference [59] to verify that equivalency ratios significantly vary with the total FFR reserve for low inertia levels.

The approximation (7.30) can alternatively be used to approximate the proportionality constants τ_i. Specifically, under the assumption that all generators have the same proportionality constant we can approximate $\tau_i \approx \frac{1}{\alpha(M)h(M,\mathbf{1}^\dagger b)}$. In this context it is particularly useful to approximate τ_i using high levels of inertia, because $\frac{1}{h(M,\mathbf{1}^\dagger b)}$ will be approximately constant. For example, using $M = 297$GWs we have $\alpha(M) = 1$ and $\frac{1}{h(M,\mathbf{1}^\dagger b)} \approx 0.25\text{s}^{-1}$ leading to a proportionality constant of $\tau_i \approx 0.25\text{s}^{-1}$.

7.5 Summary

This chapter derived various reserve requirements that couple FFR and PFR reserve and ensure sufficient reserve for arresting frequency decline in response to a large generator outage. The main reserve requirement constraint is stated in (7.1) and requires the total available PFR reserve and FFR reserve to be larger than some reserve requirement L. The

FFR reserve does not exhibit ramping limitations and thus all of the FFR reserve is considered to be available immediately to arrest frequency decline once it is triggered. On the other hand, PFR reserve exhibits ramping limitations that restrict its availability. For this reason, this chapter introduces the concept of available PFR reserve, denoted r_i, which is upper bounded by the nominal PFR reserve R_i, resulting in the limit constraint (7.9). Various other limits on the available PFR reserve are provided throughout this chapter that utilize different models of a generator's ramping ability. The rate-based PFR limit (7.23) assumes a constant ramp rate of the turbine governor. The proportional PFR limit (7.26) assumes the ramp rate of the turbine governor is proportional to the nominal PFR reserve. Finally, the equivalency ratio limit (7.29) restricts the available PFR reserve to be less than a fraction of its nominal PFR reserve. A co-optimization problem can be formulated to enforce any of the aforementioned limits on the available PFR reserve.

The next chapter will enforce reserve requirements that were derived in this chapter, particularly focusing on a comparison between the rate-based PFR limit (7.23) and the equivalency ratio PFR limit (7.29), which is consistent with the equivalency ratio requirement (7.27) from [59] as shown in Section 7.4.2. Although the equivalency ratio PFR limit is only justified empirically, it is convenient because it will result in a linearly constrained convex co-optimization problem. In contrast, the rate-based PFR limit is justified from first principles, but will result in a non-convex co-optimization problem.

Reference [59] suggested the use of equivalency ratios to formulate the reserve requirement. These equivalency ratios were previously considered to be a function of only the system inertia level and were determined empirically based on simulation studies. Section 7.4 provided an analytical expression for equivalency ratios that provides first principles insight into equivalency ratios and suggests that they may vary significantly with the total FFR reserve at low inertia levels. In other words, the analytical results in this chapter suggest that the equivalency ratio should be represented as a function of the total FFR reserve as well as the total system inertia. The empirical results provided in [59] are insufficient to empirically establish this dependence of the equivalency ratio on the FFR reserve. Future work will extend the results from [59] by empirically justifying the dependence of the equivalency ratio on the FFR reserve at low inertia levels.

Chapter 8

Real-Time Co-Optimization

ERCOT will soon implement real-time co-optimization by incorporating Primary Frequency Responsive (PFR) reserve and Fast Frequency Responsive (FFR) reserve into the economic dispatch problem [26]. Chapter 7 described both of these reserve types in detail and derived from first principles reserve requirements that couple these two reserve types. Among these reserve requirements includes a novel rate-based PFR limit and a previously proposed equivalency ratio requirement from [59]. This chapter places these two reserve requirements into two different co-optimization problems and compares their impact on the electricity market.

The recently approved Nodal Protocol Revision Request (NPRR) 863 defines a Responsive Reserve (RR) product that contains both PFR and FFR reserve types [25]. This implies that PFR reserve and FFR reserve will see the same price in the electricity market, effectively treating them as the same product. This chapter deviates from this convention by suggesting that PFR reserve and FFR reserve should be assigned different prices that accurately account for their individual effectiveness in arresting frequency decline. Specifically, *KKT prices* will be defined for both co-optimization problems presented in this chapter based on the Lagrange multipliers of the reserve requirement constraints. These KKT prices will be different for the PFR reserve product and FFR reserve product. See Remark 8.3 for further discussion.

We will begin by redefining the market participants to include PFR and FFR reserve in Section 8.1.1. This section introduces a market participant in the form of a battery providing FFR reserve and redefines the generator as a market participant that provides PFR reserve in addition to electric power generation. Section 8.2 then focuses on the *co-optimization problem with equivalency ratio requirement* that is convex and enforces a re-

serve requirement that is consistent with the empirically derived requirement from [59] as discussed in Section 7.4.2. Section 8.3 formulates the *co-optimization problem with rate-based PFR limit* that is non-convex and instead enforces the rate-based PFR limit derived in Section 7.3.2. Both Sections 8.2 and 8.3 additionally define KKT prices based on the Lagrange multipliers of their corresponding co-optimization problems. These KKT prices are analogous to the KKT prices derived in Chapter 2 but additionally include KKT prices for FFR reserve and KKT prices for nominal PFR reserve.

As explained in Chapter 1, a non-convex social welfare maximization problem could in principle result in non-zero lost opportunity costs experienced by the market participants and congestion revenue shortfalls. However, since the private constraints of all market participants are convex and the feasible set of net power injections is assumed convex in this chapter, the *co-optimization problem with rate-based PFR limit* does not exhibit either of these problems when using KKT prices. To make this explicit, both co-optimization problems studied in this chapter are shown to result in zero lost opportunity cost for all market participants when following the dispatch instructions and that congestion revenue adequacy is guaranteed when using KKT prices.

As is the case with all co-optimization problems, revenue adequacy is not necessarily guaranteed for the co-optimization problems studied in this chapter because reserve payments may be considered out-of-market payments not directly covered by another revenue stream of the ISO. Section 8.4 numerically illustrates that the rate-based PFR limit results in higher prices for FFR reserve, resulting in more reserve payments as compared to the equivalency ratio requirement. Section 8.4 also highlights another fundamental difference between the two co-optimization problems. Specifically, the rate-based PFR limit encourages PFR reserve to be evenly distributed over many generators. On the other hand, the equivalency ratio reserve requirement encourages fewer generators to provide PFR reserve. Further empirical analysis would be required to determine whether the dispersion of PFR over more generators is appropriate and necessary.

8.1 Market Participants

The co-optimization problem that will be presented in Section 8.3 is non-convex. In principle, this non-convexity could cause congestion revenue shortfalls and/or non-zero lost opportunity cost experienced by market participants. However, Section 8.3 explicitly shows that all market participants will experience zero lost opportunity cost and that congestion revenue adequacy is guaranteed when using KKT prices. To show this, we must first define the lost opportunity cost associated with each market participant. The definition of Potential Congestion Revenue Shortfall (PCRS) is unchanged from Section 2.2.3.

This section provides updated models of the market participants in a co-optimization setting. In this setting generators provide PFR reserve as well as electric power generation and a new participant is introduced in the form of a battery providing FFR reserve. The system demand and FTR holders have the same definitions as in Section 2.2.

8.1.1 Modeling Generators Providing PFR Reserve

In this part of the dissertation each generator is capable of providing two products in the electricity market, namely electric real power generation G_i and the nominal PFR reserve R_i. These two products are coupled as described by the private constraint set, denoted $\mathcal{X}^i$, from (7.4) in Section 7.1.3. In this context the generator receives a second payment in addition to the standard payment of $\lambda_i G_i$. This second payment is in the amount $\xi_i R_i$ where ξ_i is the price of PFR reserve. Furthermore, the cost function from Section 2.2.2 can be generalized to accommodate PFR reserve-related costs as $C_i(G_i, R_i)$, where this cost function is assumed jointly convex in both of its arguments. As in Chapter 2, each generator is modeled as a profit maximizer whose maximum profit is a function of its corresponding prices and is expressed as follows:

$$\Upsilon_i(\lambda_i, \xi_i) := \max_{(G_i, R_i) \in \mathcal{X}^i} \left(\lambda_i G_i + \xi_i R_i - C_i(G_i, R_i) \right). \tag{8.1}$$

As explained in Section 2.2.2 each generator is expected to provide its ISO-determined dispatched generation, denoted G_i^d. An analogous quantity determined by the ISO related to nominal PFR reserve is denoted R_i^d and is termed the *procured nominal PFR reserve* but will

also be referred to as the *procured PFR reserve.* That is, each generator is expected to provide its *procured PFR reserve*, denoted R_i^d, which is assigned to it by the ISO when the market is cleared. Similar to Section 2.2.2, some generators may have dispatched generation levels, denoted G_i^d, and/or procured PFR levels, denoted R_i^d, that do not maximize their profit in the absence of a market equilibrium. If the dispatched generation and procured PFR reserve values for generator $i \in \mathbb{N}$, denoted G_i^d and R_i^d, do not maximize the generator's profit, then the generator has an incentive to deviate from its dispatched generation and procured PFR reserve levels. If the generator follows its dispatched generation and procured PFR reserve levels, then the generator will experience lost opportunity cost in the amount that follows:

$$C_i^o(\lambda_i, \xi_i, G_i^d, R_i^d) = \sum_{i \in \mathbb{N}} \left(\Upsilon_i(\lambda_i, \xi_i) - \left(\lambda_i G_i^d + \xi_i R_i^d - C_i(G_i^d, R_i^d) \right) \right). \tag{8.2}$$

The co-optimization problem that will be presented in Section 8.3 is non-convex. As a result, generators may in principle experience non-zero lost opportunity cost. However, Section 8.3 explicitly shows that generators will experience zero lost opportunity cost when using KKT prices. This result follows from the fact that the generator private constraints are convex.

8.1.2 Modeling Batteries Providing FFR Reserve

This part of the dissertation introduces a new type of market participant in the form of a battery providing a product termed FFR reserve in the amount of b_j. The FFR reserve will be paid a price ζ_j so that its total payment is $\zeta_j b_j$. The provided FFR reserve will be constrained by the private constraints imposed by the individual battery, denoted $\mathcal{B}^j$ and defined in (7.3). Furthermore, the cost of providing an amount of FFR reserve b_j will be represented by the function $B_j(b_j)$ and is assumed to be convex. Each battery is modeled as a profit maximizer whose maximum profit is a function of its corresponding price and is expressed as follows:

$$\Gamma_j(\zeta_j) := \max_{b_j \in \mathcal{B}^j} \left(\zeta_j b_j - B_j(b_j) \right). \tag{8.3}$$

Similar to the case with generators, each battery is expected to provide its ISO-determined *procured FFR reserve*, denoted b^d, which is assigned to it by the ISO when the market is cleared. If the procured FFR reserve does not maximize the battery's profit, then the battery has an incentive to deviate. If the battery provides its procured FFR reserve value, then the battery will experience lost opportunity cost in the amount that follows:

$$C_j^b(\zeta_j, b_j^d) = \Gamma_j(\zeta_j) - \left(\zeta_j b_j^d - B_j(b_j^d)\right). \tag{8.4}$$

The co-optimization problem that will be presented in Section 8.3 is non-convex. As a result, batteries may in principle experience non-zero lost opportunity cost. However, Section 8.3 explicitly shows that batteries will experience zero lost opportunity cost when using KKT prices. This result follows from the fact that the battery private constraints are convex.

8.2 Co-Optimization with Equivalency Ratio Requirement

A co-optimization problem determines the dispatched generation and procured reserve values that meet reserve requirements described in detail in Chapter 7. This section studies a co-optimization problem that enforces a reserve requirement defined by constraints (7.1), (7.9), and (7.29), which are, respectively, as follows:

$$\mathbf{1}^\dagger r + \mathbf{1}^\dagger b \geq L, \quad r \leq R, \quad \text{and} \quad r \leq \frac{1}{\alpha(M)} R.$$

As explained in Section 7.4.3, this reserve requirement is consistent with the equivalency ratio reserve requirement from [59]. Since $\alpha(M) \geq 1$, as illustrated in Table 7.1, the constraint (7.9) can be removed because it cannot be violated without violating constraint (7.29). The intermediate variable r can then be eliminated from the reserve requirement constraints, resulting in a reserve requirement shown as constraint (8.5b) of the following *co-optimization problem with equivalency ratio requirement*:

$$\min_{(G,R)\in\mathcal{X},\ T\in\mathcal{T},b\in\mathcal{B}} \quad \sum_{i\in\mathbb{N}} C_i(G_i, R_i) + \sum_{j\in\mathbb{B}} B_j(b_j) \tag{8.5}$$

$$st: D_i - G_i + T_i = 0 \quad \forall i \in \mathbb{N} \tag{8.5a}$$

$$L \leq \frac{1}{\alpha(M)} \mathbf{1}^\dagger R + \mathbf{1}^\dagger b \tag{8.5b}$$

151

The real power balance constraints are represented by (8.5a). The reserve requirement is represented by (8.5b) and is written in terms of the constant system inertia M. Note that numerical results in Section 8.4 will study the effect of varying the inertia. The private battery constraints are represented by the set $\mathcal{B} = \{b \in \mathbb{R}^\beta : b_j \in \mathcal{B}^j \ \ \forall j \in \mathbb{B}\}$. The private generator constraints are represented by the set $\mathcal{X} = \{(G, R) \in \mathbb{R}^n \times \mathbb{R}^n : (G_i, R_i) \in \mathcal{X}^i \ \ \forall i \in \mathbb{N}\}$. Although this co-optimization problem (8.5) does not place any restrictions on the feasible set of net real power injections, denoted $\mathcal{T}$, we will henceforth assume that this set is a polytope and is thus convex. We additionally assume that this set matches the SFCs as defined in Section 2.2.3. As stated in Chapter 1, the assumption that $\mathcal{T}$ is a convex polytope is motivated by the fact that the ERCOT ISO is considering implementing market changes regarding co-optimization separately from market changes regarding transmission losses.

The co-optimization problem with equivalency ratio requirement (8.5) is simple because it results in a linearly constrained convex problem. As a result, Slater's condition necessarily holds if there exists a feasible point of the co-optimization problem. Under this mild condition strong duality must hold for the co-optimization problem and the global optimum must also solve the KKT conditions along with some optimal Lagrange multipliers. These KKT conditions can be efficiently solved to identify globally optimal dispatched generation and procured reserve, denoted (G^d, R^d, b^d), along with corresponding optimal Lagrange multipliers of constraints (8.5a) and (8.5b), denoted $\lambda^\star \in \mathbb{R}^n$ and $\mu^\star \in \mathbb{R}_+$ respectively. By the definition of strong duality, the optimal objective value of the co-optimization problem is equal to the partial Lagrangian dual function evaluated at optimal Lagrange multipliers. This partial Lagrangian dual function is written as follows:

$$\mathcal{L}(\lambda, \mu) := \sum_{i \in \mathbb{N}} \min_{(G_i, R_i) \in \mathcal{X}^i} \left(C_i(G_i, R_i) - \lambda_i G_i - \frac{\mu}{\alpha(M)} R_i \right)$$
$$+ \sum_{j \in \mathbb{B}} \min_{b_j \in \mathcal{B}^j} (B_j(b_j) - \mu b_j) + \min_{T \in \mathcal{T}} \lambda^\dagger T + \lambda^\dagger D + \mu L \qquad (8.6)$$

Similar to Chapter 2, $\lambda^\star$ represents the price for real electric power at each location in the network. Furthermore, the price for PFR reserve is the same for each generator i and is in the amount of $\xi_i := \frac{1}{\alpha(M)} \mu^\star$. The price for FFR reserve is the same for each battery j and is in the amount of $\zeta_j := \mu^\star$. This definition of the prices will be referred to as *KKT*

prices because they are derived from Lagrange multipliers that solve the KKT conditions of the co-optimization problem. Using this definition of KKT prices, the partial Lagrangian dual function (8.6) decouples into profit maximization problems associated with each of the market participants, similar to Section 6.3. With this in mind, the partial Lagrangian dual function (8.6) can be rewritten as follows:

$$\mathcal{L}(\lambda, \mu) := -\sum_{i \in \mathbb{N}} \Upsilon_i(\lambda_i, \tfrac{1}{\alpha(M)}\mu) - \sum_{j \in \mathbb{B}} \Gamma_j(\mu) - \Psi(\lambda) + \sum_{i \in \mathbb{N}} \lambda_i D_i + \mu L. \tag{8.7}$$

As mentioned previously, strong duality will hold for this co-optimization problem under the assumption that its feasible set is non-empty. For this reason, $\mathcal{L}(\lambda^\star, \mu^\star)$ is equal to the optimal value of the co-optimization problem with equivalency ratio requirement (8.5). With this in mind, two steps are taken to derive the following expression. First, we subtract the optimal value of the co-optimization problem from $\mathcal{L}(\lambda^\star, \mu^\star)$. Second, we subtract the terms $\lambda^{\star\dagger}(D - G^d + T^d) = 0$ and $\mu^\star(L - \frac{1}{\alpha(M)}\mathbf{1}^\dagger R^d - \mathbf{1}^\dagger b^d) = 0$, which evaluate to zero by the complementary slackness condition contained within the KKT conditions.

$$\sum_{i \in \mathbb{N}} C_i^o(\lambda_i^\star, \xi_i, G_i^d, R_i^d) + \sum_{j \in \mathbb{B}} C_j^b(\zeta_j, b_j^d) + C^s(\lambda^\star, G^d) = 0 \tag{8.8}$$

Since the opportunity cost for generators and batteries are non-negative and the PCRS is non-negative, each term in (8.8) must evaluate to zero. This means that congestion revenue adequacy holds and no generators or batteries experience lost opportunity cost.

Unfortunately, revenue adequacy of the ISO cannot necessarily be claimed for any co-optimization problem. In fact, ISOs in the US typically consider all reserve payments, even those not discussed in this dissertation, as out-of-market payments and redistribute this cost among the consumers in the electricity market. On the other hand, some ISOs outside of the US suggest that some or all reserve payments be recovered from the entities that cause the reserve costs. In the context of the co-optimization problem with equivalency ratio requirement (8.5), this would mean that all reserve payments be recovered by charging the costs of procuring the reserves to the two largest generators that directly contribute to the reserve requirement L. In that case the two largest generators would be charged a total amount of $\mu^\star L$, which would be exactly equal the total reserve payments $\mu^\star\left(\frac{1}{\alpha(M)}\mathbf{1}^\dagger R^d + \mathbf{1}^\dagger b^d\right)$. In summary, all reserve payments must be recovered by the ISO and the method used to recover these payments may vary between ISOs.

8.3 Co-Optimization with Rate-Based PFR Limit

This section formulates a co-optimization problem that enforces a reserve requirement defined by constraints (7.1), (7.9), and (7.23), which are, respectively, as follows:

$$\mathbf{1}^\dagger r + \mathbf{1}^\dagger b \geq L, \quad r \leq R, \quad \text{and} \quad r \leq \kappa h(M, \mathbf{1}^\dagger b).$$

This reserve requirement can be represented in a co-optimization problem by introducing the intermediate variable r_i representing the available PFR reserve for each generator i. Under the assumption that the cost function of each generator i, denoted $C_i(G_i, R_i)$, is non-decreasing in its second argument, there is no benefit to allowing the nominal PFR reserve R_i to be larger than the available PFR reserve r_i. For this reason, we will restrict these two values to be the same, e.g. $R = r$, eliminating the need for constraint (7.9). The available PFR reserve variables r can then be eliminated by replacing them with the nominal PFR reserve variables R, resulting in the reserve requirement shown as constraints (8.9b) and (8.9c) of the following *co-optimization problem with rate-based PFR limit*:

$$\min_{(G,R)\in\mathcal{X},\ T\in\mathcal{T}, b\in\mathcal{B}} \quad \sum_{i\in\mathbb{N}} C_i(G_i, R_i) + \sum_{j\in\mathbb{B}} B_j(b_j) \tag{8.9}$$

$$st: D_i - G_i + T_i = 0 \quad \forall i \in \mathbb{N} \tag{8.9a}$$

$$L \leq \mathbf{1}^\dagger R + \mathbf{1}^\dagger b \tag{8.9b}$$

$$R \leq \kappa h(M, \mathbf{1}^\dagger b) \tag{8.9c}$$

The real power balance constraints are represented by (8.9a). The reserve requirement is represented by (8.9b) and (8.9c) and is written in terms of the constant system inertia M. Again note that numerical results in Section 8.4 will study the effect of varying inertia. The private battery constraints are represented by the set $\mathcal{B} = \{b \in \mathbb{R}^\beta : b_j \in \mathcal{B}^j \quad \forall j \in \mathbb{B}\}$. The private generator constraints are represented by the set $\mathcal{X} = \{(G, R) \in \mathbb{R}^n \times \mathbb{R}^n : (G_i, R_i) \in \mathcal{X}^i \ \forall i \in \mathbb{N}\}$. As in the previous section, the co-optimization problem uses a general form of the feasible set of net real power injections, denoted $\mathcal{T}$. However, we will henceforth assume that this set is a polytope and is thus convex. We additionally assume that this set matches the SFCs as defined in Section 2.2.3.

The function $h(M, \mathbf{1}^\dagger b)$ is strictly convex in the total FFR reserve $\mathbf{1}^\dagger b$ as defined in (7.24). Since this function is strictly convex in $\mathbf{1}^\dagger b$ and appears on the RHS of constraint

(8.9c), the co-optimization problem with rate-based PFR limit is non-convex. As a result, we cannot assume that strong duality holds as was done in the previous section. Instead, this section will use the generalized KKT conditions to prove that market participants do not experience lost opportunity cost and that there is no PCRS when using KKT prices.

Below is a general definition of a KKT point for the co-optimization problem with rate-based PFR limit (8.9) where the Lagrange multipliers of constraints (8.9a), (8.9b), and (8.9c) are denoted λ, μ and γ respectively. This definition of a KKT point is similar to Definition 2.2 of a KKT price/dispatch pair from Chapter 2. This definition follows from the normal cone definition of the First Order Necessary Conditions (FONCs) as described in Appendix A (See [71] as well as Remarks 8.1 and 8.2).

Definition 8.1. A *KKT point* $(\lambda^\star, \gamma^\star, \mu^\star, G^\star, R^\star, b^\star, T^\star) \in \mathbb{R}^n \times \mathbb{R}^n_+ \times \mathbb{R}_+ \times \mathcal{X} \times \mathcal{B} \times \mathcal{T}$ is such that constraints (8.9a), (8.9b), and (8.9c) hold along with the following conditions:

$$-\lambda^\star \in \mathcal{N}_\mathcal{T}(T^\star) \tag{8.10a}$$

$$0 \in \partial \left(B_j(b_j) - \mu^\star b_j - \gamma^{\star\dagger} \kappa \nabla h(M, \mathbf{1}^\dagger b^\star) b_j \right)|_{b_j^\star} + \mathcal{N}_{\mathcal{B}^j}(b_j^\star) \quad \forall j \in \mathbb{B} \tag{8.10b}$$

$$0 \in \partial \left(C_i(G_i, R_i) - \lambda_i^\star G_i - \mu^\star R_i + \gamma_i^\star R_i \right)|_{(G_i^\star, R_i^\star)} + \mathcal{N}_{\mathcal{X}^i}(G_i^\star, R_i^\star) \quad \forall i \in \mathbb{N} \tag{8.10c}$$

$$\mu^\star(L - \mathbf{1}^\dagger R^\star - \mathbf{1}^\dagger b^\star) = 0 \tag{8.10d}$$

$$\gamma_i^\star(R_i^\star - \kappa_i h(M, \mathbf{1}^\dagger b^\star)) = 0 \quad \forall i \in \mathbb{N} \tag{8.10e}$$

where (8.10a)-(8.10c) represent the generalized stationarity condtitions for problem (8.9) and (8.10d)-(8.10e) represent the complementary slackness conditions for problem (8.9). The gradient of the function $h(M, \cdot)$ evaluated at $\mathbf{1}^\dagger b^\star$ is denoted $\nabla h(M, \mathbf{1}^\dagger b^\star)$. The normal cone of the set $\mathcal{T}$ at the point $T^\star$ is denoted $\mathcal{N}_\mathcal{T}(T^\star)$, the normal cone of the set $\mathcal{X}^i$ at the point $G_i^\star$ is denoted $\mathcal{N}_{\mathcal{X}^i}(G_i^\star)$, and the normal cone of the set $\mathcal{B}^j$ at the point $b_j^\star$ is denoted $\mathcal{N}_{\mathcal{B}^j}(b_j^\star)$. The subdifferential of a general function $g(x)$ evaluated at a point $x^\star$ is denoted $\partial(g(x))|_{x^\star}$. A formal definition of the normal cone is provided in [71] and is explained intuitively in Appendix A.

As discussed in Appendix A, standard off-the-shelf optimization software is designed to identify a KKT point as in Definition 8.1 using iterative algorithms, such as interior point algorithms. KKT prices can now be defined with respect to a KKT point. Let the KKT price for FFR reserve be defined as $\zeta_j := \mu^\star + \gamma^{\star\dagger} \kappa \nabla h(M, \mathbf{1}^\dagger b^\star)$ for each battery $j \in \mathbb{B}$,

let the KKT price for PFR reserve be defined as $\xi_i := \mu^\star - \gamma_i^\star$ for each generator $i \in \mathbb{N}$, and let the KKT price for electricity be defined as $\lambda_i^\star$ for each generator $i \in \mathbb{N}$. With this definition of the prices, the condition (8.10c) represents the FONCs of the generator profit maximization problem (8.1), the condition (8.10b) represents the FONCs of the battery profit maximization problem (8.3), and the condition (8.10a) represents the FONCs of the FTR payoff maximization problem (2.4). (Note that the normal cone definition of the FONCs are generally represented by (A.6) in Appendix A). Notice that each of these problems are convex because the feasible set of net power injections is assumed convex and the private constraint sets are convex. Since each of these problems are convex, the FONCs are sufficient for global optimality. As a result, the price, dispatched generation, and procured reserve values defined by a KKT point result in zero lost opportunity cost for generators and batteries as well as zero PCRS as defined in (8.2), (8.4), and (2.5) respectively. This is explicitly written as follows:

$$C_i^o(\lambda_i^\star, \xi_i, G_i^d, R_i^d) = 0 \ \forall i \in \mathbb{N}, \text{ and } C_j^b(\zeta_j, b_j^d) = 0 \ \forall j \in \mathbb{B}, \text{ and } C^s(\lambda^\star, G^d) = 0. \quad (8.11)$$

Intuitively, KKT prices result in zero PCRS and zero lost opportunity cost of the market participants because the only non-convex constraint (8.9c) is being priced. That is, the prices are defined based on the Lagrange multipliers of (8.9c) and all other constraints in the co-optimization problem with rate-based PFR limit (8.9) are convex.

As explained in the previous section, revenue adequacy of the ISO cannot necessarily be claimed for any co-optimization problem including the co-optimization problem with rate-based PFR limit (8.9). This is because reserve payments must be recovered by the ISO and the method used to recover these payments may vary between ISOs.

Remark 8.1. We emphasize that a KKT point may not exist in our general framework because constraint qualifications may not be satisfied for a general non-linear function $h(M, \cdot)$. It is also possible that an identified solution satisfying the KKT conditions could represent a saddle point, local maximum, or local minimum. However, a local minimum to the co-optimization problem with rate-based PFR limit (8.9) satisfying the KKT conditions has been obtained using standard off-the-shelf software for each test case in this dissertation.

Furthermore, our results regarding KKT points hold if the solution represents a saddle point, local maximum, or local minimum.

Remark 8.2. Appendix A provides an elaborate description of how the conditions from Definition 8.1 are related to the common KKT conditions. For the special case where the cost function is smooth, Appendix A.2 proves any solution $(G^\star, R^\star, b^\star, T^\star)$ that satisfies the traditional KKT conditions for the co-optimization problem with rate-based PFR limit (8.9) will also satisfy the conditions from Definition 8.1 for some Lagrange multipliers $(\lambda^\star, \gamma^\star, \mu^\star)$. In fact, there may be multiple such Lagrange multipliers $(\lambda^\star, \gamma^\star, \mu^\star)$ that satisfy the KKT conditions. Our results do not require such Lagrange multipliers to be unique.

Remark 8.3. NPRR 863 implies that PFR reserve and FFR reserve will see the same price in the electricity market in Texas [25]. In contrast, this chapter suggests that PFR reserve and FFR reserve should be assigned different prices that accurately account for their individual effectiveness in arresting frequency decline. Furthermore, this chapter suggests that the PFR reserve prices should vary between generators based on their ramping capabilities in order to accurately account for the individual generator's effectiveness in arresting frequency decline. It is also important to recognize that the FFR reserve price $\zeta_j := \mu^\star + \gamma^{\star\dagger}\kappa\nabla h(M, \mathbf{1}^\dagger b^\star)$ cannot be lower than the PFR reserve price $\xi_i := \mu^\star - \gamma_i^\star$. This is because the Lagrange multipliers $\gamma_i^\star$, the ramp rates κ, and the gradient $\nabla h(M, \mathbf{1}^\dagger b^\star)$ are all non-negative. This effectively places more value in the fast acting abilities of FFR reserve.

8.4   Numerical Results

This section intends to illustrate the effect of introducing FFR reserve into the market by increasing the total offered FFR capacity $\mathbf{1}^\dagger \bar{b}$ in a high inertia setting, representing the inertia levels experienced today. After introducing FFR reserve into the market, we will illustrate the effect of decreasing inertia to low levels that represent a future scenario where there may be significant wind and solar penetration. Section 8.4.1 will analyze the co-optimization problem with rate-based PFR limit (8.9) and Section 8.4.2 will analyze the co-optimization problem with equivalency ratio requirement (8.5).

A realistically large 2000 bus test case is used that intends to roughly approximate

the electric power system in Texas described in [7] and [93] and is based on publicly available data. We will assume the cost of FFR reserve is zero; that is $B_i(b_i) = 0$, and as a result the total procured FFR reserve $\mathbf{1}^\dagger b^d$ matches the total offered FFR capacity $\mathbf{1}^\dagger \bar{b}$. The 50 natural gas generators with the largest capacity are selected to provide PFR reserve and their offered PFR capacity is set to 20 percent of their generation capacity, e.g. $\bar{R}_i = 0.2\bar{G}_i$, consistent with the analysis in Section 7.1.3.2. The frequency thresholds are set to values that match the ERCOT NPRR 863 [25]. Specifically, the PFR threshold is $\omega_1 = 59.9833$Hz, the FFR threshold is $\omega_2 = 59.8$Hz, and the minimum frequency threshold is $\omega_{\min} = 59.4$Hz. We additionally analyze a loss of generation in the amount of $L = 2750$MW, which represents the two largest nuclear plants in Texas.

8.4.1 Co-optimization with Rate-Based PFR Limit

Let's first analyze the co-optimization problem with rate-based PFR limit (8.9). The co-optimization problem (8.9) is solved using the interior point algorithm from the MATLAB package TOMLAB [44]. This algorithm is not guaranteed to find a globally optimal solution; however, it seems to perform well and always identifies a KKT point as in Definition 8.1. Furthermore, the ramp rate $\kappa_i = 20$MW/s and the delay $\epsilon = 0.5$s are approximated as being the same for each generator i providing PFR reserve and were determined using a dynamic simulation of a loss of the two largest generators, which amounts to approximately 2750MW. The dynamic simulations were performed using PowerWorld.

We will first consider the effect of introducing FFR reserve into the market and then consider the effect of reducing the inertia after FFR reserve has been introduced into the market.

8.4.1.1 Introducing FFR Reserve to Market

Consider a high inertia scenario $M = 300$GWs, which represents an inertia value typical today in Texas. The limit function at this inertia level is plotted in Figure 7.4. Figures 8.1 and 8.2 analyze the effect of introducing FFR reserve into the market by increasing the total offered FFR capacity $\mathbf{1}^\dagger \bar{b}$ from 0 to 1000MW. Figure 8.1 plots the procured PFR

reserve for each generator as the total offered FFR capacity $\mathbf{1}^\dagger \bar{b}$ increases. When the total of-fered FFR capacity increases past 1000MW the price of both PFR and FFR reserve becomes zero and the co-optimization problem has multiple solutions, making it difficult to analyze. Notice that Assumption 7.1 from Section 7.2.2 is satisfied with the selected parameters and for the selected range of total offered FFR capacity. As the total offered FFR capacity increases the procured FFR reserve replaces the most expensive PFR reserve in turn from highest procurement cost to lowest procurement cost. As a result the procured PFR reserve does not decrease uniformly among all generators, but instead decreases to zero for only one or two generators at a time.
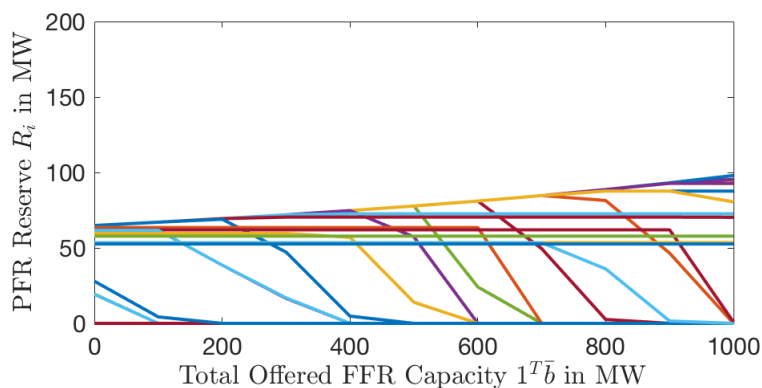

Figure 8.1: Procured PFR reserve for increasing total offered FFR capacity using the co-optimization problem with rate-based PFR limit (8.5). Each trajectory represents the procured PFR reserve to a specific generator.

The upper bound on the procured PFR reserve from the rate-based PFR limit con-straint (8.9c) increases as the total offered FFR capacity $\mathbf{1}^\dagger \bar{b}$ increases. Generators that exhibit high generation costs, low PFR reserve costs and high capacity $\bar{G}_i$ are operating at this upper bound and see increasing procured PFR reserve as the total offered FFR capacity increases. As a result we see the procured PFR reserve increasing for many generators from approximately 65MW to approximately 100MW. On the other hand, generators that exhibit high generation costs, low PFR reserve costs, and low capacity $\bar{G}_i$ are limited by their offered PFR capacity $\bar{R}_i = 0.2\bar{G}_i$ and do not experience this increase in procured PFR reserve.

Figure 8.2 shows the trajectory of reserve payments as the offered FFR capacity $\mathbf{1}^\dagger \bar{b}$ increases. Notice that the total FFR reserve payments initially increase because the procured

FFR reserve is increasing. However, when the total offered FFR capacity $\mathbf{1}^\dagger \bar{b}$ reaches 500 MW the total FFR reserve payments begin to decrease because the reserve price is dropping. On the other hand, the total PFR reserve payments experiences a steady decline. The total reserve payments (including both FFR and PFR reserve payments) also decreases as more FFR reserve is introduced.
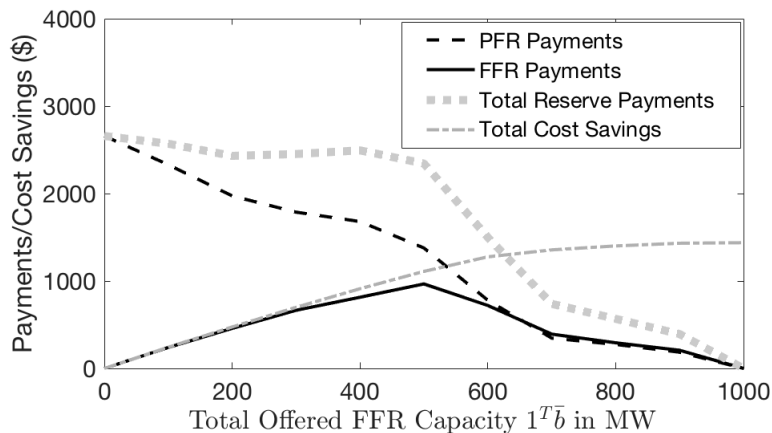

Figure 8.2: Reserve payments and cost savings for increasing total offered FFR capacity using the co-optimization problem with rate-based PFR limit (8.5).

Increasing FFR reserve also has the benefit of reducing total system costs, or equivalently increasing social welfare. The total system costs at the total offered FFR capacity of $\mathbf{1}^\dagger \bar{b} = 0$ is approximately $\$1.2 \times 10^6$. Figure 8.2 additionally plots the total cost savings, which are increasing. Notice that increasing offered FFR capacity increases cost savings in two ways. First, it allows for lower amounts of procured PFR reserve, in turn, allowing for low cost generation to be dispatched upward. Second, it increases the PFR reserve limit from constraint (8.9c), allowing the procured PFR reserve to increase from generators with low procurement costs.

8.4.1.2 Reducing the Total System Inertia

Figures 8.3 and 8.4 fix the total offered FFR capacity to $\mathbf{1}^\dagger \bar{b} = 1000$MW and analyze the effect of decreasing inertia values from 300GWs to 150GWs. This intends to represent the future scenario of decreasing inertia caused by an increase of wind and solar energy penetration. Figure 8.3 plots the procured PFR reserve for each generator as the total

160

system inertia M decreases. As the inertia drops, the limit function $h(\cdot, \mathbf{1}^\dagger b)$ decreases and the rate-based PFR limit becomes tighter. This limit constraint causes the procured PFR reserve to decrease for many generators with low procurement costs and increase for many generators with high procurement costs. When the inertia reaches its lowest value of 150GWs, the procured PFR reserve for many generators matches their rate-based PFR limit. It is apparent that the co-optimization problem (8.9) accommodates low inertia values by diversifying the procured PFR reserve, effectively distributing PFR reserve more evenly among the generators.
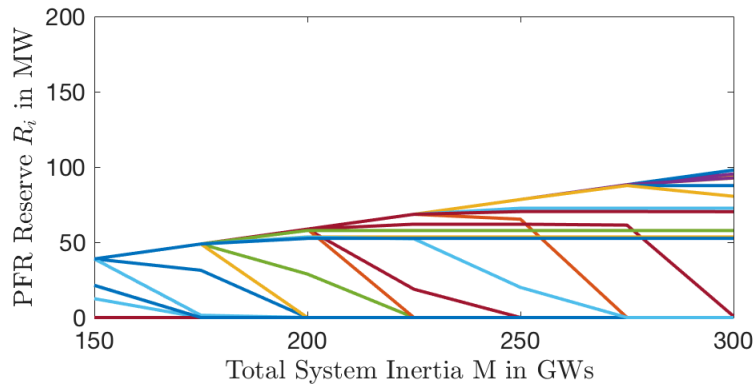

Figure 8.3: Procured PFR reserve for decreasing inertia values using the co-optimization problem with rate-based PFR limit (8.5). Each trajectory represents the procured PFR reserve for a specific generator.

Figure 8.4 shows the trajectory of PFR and FFR reserve payments as the inertia drops. As the inertia drops from $M = 300$GWs the reserve prices and payments remain zero until approximately $M = 275$GWs at which point the PFR and FFR reserve payments begin to increase. For all values of inertia the total FFR reserve payments approximately double the total PFR reserve payments despite the fact that the total procured FFR reserve is lower than the total procured PFR reserve. Specifically, the total procured FFR reserve is 1000MW and the total procured PFR reserve is 1750MW at all inertia levels. This means that the FFR reserve price is significantly larger than the PFR reserve price as discussed in Section 8.3. This higher FFR reserve price places more value in the FFR reserve because of its ramping capabilities.
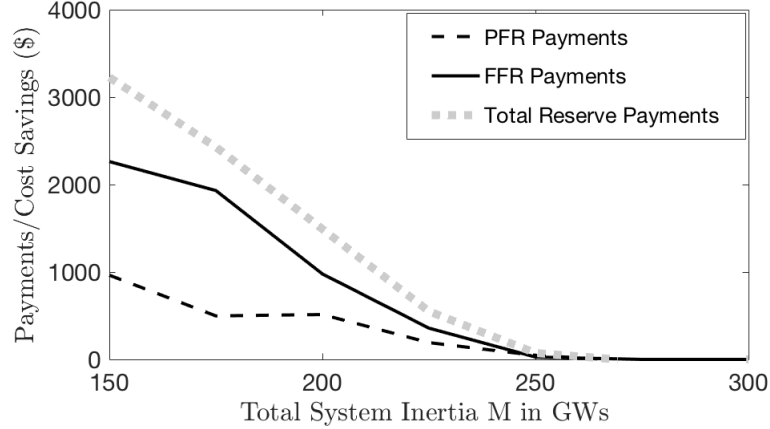
Figure 8.4: Reserve payments and cost savings for decreasing inertia values using the co-optimization problem with rate-based PFR limit (8.5).

8.4.2 Co-optimization with Equivalency Ratio Requirement

Let's now analyze the co-optimization problem with equivalency ratio requirement (8.5). The co-optimization problem (8.5b) is convex and quadratic due to quadratic cost functions in the 2000 bus test case. This problem is solved using the quadratic programming software in MATLAB's optimization toolbox, which is guaranteed to converge to a globally optimal solution. The equivalency ratio will take the values from Table 7.1, which were identified empirically by [59].

Similar to the previous section, we will first consider the effect of introducing FFR reserve into the market and then consider the effect of reducing the inertia after FFR reserve has been introduced into the market.

8.4.2.1 Introducing FFR Reserve to Market

Consider a high inertia scenario $M = 300$GWs, which represents an inertia value typical today in Texas. According to Table 7.1 the equivalency ratio at this inertia level should be $\alpha(M) = 1$. Figures 8.5 and 8.6 analyze the effect of introducing FFR reserve into the market by increasing the total offered FFR capacity $\mathbf{1}^\dagger \bar{b}$ from 0 to 1000MW. Figure 8.5 plots the procured PFR reserve for each generator as the total offered FFR capacity $\mathbf{1}^\dagger \bar{b}$ increases. When the total offered FFR capacity increases past 600MW the price of both PFR and FFR reserve becomes zero and the co-optimization problem has multiple solutions,

making it difficult to analyze. We will focus our analysis on total offered FFR capacity levels below 600MW, in which case the prices are positive and the total procured FFR reserve $\mathbf{1}^\dagger b^d$ equals the total offered FFR capacity $\mathbf{1}^\dagger \bar{b}$. As the total procured FFR reserve increases it replaces the most expensive PFR reserve in turn from highest procurement cost to lowest procurement cost. As a result the procured PFR reserve does not decrease uniformly among all generators, but instead decreases to zero for only one or two generators at a time.
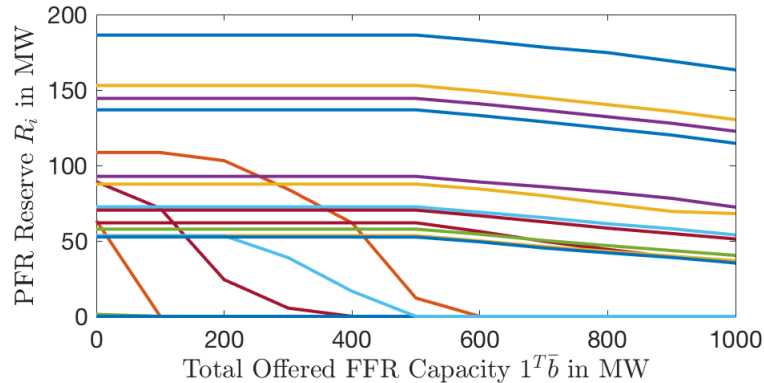

Figure 8.5: Procured PFR reserve for increasing total offered FFR capacity using the co-optimization problem with equivalency ratio requirement (8.5). Each trajectory represents the procured PFR reserve for a specific generator.

As compared to the co-optimization problem with rate-based PFR limit (8.9) the co-optimization problem with equivalency ratio requirement (8.5) results in large amounts of procured PFR reserve for some generators because they do not exhibit a tight PFR limit. This can be seen by comparing the two Figures 8.5 and 8.1. Furthermore, when using the equivalency ratio requirement, fewer generators are effected by the introduction of FFR reserve into the market. First, the equivalency ratio does not change with the total offered FFR capacity and so most generators maintain constant procured PFR reserve. Second, less generators are replaced by the newly introduced low cost FFR reserve in the sense that their procured PFR reserve falls to zero. Notice that only four generators are replaced by FFR reserve in Figure 8.5 and twelve generators are replaced by FFR reserve in Figure 8.1.

Figure 8.6 shows the trajectory of reserve payments as the total offered FFR capacity $\mathbf{1}^\dagger \bar{b}$ increases. Although this figure sees similar trends as in Figure 8.2, we see slightly less PFR reserve payments and significantly less payment to FFR reserve. Notice that the total

FFR reserve payments initially increase because the total procured FFR reserve is increasing. However, when the total offered FFR capacity $\mathbf{1}^\dagger \bar{b}$ reaches 350 MW the total FFR reserve payments begin to decrease because the reserve price is dropping. On the other hand, total PFR reserve payments steadily decline. The total reserve payments (including both FFR and PFR reserve payments) also decreases as more FFR reserve is introduced.

As compared to the co-optimization problem with rate-based PFR limit (8.9) the co-optimization problem with equivalency ratio requirement (8.5) lowers the operating cost by approximately \$1200 at the total offered FFR capacity level of $\mathbf{1}^\dagger \bar{b} = 0$. Figure 8.6 additionally plots the total cost savings with respect to the case with zero total offered FFR capacity for the co-optimization problem with equivalency ratio requirement (8.5). As expected the total cost savings are increasing in the total offered FFR capacity.

Figure 8.6: Reserve payments and cost savings for increasing total offered FFR capacity using the co-optimization problem with equivalency ratio requirement (8.5).

8.4.2.2 Reducing the Total System Inertia

Figures 8.7 and 8.8 fix the total offered FFR capacity to $\mathbf{1}^\dagger \bar{b} = 1000$MW and analyze the effect of decreasing inertia values from 300GWs to 150GWs. This intends to represent the future scenario of decreasing inertia caused by an increase of wind and solar energy penetration. The reserve prices and payments are zero for inertia at or above $M = 230$GWs and thus the co-optimization problem has multiple solutions, making it difficult to analyze. We will focus our analysis on inertia values falling below $M = 230$GWs, in which case the

prices are positive and the total procured FFR reserve $\mathbf{1}^\dagger b$ is equal to the total offered FFR capacity $\mathbf{1}^\dagger \bar{b}$.

Figure 8.7 plots the procured PFR reserve for each generator as the total system inertia M decreases. The fundamental difference between the reserve requirements in problems (8.5) and (8.9) is well illustrated by Figures 8.7 and 8.3. Specifically, Figure 8.7 shows that problem (8.5) accommodates low inertia values by simply increasing the procured PFR reserve. Notice that all procured PFR reserve trajectories increase as the inertia decreases in Figure 8.7, which contrasts with Figure 8.3. On the other hand, Figure 8.3 shows that problem (8.9) accommodates low inertia values by distributing the procured PFR reserve among more generators. Notice that the total procured reserve (including FFR and PFR) is equal to $L = 2750$MW at all inertia values in Figure 8.3, whereas the total procured reserve is more than $L = 2750$MW at low inertia values in Figure 8.7.
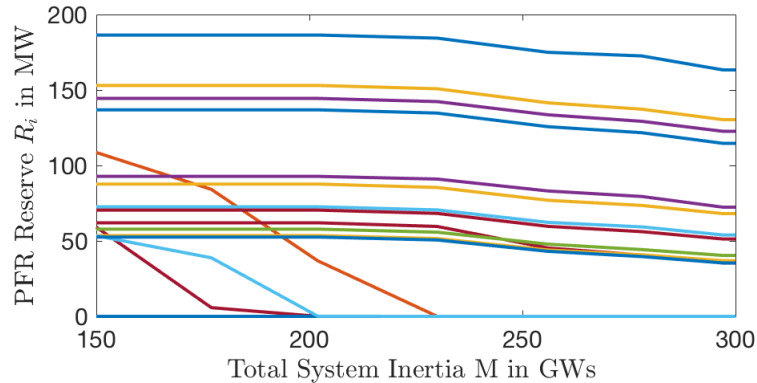
Figure 8.7: Procured PFR reserve for decreasing inertia values using the co-optimization problem with equivalency ratio requirement (8.5). Each trajectory represents the procured PFR reserve to a specific generator.

Figure 8.8 shows the trajectory of reserve payments as the total system inertia drops. As the inertia drops the reserve prices and payments remain zero until approximately $M = 230$GWs at which point the PFR and FFR reserve payments begin to increase. For all inertia levels the total PFR reserve payments approximately double the total FFR reserve payments, which is the opposite of what was witnessed in Figure 8.4. Notice that the trajectory of total PFR reserve payments is very similar for both figures; however, Figure 8.8 experiences a drastic reduction in total FFR reserve payments. In fact, the co-optimization

problem with equivalency ratio requirement (8.5) results in considerably lower prices for FFR reserve as compared to the co-optimization problem with rate-based PFR limit (8.9).
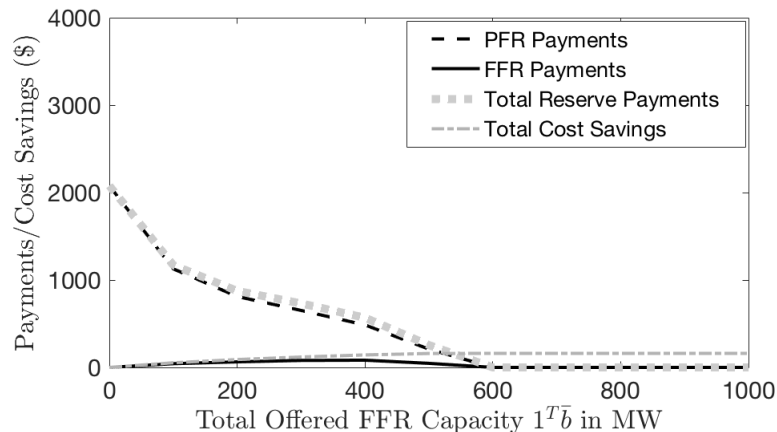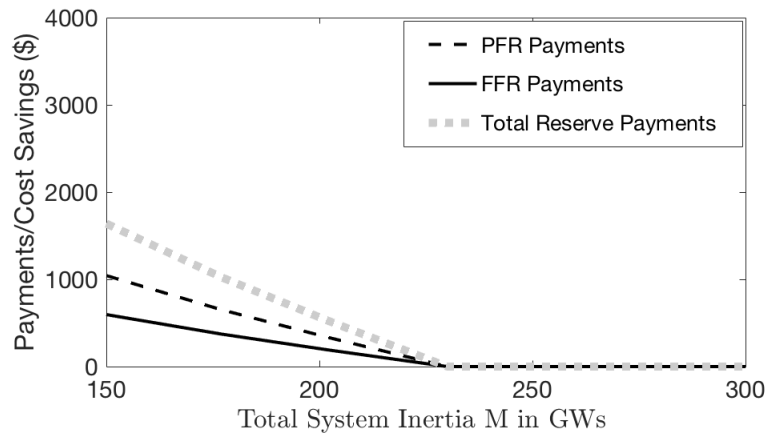

Figure 8.8: Reserve payments and cost savings for decreasing inertia values using the co-optimization problem with equivalency ratio requirement (8.5).

8.5 Summary

This chapter analyzed two different co-optimization problems. The first co-optimization problem uses an equivalency ratio reserve requirement and is consistent with the empirically derived requirement from [59]. The second co-optimization problem uses the rate-based PFR limit derived in Chapter 7. Using KKT prices, all market participants are proven to have zero lost opportunity cost and congestion revenue adequacy is guaranteed.

Numerical results are provided that illustrate the main differences between the two co-optimization problems. The equivalency ratio reserve requirement is shown to concentrate large amounts of PFR reserve to generators with low procurement costs at low inertia levels. In contrast, the rate-based PFR limit disperses the procured PFR reserve more evenly among many generators. The equivalency ratio reserve requirement is also shown to result in less reserve payments, which is desirable from a revenue adequacy standpoint. In contrast the rate-based PFR limit results in significantly higher prices for FFR reserve effectively placing value in the ramping ability of FFR reserve and resulting in large FFR reserve payments.

Part III
Conclusions and Future Work

Chapter 9

Conclusions and Future Work

Parts I and II of this dissertation were motivated by two recently proposed market rule changes in the Electric Reliability Council of Texas (ERCOT). Part I aimed to incorporate non-linear transmission models into the electricity market that account for transmission losses. This part of the dissertation was primarily based on [31–33]. Part II aimed to incorporate interdependent reserve types for primary frequency response into a real-time co-optimization problem. This part of the dissertation extended the work from [30]. Part III will now conclude the dissertation by summarizing the main findings and suggesting future research directions.

9.1 Economic Dispatch: Non-Linear Transmission Models

Part I of this dissertation focused on incorporating accurate non-linear transmission models into the myopic economic dispatch problem. Chapter 3 formulated the most accurate myopic economic dispatch problem, which is termed the Alternating Current Optimal Power Flow (AC OPF) problem. Due to the inherent non-convexity of the AC OPF problem it is generally difficult to solve and it would also result in an electricity market that cannot guarantee congestion revenue adequacy. This is one reason why ISOs today solve economic dispatch problems that serve as convex approximations of the AC OPF problem. These convex approximations were derived in Chapters 4 and 5. On the other hand, Chapter 6 attempted to accommodate non-convexity of the AC OPF problem by using algorithms that identify a potentially sub-optimal solution and by mitigating the congestion revenue adequacy problem using convex hull prices.

9.1.1 Convex Approximations of the AC OPF Problem

A non-linear transmission line model was derived in Chapter 4 that approximates the fully detailed AC transmission line model used in the AC OPF problem. The proposed non-linear transmission line model is a generalization of the commonly used quadratic loss model, incorporates a Fictitious Nodal Demand (FND) representation of losses, and was used to formulate the Transmission Constrained Economic Dispatch (TCED) problem, which approximates the AC OPF problem. Chapter 4 additionally contributed to the literature by deriving various line limit constraints and by providing rigorous justification that the FND representation of transmission losses should allocate half of the losses of each transmission line to the busses on either side of the line.

The TCED problem derived in Chapter 4 is convenient because it can easily be made convex by use of the load over-satisfaction relaxation, which is capable of recovering the exact solution of the TCED problem under the condition that Locational Marginal Prices (LMPs) are positive. The Independent System Operator (ISO) in New Zealand rarely sees non-positive prices because they restrict market participants to provide non-negative marginal cost offers in the electricity market. For this reason, New Zealand uses the load over-satisfaction relaxation in their market clearing process. Unfortunately, ISOs in the United States (US) frequently see negative prices and so they could not directly use the load over-satisfaction relaxation without modification or post-processing. To make this approach applicable to ISOs in the US, future work will focus on post-processing methods that can recover a nearly optimal feasible solution to the TCED problem from the minimizer of the convex relaxed TCED problem.

ISOs in the US use linearization techniques to approximate the solution to the TCED problem and these techniques do not require the prices to be positive. Chapter 5 studied a linearized version of the TCED problem termed the *common LCED problem* because it represents an economic dispatch problem used by ISOs in the US. This chapter contributed to the literature by characterizing the approximation errors associated with each of the three assumptions required to accurately recover the optimal dispatch of the non-convex TCED problem from the solution of the common LCED problem. This chapter observed that the

common LCED problem may have multiple minimizers, in which case small perturbations of the base-case state may result in large dispatch approximation error. Future work will identify the economic impacts of this seemingly unavoidable dispatch approximation error.

Another identified source of dispatch approximation error lies in the inaccurate choice of Loss Distribution Factors (LDFs). Even if the base-case state matches a minimizer of the non-convex TCED problem, Chapter 5 proved that there does not always exist a choice of LDFs such that the optimal dispatch of the TCED problem is also optimal for the common LCED problem. For the situations where such LDFs do not exist, future work will focus on identifying LDFs that minimize dispatch approximation error. On the other hand, Chapter 5 showed that such LDFs do exist and identified such LDFs for the special case where no line limits are binding.

9.1.2   Accommodating the AC OPF Problem by use of Convex Hull Pricing

As illustrated in Chapter 4, iterative methods, such as interior point algorithms, can be used to effectively approximate a minimizer of the AC OPF problem. Although these algorithms are only, at best, guaranteed to converge to a local minimum, they often converge to a point that is nearly globally optimal. Chapter 6 suggested dispatching the resulting identified solution of the AC OPF problem that is not guaranteed to be globally optimal. As a result congestion revenue adequacy cannot be guaranteed, or equivalently Financial Transmission Right (FTR) uplift may be positive, as illustrated in Chapter 3. For this reason Chapter 6 proposed using Convex Hull Prices (CHPs) that solve a novel multi-objective minimum uplift problem that balances a tradeoff between generator uplift and FTR uplift. The proposed multi-objective minimum uplift problem includes a weight parameter representing the relative value of FTR uplift to generator uplift. Although this chapter illustrates the effect of varying this weight parameter, it does not identify a proper method of choosing this parameter. Future work will focus on methods of properly choosing this weight parameter.

Chapter 6 continued by providing the first proposed method of approximating CHPs in polynomial-time using a transmission network model that is general enough to accom-

modate the AC OPF problem. The approximate CHPs were computed using convex relaxations of the AC OPF problem that have been developed in previous work. Numerical results showed that the Semi-Definite Programming (SDP) relaxation effectively approximates CHPs but exhibits computational limitations on large systems. Furthermore, the Quadratic Convex (QC) and Second-Order Cone (SOC) relaxations are computationally efficient but are not as effective in approximating CHPs. Future work will aim to improve upon the convex relaxations studied in this dissertation by developing tight relaxations that are computationally efficient.

The results in this dissertation focus on an economic dispatch problem that is myopic the sense that (in its basic formulation) it only optimizes over a single time interval. However, convex hull pricing is typically studied in the context of the Unit Commitment (UC) problem, which optimizes over a time horizon and considers non-convex private generator constraints. The results provided in Chapter 6 will be extended to accommodate a UC problem. Remark 6.1 illustrates how this extension can be made. In this context it would also be useful to approximate convex hull prices using a quadratic loss model as derived in Chapter 4 along with the load over-satisfaction relaxation. Future work will also identify special cases where the proposed approximation of CHPs are guaranteed to exactly match the actual CHPs.

Electricity markets today require each FTR allocation vector to be balanced in the sense that the elements sum to zero. With the goal of introducing loss modeling into the electricity market, the convex hull pricing work in Chapter 6 assumed a more general definition of FTRs that allow FTR allocation vectors to be *unbalanced* in the sense that their elements may not sum to zero, e.g. $\mathbf{1}^{\dagger} f^{(\xi)} \neq 0$. Unbalanced FTRs have been studied well in the literature [37, 40] and allow FTRs to hedge locational price differences caused by losses as well as congestion. That being said, no electricity markets today allow for unbalanced FTRs and so future work will investigate implementation challenges regarding unbalanced FTRs.

9.2 Co-Optimization: Interdependent Reserve Types

Part II of this dissertation introduced interdependent reserve types for primary frequency response into the economic dispatch problem, resulting in a co-optimization problem. Two types of reserve were considered. The first type was Primary Frequency Responsive (PFR) reserve, which intends to accommodate standard droop control. The second type was Fast Frequency Responsive (FFR) reserve, which was recently introduced to the ERCOT market and intends to accommodate fast acting battery resources. Chapter 7 derived reserve requirements from first principles that couple FFR and PFR reserve. Chapter 8 then placed these reserve requirements into a co-optimization problem that would be solved by the ERCOT ISO to determine dispatch of generation and procurement of reserves. This chapter compared a non-convex co-optimization problem that enforces the newly proposed *rate-based PFR limit* to a previously formulated convex co-optimization problem that enforces a reserve requirement based on equivalency ratios.

9.2.1 Reserve Requirements

Chapter 7 distinguished between *nominal PFR reserve,* as determined by a generator's head-room, and *available PFR reserve,* as determined by the ramping limitations of a generator's turbine governor. This chapter provided a simple model of available PFR reserve that intended to capture the ramping limitations of droop control by use of a fixed time delay followed by a fixed ramp rate. Using this model, Chapter 7 derived a novel rate-based PFR limit that ensures PFR reserve has sufficient ramping ability to effectively arrest frequency decline in response to a generator outage under certain assumptions. Specifically, the FFR reserve deployment was assumed to occur during the PFR reserve ramping period and was assumed not to overshoot; that is, the power imbalance is assumed to not become instantly positive. Finally, Chapter 7 used the rate-based PFR limit to derive the equivalency ratio reserve requirement by modeling the fixed ramp rate exhibited by each PFR reserve generator as being proportional to the nominal PFR reserve of that generator. The resulting equivalency ratio depends on the system inertia as well as the total FFR reserve. It was shown that the proposed equivalency ratio is approximately constant in the total FFR reserve for high inertia levels, yielding a reserve requirement very similar in form to the equivalency ratio

reserve requirement from [59]. This first principles derivation of the equivalency ratio reserve requirement is novel because previous work has only studied equivalency ratios empirically through simulation [59].

The assumptions used to derive the rate-based PFR limit will be removed in future work. Specifically, each possible combination of scenarios will be considered where the FFR reserve deployment occurs before or after the PFR reserve ramp and where the FFR reserve does overshoot. Furthermore, future work will determine which turbine governor models are best represented as having a constant ramp rate versus a ramp rate that is proportional to the generator's nominal PFR reserve. In this context, proper ramp rates and proportional constants will be empirically verified using extensive simulation results of large generator outages. Finally, future work will use the rate-based PFR limit to provide insight into offered PFR capacity limits that are enforced in practice through ISO protocols.

9.2.2   Real-Time Co-Optimization

Chapter 8 formulated two co-optimization problems. The first was non-convex and enforced the newly proposed rate-based PFR limit, which varied non-linearly with the procured FFR reserve. The second was convex and enforced the equivalency ratio requirement from [59]. It was proven that both problems result in zero lost opportunity cost for generators/batteries and zero FTR uplift when using the proposed KKT prices. As compared to the co-optimization problem with equivalency ratio requirement, numerical results illustrated that the co-optimization problem with rate-based PFR limit encouraged the procured PFR reserve to be more evenly dispersed among generators. Furthermore, the co-optimization problem with rate-based PFR limit resulted in higher prices for FFR reserve, which would encourage additional investment in FFR reserve but also result in larger reserve payments, which may be considered out-of-market payments.

The co-optimization problem with rate-based PFR limit is non-convex and is generally difficult to solve. This dissertation suggested solving this co-optimization problem using interior point methods, which are only, at best, guaranteed to converge to local minimum. Future work will identify efficient ways of approximately solving this non-convex

co-optimization problem. For example, [30] briefly suggests an accurate approximate formulation that uses a piecewise linearization of the PFR reserve limit constraint that only requires the introduction of a few integer variables.

Appendices

Appendix A

Generalized KKT Conditions using the Normal Cone

This appendix outlines the relationship between the common KKT conditions and the generalized KKT conditions used in Chapters 8 and 2. Section A.1 intuitively explains the relationship between the normal cone definition of the First Order Necessary Conditions (FONCs) from [71] and the common KKT conditions. This section additionally shows that the common KKT conditions imply the normal cone definition of the FONCs. Section A.2 then explicitly states the common KKT conditions for the co-optimization problem with rate-based PFR limit (8.9) for the special case where the cost function is smooth and proves that these conditions imply the generalized KKT conditions from Definition 8.1. The KKT price/dispatch pair from Definition 2.2 follows by recognizing that the KKT conditions for the general ED problem (2.6) are a special case of the KKT conditions for the co-optimization problem with rate-based PFR limit (8.9) where the reserve requirement L is zero, the PFR reserve offer $\bar{R}$ is zero, and the FFR reserve offer $\bar{b}$ is zero.

The notation in this section of the appendix is consistent with the introduction and Part II of this dissertation, where the generalized KKT conditions are defined. However, this notation is not completely consistent with Part I of this dissertation because some symbols are redefined.

A.1 The FONCs, the Normal Cone, and the KKT Conditions

Section A.1.1 will quickly derive the normal cone definition of the FONCs. Section A.1.2 will provide geometric insight into the normal cone definition of the FONCs. Finally, Section A.1.3 will quickly derive the KKT conditions from the normal cone definition of the FONCs, intuitively showing that both are equivalent.

We adopt the following optimization problem:

$$\min_{x \in \mathcal{F}} \quad \psi(x) \tag{A.1}$$

where $\mathcal{X}$ represents the feasible set of the optimization problem and $\psi : \mathcal{X} \to \mathbb{R}$ represents the objective function.

A.1.1 General First Order Necessary Condition using Normal Cones

The optimization problem (A.1) can be equivalently written as the following problem that implicitly enforces the constraints using an indicator function:

$$\min_{x \in \mathbb{R}^\psi} \quad \psi(x) + \mathbb{I}_{\mathcal{F}}(x) \tag{A.2}$$

where the indicator function is defined as follows:

$$\mathbb{I}_{\mathcal{F}}(x) := \begin{cases} 0 & \text{if } x \in \mathcal{F} \\ \infty & else \end{cases} \tag{A.3}$$

The FONCs of this unconstrained problem require the zero vector to fall in the sub-gradient of the objective. Before writing this mathematically, let's first note that the sub-gradient of the indicator function evaluated at x is the normal cone of the set $\mathcal{F}$ evaluated at x and is denoted $\mathcal{N}_{\mathcal{F}}(x)$. The normal cone of the set $\mathcal{F}$ evaluated at $x^\star$ is formally defined in [71] as follows:

$$\mathcal{N}_{\mathcal{F}}(x^\star) := \{y : y(x - x^\star) \leq 0 \ \ \forall x \in \mathcal{C}_{\mathcal{F}}(x^\star)\}, \tag{A.4}$$

where $\mathcal{C}_{\mathcal{F}}(x^\star)$ is called the *tangent cone* of the set $\mathcal{F}$ evaluated at some point $x^\star$ and represents all feasible directions in the set $\mathcal{F}$ starting at point $x^\star$. With this in mind, we have the following equality:

$$\partial\left(\mathbb{I}_{\mathcal{F}}(x)\right) = \mathcal{N}_{\mathcal{F}}(x) \tag{A.5}$$

Recall that the FONCs of this unconstrained problem require the zero vector to fall in the sub-gradient of the objective. The FONCs can now be written as follows, where the addition of two sets represents the Minkowski sum:

$$\mathbf{0} \in \partial\left(\psi(x) + \mathbb{I}_{\mathcal{F}}(x)\right) = \partial\left(\psi(x)\right) + \partial\left(\mathbb{I}_{\mathcal{F}}(x)\right) = \partial\left(\psi(x)\right) + \mathcal{N}_{\mathcal{F}}(x) \tag{A.6}$$

In the special case where the objective function $\psi(x)$ is smooth, its sub-gradient is a singleton and the FONCs reduce to the following:

$$-\nabla\psi(x^\star) \in \mathcal{N}_\mathcal{F}(x^\star) \tag{A.7}$$

A.1.2 Geometric Interpretation of the FONCs with Smooth Objective Function

The normal cone definition of the FONCs has an intuitive geometric interpretation. Consider some point $x^\star \in \mathcal{F}$. Intuitively, if $x^\star$ is optimal, then the gradient of the objective evaluated at $x^\star$, denoted $\nabla\psi(x^\star)$, should have a non-negative dot product with all feasible directions. This can be expressed as follows:

$$\nabla\psi(x^\star)^\dagger(x - x^\star) \geq 0 \quad \forall x \in \mathcal{C}_\mathcal{F}(x^\star) \tag{A.8}$$

With this in mind, the normal cone of the normal cone of the set $\mathcal{F}$ evaluated at x, denoted $\mathcal{N}_\mathcal{F}(x^\star)$, represents all vectors with negative dot product with all feasible directions as defined in (A.4).

These concepts are intuitively demonstrated in a simple two dimensional example with a smooth objective function from Figure A.1. In this example the feasible set is defined as $\mathcal{F} = \{x \in \mathbb{R}^2 : \phi(x) \leq 0\}$ where $\phi : \mathbb{R}^2 \to \mathbb{R}^2$ is the vector valued constraint function and the point $x^\star$ satisfies the FONCs. The tangent cone $\mathcal{C}_\mathcal{F}(x^\star)$ is illustrated by the orange area in Figure A.1. The normal cone $\mathcal{N}_\mathcal{F}(x^\star)$ is illustrated by the blue area in Figure A.1. Intuitively, if $x^\star$ is optimal, then the gradient of the objective evaluated at $x^\star$, denoted $\nabla\psi(x^\star)$, should have a non-negative dot product with all feasible directions.

A.1.3 Deriving the KKT Conditions

Let's now assume the feasible set is defined as follows, where the vector valued constraint function $\phi : \mathbb{R}^{\underline{\psi}} \to \mathbb{R}^{\bar{\phi}}$ is smooth and thus its gradient is well-defined:

$$\mathcal{F} = \{x \in \mathbb{R}^{\underline{\psi}} : \phi(x) \leq \mathbf{0}\} \tag{A.9}$$

In this case the normal cone of $\mathcal{F}$ evaluated at the point $x^\star$ can be written as follows:

$$\mathcal{N}_\mathcal{F}(x^\star) = \begin{cases} \{y \in \mathbb{R}^{\underline{\psi}} : \exists \lambda \in \mathbb{R}_+^{\bar{\phi}} \text{ where } y = \nabla\phi(x^\star)\lambda, \text{ and } \phi_i(x^\star)\lambda_i = 0 \; \forall i \in [1, \bar{\phi}]\} & \text{if } x^\star \in \mathcal{F} \\ \emptyset & \text{else} \end{cases}$$
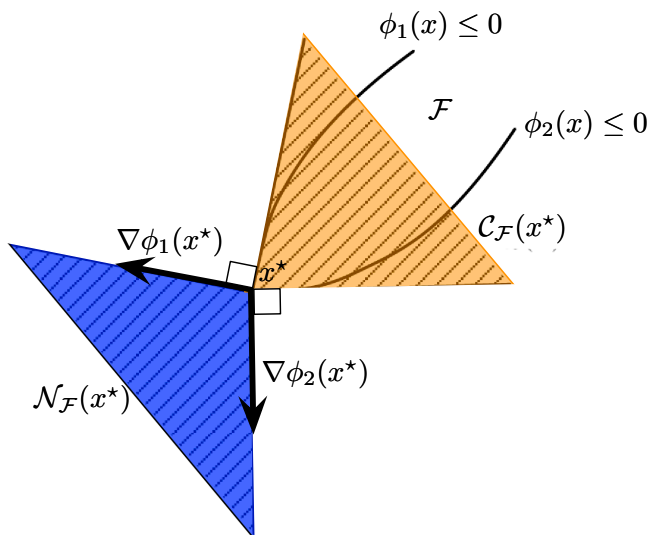
Figure A.1: Normal Cone Illustration

Notice that this definition is interpreted as a cone with basis vectors being the columns of $\nabla\phi(x^\star)$. Furthermore, the ith column is used in the basis only if the ith constraint is binding, e.g. $\phi_i(x^\star)\lambda_i = 0$. The general FONCs from (A.6) can now be rewritten. Specifically, a point $x^\star$ satisfies the general FONCs from (A.6) if the following KKT conditions hold:

$$\exists\lambda \in \mathbb{R}^{\bar{\phi}} \text{ and } \exists y \in \partial(\psi(x^\star)) \text{ such that:} \tag{A.10}$$

$$x^\star \in \mathcal{F} \tag{A.10a}$$

$$y = \nabla\phi(x^\star)\lambda \tag{A.10b}$$

$$\lambda \geq \mathbf{0} \tag{A.10c}$$

$$\phi_i(x^\star)\lambda_i = 0 \tag{A.10d}$$

Constraint (A.10a) is called the *primal feasibility* condition and follows from the fact that the normal cone evaluates to the null set if $x^\star \notin \mathcal{F}$. Constraint (A.10b) is called the stationarity condition and is interpreted as basis vectors of the normal cone being the columns of $\nabla\phi(x^\star)$. Constraint (A.10c) is called the *dual feasibility* condition and is interpreted as the cone weights being non-negative. Constraint (A.10d) is called the *complimentary slackness* condition and allows the ith column of $\nabla\phi(x^\star)$ to be a basis vector only if the jth constraint

is binding, e.g. $\phi_j(x^\star) = 0$.

The conditions (A.10) are the KKT conditions for optimization problem (A.1) with feasible set (A.9), with a general non-smooth objective function $\psi(x)$, and a smooth constraint function $\phi(x)$. Most off-the-shelf optimization software aims to identify a solution $x^\star$ that satisfies the KKT conditions (A.10) along with corresponding Lagrange multipliers $\lambda^\star$. In the case where the constraint function $\phi(x)$ is smooth, these KKT conditions imply the normal cone definition of the FONCs (A.6).

A.2   Generalized KKT Conditions for the Co-Optimization Problem

This section analyzes the co-optimization problem with rate-based PFR limit (8.9) for the special case where that the constraint sets $\mathcal{X}^i$, $\mathcal{B}^j$, and $\mathcal{T}$ are defined by smooth vector valued constraint functions and the cost function is smooth. We show that any point satisfying the common KKT conditions of the co-optimization problem with rate-based PFR limit (8.9) along with some Lagrange multipliers must also solve the definition of a KKT point 8.1.

Consider the general co-optimization problem (8.9) with the feasible set of net real power injections and the private constraint sets defined as follows:

$$\mathcal{T} = \{T \in \mathbb{R}^n : \sigma(T) \leq 0\}$$

$$\mathcal{X}^i = \{(G_i, R_i) \in \mathbb{R} \times \mathbb{R} : \rho_i(G_i, R_i) \leq 0\} \quad \forall i \in \mathbb{N}$$

$$\mathcal{B}^j = \{b_j \in \mathbb{R} : \theta_j(b_j) \leq 0\} \quad \forall j \in \mathbb{B}$$

where the vector valued constraint functions are defined as $\sigma : \mathbb{R}^n \to \mathbb{R}^{\bar{\sigma}}$, $\rho_i : \mathbb{R} \times \mathbb{R} \to \mathbb{R}^{\bar{\rho}}$, and $\theta : \mathbb{R} \to \mathbb{R}^{\bar{\theta}}$ and are assumed smooth so they have a unique gradient. Notice that these symbols have different meaning in Part I of this dissertation, but are consistent with the notation in the introduction and Part II of this dissertation. Using these definitions the co-optimization problem can now be written as follows:

$$\min_{(G,R)\in\mathbb{R}^n\times\mathbb{R}^n,\ T\in\mathbb{R}^n,b\in\mathbb{R}^\beta} \quad \sum_{i\in\mathbb{N}} C_i(G_i,R_i) + \sum_{j\in\mathbb{B}} B_j(b_j) \tag{8.9}$$

$$st : D_i - G_i + T_i = 0 \quad \forall i \in \mathbb{N} \tag{8.9a}$$

$$L \le \mathbf{1}^\dagger R + \mathbf{1}^\dagger b \tag{8.9b}$$

$$R_i \le \kappa_i h(M, \mathbf{1}^\dagger b) \quad \forall i \in \mathbb{N} \tag{8.9c}$$

$$\rho_i(G_i, R_i) \le 0 \quad \forall i \in \mathbb{N} \tag{8.9d}$$

$$\theta_j(b_j) \le 0 \quad \forall j \in \mathbb{B} \tag{8.9e}$$

$$\sigma(T) \le 0 \tag{8.9f}$$

A point $(G^\star, R^\star, b^\star, T^\star) \in \mathbb{R}^n \times \mathbb{R}^n \times \mathbb{R}^\beta \times \mathbb{R}^n$ is said to satisfy the KKT conditions for problem (8.9) if there exist Lagrangian dual variables $(\lambda, \mu, \gamma, \varphi, \chi, \varsigma) \in \mathbb{R}^n \times \mathbb{R} \times \mathbb{R}^\beta \times \mathbb{R}^{\bar\rho \times n} \times \mathbb{R}^{\bar\theta \times \beta} \times \mathbb{R}^{\bar\sigma}$ such that the following conditions hold:

$$\nabla_{G_i} C_i(G_i^\star, R_i^\star) - \lambda_i + \nabla_{G_i} \rho_i(G_i^\star, R_i^\star)\varphi_i = 0 \qquad \forall i \in \mathbb{N} \tag{A.12}$$

$$\nabla_{R_i} C_i(G_i^\star, R_i^\star) - \mu + \gamma_i + \nabla_{R_i} \rho_i(G_i^\star, R_i^\star)\varphi_i = 0 \qquad \forall i \in \mathbb{N} \tag{A.13}$$

$$\nabla B_j(b_j^\star) - \mu - \kappa^\dagger \gamma \nabla h\left(M, \mathbf{1}^\dagger b^\star\right) + \nabla \theta_j(b_j^\star)\chi_j = 0 \qquad \forall j \in \mathbb{B} \tag{A.14}$$

$$\lambda + \nabla \sigma(T^\star)\varsigma = 0 \tag{A.15}$$

$$D - G^\star + T^\star = 0 \tag{A.16}$$

$$L \leq \mathbf{1}^\dagger R^\star + \mathbf{1}^\dagger b^\star \tag{A.17}$$

$$R_i^\star \leq \kappa_i h_i(M, \mathbf{1}^\dagger b^\star) \tag{A.18}$$

$$G_i^\star \in \mathcal{X}^i \qquad \forall i \in \mathbb{N} \tag{A.19}$$

$$b_j^\star \in \mathcal{B}^j \qquad \forall j \in \mathbb{B} \tag{A.20}$$

$$T^\star \in \mathcal{T} \tag{A.21}$$

$$\mu \geq \mathbf{0} \tag{A.22}$$

$$\gamma \geq \mathbf{0} \tag{A.23}$$

$$\varphi \geq \mathbf{0} \tag{A.24}$$

$$\chi \geq \mathbf{0} \tag{A.25}$$

$$\varsigma \geq \mathbf{0} \tag{A.26}$$

$$\mu(L - \mathbf{1}^\dagger R^\star - \mathbf{1}^\dagger b^\star) = 0 \tag{A.27}$$

$$\gamma_i^\dagger(R_i^\star - \kappa_i h_i(M, \mathbf{1}^\dagger b^\star)) = \mathbf{0} \qquad \forall i \in \mathbb{N} \tag{A.28}$$

$$\varphi_i^\dagger \rho_i(G_i^\star, R_i^\star) = \mathbf{0} \qquad \forall i \in \mathbb{N} \tag{A.29}$$

$$\chi_j^\dagger \theta_j(b_j^\star) = \mathbf{0} \qquad \forall j \in \mathbb{B} \tag{A.30}$$

$$\varsigma^\dagger \sigma(T^\star) = \mathbf{0} \tag{A.31}$$

Recall from Definition 8.1 that $\nabla h\left(M, \mathbf{1}^\dagger b^\star\right)$ represents the gradient of the function $h(M, \cdot)$ evaluated at $\mathbf{1}^\dagger b^\star$ and is smooth. Furthermore, $\nabla_{G_i} C_i(G_i^\star, R_i^\star)$ represents the gradient of the function $C_i(\cdot, R_i^\star)$ evaluated at $G_i^\star$ and $\nabla_{R_i} C_i(G_i^\star, R_i^\star)$ represents the gradient of the function $C_i(G_i^\star, \cdot)$ evaluated at $R_i^\star$. All other gradient notation matches the standard conventions from the body of the dissertation.

The stationarity condition is represented by (A.12)-(A.15). The primal feasibility condition is represented by (A.16)-(A.21). The dual feasibility condition is represented by (A.22)-(A.26). The complementary slackness condition is represented by (A.27)-(A.31).

The conditions (A.15), (A.21), (A.26) and (A.31) represent the KKT conditions for the FTR payoff maximization problem (2.4) and thus the general FONCs from (A.6) are satisfied for this problem. As a result, the following must be satisfied:

$$-\lambda \in \mathcal{N}_{\mathcal{T}}(T) \tag{A.32}$$

The conditions (A.12), (A.13), (A.19), (A.24) and (A.29) represent the KKT conditions for the individual generator profit maximization problems (8.1) and thus the general FONCs from (A.6) are satisfied for this problem. As a result, the following must be satisfied:

$$0 \in \partial \left(C_i(G_i, R_i) - \lambda_i^\star G_i - \mu^\star R_i + \gamma_i^\star R_i \right)\big|_{(G_i^\star, R_i^\star)} + \mathcal{N}_{\mathcal{X}^i}(G_i^\star, R_i^\star) \quad \forall i \in \mathbb{N} \tag{A.33}$$

The conditions (A.14), (A.20), (A.25) and (A.30) represent the KKT conditions for the individual battery profit maximization problems (8.3) and thus the general FONCs from (A.6) are satisfied for this problem. As a result, the following must be satisfied:

$$0 \in \partial \left(B_j(b_j) - \mu^\star b_j - \gamma^{\star\dagger} \kappa \nabla h(M, \mathbf{1}^\dagger b^\star) b_j \right)\big|_{b_j^\star} + \mathcal{N}_{\mathcal{B}^j}(b_j^\star) \quad \forall j \in \mathbb{B} \tag{A.34}$$

Conditions (A.32)-(A.34) represent the generalized stationarity conditions (8.10a)-(8.10c) from Definition 8.1. The non-negativity constraints on μ and γ in Definition 8.1 are implied by conditions (A.22) and (A.23). The complimentary slackness equations from Definition 8.1 are implied by (A.27) and (A.28). The primal feasibility conditions from Definition 8.1 are implied by conditions (A.16)-(A.21).

The conditions from Definition 8.1 represent the generalized KKT conditions for the co-optimization problem with rate-based PFR limit (8.9), which is a generalization of the general ED problem (2.6). Specifically, the general ED problem (2.6) is attained from the co-optimization problem with rate-based PFR limit (8.9) by setting the reserve requirement to $L = -1$, by setting the FFR reserve offers to zero for each battery, e.g. $\bar{b} = 0$, and by setting the PFR reserve offers to zero for each generator $\bar{R} = 0$. In this case constraints (8.9b) and (8.9c) are never binding and thus their corresponding Lagrange multipliers must be zero by the complimentary slackness conditions (A.27) and (A.27). With this in mind, it is straight forward to see that the generalized KKT conditions for the general ED problem (2.6) in Definition 2.2 represent a special case of the more general KKT conditions for the co-optimization with rate-based PFR limit (8.9) in Definition 8.1.

Appendix B

Proof of Theorem 5.1

This proof will begin by splitting the congestion revenue into two parts denoted Γ and Ω such that $\lambda^\dagger(D - G^\star) = \Gamma + \Omega$. Subsequently, the first part of the congestion revenue will be proven greater than the FTR payoffs, e.g. $\Gamma \geq -c^\dagger f$. Finally, the second part of the congestion revenue will be proven non-negative, e.g. $\Omega \geq 0$. Let's begin.

The stationarity condition with respect to N as shown in (5.2) and (5.4) leads to the following:

$$0 = \kappa^\star + \gamma_\sigma^\star, \tag{B.1}$$

$$\mathbf{0} = \kappa^\star \mathbf{1} + \left(\mathring{\mathbf{I}}^\dagger + \tfrac{1}{2}\mathring{H}^{-1}\dot{A}^\dagger \nabla L(\dot{A}\dot{\theta}^\star)|A|\right)\gamma^\star + S^\dagger(\underline{\mu}^\star - \bar{\mu}^\star), \tag{B.2}$$

Notice that this implies $\gamma^\star$ is the negative of the LMP λ by (5.13), (5.14), and (5.15). This relationship between $\gamma^\star$ and λ will be referenced later in the proof.

$$\gamma^\star = -\lambda \tag{B.3}$$

Let's introduce a vector $\varrho = \frac{N^\star}{\mathbf{1}^\dagger N^\star}$ that sums to one. Left multiply both sides of (B.1) and (B.2) by ϱ_σ and $\mathring{\varrho}^\dagger$ respectively and sum both sides of the resulting two equations to achieve the following:

$$\kappa^\star = -\varrho_\sigma\gamma_\sigma^\star - \mathring{\varrho}^\dagger\left(\mathring{\mathbf{I}}^\dagger + \tfrac{1}{2}\mathring{H}^{-1}\dot{A}^\dagger\nabla L(\dot{A}\dot{\theta}^\star)|A|\right)\gamma^\star - \mathring{\varrho}^\dagger S^\dagger(\underline{\mu}^\star - \bar{\mu}^\star) \tag{B.4}$$

Notice that energy component of the LMP $e = -\kappa^\star \mathbf{1}$ and the LMP $\lambda = e + l + c$ can now be written in terms of the Lagrange multipliers $\gamma^\star$, $\underline{\mu}^\star$, and $\bar{\mu}^\star$. We can now decompose the revenue into two parts. The first part of the revenue, denoted Γ, will be defined by a price component that incorporates the Lagrange multipliers of the line limit constraints $\underline{\mu}^\star$ and $\bar{\mu}^\star$. The second part of the revenue, denoted Ω, will be defined by a price component

that incorporates the Lagrange multipliers of the loss constraints $\gamma^\star$. From (B.4) it is easy to see that the congestion revenue $\lambda^\dagger(D - G^\star)$ is equal to $\Gamma + \Omega$.

$$\Gamma := (c - \mathring{\varrho}^\dagger S^\dagger(\underline{\mu}^\star - \bar{\mu}^\star)\mathbf{1})^\dagger (D - G^\star) \tag{B.5}$$

$$\Omega := \left(l - \varrho_\sigma \gamma_\sigma^\star \mathbf{1} - \mathring{\varrho}^\dagger \left(\mathring{\mathbf{I}}^\dagger + \tfrac{1}{2}\mathring{H}^{-1}\dot{A}^\dagger \nabla L(\dot{A}\dot{\theta}^\star)|A|\right)\gamma^\star \mathbf{1}\right)^\dagger (D - G^\star) \tag{B.6}$$

The remainder of the proof is split into two parts. Section B.1 provides Part A of the proof and shows that Γ is at always greater than or equal to the FTR payoff $-c^\dagger f$. Section B.2 provides Part B of the proof and shows that Ω is non-negative under the assumption that the LMPs, $\lambda = -\gamma^\star$, are non-negative. Theorem 5.1 is then implied.

B.1 Part A of Proof

The following steps are taken to prove that $\Gamma \geq -c^\dagger f$. The first expression (B.7) follows directly from (B.5). Step (B.7)-(B.8) uses the definition of c from (5.15). Step (B.8)-(B.9) follows algebraically. Step (B.9)-(B.10) substitutes the definition of $\varrho = \frac{N^\star}{\mathbf{1}^\dagger N^\star}$ and uses the constraint $(j1)$, which states that $\mathbf{1}^\dagger(D - G^\star) = -\mathbf{1}^\dagger N^\star$. Step (B.10)-(B.11) follows algebraically. Step (B.11)-(B.12) uses the complementary slackness condition for constraints $(j4)$. Step (B.12)-(B.13) uses the upper and lower bounds enforced by the SFC in definition (5.16). Step (B.13)-(B.14) follows algebraically. Step (B.13)-(B.14) uses the definition of c from (5.15).

$$\Gamma := c^\dagger (D - G^\star) - (\underline{\mu}^\star - \bar{\mu}^\star)^\dagger S \mathring{\varrho}\mathbf{1}^\dagger (D - G^\star) \tag{B.7}$$

$$= (\underline{\mu}^\star - \bar{\mu}^\star)^\dagger S \left(\mathring{D} - \mathring{G}^\star\right) - (\underline{\mu}^\star - \bar{\mu}^\star)^\dagger S \mathring{\varrho}\mathbf{1}^\dagger (D - G^\star) \tag{B.8}$$

$$= (\underline{\mu}^\star - \bar{\mu}^\star)^\dagger S \left(\left(\mathring{D} - \mathring{G}^\star\right) - \mathring{\varrho}\mathbf{1}^\dagger (D - G^\star)\right) \tag{B.9}$$

$$= (\underline{\mu}^\star - \bar{\mu}^\star)^\dagger S \left(\left(\mathring{D} - \mathring{G}^\star\right) + \tfrac{\mathring{N}^\star}{\mathbf{1}^\dagger N^\star}\mathbf{1}^\dagger N^\star\right) \tag{B.10}$$

$$= (\underline{\mu}^\star - \bar{\mu}^\star)^\dagger S \left(\mathring{D} - \mathring{G}^\star + \mathring{N}^\star\right) \tag{B.11}$$

$$= -\underline{\mu}^{\star\dagger} F + \bar{\mu}^{\star\dagger} \bar{F} \tag{B.12}$$

$$\geq -\underline{\mu}^\dagger S \mathring{f} + \bar{\mu}^\dagger S \mathring{f} \tag{B.13}$$

$$= (\bar{\mu} - \underline{\mu})^\dagger S \mathring{f} \tag{B.14}$$

$$= -c^\dagger f \tag{B.15}$$

B.2 Part B of Proof

The following steps are taken to prove that $\Omega \geq 0$. The first expression (B.16) follows directly from (B.6). Step (B.16)-(B.17) and step (B.17)-(B.18) follow algebraically. Step (B.18)-(B.19) substitutes the definition of $\varrho = \frac{N^\star}{1^\dagger N^\star}$ and the constraint $(j1)$, which states that $1^\dagger(D - G^\star) = -1^\dagger N^\star$. Step (B.19)-(B.20) follows algebraically. Step (B.20)-(B.21) follows from the definition of $\dot{\theta}^\star := \mathring{H}^{-\dagger}\left(\mathring{D} - \mathring{G}^\star + \mathring{N}^\star\right)$. Step (B.21)-(B.22), step (B.22)-(B.23), and step (B.23)-(B.24) follow algebraically. Step (B.24)-(B.25) uses the first order definition of convexity for the vector-valued function $L(\cdot)$. In this context the first order definition of convexity states that $0 = L(0) \geq L(\dot{A}\dot{\theta}^\star) + \nabla L^\dagger(\dot{A}\dot{\theta}^\star)(0 - \dot{A}\dot{\theta}^\star)$. The final inequality follows from this first order definition of convexity along with (B.3) and the assumption that the LMPs λ are non-negative.

$$\Omega := l^\dagger(D - G^\star) - \left(\varrho_\sigma \gamma_\sigma^\star + \mathring{\varrho}^\dagger\left(\mathring{\mathbf{I}}^\dagger + \tfrac{1}{2}\mathring{H}^{-1}\dot{A}^\dagger\nabla L(\dot{A}\dot{\theta}^\star)|A|\right)\gamma^\star\right)1^\dagger(D - G^\star) \tag{B.16}$$

$$= \left(\tfrac{1}{2}\mathring{H}^{-1}\dot{A}^\dagger\nabla L(\dot{A}\dot{\theta}^\star)|A|\gamma^\star\right)^\dagger\left(\mathring{D} - \mathring{G}^\star\right) - \varrho_\sigma\gamma_\sigma^\star 1^\dagger(D - G^\star)$$
$$\quad - \mathring{\varrho}^\dagger\mathring{\mathbf{I}}^\dagger\gamma^\star 1^\dagger(D - G^\star) - \tfrac{1}{2}\mathring{\varrho}^\dagger\mathring{H}^{-1}\dot{A}^\dagger\nabla L(\dot{A}\dot{\theta}^\star)|A|\gamma^\star 1^\dagger(D - G^\star) \tag{B.17}$$

$$= \tfrac{1}{2}\gamma^{\star\dagger}|A|^\dagger\nabla L^\dagger(\dot{A}\dot{\theta}^\star)\dot{A}\mathring{H}^{-\dagger}\left(\mathring{D} - \mathring{G}^\star\right) - \gamma_\sigma^\star\varrho_\sigma 1^\dagger(D - G^\star)$$
$$\quad - \gamma^{\star\dagger}\mathring{\mathbf{I}}\mathring{\varrho}1^\dagger(D - G^\star) - \tfrac{1}{2}\gamma^{\star\dagger}|A|^\dagger\nabla L^\dagger(\dot{A}\dot{\theta}^\star)\dot{A}\mathring{H}^{-\dagger}\mathring{\varrho}1^\dagger(D - G^\star) \tag{B.18}$$

$$= \tfrac{1}{2}\gamma^{\star\dagger}|A|^\dagger\nabla L^\dagger(\dot{A}\dot{\theta}^\star)\dot{A}\mathring{H}^{-\dagger}\left(\mathring{D} - \mathring{G}^\star\right) + \gamma_\sigma^\star\tfrac{N_\sigma^\star}{1^\dagger N^\star}1^\dagger N^\star$$
$$\quad + \gamma^{\star\dagger}\mathring{\mathbf{I}}\tfrac{\mathring{N}^\star}{1^\dagger N^\star}1^\dagger N^\star + \tfrac{1}{2}\gamma^{\star\dagger}|A|^\dagger\nabla L^\dagger(\dot{A}\dot{\theta}^\star)\dot{A}\mathring{H}^{-\dagger}\tfrac{\mathring{N}^\star}{1^\dagger N^\star}1^\dagger N^\star \tag{B.19}$$

$$= \tfrac{1}{2}\gamma^{\star\dagger}|A|^\dagger\nabla L^\dagger(\dot{A}\dot{\theta}^\star)\dot{A}\mathring{H}^{-\dagger}\left(\mathring{D} - \mathring{G}^\star + \mathring{N}^\star\right) + \gamma_\sigma^\star N_\sigma^\star + \mathring{\gamma}^{\star\dagger}\mathring{N}^\star \tag{B.20}$$

$$= -\tfrac{1}{2}\gamma^{\star\dagger}|A|^\dagger\nabla L^\dagger(\dot{A}\dot{\theta}^\star)\dot{A}\dot{\theta}^\star + \gamma^{\star\dagger}N^\star \tag{B.21}$$

$$= \gamma^{\star\dagger}\left(-\tfrac{1}{2}|A|^\dagger\nabla L^\dagger(\dot{A}\dot{\theta}^\star)\dot{A}\dot{\theta}^\star + N^\star\right) \tag{B.22}$$

$$= \gamma^{\star\dagger}\left(\tfrac{1}{2}|A|^\dagger\nabla L^\dagger(\dot{A}\dot{\theta}^\star)(0 - \dot{A}\dot{\theta}^\star) + N^\star\right) \tag{B.23}$$

$$= \gamma^{\star\dagger}\tfrac{1}{2}|A|^\dagger\left(\nabla L^\dagger(\dot{A}\dot{\theta}^\star)(0 - \dot{A}\dot{\theta}^\star) + L(\dot{A}\dot{\theta}^\star)\right) \tag{B.24}$$

$$\geq 0 \tag{B.25}$$

$\square$

Appendix C

Power Flow and Current Flow Quantities

This appendix derives the power flow quantity $\hat{F}_\ell(\Theta_\ell, d)$ from Section 4.1.1 and the current flow quantity $\hat{\mathcal{I}}_{ij}(\Theta_\ell)$ from Section 4.1.5. Both quantities are derived based on the equivalent-Π model of a transmission line provided in Figure 4.1. As stated in Chapter 4 voltage magnitudes are assumed fixed.

C.1 Real and Reactive Power Flow Quantities

This section derives the function $\hat{F}_\ell(\Theta_\ell, d)$ in Section 4.1.1. In accordance with Figure 4.1, this function represents the real power flowing through node c in the series element of the equivalent-Π model of a transmission line in the direction of bus j at an arbitrary fractional distance d. First, let S_ℓ^d denote the complex power flowing through node c toward bus j. The voltage at node c relative to ground is v_c and the current flowing through node c toward bus j is I_c.

$$S_\ell^d = v_c I_c^* = \left(v_j + d\left(\frac{v_i}{a_\ell} - v_j \right) \right) \left(\frac{\frac{v_i^*}{a_\ell^*} - v_j^*}{z_\ell^*} \right) \tag{C.1}$$

$$= \frac{1}{z_\ell^*} \left(V_j \angle (\theta_j) + d\left(\frac{V_i}{\tau_\ell} \angle (\theta_i - \psi_\ell) - V_j \angle (\theta_j) \right) \right) \left(\frac{V_i}{\tau_\ell} \angle (\psi_\ell - \theta_i) - V_j \angle (-\theta_j) \right) \tag{C.2}$$

$$= \frac{1}{z_\ell^*} \left(\frac{V_i V_j}{\tau_\ell} \angle (\psi_\ell - \theta_i + \theta_j) + \frac{dV_i^2}{\tau_\ell^2} - \frac{dV_j V_i}{\tau_\ell} \angle (\psi_\ell - \theta_i + \theta_j) - V_j^2 - V_j d\frac{V_i}{\tau_\ell} \angle (-\theta_j + \theta_i - \psi_\ell) + dV_j^2 \right) \tag{C.3}$$

$$= \frac{1}{z_\ell^*} \left(\frac{dV_i^2}{\tau_\ell^2} - (1-d)V_j^2 + \frac{V_j V_i}{\tau_\ell} \angle (\psi_\ell - \theta_i + \theta_j) - \frac{dV_i V_j}{\tau_\ell} \left(1\angle (\psi_\ell - \theta_i + \theta_j) + 1\angle (-\theta_j + \theta_i - \psi_\ell) \right) \right) \tag{C.4}$$

$$= \frac{1}{z_\ell^*} \left(\frac{dV_i^2}{\tau_\ell^2} - (1-d)V_j^2 + \frac{V_j V_i}{\tau_\ell} \angle (\psi_\ell - \Theta_\ell) - \frac{dV_i V_j}{\tau_\ell} \left(1\angle (\psi_\ell - \Theta_\ell) + 1\angle (\Theta_\ell - \psi_\ell) \right) \right) \tag{C.5}$$

$$= \frac{1}{z_\ell^*} \left(\frac{dV_i^2}{\tau_\ell^2} - (1-d)V_j^2 + \frac{V_j V_i}{\tau_\ell} \left(\cos(\psi_\ell - \Theta_\ell) + \mathbf{i}\sin(\psi_\ell - \Theta_\ell) \right) - \frac{2dV_i V_j}{\tau_\ell} \cos(\Theta_\ell - \psi_\ell) \right) \tag{C.6}$$

$$= (g_\ell - \mathbf{i}b_\ell) \left(\frac{dV_i^2}{\tau_\ell^2} - (1-d)V_j^2 + \frac{V_j V_i}{\tau_\ell}(1-2d)\cos(\Theta_\ell - \psi_\ell) - \mathbf{i}\frac{V_j V_i}{\tau_\ell}\sin(\Theta_\ell - \psi_\ell) \right) \tag{C.7}$$

The function $\hat{F}_\ell(\Theta_\ell, d)$ should represent the real part of S_ℓ^d. This is expressed as follows.

$$\text{Re}(S_\ell^d) = g_\ell \left(\frac{dV_i^2}{\tau_\ell^2} - (1-d)V_j^2 + \frac{V_j V_i}{\tau_\ell}(1-2d)\cos(\Theta_\ell - \psi_\ell) \right) - b_\ell \frac{V_j V_i}{\tau_\ell}\sin(\Theta_\ell - \psi_\ell) \quad \text{(C.8)}$$

C.2   Derivation of Squared Current Magnitude

This section derives the function $\hat{\mathcal{I}}_{ij}(\Theta_\ell)$ in Section 4.1.5. In accordance with Figure 4.1, this function represents the squared current magnitude flowing into the transmission line from bus i and is written as follows:

$$\hat{\mathcal{I}}_{ij}(\Theta_\ell) := \frac{|y_\ell|^2}{\tau_\ell^2}\left(\frac{\alpha_\ell^2}{\tau_\ell^2}V_i^2 + V_j^2 - \frac{2\alpha_\ell}{\tau_\ell}V_i V_j \cos(\phi_\ell - \psi_\ell + \Theta_\ell) \right), \quad \text{(4.12)}$$

Let's derive this function. First, let the complex current flowing into the line from bus i be denoted I_{ij}. Recognize that the current on the receiving end of the ideal transformer is $a_\ell I_{ij}$ and is equivalent to the sum of current flowing through the shunt element located at bus i, written as $\frac{v_i}{a_\ell}y_\ell^{(s)}$, and the current flowing through the series impedance, written $(\frac{v_i}{a_\ell} - v_j)y_\ell$. The squared current magnitude flowing into the transmission line from bus i is written as follows. The squared current magnitude function $\hat{\mathcal{I}}_{ij}(\Theta_\ell)$ represents the squared magnitude of the sum of these terms divided by the squared magnitude of the off-nominal tap ratio and can be expressed as follows.

$$\hat{\mathcal{I}}_{ij}(\Theta_\ell) = \left| \frac{v_i}{a_\ell}y_\ell^{(s)} + \left(\frac{v_i}{a_\ell} - v_j \right)y_\ell \right|^2 \frac{1}{|a_\ell|^2} \quad \text{(C.9)}$$

$$= \left| \left(z_\ell \left(y_\ell^{(s)} + y_\ell \right)\frac{v_i}{a_\ell} - v_j \right)y_\ell \right|^2 \frac{1}{\tau_\ell^2} \quad \text{(C.10)}$$

$$= \left| \left(\alpha_\ell \frac{V_i}{\tau_\ell}\angle(\theta_i + \phi_\ell - \psi_\ell) - V_j\angle\theta_j \right)y_\ell \right|^2 \frac{1}{\tau_\ell^2} \quad \text{(C.11)}$$

$$= \left(\frac{\alpha_\ell V_i}{\tau_\ell}\angle(\theta_i + \phi_\ell - \psi_\ell) - V_j\angle\theta_j \right)\left(\frac{\alpha_\ell V_i}{\tau_\ell}\angle(-\theta_i - \phi_\ell + \psi_\ell) - V_j\angle -\theta_j \right)\frac{|y_\ell|^2}{\tau_\ell^2} \quad \text{(C.12)}$$

$$= \left((\frac{\alpha_\ell V_i}{\tau_\ell})^2 + V_j^2 - \frac{\alpha_\ell}{\tau_\ell}V_i V_j\angle(\Theta_\ell + \phi_\ell - \psi_\ell) - \frac{\alpha_\ell}{\tau_\ell}V_i V_j\angle(-\Theta_\ell - \phi_\ell + \psi_\ell) \right)\frac{|y_\ell|^2}{\tau_\ell^2} \quad \text{(C.13)}$$

$$= \left((\frac{\alpha_\ell}{\tau_\ell}V_i)^2 + V_j^2 - \frac{2\alpha_\ell}{\tau_\ell}V_i V_j \cos(\Theta_\ell + \phi_\ell - \psi_\ell) \right)\frac{|y_\ell|^2}{\tau_\ell^2} \quad \text{(C.14)}$$

Step (C.10) simply factors out y_ℓ^*. Steps (C.10)-(C.11) place complex numbers in polar form and use the definitions of α_ℓ and ϕ_ℓ. Steps (C.11)-(C.12) expresses squared magnitude as the multiplication of complex conjugates. Steps (C.12)-(C.13) use simple multiplication.

188

Steps (C.13)-(C.14) uses Eulers formula, recognize that the sum of complex conjugates of any number is two times the real part of that number.

Index

Bibliography

[1] Tohid Akbari and Mohammad Tavakoli Bina. A linearized formulation of ac multi-year transmission expansion planning: A mixed-integer linear programming approach. *Electric Power Systems Research*, 114:93–100, 2014.

[2] Farid Alizadeh. Interior point methods in semidefinite programming with applications to combinatorial optimization. *SIAM journal on Optimization*, 5(1):13–51, 1995.

[3] Paul M Anderson and Aziz A Fouad. *Power system control and stability.* John Wiley & Sons, 2008.

[4] MOSEK ApS. *The MOSEK optimization toolbox for MATLAB manual. Version 8.1.*, 2017.

[5] Ross Baldick. *Applied optimization: formulation and algorithms for engineering systems.* Cambridge University Press, 2006.

[6] Daniel Bienstock and Abhinav Verma. Strong NP-hardness of AC power flows feasibility. *arXiv preprint arXiv:1512.07315*, 2015.

[7] Adam B Birchfield, Ti Xu, Kathleen M Gegner, Komal S Shetye, and Thomas J Overbye. Grid structural characteristics as validation criteria for synthetic networks. *IEEE Transactions on power systems*, 32(4):3258–3265, 2017.

[8] Subhonmesh Bose and Steven H Low. Some emerging challenges in electricity markets. In *Smart Grid Control*, pages 29–45. Springer, 2019.

[9] Waqquas A Bukhsh, Andreas Grothey, Ken IM McKinnon, and Paul A Trodden. Local solutions of the optimal power flow problem. *IEEE Transactions on Power Systems*, 28(4):4780–4788, 2013.

[10] Richard H Byrd, Jorge Nocedal, and Richard A Waltz. Knitro: An integrated package for nonlinear optimization. In *Large-scale nonlinear optimization*, pages 35–59. Springer, 2006.

[11] Mary B Cain, Richard P O'neill, and Anya Castillo. History of optimal power flow and formulations. *Federal Energy Regulatory Commission*, pages 1–36, 2012.

[12] J Carpentier. Optimal power flows. *International Journal of Electrical Power & Energy Systems*, 1(1):3–15, 1979.

[13] Anya Castillo, Paula Lipka, Jean-Paul Watson, Shmuel S Oren, and Richard P O'Neill. A successive linear programming approach to solving the IV-ACOPF. *IEEE Transactions on Power Systems*, 31(4):2752–2763, 2016.

[14] Anya Castillo and Richard P O'Neill. Computational performance of solution techniques applied to the acopf. *Federal Energy Regulatory Commission, Optimal Power Flow Paper*, 5, 2013.

[15] Héctor Chávez, Ross Baldick, and Sandip Sharma. Governor rate-constrained opf for primary frequency control adequacy. *IEEE Transactions on Power Systems*, 29(3):1473–1480, 2014.

[16] Carleton Coffrin, Russell Bent, Kaarthik Sundar, Yeesian Ng, and Miles Lubin. Powermodels. jl: An open-source framework for exploring power flow formulations. *arXiv preprint arXiv:1711.01728*, 2017.

[17] Carleton Coffrin, Dan Gordon, and Paul Scott. NESTA, the NICTA energy system test case archive. *arXiv preprint arXiv:1411.0359*, 2014.

[18] Carleton Coffrin, Hassan L Hijazi, and Pascal Van Hentenryck. The QC relaxation: A theoretical and computational study on optimal power flow. *IEEE Trans. on Power Systems*, 31(4):3008–3018, 2016.

[19] Carleton Coffrin and Pascal Van Hentenryck. A linear-programming approximation of AC power flows. *INFORMS Journal on Computing*, 26(4):718–734, 2014.

[20] Carleton Coffrin, Pascal Van Hentenryck, and Russell Bent. Approximating line losses and apparent power in AC power flow linearizations. In *Power and Energy Society General Meeting, 2012 IEEE*, pages 1–8. IEEE, 2012.

[21] Brent Eldridge, Richard O'Neill, and Anya Castillo. An improved method for the DCOPF with losses. *IEEE Transactions on Power Systems*, 33(4):3779–3788, 2018.

[22] Brent Eldridge, Richard P O'Neill, and Anya Castillo. Marginal loss calculations for the DCOPF. *Federal Energy Regulatory Commission, Tech. Rep*, 2017.

[23] ERCOT. BAL-001-TRE-1 - primary frequency response in the ERCOT region. Technical report, ERCOT, February 2014.

[24] ERCOT. NPRR 581: Add fast responding regulation service as a subset of regulation service. Technical report, ERCOT, February 2014.

[25] ERCOT. NPRR 863: Creation of primary frequency response service product and revisions to responsive reserve. Technical report, ERCOT, January 2018.

[26] ERCOT. Study of the operational improvements and other benefits associated with the implementation of real-time co-optimization of energy and ancillary services. Technical report, ERCOT, June 2018.

[27] ERCOT. Study of the system benefits of incorporating marginal losses in security-constrained economic dispatch. Technical report, ERCOT, June 2018.

[28] James E Falk. Lagrange multipliers and nonconvex programs. *SIAM Journal on Control*, 7(4):534–545, 1969.

[29] Francisco Flores-Espino, Tian Tian, Ilya Chernyakhovskiy, Ilya Chernyakhovskiy, and Mackay Miller. Competitive electricity market regulation in the United States: A primer. Technical report, National Renewable Energy Lab.(NREL), Golden, CO (United States), 2016.

[30] Manuel Garcia and Ross Baldick. Real-time co-optimization: Interdependent reserve types for primary frequency response. In *Proceedings of the Tenth ACM International Conference on Future Energy Systems*, pages 550–555. ACM, 2019.

[31] Manuel Garcia and Ross Baldick. Approximating economic dispatch by linearizing transmission losses. In *IEEE Transactions on Power Systems*, (Accepted) 2019.

[32] Manuel Garcia, Ross Baldick, and Shams Siddiqi. A general economic dispatch problem with marginal losses. In *2019 American Control Conference (ACC)*, pages 2588–2595. IEEE, 2019.

[33] Manuel Garcia, Harsha Nagarajan, and Ross Baldick. Convex hull pricing for the AC optimal power flow problem. *IEEE Transactions on Control of Network Systems*, (Accepted) 2019.

[34] Michael Grant, Stephen Boyd, and Yinyu Ye. CVX: Matlab software for disciplined convex programming, 2008.

[35] Paul R Gribik, William W Hogan, and Susan L Pope. Market-clearing electricity prices and energy uplift. *Cambridge, MA*, 2007.

[36] Chris Harris. *Electricity markets: pricing, structures and economics*, volume 565. John Wiley & Sons, 2011.

[37] Scott M Harvey and William W Hogan. Loss hedging financial transmission rights. *Center for Business and Government, Harvard University*, 15(2002), 2002.

[38] Benjamin F Hobbs, Glenn Drayton, Emily Bartholomew Fisher, and Wietze Lise. Improved transmission representations in oligopolistic market models: quadratic losses, phase shifters, and DC lines. *IEEE Transactions on Power Systems*, 23(3):1018–1029, 2008.

[39] Benjamin F Hobbs, Michael H Rothkopf, Richard P O'Neill, and Hung-po Chao. *The next generation of electric power unit commitment models*, volume 36. Springer Science & Business Media, 2006.

[40] William Hogan. Financial transmission right formulations. *Report, Center for Business and Government, John F. Kennedy School of Government, Harvard University, Cambridge, MA*, 2002.

[41] William W Hogan. Financial transmission rights, revenue adequacy and multi-settlement electricity markets. *unpublished. [Online]. Available Harvard University web site: https://sites.hks.harvard.edu/fs/whogan/Hogan_FTR_Rev_Adequacy_031813.pdf*, 2013.

[42] William W Hogan and Susan Pope. Priorities for the evolution of an energy-only electricity market design in ercot. *FTI Consulting*, 2017.

[43] William W Hogan and Brendan J Ring. On minimum-uplift pricing for electricity markets. *Electricity Policy Group*, 2003.

[44] Kenneth Holmström, Anders O Göran, and Marcus M Edvall. Users guide for tomlab 7. *Tomlab Optimization Inc*, 2010.

[45] Bowen Hua and Ross Baldick. A convex primal formulation for convex hull pricing. *IEEE Transactions on Power Systems*, 32(5):3814–3823, 2017.

[46] Rabih A Jabr. Radial distribution load flow using conic programming. *IEEE Trans. on power systems*, 21(3):1458–1459, 2006.

[47] Cédric Josz, Stéphane Fliscounakis, Jean Maeght, and Patrick Panciatici. AC power flow data in MATPOWER and QCQP format: iTesla, RTE snapshots, and PEGASE. *arXiv preprint arXiv:1603.01533*, 2016.

[48] Daniel S Kirschen and Goran Strbac. *Fundamentals of power system economics*. John Wiley & Sons, 2018.

[49] Burak Kocuk, Santanu S Dey, and X Andy Sun. Strong SOCP relaxations for the optimal power flow problem. *Operations Research*, 64(6):1177–1196, 2016.

[50] Prabha Kundur, Neal J Balu, and Mark G Lauby. *Power system stability and control*, volume 7. McGraw-hill New York, 1994.

[51] Javad Lavaei and Steven H Low. Zero duality gap in optimal power flow problem. *IEEE Transactions on Power Systems*, 27(1):92–107, 2012.

[52] Javad Lavaei and Somayeh Sojoudi. Competitive equilibria in electricity markets with nonlinearities. In *American Control Conference (ACC), 2012*, pages 3081–3088. IEEE, 2012.

[53] Javad Lavaei, David Tse, and Baosen Zhang. Geometry of power flows and optimization in distribution networks. *IEEE Trans. on Power Systems*, 29(2):572–583, 2014.

[54] Karsten Lehmann, Alban Grastien, and Pascal Van Hentenryck. AC-feasibility on tree networks is NP-hard. *IEEE Transactions on Power Systems*, 31(1):798–801, 2016.

[55] Bernard C Lesieutre and Ian A Hiskens. Convexity of the set of feasible injections and revenue adequacy in FTR markets. *IEEE Trans. on Power Systems*, 20(4):1790–1798, 2005.

[56] Fangxing Li. Fully reference-independent lmp decomposition using reference-independent loss factors. *Electric Power Systems Research*, 81(11):1995–2004, 2011.

[57] Fangxing Li and Rui Bo. DCOPF-based lmp simulation: algorithm, comparison with acopf, and sensitivity. *IEEE Transactions on Power Systems*, 22(4):1475–1485, 2007.

[58] Eugene Litvinov, Tongxin Zheng, Gary Rosenwald, and Payman Shamsollahi. Marginal loss modeling in LMP calculation. *IEEE Transactions on Power Systems*, 19(2):880–888, 2004.

[59] Cong Liu and Pengwei Du. Participation of load resources in day-ahead market to provide primary-frequency response reserve. *IEEE Transactions on Power Systems*, 33(5):5041–5051, 2018.

[60] Steven H Low. Convex relaxation of optimal power flow-part I: Formulations and equivalence. *IEEE Trans. on Control of Network Systems*, 1(1):15–27, 2014.

[61] Steven H Low. Convex relaxation of optimal power flow-part II: Exactness. *IEEE Trans. on Control of Network Systems*, 1(2):177–189, 2014.

[62] Mowen Lu, Harsha Nagarajan, Russell Bent, Sandra Eksioglu, and Scott Mason. Tight piecewise convex relaxations for global optimization of optimal power flow. In *Power Systems Computation Conf.*, pages 1–7. IEEE, 2018.

[63] Mehdi Madani, Carlos Ruiz, Sauleh Siddiqui, and Mathieu Van Vyve. Convex hull, ip and european electricity pricing in a european power exchanges setting with efficient computation of convex hull prices. *arXiv:1804.00048*, 2018.

[64] Ramtin Madani, Morteza Ashraphijuo, and Javad Lavaei. SDP solver of optimal power flow users manual. 2014.

[65] Rakesh Maurya, Harris Loizou, and Himali Parmar. White paper: Here's what may happen if ercot introduces marginal losses. Technical report, ICF International, Inc, May 2017.

[66] Daniel K Molzahn and Ian A Hiskens. Convex relaxations of optimal power flow problems: An illustrative example. *IEEE Transactions on Circuits and Systems I: Regular Papers*, 63(5):650–660, 2016.

[67] Daniel K Molzahn, Ian A Hiskens, et al. A survey of relaxations and approximations of the power flow equations. *Foundations and Trends® in Electric Energy Systems*, 4(1-2):1–221, 2019.

[68] Daniel K Molzahn, Jesse T Holzer, Bernard C Lesieutre, and Christopher L DeMarco. Implementation of a large-scale optimal power flow solver based on semidefinite programming. *IEEE Transactions on Power Systems*, 28(4):3987–3998, 2013.

[69] Young-Hyun Moon, Byoung-Kon Choi, Heon-Su Ryu, Jae-Suk Jung, and Ho-Min Park. Slack-bus independent penalty factor for spot pricing under deregulation. In *Power Engineering Society Winter Meeting, 2000. IEEE*, volume 2, pages 1017–1021. IEEE, 2000.

[70] FERC Order No. 844, uplift cost allocation and transparency in markets operated by regional transmission organizations and independent system operators. *Federal Energy Regulatory Commission*, 2018.

[71] Jorge Nocedal and Stephen Wright. *Numerical optimization.* Springer Science & Business Media, 2006.

[72] James Ostrowski, Miguel F Anjos, and Anthony Vannelli. Tight mixed integer linear programming formulations for the unit commitment problem. *IEEE Transactions on Power Systems*, 27(1):39–46, 2011.

[73] Thomas J Overbye, Xu Cheng, and Yan Sun. A comparison of the AC and DC power flow models for lmp calculations. In *37th Annual Hawaii International Conference on System Sciences, 2004. Proceedings of the*, pages 9–pp. IEEE, 2004.

[74] Narayana Prasad Padhy. Unit commitment-a bibliographical survey. *IEEE Trans. on power systems*, 19(2):1196–1205, 2004.

[75] Rodrigo Palma-Benhke, Andy Philpott, Alejandro Jofré, and Marcelo Cortés-Carmona. Modelling network constrained economic dispatch problems. *Optimization and Engineering*, 14(3):417–430, 2013.

[76] A Philpott. Experiments with load flow pricing models. In *Proceedings of CRNEC Policy Conference, Centre for Research in Network Economics and Communications, Univ. Auckland, New Zealand*, 1999.

[77] Andy Philpott and Geoffrey Pritchard. Financial transmission rights in convex pool markets. *Operations Research Letters*, 32(2):109–113, 2004.

[78] PJM. Marginal losses implementation training. `http://www.pjm.com`, Winter and Spring. 2007.

[79] Jose Luis Martinez Ramos, Antonio Gomez Exposito, FJC Moron, and SN Becerra. On the use of loss penalty factors for generation scheduling. In *2003 IEEE Power Engineering Society General Meeting (IEEE Cat. No. 03CH37491)*, volume 2, pages 926–931. IEEE, 2003.

[80] Dane A Schiro, Tongxin Zheng, Feng Zhao, and Eugene Litvinov. Convex hull pricing in electricity markets: Formulation, analysis, and implementation challenges. *IEEE Transactions on Power Systems*, 31(5):4068–4075, 2016.

[81] Fred C Schweppe, Michael C Caramanis, Richard D Tabors, and Roger E Bohn. *Spot pricing of electricity*. Springer Science & Business Media, 2013.

[82] Mohammad Shahidehpour, Hatim Yamin, and Zuyi Li. Market overview in electric power systems. *Market Operations in Electric Power Systems: Forecasting, Scheduling, and Risk Management*, pages 1–20, 2002.

[83] Steven Stoft. Power system economics. *Journal of Energy Literature*, 8:94–99, 2002.

[84] Brian Stott, Jorge Jardim, and Ongun Alsaç. DC power flow revisited. *IEEE Transactions on Power Systems*, 24(3):1290–1300, 2009.

[85] Kaarthik Sundar, Harsha Nagarajan, Sidhant Misra, Mowen Lu, Carleton Coffrin, and Russell Bent. Optimization-based bound tightening using a strengthened QC-relaxation of the optimal power flow problem. *arXiv preprint arXiv:1809.04565*, 2018.

[86] Cyriel Van Nuffelen. On the incidence matrix of a graph. *IEEE Transactions on Circuits and Systems*, 23(9):572–572, 1976.

[87] Andreas Wächter and Lorenz T Biegler. On the implementation of an interior-point filter line-search algorithm for large-scale nonlinear programming. *Mathematical programming*, 106(1):25–57, 2006.

[88] Congcong Wang, Peter B Luh, Paul Gribik, Tengshun Peng, and Li Zhang. Commitment cost allocation of fast-start units for approximate extended locational marginal prices. *IEEE Trans. on Power Systems*, 31(6):4176–4184, 2016.

[89] Congcong Wang, Tengshun Peng, Peter B Luh, Paul Gribik, and Li Zhang. The subgradient simplex cutting plane method for extended locational marginal prices. *IEEE Trans. on Power Systems*, 28(3):2758–2767, 2013.

[90] Gui Wang, Uday V Shanbhag, Tongxin Zheng, Eugene Litvinov, and Sean Meyn. An extreme-point subdifferential method for convex hull pricing in energy and reserve markets-part I: Algorithm structure. *IEEE Trans. on Power Systems*, 28(3):2111–2120, 2013.

[91] MQ Wang, Hoay Beng Gooi, SX Chen, and Shaofeng Lu. A mixed integer quadratic programming for dynamic economic dispatch with valve point effect. *IEEE Transactions on Power Systems*, 29(5):2097–2106, 2014.

[92] Felix Wu, Pravin Varaiya, Pablo Spiller, and Shmuel Oren. Folk theorems on transmission access: Proofs and counterexamples. *Journal of Regulatory Economics*, 10(1):5–23, 1996.

[93] Ti Xu, Adam B Birchfield, and Thomas J Overbye. Modeling, tuning, and validating system dynamics in synthetic electric grids. *IEEE Transactions on Power Systems*, 33(6):6501–6509, 2018.

[94] Zhifang Yang, Anjan Bose, Haiwang Zhong, Ning Zhang, Jeremy Lin, Qing Xia, and Chongqing Kang. LMP revisited: A linear model for the loss-embedded LMP. *IEEE Transactions on Power Systems*, 32(5):4080–4090, 2017.

[95] Zhifang Yang, Tongxin Zheng, Juan Yu, and Kaigui Xie. A unified approach to pricing under nonconvexity. *IEEE Trans. on Power Systems*, 2019.

[96] Zhifang Yang, Haiwang Zhong, Anjan Bose, Tongxin Zheng, Qing Xia, and Chongqing Kang. A linearized OPF model with reactive power and voltage magnitude: a pathway to improve the Mw-only DC OPF. *IEEE Transactions on Power Systems*, 33(2):1734–1745, 2018.

[97] Hui Zhang, Gerald T Heydt, Vijay Vittal, and Jaime Quintero. An improved network model for transmission expansion planning considering reactive power and network losses. *IEEE Transactions on Power Systems*, 28(3):3471–3479, 2013.

[98] Ray Daniel Zimmerman, Carlos Edmundo Murillo-Sánchez, and Robert John Thomas. Matpower: Steady-state operations, planning, and analysis tools for power systems research and education. *IEEE Transactions on power systems*, 26(1):12–19, 2011.

Vita

Manuel Joseph Garcia is a doctoral candidate in the Electrical and Computer Engineering department at the University of Texas at Austin, where he held the Cockrell School of Engineering Fellowship. He earned a B.S. and M.S. degree from the Mechanical Engineering department at the University of California at Berkeley. Before attending the University of Texas he held a two-year Post-Masters Internship position in the Theoretical Division at Los Alamos National Laboratory. As a student at the University of Texas he held internship positions at Los Alamos National Laboratory, Argonne National Laboratory, the Massachusetts Institute of Technology, and the Pontifical Catholic University of Chile. In each of these positions Manuel performed academic research in the field of electric power systems. Manuel was born and raised in Redding California and graduated from Shasta High School and Shasta College before moving to Berkeley.

Permanent address: mogarcia723@gmail.com

This dissertation was typeset with LaTeX by the author.

LaTeX is a document preparation system developed by Leslie Lamport as a special version of Donald Knuth's TeX Program.